# Hungry for More: Measuring Metabolomic Responses in ANCA-Activated Monocytes

**Emma Leacy**

**B.Sc. Human Health & Disease**

A thesis submitted to Trinity College Dublin

For the degree of Doctor of Philosophy

Supervisors: Prof. Mark Little, Prof. Gareth Brady, Dr. Hania Khouri

School of Medicine

Trinity College Dublin

2022

## Declaration

I declare that this thesis has not been submitted as an exercise for a degree at this or any other university and it is entirely my own work, with the exception of the following figures:

- Figure 1.4.1, taken from Vegting *et al.* [1].
- Figure 1.4.2 & Figure 3.3.8A, which was carried out by Dr. Eóin O'Brien, Trinity College Dublin
- Figure 3.3.9, which was carried out by Laetitia Sanelli, Maastricht University
- Figure 3.3.11, which was carried out by Michéle O'Sullivan, Trinity College Dublin
- Figure 3.3.17, which was carried out by Mark McFeely, Trinity College Dublin
- Figure 5.3.17B-D, which was carried out by Dr. Jason Wyse, Trinity College Dublin

I agree to deposit this thesis in the University's open access institutional repository or allow the library to do so on my behalf, subject to Irish Copyright Legislation and Trinity College Library conditions of use and acknowledgement.

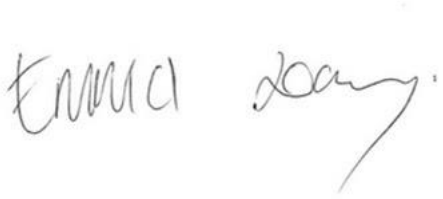

Emma Leacy

## Acknowledgements

I have dreamed about doing a PhD for as long as I can remember, but never thought about actually getting to this point. I have imagined myself sitting in this specific apartment writing my thesis, and have had the past 18 months to do nothing but that. To (obnoxiously) quote Orwell: "It was like struggling with some crushing physical task, something which one had the right to refuse and which was nevertheless neurotically anxious to accomplish [2]". There are countless people who have contributed to my success over the years and I will do my best to give them their due credit here.

I must first thank my Supervisors – Prof. Mark Little, Prof. Gareth Brady and Dr. Hania Khouri – for your constant support and guidance throughout my PhD research. Mark took me on and set me the task of solving the ANCA-monocyte-metabolism riddle. Your consistent, critical feedback has helped strengthen this work, and I hope this piece of the AAV puzzle helps put together the big picture. Gareth has helped to shape this work by asking difficult questions, but has always helped to make the impossible tasks seem doable. Your “See, Do, Teach” approach has been invaluable for me to improve my lab skills. Hania has taught me everything I know about mass spec and without her none of this work would exist. She is one of the smartest and most capable women I’ve had the pleasure of meeting and I’ve learned so much from her. So many things have gotten lost in translation, but make no mistake; I have the utmost admiration and respect for you, Hania.

There have been countless other teachers who have supported me over the years. In particular, Ms. Holden, Ms. Flatley, Ms. King, and Ms. O’Toole made me feel smart and brave enough to pursue a career in science. The lessons these educators have thought me will be extremely helpful going forward in my career and life. They have made me the scientist I am today.

I have to give huge thanks to everyone in the RIG/TIRG/IRG labs past and present, for their assistance in the lab, and for their patience at every data meeting I’ve presented at. Aisling, Amrita, Izzy and Tom – you have made this feel less like work and more like a Leaving Cert Holiday. My work wife Gráinne has been a lifesaver

both in and out of the lab. Everyone else in TTMI who joined in on the 2018 World Cup Sweepstakes – this was the beginning of a beautiful inter-lab collaboration where the key outputs were laughs and good times. Everyone in the “Live, Lab, Love” WhatsApp group is a diamond. Thank you for the memes and for listening to my terrible jokes and complaints for four years. Special shoutouts to Derv, Adam, Anna, Ola, Stephen, Niall, Sam and Andreas.

Despite several delays and obstacles, I’ve had the pleasure of working with some outstanding individuals who have consistently delivered to allow this and other projects to work seamlessly. For being excellent at their jobs and helping to put my frantically anxious mind to rest I want to thank: Pamela O'Neill, Jona Yusingco, Dr. Jean Dunne, Dr. Michelle O'Shaughnessy, Dr. Lina Zgaga, Caroline Kosgiec, Binny Benny, Carol Cunniam, and the brilliant team in CPL – Rachel, Aifric, and Caroline. There have also been countless RKD interns and research students I've gotten emotionally attached to and who made work a joy. Namely Laetitia, Michèle and Mark for allowing me to supervise their final year projects and highlight their work here.

I am incredibly blessed to have supportive friends and family. Gary, Amy, Tanya, Sibéal, Nicole – thank you for helping me feel like the capable scientist you believe me to be. To Dave, thank you for letting me back into your life and helping me to believe in myself again. To Conor, Laura, and Niamh: this proves that I am once again the smartest in the family. My parents – Nuala and Dave – endlessly warm my heart with their enthusiasm for my work. Their pride in me has helped to power me through the tough days. I would like to dedicate this work to my grandfather Pat. I hope that I can do him justice as the first Dr. Leacy.

# Abstract

Immunometabolism examines the links between immune cell function and their metabolism. Advances in liquid chromatography mass spectrometry (LC-MS) technologies have uncovered unique insights into cellular metabolomics. Dysregulation of immune cell metabolism is now an established feature of many autoimmune diseases. One such condition is anti-neutrophil cytoplasmic antibody (ANCA) associated vasculitis (AAV), where monocyte metabolism is disrupted following ANCA stimulation leading to pathogenic inflammation. In this thesis I have optimised LC-MS methods for metabolomic profiling of primary monocytes, and investigated the role of metabolism in response to ANCA stimulation.

I first defined optimum cell culture conditions and experimental protocols for ANCA stimulation of primary monocytes. I then investigated ways to better combine immunologic and metabolic readouts in these cells. Flow cytometry, histology, ELISA, RT-qPCR, and western blots can all be completed in a single four-hour stimulation experiment alongside the core LC-MS analysis, but Seahorse investigations must be completed in parallel. Pilot investigations also uncovered changes in ANCA antigen expression with age and links to amino acid production via glycolysis.

Next, I optimised sample preparation and LC-MS conditions for metabolomic profiling of these cells. A methanol-based metabolite extraction protocol was deemed most appropriate, and a Hydrophilic Interaction Liquid Chromatography (HILIC) LC-MS method provided excellent coverage of the monocyte metabolome. The analysis pipeline requires sample normalisation to account for technical and biological variation. I have validated measurement of the residual protein content of the metabolite fraction as a means of normalising primary cellular metabolomic data, and have optimised a commercial assay protocol for this purpose.

Finally, these optimised experiments were completed in a cohort of healthy donor monocytes stimulated with ANCA. Alterations in several amino acids and several lipid species were discovered, with a greater effect seen in cells activated with anti-myeloperoxidase (MPO). Increases in several metabolites also appear to be linked to ANCA antigen expression. While the changes in cellular metabolism at this early (4 hour) timepoint are subtle, they do suggest a link between metabolic activation and upregulation of inflammatory responses.

These data implicate changes in monocyte metabolism in the pathogenesis of AAV. This hypothesis-generating work should be further validated to determine the specific role of these metabolites in ANCA-induced inflammation. These metabolic pathways may also hold potential as therapeutic targets for AAV.

# Table of Contents

# List of Figures

# List of Tables

# Publications & Presentations Arising from this Work

## Publications

- Dooley, D., M. M. van Timmeren, V. P. O'Reilly, G. Brady, E. C. O'Brien, B. Fazekas, F. B. Hickey, E. Leacy, C. D. Pusey, F. W. K. Tam, T. Mehrling, P. Heeringa and M. A. Little (2018). "Alkylating histone deacetylase inhibitors may have therapeutic value in experimental myeloperoxidase-ANCA vasculitis." Kidney Int 94(5): 926-936.
- Leacy, E., G. Brady and M. A. Little (2020). "Pathogenesis of ANCA-associated vasculitis: an emerging role for immunometabolism." Rheumatology (Oxford) 59(Supplement_3): iii33-iii41.
- O'Brien, E. C., C. A. White, J. Wyse, E. Leacy, R. K. Porter, M. A. Little and F. B. Hickey (2020). "Pro-inflammatory Stimulation of Monocytes by ANCA Is Linked to Changes in Cellular Metabolism." Frontiers in Medicine 7.

## Presentations

- Cross-Instrument Metabolic and Cellular Energetic Profiling of Monocytes in ANCA-Associated Vasculitis
    - Oral Presentation, European Forum on Applied Metabolomics, 2018
- Metabolic Profiling of Monocytes in ANCA-Vasculitis
    - Oral Presentation, TTMI Research Blitz, 2019
        - Awarded Best Postgraduate Speaker
- Altered Intracellular Amino Acid Metabolism in Monocytes Correlates with Increased Glycolysis upon ANCA Stimulation
    - Poster Presentation, Vasculitis Workshop Philadelphia, 2019
- Proteomic and Genetic Expression of Chemokines in ANCA-Stimulated Monocytes
    - Poster Presentation, Irish Nephrology Society, 2019
- Sample Preparation Optimisation in Primary Immune Cells for Untargeted Metabolomics
    - Oral Presentation, Irish Mass Spectrometry Society, 2019
- Increased Monocyte Glycolysis upon ANCA stimulation Correlates with Intracellular Amino Acid Levels
    - Poster Presentation, Irish Society of Immunology, 2019

- Assessment of Normalisation Strategies for Untargeted Metabolomic Analysis of Primary Immune Cells in ANCA-Associated Vasculitis
    - Oral Presentation, Irish Mass Spectrometry Society, 2021
- Untargeted Metabolomic Profiling of Primary Monocytes Reveals Alterations in Amino Acid and Lipid Metabolism Following LPS and ANCA Stimulation
    - Poster Presentation Annual Conference of the Metabolomics Society, 2021
        - Awarded Best Student Poster by Early Career Members Network
- Alterations in Amino Acid and Lipid Metabolism in ANCA-Stimulated Monocytes
    - Poster Presentation, American Society of Nephrology, 2021

# Abbreviations

| Abbreviation | Description |
|---|---|
| .CEF | Compound Exchange Format |
| 2-DG | 2-Deoxyglucose |
| α-KG | alpha-Ketoglutarate |
| 4-ABAH | 4-Aminobenzoic Acid Hydrazide |
| AAV | ANCA Associated Vasculitis |
| ACN | Acetonitrile |
| ACS | American Chemical Society |
| AIF | All-Ion Fragmentation |
| AMW | Acetonitrile:Methanol:Water |
| ANCA | Anti-Neutrophil Cytoplasmic Antibody |
| ATP | Adenosine Triphosphate |
| AUC | Area Under the Curve |
| BC | Buffy Coat |
| BMDM | Bone Marrow Derived Macrophage |
| BSA | Bovine Serum Albumin |
| $C_2H_7NO_2$ | Ammonium Acetate |
| CV | Coefficient of Variation |
| CXCL | C-X-C motif chemokine Ligand |
| DMEM | Dulbecco's Modified Eagle's Medium |
| DMSO | Dimethyl Sulfoxide |
| DNA | Deoxyribonucleic Acid |
| ECAR | Extracellular Acidification Rate |
| EGPA | Eosinophilic Granulomatosis With Polyangiitis |
| ELISA | Enzyme-Linked Immunosorbent Assay |
| ESI | Electrospray Ionization |
| ETC | Electron Transport Chain |
| FACS | Fluorescence Associated Cell Sorting |
| FAO | Fatty Acid Oxidation |
| FAS | Fatty Acid Synthesis |
| FBS/FCS | Foetal Bovine Serum/Foetal Calf Serum |
| FC | Fold Change |
| FDR | False Discovery Rate |
| FMO | Fluorescence Minus One |
| GN | Glomerulonephritis |
| GPA | Granulomatosis With Polyangiitis |
| $H_2O$ | Water |
| HBSS | Hanks Buffered Salt Solution |

| | |
|---|---|
| HGF | Haematopoietic Growth Factor |
| HILIC-Z | Hydrophilic Interaction Liquid Chromatography - Zwitterionic |
| HK-1 | Hexokinase-1 |
| HLA | Human Leukocyte Antigen |
| HRP | Horseradish Peroxidase |
| IBTS | Irish Blood Transfusion Service |
| IgG | Immunoglobulin G |
| IL | Interleukin |
| ISO | Isotype |
| LC-MS | Liquid Chromatography-Mass Spectrometry |
| LDH | Lactate Dehydrogenase |
| LDL | Low Density Lipoprotein |
| LPS | Lipopolysaccharide |
| *m/z* | Mass-to-Charge Ratio |
| mAb | Monoclonal Antibody |
| MACS | Magnetic Activated Cell Sorting |
| MAD | Median Absolute Deviation |
| MCP | Monocyte Chemoattractant Protein |
| MeOH | Methanol |
| MFE | Molecular Feature Extraction |
| MFI | Median Fluorescence Intensity |
| MHC | Major Histocompatibility Complex |
| MMP | Matrix Metalloproteinase |
| MPA | Microscopic Polyangiitis |
| MPO | Myeloperoxidase |
| MPP | Mass Profiler Professional |
| MRM | Multiple Reaction Monitoring |
| mTOR | Mechanistic Target Of Rapamycin |
| NAD+ | Nicotinamide Adenine Dinucleotide |
| OCR | Oxygen Consumption Rate |
| OD | Optical Density |
| OSM | Oncostatin M |
| OXPHOS | Oxidative Phosphorylation |
| PAM3 | Pam3CSK4 |
| PAMP | Pathogen-Associated Molecular Pattern |
| PBMC | Peripheral Blood Mononuclear Cells |
| PBS | Phosphate Buffered Saline |
| PCA | Principal Component Analysis |
| PCDL | Personal Compound Database And Library |

| | |
|---|---|
| pHILIC-Z | PEEK (polyetheretherketone)-Lined HILIC-Z |
| PPP | Pentose Phosphate Pathway |
| PQN | Probabilistic Quotient Normalization |
| PR3 | Proteinase-3 |
| PRR | Pattern Recognition Receptor |
| PUFA | Polyunsaturated Fatty Acid |
| Q-ToF | Quadrupole Time Of Flight |
| QC | Quality Control |
| RFE | Recursive Feature Extraction |
| RKD | Rare Kidney Disease |
| RNA | Ribonucleic Acid |
| ROS | Reactive Oxygen Species |
| RPMI | Roswell Park Memorial Institute |
| RSD | Relative Standard Deviation |
| RT | Retention Time |
| RT-qPCR | Real-Time Quantitative Reverse Transcription Polymerase Chain Reaction |
| SDW | Sterile Distilled Water |
| SEM | Standard Error of the Mean |
| SFM | Serum-Free Media |
| SJH | St. James's Hospital |
| SLE | Systemic Lupus Erythematosus |
| SSE | Sample Size Estimate |
| SVV | Small Vessel Vasculitis |
| TAK | Takayasu's Arteritis |
| TCA | Tricarboxylic Acid Cycle |
| TFE | Targeted Feature Extraction |
| TIC | Total Ion Chromatogram |
| TLR | Toll-Like Receptor |
| TMAO | Trimethylamine N-Oxide |
| TMB | 3, 3’, 5, 5’ – Tetramethylbenzindine |
| TNF | Tumour Necrosis Factor |
| Treg | Regulatory T Cell |

# Chapter 1: Introduction

## 1.1 Immunometabolism

Immunometabolism is a burgeoning field which examines the links between immune cell function and metabolism. Metabolic pathways and immunologic functions are now recognised as a complex concatenation of processes with distinct outputs based on context. Cellular metabolism is the process by which cells generate energy in the form of adenosine triphosphate (ATP)[3]. There are two primary pathways used by cells to generate ATP: the glycolytic pathway (glycolysis) and oxidative phosphorylation (OXPHOS). These pathways are linked by the production of pyruvate, produced via pyruvate kinase during the final step of glycolysis. Pyruvate then moves from the cytoplasm into the mitochondrion where it is converted to acetyl-CoA to feed the tricarboxylic acid (TCA) cycle (a.k.a. Krebs cycle). A summary of the major metabolic pathways in human cells and some of their interconnections is shown in Figure 1.1.1.

Glucose is the primary fuel used by immune cells to produce energy. Glycolysis – the breakdown of glucose – is a fundamental metabolic process for energy generation in the human body. Glycolytic intermediates can be hijacked to feed other metabolic pathways. The pentose phosphate pathway (PPP), tricarboxylic acid (TCA) cycle, and lipid synthesis pathways can all be fuelled by branches of glycolysis [3]. The field of immunometabolism was initially born from the discovery that cancer cells primarily produce ATP via glycolysis [4]. Despite this pathway yielding significantly less ATP than OXPHOS, glycolysis produces ATP at a much faster rate [5, 6]. Glycolysis supports these cells' need for rapid proliferation in a process called the "Warburg effect" [4]. A similar phenomenon has also been demonstrated in immune cells. In general, quiescent immune cells transfer pyruvate generated from glycolysis into the TCA to meet their low energy demands. Upon activation these cells require much more energy to carry out their varied functions, and generally favour glycolysis.

Immunometabolism provides deeper phenotypic profiling of the influence of specific immune cell types in health and disease. Modern immunometabolism was born from discoveries linking succinate accumulation to interleukin (IL)-1β [7, 8] in macrophages. Monocytes extravasate and differentiate into macrophages (or

dendritic cells [DCs]) in tissues where they adopt a specific functional niche determined by microenvironmental signals. Macrophages play diverse functional roles depending on their phenotype, compartment, and origin, but can be broadly characterised into a pro- inflammatory (M1) and an anti-inflammatory (M2) profile [9]. M1 macrophages initiate and sustain inflammatory responses by secreting pro-inflammatory cytokines and chemokines, and M2 macrophages are pro-resolving, phagocytosing, and produce anti-inflammatory signalling compounds [9, 10]. Further to their opposing pro- and anti-inflammatory roles, macrophages have distinct metabolic profiles depending on the stimuli received [10-12]. M1 macrophages undergo Warburg metabolic reprogramming towards glycolysis, the PPP and fatty acid synthesis (FAS). There are also distinct TCA cycle breaks which lead to succinate and itaconate accumulation, and citrate efflux [13]. These pathways fuel the pro-inflammatory functions of these cells. Conversely, pro-resolving M2 macrophages preferentially utilise OXPHOS metabolism, FAO, and glutaminolysis as a means of energy generation. Metabolism of amino acids arginine, proline, alanine, aspartate, and tryptophan defined the M2 phenotype during macrophage differentiation [14]. Inhibition of glycolysis also affected M2 differentiation and function [15]. The immunometabolism of monocytes has been less well defined, particularly in the context of autoimmune disease.

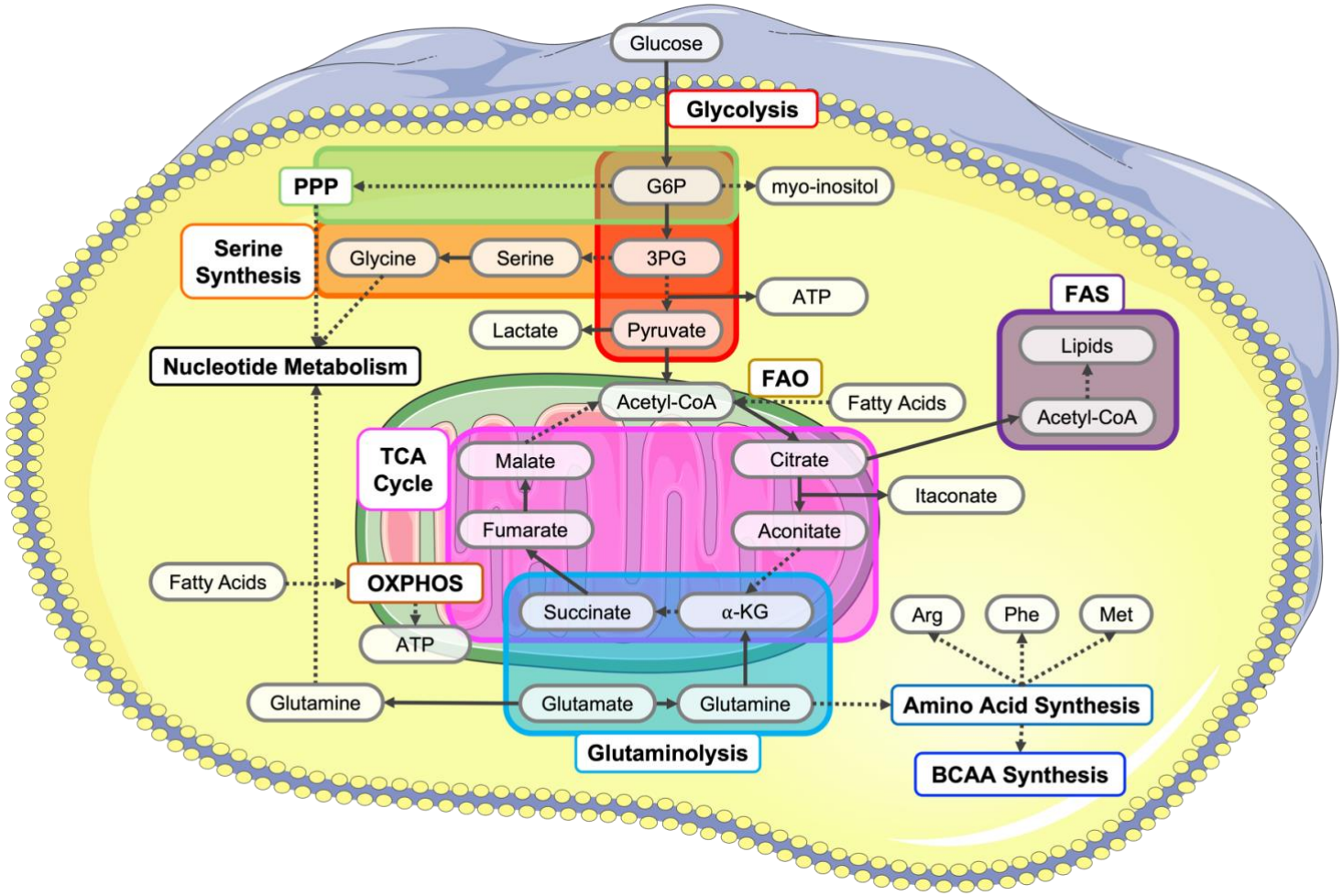


**Figure 1.1.1: Summary of major metabolic pathways utilized by primary immune cells.** Metabolic processes are colour coded and key metabolites highlighted in grey. Solid lines are direct conversions and dashed lines are multi-step reactions. Edited from Buck et al. [10.1084/jem.20151159]. PPP: Pentose Phosphate Pathway; G6P: Glucose-6-Phosphate; 3PG: 3-Phosphoglycerate; ATP: Adenosine Triphosphate; FAS: Fatty Acid Synthesis; FAO: Fatty Acid (β-)Oxidation; TCA Cycle: Tricarboxylic Acid/Krebs cycle; α-KG: alpha-Ketoglutarate; OXPHOS: Oxidative Phosphorylation; Arg: Arginine; Phe: Phenylalanine; Met: Methionine; BCAA: Branched Chain Amino Acid

## 1.2 Metabolomics

Metabolomics is the comprehensive measurement of all metabolites and low-molecular-weight molecules in a biological specimen. Metabolomic profiling refers to the identification and quantitation of the compounds of metabolism. This can be examined in the context of disease phenotypes, genetic differences, environmental influences, and pharmacological perturbations. Variation in the metabolomic profile will reflect biochemical changes caused by physiological or pathological processes. Untargeted metabolomics is commonly used for biomarker discovery in mammalian models and has also been applied to the study of microbes, plants, food products, and environmental systems. Metabolomic profiling also has clinical and industrial relevance. Metabolomic assays are increasingly used to screen and diagnose inborn errors of metabolism in neonates [16, 17], and analysis of primary and secondary metabolites is used to optimise cell culture conditions for biotechnological applications [18].

Untargeted metabolomics is an important first step in biomarker discovery. Metabolite activity screening [19] integrates metabolomics data with systems biology information to identify metabolites and pathways that moderate a given phenotype. This is particularly relevant in the context of cellular metabolomics, where different cells and tissues can be affected in a given condition. Metabolism can drive energy production, macromolecule synthesis, control intracellular signalling, post- translational modifications, and impact cell survival. Certain metabolites have also been shown to play a role in epigenetic modifications that drive inflammation in monocytes [20-22]. There are 114,100 metabolites currently identified by the Human Metabolome Database (HMDB; https://hmdb.ca/about)[23]. Only 21,000 have been detected and identified, and approximately 2,000 are considered major (or primary) metabolites in the global human metabolome [24]. There are five hierarchical levels of chemical metabolite classification. Level 1 – a confirmed structure with ≥2 orthogonal properties from a pure reference standard acquired under identical analytical conditions – represents the highest quality identification standard [25]. Thus, a major bottleneck of metabolomic analysis is sufficient optimisation to reliably identify such an extensive range of compounds.

### 1.2.1 Liquid Chromatography Mass Spectrometry (LC-MS)

Liquid-chromatography mass spectrometry (LC-MS) is the gold standard for metabolomic analyses because of its high sensitivity, specificity, and reproducibility [19, 26]. Modern quadrupole time-of-flight (Q-ToF) spectrometers are capable of measuring across five orders of magnitude and into the picomolar range while still allowing effective molecular identification. Given the diversity of ionic and polar properties across metabolite classes, there is no single LC-MS assay or method capable of comprehensively measuring the full metabolome of a given sample. Gas chromatography (GC)-MS can complement untargeted analyses by allowing detection of low-molecular-weight and volatile analytes [27]. Changes in study design and analytical strategy can influence the quality of the data acquired and how it is interpreted. A schematic overview of LC-MS instrumentation is shown in Figure 1.2.1.

Commercial metabolomics platforms such as Metabolon Inc. (https://www.metabolon.com/) and the Broad Institute (https://www.broadinstitute.org/metabolomics) analyse each experimental sample using four distinct LC-MS methods [28]. This enables broad metabolome coverage covering a range of analyte polarity and chemical properties. However, a number of key studies regularly cited in the literature (and indeed in this work) do not describe these LC-MS methods or sample preparation techniques in sufficient detail to allow replication defined by minimum required reporting guidelines [29]. Furthermore, these methods may not be optimised for the specific sample matrix or experimental conditions, but rather fit into a one-size-fits-all approach to standardise metabolomic profiling.

#### 1.2.1.1 High Performance Liquid-Chromatography (HPLC)

Compounds are separated by high performance liquid chromatography (HPLC) based on three primary characteristics: polarity, electrical charge, and molecular size. Metabolites can have a very wide range of structures and physicochemical characteristics, which will ultimately affect their polarity. To achieve optimal coverage of the metabolome a multi-method LC-MS strategy is often employed [30-35]. This typically involves a combination of hydrophilic interaction chromatography (HILIC) and reverse-phase (RP) chromatography optimised for polar and non-polar compounds, respectively.

In LC method development there are two key ways to manipulate chemical attractions: the mobile phase(s) and the stationary phase. The stationary phase pertains to the packing material within the chromatographic column. HILIC chromatography contains a stationary phase (e.g. silica, amine, zwitterionic etc.) which favours polar metabolite retention (amino acids, nucleic acids, sugars and small organic acids) when coupled with an appropriate organic mobile phase gradient [36](see below). RP chromatography bonds carbon tails (C8/C18/C30) to the silica layer and is optimized for binding of non-polar compounds such as lipids. Chromatographic columns can also vary on column length or diameter and packing material or size. RP chromatography is not optimized for polar compounds, and because these metabolites are not effectively retained within the column they elute early in the method (and vice versa for HILIC). Many metabolites eluting at this void/dead volume means more optimization is required for the LC method.

Mobile phases can affect compound separation and elution in LC-MS experiments. Gradient elution can improve separation of complex sample matrices, sharpen peaks, and reduce total method time. A gradient elution with two or more different mobile phases allows control of the levels of organic solvent and can alter the retention of metabolites within the column. The percentage of organic solvent (typically mobile phase B) is carefully manipulated to enhance separation of metabolite classes. The water content of gradients is important for HILIC chromatography, where metabolites bind to a polar stationary phase and are eluted by increasing water content [27] with an organic to aqueous gradient. For untargeted metabolomic analyses an LC method with a varied gradient over 15-20 mins is generally sufficient to cover broad metabolite species and effectively separate many isomers (molecules with identical molecular formulas but distinct structural arrangements) and metabolites with similar masses. The interaction of the mobile phase with the stationary is crucial for efficient separation of metabolites. HILIC columns are suited to more polar solvents (methanol, acetonitrile), and RP chromatography demand less polar (chloroform, isopropanol).

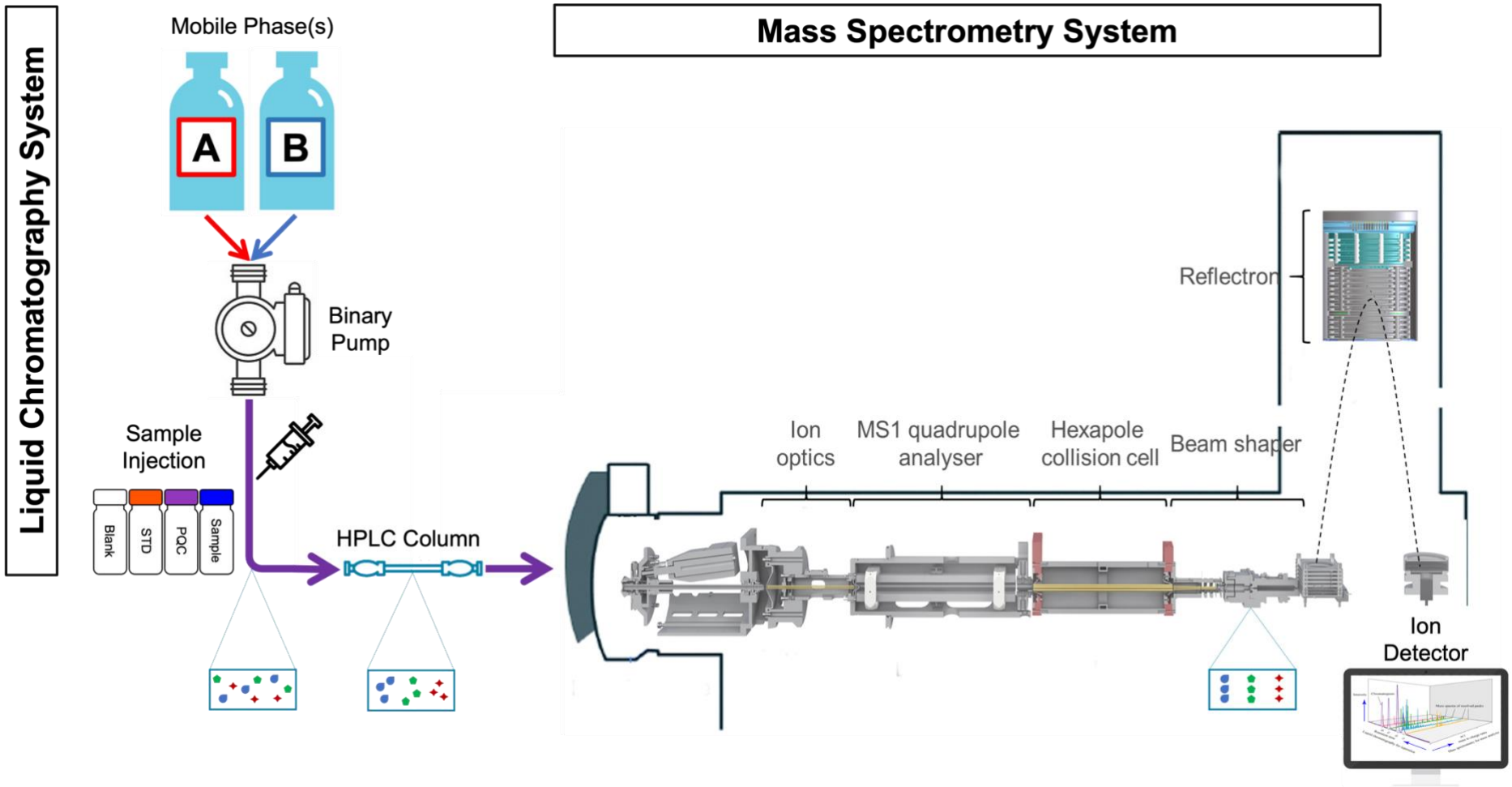


**Figure 1.2.1: Schematic Overview of Liquid Chromatography Mass Spectrometry (LC-MS) Instrumentation.** Mixing of mobile phases by the binary pump creates a gradient of organic and inorganic solvent which moves through the HPLC column at a defined flow rate. This process allows separation of the heterogenous metabolite matrix of samples loaded onto the HPLC column. Upon vaporisation in the mass spectrometer samples are ionised (in this case by electrospray ionisation) and accelerated through the drift tube. The collision cell fragments charged ions and pulses them up the MS funnel until they are received by the ion detector and visualised using the appropriate software. *HPLC:* High Performance Liquid Chromatography.

Another way to separate isomers and improve chromatography is to incorporate mobile phase additives. Mobile phase components must be sufficiently volatile to allow vaporisation in the ESI source, and free from impurities that can impact sensitivity by adduct formation or increasing background. Additives are typically acids or ammonium salts which are used to buffer mobile phases to improve ionization of analytes and stationary phase, while improving chromatography and retention time reproducibility [37]. Mobile phase additives can alter compound retention and peak shape, affecting retention time and abundance measurements, respectively. The pH of the mobile phase is another crucial consideration that can dramatically affect analyte retention behaviour. Retention of acidic or basic functional groups can be drastically altered by the pH of the mobile phase, which should be strictly controlled. A high pH mobile phase can often improve MS sensitivity, metabolite detection and peak shape [38, 39], particularly for HILIC-based methods.

Analysis of polar metabolites by RP chromatography is challenging but can be achieved by manipulating mobile phase conditions. Addition of an ion-pairing agent to mobile phases can improve retention and detection of charged polar metabolites [40]. Ion pairing agents (quaternary amines, alkyl-sulfonates/-sulphate/alkylammonium salt, volatile acids, etc.) are compounds that contain both an ionic functional group and a hydrophobic portion. They act by interacting with counter-ions in the sample matrix to form pseudo-neutral complexes. This can greatly improve chromatographic peak quality [27, 41]. However, the use of ion-pairing agents in LC-MS requires very careful consideration and comes with a number of caveats. Most notably, ion-pairing agents are challenging to remove completely from the LC system/column once introduced, and generally require dedicated instrumentation [42]. They can also diminish column performance over time requiring additional column maintenance and, in some cases, suppress biologically relevant signals.

Changes to mobile phase composition, gradient, or column type will affect metabolite coverage and retention. Both flow rate and injection volume can affect retention time, and injection volume (and its relationship with column size & diameter) can additionally impact metabolite abundance measurements and chromatography [43, 44]. There are countless variables to consider across the LC-

MS platform, and those affecting chromatography can have knock-on effects to MS detection.

#### 1.2.1.2 Mass Spectrometry (MS)

After metabolite separation (by LC as described above) mass spectrometry (MS) is used to detect and identify compounds in a given sample matrix [24]. Most metabolomic LC-MS methods rely on electrospray for ionisation and detection of charged metabolites [27]. Quadrupole time-of-flight mass spectrometry (QToF-MS) is the method of choice for metabolomic investigations. These instruments combine ToF and quadrupole instruments to generate spectra with high mass accuracy, speed and sensitivity [45]. Mass-to-charge ratios are determined by the speed that ions move down the flight tube to the detector. QToF-MS analysers provide excellent dynamic range, high mass resolution and mass accuracy.

Metabolite abundances are determined by measuring the area under the curve (AUC) of chromatographic peaks. However, this AUC readout alone is not a quantitative metabolite measurement. Ion counts can be affected by ionisation efficiency, and ion suppression is common in ESI-MS. Inefficient separation of isomers can confound metabolite measurements. Without the addition of a standard curve via repeated injections of a known standard(s)(or development of a targeted method) it is not possible to quantitatively measure metabolites as part of an untargeted LC-MS experiment [46]. Thus, for untargeted metabolomics relative quantitation by comparing metabolite differences from one group to another is the modus operandi for comparing experimental conditions/groups. LC-MS can be less reproducible than gas chromatography (GC), with variation arising from the ESI source, column deterioration, and mobile phase composition [47]. Ion suppression is an important issue in LC-MS investigations particularly in the analysis of complex samples such as cell lysates by ESI. This occurs when a high abundance ion inhibits the electrospray ionization and thus the signal of coeluting ions [48, 49]. This can be caused by mobile phase additives (particularly salts or ion pairing agents [see above]) or by metabolites themselves. A related issue is adduct formation, where additional peaks appear in a chromatogram mimicking a metabolite feature [24]. These are important issues which can affect interpretation of metabolomic data and should be carefully considered during method development and data analysis.

### 1.2.1.3 Sample Preparation for LC-MS

Sample preparation is the first step in ensuring reproducibility and accuracy for metabolomics analyses. There are two key sample preparation steps in cellular metabolomics: quenching and metabolite extraction. Quenching is necessary to halt enzymatic activity to prevent metabolite degradation. This needs to be carried out immediately following sample collection to preserve sample composition. Quenching can be easily achieved in suspension cells by rapidly altering the temperature or pH of the sample. Altering pH can modify the chemical composition of metabolites, and higher temperatures may cause the loss of heat-sensitive metabolites and build-up of degradation products. Rapid cooling in liquid nitrogen, dry ice, or cooled buffers/extraction solvents is commonly used to quench mammalian cells [50]. Suspension cells (such as primary human monocytes) do not require cell harvesting by scraping or trypsin-EDTA, steps which have been shown to influence the intracellular metabolome [51, 52]. These cells can be quenched immediately after separation from culture medium by (chilled) centrifugation. Rapid filtration steps have been developed in lieu of centrifugation and are used in large cohort studies and biotechnological applications [53]. Even with efficient quenching, the turnover rate of some metabolites is so high that they will begin to degrade within seconds

Organic solvents are used in metabolomics studies to extract the metabolite fraction by precipitating protein (and nucleic acids) from the sample matrix. The choice of extraction solvent has less to do with the material being examined, but profoundly impacts metabolome coverage, and thus is an important consideration. Metabolite extraction should be universal to recover as many metabolites as possible, however this presents an intrinsic problem. The chemical diversity (molecular weight, polarity, acidity, stability, function) of metabolites is such that their polarity ranges from very hydrophilic compounds, such as lactate, amino acids, and tricarboxylic acid (TCA) cycle intermediates, to hydrophobic compounds, such as lipids and fatty acids. Thus, the extraction protocol can be considered the limiting step in intracellular metabolite profiling. To overcome this problem, multi-step extraction and biphasic protocols have been developed. The classic extraction protocol developed by Bligh and Dyer [54] was optimized for lipid analysis and combined chloroform, methanol (MeOH), and water. This separates hydrophobic, non-polar compounds in the

chloroform layer at the bottom, from more hydrophilic, polar metabolites in the upper MeOH/water layer. The interface between the two layers contains proteins and ribonucleic acid (RNA) which can be preserved for subsequent analyses [55-57]. Other extraction protocols split samples to incorporate multiple extraction solvents optimized for different analytical methods or sub-metabolomes [52]. Despite these comprehensive extraction protocols, many studies in mammalian cells have found monophasic methanolic extractions to be sufficient for metabolomic analyses. Indeed, the majority of intracellular metabolites are small polar molecules amenable to detection by a variety of solvents. An 80/20 solution of MeOH/$H_2O$ (80% MeOH) has been used in a wide variety of metabolomics investigations [58], is proven to be effective in the Jurkat T-cell line [59, 60], and can detect a broad range of metabolite classes [61]. Acetonitrile (ACN) at various concentrations has also proven effective [62]. Isotopically labelled standards from a range of metabolite classes can also be added to extraction solvents for compensation of technical/experimental variability.

### 1.2.2 LC-MS Data Analysis

Once LC-MS data has been acquired there are several additional steps that need to be completed before the results can be appropriately interpreted. The essential stages in the metabolomic data pre-processing workflow are: peak picking, peak filtering, peak alignment, chromatograph integration, and spectral processing. The process can be strengthened with appropriate quality and experimental controls [63, 64]. Some chromatographic peaks require manual review, particularly where there is evidence of peak splitting, shouldering, or suboptimal separation of isomers [65]. Subsequent quality control (QC) filtering can be performed to ensure that only high quality metabolite features are brought forward for statistical analysis [47]. Additional post-processing steps can include missing value imputation [66], data normalisation (see below), and machine learning for class prediction and pathway analysis.

Metabolite identification is a crucial step in an untargeted metabolomics workflow that causes substantial bottlenecks. There are five levels of confidence for metabolite IDs [25] and the top three are considered acceptable for reliable identification/annotation [47]. There are major differences in identification workflows between analytical techniques. For LC-MS feature annotation is achieved by comparing the detected masses and isotopic profile generated from experimental

data to databases of known metabolites within an appropriate mass tolerance window [25]. Today there are a number of high quality, curated, open source databases with MS1 and MS/MS information, including HMDB [23], METLIN [67, 68], MassBank [69], and LIPIDMAPS [70]. Still, metabolite features can be annotated with multiple potential IDs or in many cases not at all. Appropriate statistical analyses are dependent on the experimental design, and the massive amounts of data generated from MS experiments can be challenging to work with. There are several open source and vendor-specific options for statistical analysis of metabolomic data, and here we have utilised the Agilent MassHunter suite.

#### 1.2.2.1 Metabolomic Data Normalisation

Before we can extract meaningful data from complex and noisy datasets [47], data normalisation must be performed. This is especially pertinent for cellular metabolomic data, which is particularly susceptible to interpersonal and experimental variation in metabolomic data [71]. There are two main sources of variability in metabolomic data; confounding variables from experimental sources such as sample preparation and LC-MS conditions (e.g. instrument settings, signal drift, MS source contamination, column performance, mobile phase preparation etc. [72]), and interpersonal biological variations (physiological differences, sample degradation, variation in sample measurements, etc.) between samples [47, 73-75]. It is impossible to correct for *all* of these confounding variables in the course of a defined metabolomics investigation, but there are normalisation strategies that can improve quality of results. Few metabolomics investigations report their normalisation approaches in great detail, and as with sample preparation, there is no consensus strategy for normalising metabolomic data. Multiple normalisation strategies are recommended to strengthen metabolomics data integrity [47, 72, 76, 77]. Gagnebin *et al.* [78] have proposed a sequential normalisation strategy to improve data quality. A two-pronged approach combining biologic normalisation to account for technical variation and statistical normalisation to correct interpersonal differences may be appropriate for investigations of primary cellular metabolism. In addition to calculating accuracy of normalisation strategies, biological relevance, convenience, and cost should also be considered [75]. Normalisation approaches typically fall into one of two categories: sample-based or data-based.

#### 1.2.2.1.1 Sample-Based Normalisation Approaches

##### 1.2.2.1.1.1 Housekeeping Metabolites

Efforts have been made to identify metabolites present at stable and consistent concentrations that can be used for data normalisation as is the case for housekeeping genes [79]. Creatinine is routinely used for normalisation in urinary metabolomic studies where it's concentration is relatively stable [76]. However levels can vary by age, sex, race, diet, activity, and health/disease status [80] – similar to sources of variation in the human metabolome. It is recommended that normalisation to creatinine be combined with additional normalisation techniques such as osmolality [76] or integrated into sequential normalisation strategies [78]. Dilution of urine based on creatinine content to correct differences in total urine volume/output can be easily incorporated into a sample preparation protocol prior to sample processing and LC-MS analysis [81]. Given the dynamic nature of cellular metabolism, finding a single "housekeeping metabolite" for normalisation of cellular metabolomic data has been more challenging [71]. Relying on a single compound to evaluate the overall sample concentration is not recommended. Slight inaccuracies in measurement or interpersonal variations (from inefficient quenching for example) can introduce bias to the sample matrix. Furthermore, metabolite levels can change in disease states and could potentially alter flux of other metabolic pathways. Thus, normalising to a single metabolite could mask these differences.

Where isotopically-labelled standards have been included in the extraction solvents, these can be used to account for technical variation in the sample preparation process. For untargeted metabolomics it is recommended that a range of standards representing several metabolite classes be used [64]. The sum of detected phospholipids in HepG2 cells was presumed to be a surrogate measure of cellular membrane content and used for metabolomic data normalisation [82]. Cao *et al.* [83] identified a panel of 11 intracellular metabolites that were equally as effective as protein content for normalisation of metabolomic data in the MDCK canine kidney cell line. Given the diversity of energy utilisation across human cells, it is unlikely that a single metabolite (or selection of metabolites) remains constant in other matrices and can be used to normalise metabolomic data. Their utility is further limited by the need for validation for each cell type and application under investigation – an ideal "housekeeper" should remain constant across all cell lines

and treatments in the experiment. Human primary cells are massively dependent on glucose as a fuel source. Studies have shown that there are just four key enzymatic steps in this pathway that control glycolytic flux [84]. The metabolite products of these reactions may give an insight into the state of the cell's metabolism. In the context of monocytes Raulien *et al.* [85] observed changes in α-ketoglutarate, aspartate, and malate in response to the gram-negative bacterial product lipopolysaccharide (LPS) at early timepoints. These metabolites may be considered benchmarks of activated monocyte metabolism – in the same way creatinine is to urine output and total metabolite volume – and may be applicable to our experimental design.

Where single metabolites may not be relevant for data normalisation, measuring the entire metabolome content by calculating the area of the total ion chromatogram (TIC) may be a solution. This method is routinely used for normalisation of proteomic data but has also been used in metabolomics [86, 87]. The underlying assumption for TIC normalisation is that the total intensity of the spectrum should be proportional to the total concentration in the sample, and that if there is an equal amount of sample, then the summed intensity in the spectrum should be the same across all spectra. Normalisation by TIC uses the AUC value as a scalar to correct each individual spectrum to the same total metabolite intensity. This method is sensitive to the technical difficulties of LC-MS, namely ion suppression and batch variability. Some normalisation algorithms have been developed on similar principles. MS "total useful signal" (MSTUS) was first introduced by Warrack *et al.* [76] for normalisation of urinary metabolomic data, where it performed comparably to urine osmolality. This was in line with the group's recommendation that multiple normalisation techniques be employed as opposed to a single metabolite/biological readout.

##### 1.2.2.1.1.2 Biomass Normalisation

Metabolite intensity is proportional to cell number [88], and the efficacy of metabolomic normalisation strategies can be calculated by their correlation to cell number. While cell number alone is a commonly used method for metabolomic data normalisation [58], it is still subjective. Therefore, robust quantitative readouts of cell volume are required to accurately improve technical variability for normalisation purposes. Dry weight is commonly used in tissue and plant metabolomics as samples can be reliably measured prior to metabolite extraction. Measuring cell

weight is more difficult due to issues with sensitivity, yet has been employed in some cellular metabolomics investigations [89, 90]. Estimating cellular membrane content by measuring phospholipids has been used to normalise metabolite readouts from HepG2 cells [82]. A number of intrinsic sample-based normalisation readouts have been shown to correlate well with cell number.

Normalisation to deoxyribonucleic acid (DNA) concentration of residual cell pellets was first suggested by Silva *et al.* [88], and has been employed in various metabolomic analyses [91, 92]. DNA concentration typically remains constant across cell types and correlates well with protein and metabolite concentrations [71, 88]. DNA content can be stably measured post-metabolite extraction and allows absolute quantification of transcripts, proteins and metabolites in cells [74]. More recently thymine concentration alone has been proposed as a more accurate normalisation strategy for metabolomics investigations [93]. While RNA may be detectable in the cell pellet, it is unlikely to remain stable enough during extraction and storge for use as a normalisation factor.

Despite protein precipitation being a fundamental step of the sample preparation process, sample normalisation by protein content is commonly used to normalise metabolomic data. This is usually done by measuring protein content in the cell pellet following isolation of the metabolite fraction, and most commonly by bicinchoninic acid (BCA) assay. Protein (and DNA) content correlate well with cell number [94] and have been used for normalisation in many cellular metabolomic investigations [89, 95-97]. This technique is also employed by Metabolon for normalisation of cellular metabolomic data [96-98]. Despite its common use for metabolomic normalisation it is not specified whether the protein content is measured in the metabolite fraction or the cell pellet. The majority of the protein present in the cell should precipitate to the bottom during high-speed centrifugation, and the metabolite fraction should only contain low molecular weight compounds for analysis. However residual protein can be measured in the metabolite fraction and used to normalise metabolomic data.

#### 1.2.2.2 Data-Based Normalisation Approaches

Given the massive inter-personal variation in metabolism, large cohorts are often necessary to sufficiently power untargeted metabolomics investigations. This

presents a challenge for measuring large numbers of samples in a single MS experimental worklist. It is not uncommon for experiments to be split across several instrument runs, particularly where samples are measured with multiple methods. For instance, the Human Serum Metabolome (HUSERMET) Consortium have been measuring healthy human serum by GC-MS, UPLC-MS, and NMR spectroscopy for several years [64]. Correcting for inter-batch variation is crucial to account for differences in instrument variation (e.g., signal drift, MS source contamination, column performance, mobile phase preparation etc.). This inter-batch error can compromise the technical precision of LC-MS measurements and obscure biologically relevant signals. To overcome this many LC-MS-based metabolomics data processing workflows monitor (and correct for) signal intensity drift using pooled quality control (PQC) samples [63]. This involves combining an equal volume of all samples in a given experiment. These PQC samples can be used for method development and validation to assess metabolome coverage, correct for batch variability, and prime the LC-MS for the relevant sample matrix. Data-based batch correction algorithms have also been developed [99-101] and can easily be integrated into data analysis workflows [102].

There have been countless data normalisation programs developed for untargeted metabolomic data [103-109], many of which overlap in their methodology. One such platform is NOREVA [102], which combines 24 different normalisation methods to compare efficacy across five different criteria. This platform was recently upgraded [110] to allow time-course and multi-class analyses in a total of 168 normalisation strategies. Statistical normalisation strategies typically fall into two categories: those which remove unwanted sample-to-sample variations and those which adjust biases among various metabolites to reduce heteroscedasticity. PQC samples can also be integrated into normalisation strategies, or periodically analysed throughout an LC-MS analytical run to provide robust per-metabolite quality assurance [64, 104].

## 1.3 Monocytes

Monocytes are myeloid cells accounting for approximately 10% of circulating leukocytes whose primary role is immune defence. These cells are derived from myeloid bone marrow precursors and can transmigrate into tissues to differentiate into macrophages or dendritic cells. In humans, monocytes are identified by surface expression of CD14 and can be further characterised into three subsets; classical

(CD14++CD16-), intermediate (CD14++CD16+) and non-classical (CD14+CD16++), based on increasing expression of the FcγIII receptor CD16 [111] among other markers. These subsets are also functionally and transcriptionally distinct [112-114]. Despite these discrete transcriptional and proteomic [115] profiles, whether they represent different cell types or simply transitional developmental stages is not yet understood [116].

Long considered a circulating precursor of macrophages and dendritic cells, monocytes are becoming more recognised for their heterogeneous responses to inflammation and roles in tissue repair and trained immunity [117]. Prior to differentiation monocytes are typically pro-inflammatory cells. Monocytes can rapidly propagate inflammation directly by phagocytosis and antigen presentation, as well as through release of cytokines, reactive oxygen species (ROS) and other inflammatory signalling molecules [118]. Importantly, IL-1β can be produced by both the traditional NLRP3 inflammasome [119, 120] and an alternative, potassium-independent pathway in these cells [121]. During inflammation (sterile or infectious), circulating monocytes extravasate to inflamed tissues via the leukocyte recruitment cascade of rolling, adhesion, and transmigration. Key chemokines for monocytes recruitment include monocyte chemoattractant protein (MCP) 1-4, and other members of the CCL and CXC families [122]. Monocytes can rapidly become the dominant infiltrating mononuclear phagocyte in damaged tissues and draining lymph nodes. In inflamed tissues (and in the circulation) monocytes have distinct roles in propagating inflammation [123].

### 1.3.1 Monocyte Metabolism

In order to perform these diverse functions, monocytes need effective energy processing systems. *In vitro* stimulation of myeloid cells with LPS has pinpointed an increase in glycolysis and a decrease in OXPHOS as a defining event of pro-inflammatory innate immune activation (Figure 1.3.1). However, unlike the observed Warburg effect in macrophages, decreased OXPHOS is not a universal myeloid response to pathogenic stimuli in monocytes. These cells exhibit differing metabolic and inflammatory responses to different microbial stimuli. Lachmandas *et al.* investigated the differential metabolomic effects of various microbial stimulants in human monocytes and found diverse metabolic and inflammatory phenotypes [97]. LPS did increase glycolysis rates at the expense of OXPHOS, however Pam3CysK4

and other bacterial lysates increased oxygen consumption. *Candida albicans (C. albicans*) stimulation for instance led to sustained increases in both glycolysis and OXPHOS for up to 24 hours [124].

Disparities in metabolic activation may result from differential toll-like receptor (TLR) signalling [125]. TLRs are pattern recognition receptors (PRRs) which recognise molecular signatures of microbial pathogens and are crucial in innate immune responses. Monocytes express all known TLRs, with TLRs 1, 2 and 4 present at high levels [125, 126]. TLR4 recognizes LPS and initiates a signalling cascade via MyD88 or TRIF leading to NF-κB/MAPK/IRF5 or IRF3 activation, respectively [127]. This ultimately alters inflammatory gene regulation. TLR4 activation can influence NAD+ levels in macrophages [128], and in monocytes NAD+ depletion inhibited TLR4 signalling, ultimately abrogating IL-1β production [129]. The decrease in OXPHOS typically seen with LPS stimulation can be reversed by blocking microRNA-125b (miR-125b), which reduces mitochondrial respiration and promotes elongation of mitochondria [130]. Glycolysis and PPP activity are upregulated in macrophages in response to LPS, leading to succinate accumulation and HIF-1α stabilisation to sustain IL-1β production [8, 128]. This metabolite can act as a node for various metabolic pathways [131, 132], or induce a net anti-inflammatory effect via SIRT1 [128]. Here succinate appears to act as signalling molecule within the broader network of TLR signalling. Whether they play a similar role in monocyte activation remains to be seen.

Primary monocytes show remarkable metabolic plasticity in instances of nutrient deprivation. This flexibility is particularly beneficial during periods of oxygen or glucose deprivation. Under hypoxic conditions monocytes can shift away from mitochondrial-associated metabolism and increase glycolytic flux. Rodgers *et al.* [86] simulated the rheumatoid arthritis (RA) synovial environment, which has an extremely limited oxygen supply. Indeed, these conditions increase glycolytic and purine metabolism intermediates and decrease TCA cycle metabolites. Synovial monocytes compensate for these hostile conditions by shuttling carnitine to the mitochondria and maintain fatty acid oxidation (FAO). Conversely, in low glucose conditions (or where competition for glucose is high) monocytes increase FAO via oxidative phosphorylation to meet their energy demands [85]. Recent work

demonstrated how dietary fructose can disrupt this metabolic flexibility. Fructose reprogramed primary monocytes to favour glutaminolysis and oxidative metabolism above glycolysis, and increased pro-inflammatory cytokine levels in *in vitro* and in *in vivo* models [133]. Excess lactate production (likely from glycolysis) can also induce an anti-inflammatory phenotype in primary monocytes [134]. Both nutrient availability and stimulus are crucial to determine the metabolic and inflammatory response in these cells.

As in macrophages, gylcolysis is an important metabolic pathway for monocytes. Upon activation these cells increase glucose uptake and glycolytic metabolism [135]. This increase in glycolysis was regulated by mTOR-induced glucose transporter (GLUT)-1 expression. GLUT1 is typically stored intracellarly [135], but can be expressed on the cell surface in times of nutrient stress. Glycolysis in monocytes is essential for effective vascular adhesion [136], differentiation [15], and cytokine production [97, 124]. Given that gylcolysis is a less efficient energy generating pathway than OXPHOS, it seems unlikely that this pathway is being used purely for cellular metabolism. The glycolytic switch in monocytes could create substrates for DNA and cell membrane synthesis to facilitate cell growth and differentiation [137]. Recently certain metabolites have been shown to play a role in epigenetic modifications that drive inflammation in monocytes [20-22]. Further work is needed to profile the precise role of metabolites (and their associated pathways) with monocyte function.

### 1.3.2 Monocytes in Disease

Persistent activation of monocytes at disease sites has been implicated in the pathogenesis of a number of conditions. Defects in monocyte metabolism have been demonstrated in a range of acute and chronic diseases, and most recently in COVID-19 [138-141]. In many of these conditions, macrophages are the primary drivers of inflammation. Before monocytes infiltrate disease sites and differentiate into macrophage subtypes, they undergo metabolic and inflammatory changes in the circulation that can drive systemic inflammation.

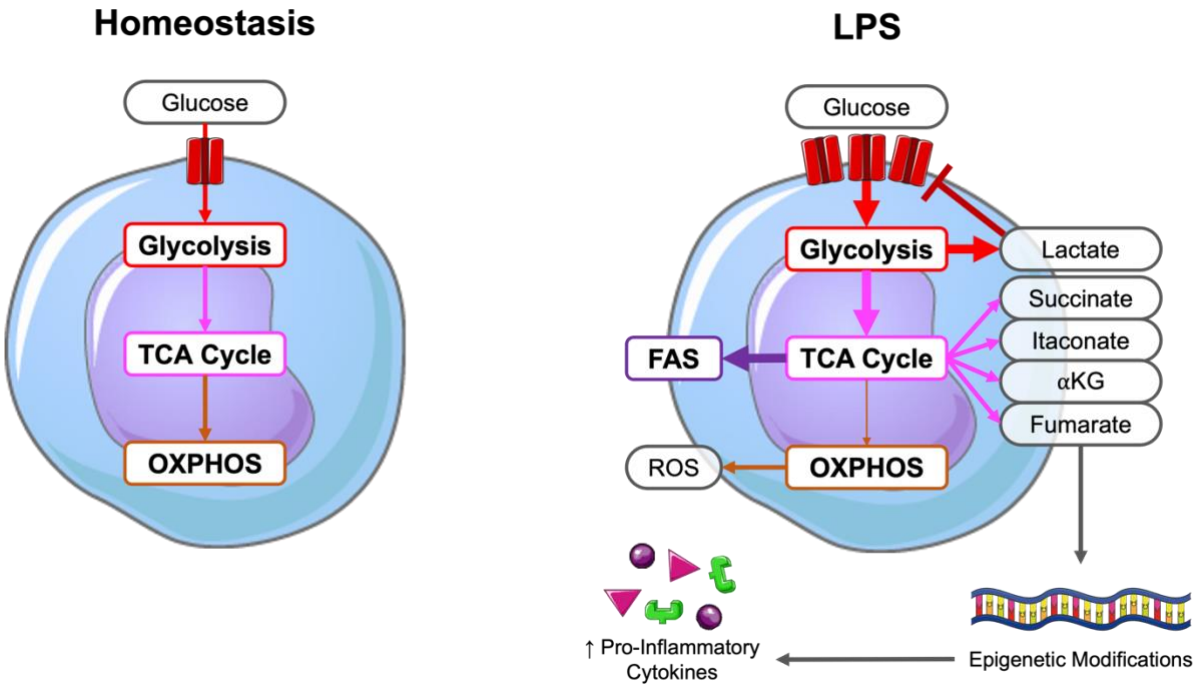


**Figure 1.3.1: Summary of Metabolomic Alterations and Activated Pathways in LPS-Activated Monocytes.** LPS activation in monocytes promotes Warburg metabolism. Increased glucose uptake (via GLUT1) drives increased glycolysis and flux through the TCA cycle. TCA cycle intermediates such as fumarate and α-KG can trigger epigenetic changes to drive pro-inflammatory cytokine production. TCA Cycle activity can also feed FAS, and cholesterol synthesis can have similar effects on cytokine synthesis. Simultaneously, OXPHOS is decreased in response to LPS. α-KG: alpha-Ketoglutarate; FAS: Fatty Acid Synthesis; LPS: Lipopolysaccharide; OXPHOS: Oxidative Phosphorylation; ROS: Reactive Oxygen Species; TCA Cycle: Tricarboxylic Acid/Krebs cycle.

### 1.3.2.1 Rheumatoid Arthritis (RA)

Rheumatoid Arthritis (RA) is the most common inflammatory joint disease in the world. This systemic autoimmune disease is characterised by chronic synovial inflammation causing pain, dysfunction, and ultimately destruction of cartilage and bone in affected joints [142]. Monocytes – in particular the CD14+CD16+ intermediate monocyte subset – have been heavily implicated in the pathogenesis of RA. This subset is expanded in RA patients compared to healthy controls [143] and positively correlates with disease activity [144]. Systemic MCP-1 levels were significantly increased in the years preceding disease onset [145], implicating early monocyte chemotaxis in the initiation of RA. Higher absolute monocyte levels in treatment-naïve patients are predictive of a reduced response to treatment with methotrexate [146]. These cells are a major source of inflammatory cytokines and were potent inducers of T helper (Th)17 cell expansion [145].

Monocytes (and macrophages [147, 148]) have demonstrated aberrant metabolic phenotypes in RA [149]. These cells are present in affected joints where they drive pathogenesis by propagating inflammation in the synovial microenvironment. In a mouse model of RA, synovial fluid-derived succinate promoted IL-1β release from macrophages [150]. Low oxygen levels in the synovium can contribute to this metabolic dysfunction. Hypoxia exacerbated inflammatory cytokine release and increased fatty acid oxidation (FAO) in monocytes exposed to RA synovial fluid [86]. These oxygen-deprived monocytes showed a distinct switch from glycolysis to FAO compared to their circulating counterparts. Peripheral blood monocytes of RA patients display a hypermetabolic phenotype with both enhanced mitochondrial metabolism and increased expression of glycolytic enzymes [151]. These cells rely heavily on glycolysis during subsequent LPS activation. The glycolytic enzyme α-enolase is highly expressed on the cell surface of monocytes/macrophages from RA patients where it can be activated by autoantibodies to induce pro-inflammatory cytokine production [152]. These data collectively demonstrate the metabolic plasticity of monocytes in RA.

#### 1.3.2.2 Atherosclerosis & CVD/CAD

Inflammation plays a key role in the pathogenesis of atherosclerosis, and monocytes contribute considerably to this. Foam cells derived from circulating monocytes accumulate lipids in atherosclerotic plaques and propagate a hyperinflammatory microenvironment [153]. Monocytes and monocyte-derived cells also share metabolic abnormalities that contribute to this pathogenic phenotype. These cells typically have increased glucose consumption, ATP production, and cytokine production compared to their healthy equivalents. It has recently been suggested that innate trained immunity – transcriptional and epigenetic changes – are important in the pathogenesis of atherosclerosis [154]. Cholesterol synthesis is a fundamental requirement for the induction of trained immunity [20, 21], and the lipid-rich plaque environment disrupts monocyte fatty acid metabolism leading to increased pro-inflammatory cytokine production [155]. Atherosclerosis is typically treated with statins – lipid lowering drugs which inhibit cholesterol synthesis. Secondary to their systemic cholesterol-lowering effects, statins can offset inflammatory responses to LPS in monocytes [156-159] and may be useful cell-specific metabolic therapy in other autoimmune conditions.

### 1.3.2.3 Human Immunodeficiency Virus (HIV)

Monocytes play key pathogenic roles throughout the course of Human Immunodeficiency Virus (HIV) infection and its associated co-morbidities [137, 160]. HIV+ individuals showed higher monocyte GLUT1 expression, in particular the non-classical and intermediate subsets [135]. These subsets are associated with inflammation and peripheral immune activation during HIV infection [161, 162]. As these subsets expand during disease progression, so too does the demand for glucose. HIV+ individuals also present with impaired glucose tolerance, insulin resistance, altered glucose metabolism, and dyslipidaemia [163]. Systemic metabolomic profiling has revealed HIV signatures for various subgroups and biomarkers of HIV infection [164-167]. Despite these data there are currently no confirmed mechanistic links between the increase in monocyte glucose metabolism and inflammation in HIV-infected individuals. Some recent works have highlighted a lipidomic signature of HIV infection which correlates with some monocyte readouts [168-170]. These results may be strengthened/complimented by well-considered cellular metabolomics investigations.

## 1.4 Anti-Neutrophil Cytoplasmic Antibody (ANCA)-Associated Vasculitis (AAV)

Autoimmune disease affects up to 10% of the world's population with a considerable burden of morbidity and mortality [171, 172]. Anti-Neutrophil Cytoplasmic Antibody (ANCA)-Associated Vasculitis (AAV) is a rare autoimmune disease affecting the microvasculature. The disease is characterised by the presence of autoantibodies directed against two proteins: myeloperoxidase (MPO) and proteinase-3 (PR3). These proteins are found in the cytoplasmic granules of innate immune cells and translocate to the plasma membrane following immune challenge [173]. There are three AAV subtypes – granulomatosis with polyangiitis (GPA), microscopic polyangiitis (MPA), and eosinophilic GPA (EGPA) – which are defined by their clinical presentation. GPA is traditionally associated with PR3-ANCA, whereas MPA and EGPA patients are more commonly anti-MPO+ [174, 175]. AAV can involve any small blood vessels in the body but most commonly affects the respiratory tract and kidneys. Incidence rates range from 0.4 to 24.0 cases per million person-years across the disease phenotypes, with additional differences in age, sex, and location [174, 176, 177]. There is no known cure for AAV, and there are substantial quality-of-life burdens associated with the condition. AAV patients have a 2.7-fold increase

in mortality compared to the general population [178]. Current treatment strategies involve immunosuppression to induce remission, before a switch to maintenance therapy to prevent disease relapse [179].

### 1.4.1 Pathophysiology of AAV

Much of our understanding of the pathophysiology of AAV comes from experiments carried out in neutrophils. ANCAs were first identified in neutrophils in 1982 as anti-cytoplasmic antibodies with unknown specificity [180]. Once considered to be biomarkers of disease activity, ANCAs are now recognised as pathogenic drivers of AAV [181, 182]. Different cytokine profiles have also been defined for anti-MPO and anti-PR3 positive disease [183]. However, these antibodies have similar pro-inflammatory effects on neutrophils *in vitro*. This supports the idea that other cell types are involved in the pathogenesis and disease activity of AAV.

AAV pathogenesis involves dysregulation of both the innate and adaptive immune systems. A combination of genetic factors, environmental exposures/infections, ageing, and dysfunction of the innate and adaptive immune system can lead to ANCA development [174, 182, 184]. Malfunctioning of the regulatory lymphocyte compartment leads to loss of tolerance and the development of autoreactive B and T cells which produce and recognise ANCA, respectively [185]. Once in the circulation ANCA can activate (primed) neutrophils and monocytes expressing ANCA on their cell surface (see Section 1.4.2.4). These innate immune cells mediate acute injury and are important in the early stages of disease. Persistent T cell activation (in particular Th17 cells) is a hallmark of AAV. T cells and mature macrophages orchestrate the tissue response to ANCA-induced tissue damage and induce a remission state in the later stages. Given how the function of immune cell subtypes is intricately linked to their metabolism, there may well be a fundamental role for immunometabolism in AAV pathogenesis (reviewed in [186]). The precise mechanisms of these metabolic interactions remain to be revealed.

### 1.4.2 Monocytes in AAV

The role of monocytes in AAV has been thoroughly revied by Brunini *et al.*[187] and more recently by Vegting *et al.* [1]. Figure 1.4.1 is adapted from the latter and summarises the role of these cells in the pathophysiology of AAV. Here we expand upon a number of these key areas.

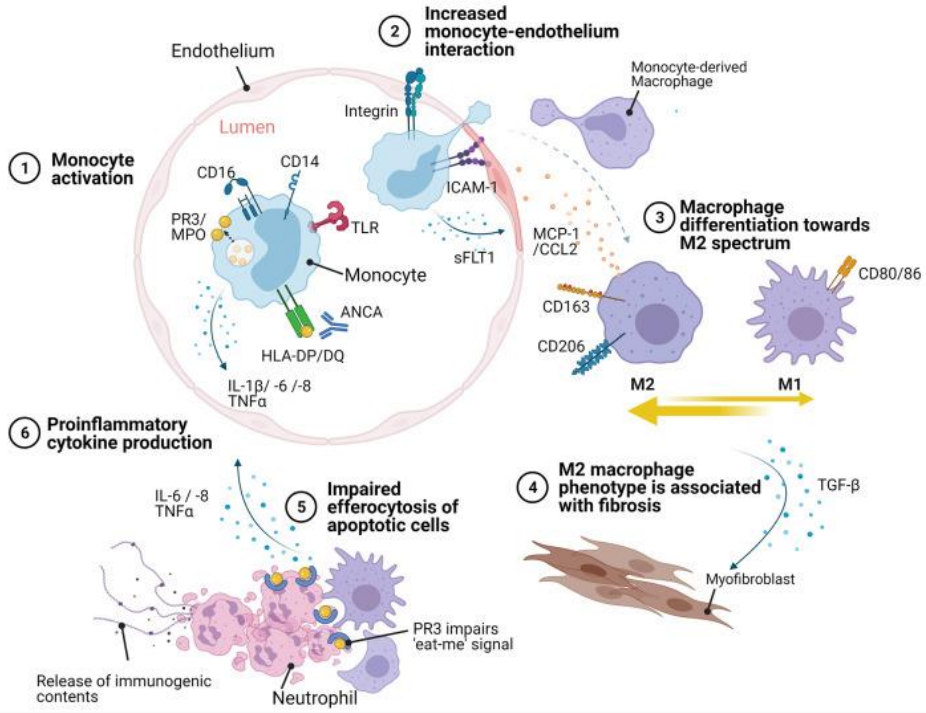


**Figure 1.4.1: Overview on the Role of Monocytes (and Macrophages) in the Pathophysiology of AAV.** Taken from Vegting *et al.* [1]**.**

### 1.4.2.1 Transmigration & Organ Infiltration

Circulating and patrolling monocytes are recruited to sites of inflammation by chemokine gradients [122, 188]. MCP-1 is a key chemokine for monocyte chemoattraction. Increased MCP-1 is found in AAV patient kidney biopsies and urine, with urine levels correlating with disease activity [189, 190]. Another promoter of monocyte recruitment and macrophage proliferation is macrophage colony stimulating factor (M-CSF), which is increased systemically in AAV [191]. This suggests that monocytes are rapidly recruited to disease sites. Indeed monocytes/macrophages are the predominant infiltrating immune cell found in the early glomerular lesions [192, 193]. Soluble CD163 (sCD163) is shed by activated monocytes and macrophages and is used as a biomarker of renal flare in AAV [194, 195]. This increase in sCD163 is likely a result of excessive macrophage activation in affected glomeruli. Depletion of inflammatory CCR2+ monocytes significantly reduced serum sCD163, glomerular necrosis and crescent formation and in an anti-MPO mouse model of AAV [196]. Infiltration of monocyte-lineage cells into affected kidneys was greatly reduced with no effect on neutrophils. Monocyte exposure to MPO-ANCA increased survival and enhanced macrophage differentiation [197]. These macrophages had enhanced transforming growth factor (TGF)-β secretion and promoted expansion of CD4+ T cells. Monocytes (and neutrophils) form the

core of granulomas where they orchestrate systemic T cell responses [187]. T cells are key for induction of tissue damage in ANCA glomerulonephritis [198-200]. As is seen in RA [201], T cells and monocytes/macrophages may synergise to drive damage at disease sites. While the exact monocyte interactions in AAV granulomas are still incompletely understood, the presence of these cells in early lesions coupled with macrophage domination in later stages of ANCA-induced glomerulonephritis points to an important role for monocytes in AAV granulomatosis.

#### 1.4.2.2 Monocyte Subsets in AAV

Disruption of monocyte subsets can contribute to persistent inflammation in autoimmune conditions [202]. The intermediate CD14++CD16+ monocyte subset has been shown to be enriched in AAV patients compared to healthy controls [203, 204]. These cells also produced the highest levels of pro-inflammatory cytokines in response to anti-MPO (but not anti-PR3). Intermediate monocytes have subsequently been recognized as a predictor of disease relapse [205]. The function of these cells overlaps with the classical and non-classical subsets, but they are typically involved in phagocytosis, antigen presentation, cytokine secretion, apoptosis regulation, and differentiation [202, 206]. Intermediate monocytes are increased in RA, where they induce Th17 expansion and produce high levels of pro-inflammatory cytokines [145]. Persistent activation and expansion of Th17 cells is also well documented in AAV [184, 185, 207] and contributes to disease pathogenesis. Classical monocyte numbers are increased in giant cell arteritis (GCA) - a large vessel vasculitis – and returned to normal levels following treatment [208]. High levels of inflammatory macrophage infiltration at disease sites are a consequence of this monocyte enrichment. Whether the intermediate monocyte subset is the main pathogenic driver of inflammation in AAV monocytes is not yet clear.

#### 1.4.2.3 Cell “Priming”

When assessing neutrophil responses to ANCA *in vitro* it is important to replicate the biological microenvironment. To achieve this most studies of cellular function in AAV incorporate a cell priming step. Given that ANCA titres do not necessarily correlate with disease activity [209], the priming events which facilitate ANCA

binding and cellular activation may be a key factor in mediating a pathological response to these antibodies. *In vivo* priming can occur during disease or infection [210, 211], either directly by pathogen-associated molecular pattern (PAMP) stimulation or indirectly via the resulting milieu of pro-inflammatory cytokines. A number of stimuli have been used to prime immune cells for susceptibility to the effects of circulating ANCA, including tumour necrosis factor (TNF)-α, LPS, complement anaphylatoxin C5a, high mobility group box (HMGB)-1 and cytokines such as IL-1β, IL-6, and IL-18 [173, 182, 184].

The most commonly used priming agent in studies of neutrophil function is TNF-α. This facilitates p38 and extracellular signal regulated kinase (ERK) and mitogen-activated protein kinase (MAPK) pathway activation prior to ANCA stimulation [212-218]. These pathways appear to be important for translocation of MPO and PR3 from cytoplasmic granules to the plasma membrane. These studies have generally used priming TNF-α concentrations of 2ng/ml. However, there are disparities between clinically relevant levels of priming factors and those described in the literature. This 2ng/ml benchmark is significantly higher than concentrations commonly found in the circulation even of septic patients (30–1,300 pg/ml)[219]. Locally increased TNF-α production from immune infiltrates and activated epithelial cells may be higher and explain this disparity [220, 221]. *In-vitro* concentrations of LPS can have differing effects on IL-1β production and cellular metabolism [97], and priming concentrations of TNF-α can vary in *in-vitro* studies of neutrophil function. Given the pleiotropic nature of these priming agents, specific investigations into their effects at clinically relevant concentrations in ANCA-activated immune cells are warranted. Separating the immunologic and metabolic outputs will also be important to reveal the ANCA-specific effects of these stimuli.

#### 1.4.2.4 Surface Marker Expression

Monocytes are identified by expression of CD14, a Toll-like receptor 4 (TLR4) co-receptor that recognised bacterial LPS. Upon LPS binding a signalling cascade is triggered ultimately ending in pro-inflammatory cytokine production [222]. Patients with AAV express higher levels of CD14 on their monocytes [223]. ANCA binding further increases expression of CD14 and other toll-like receptors (TLRs) on monocytes [224-226], which suggests that these cells may be more readily activated by TLR-mediated stimuli. CD14 expression can correlate with both PR3 and MPO

expression on classical monocytes in AAV patients [223]. This suggests a link between monocyte phenotype and ANCA pathology.

Because monocytes express ANCA antigens on their cell surface they can mediate many of the systemic inflammatory effects seen in AAV. TNF-α is required to prime neutrophils to express MPO and PR3 on their cell surface [227]. Monocytes can be activated in the same fashion, however ANCA antigens were also constitutively expressed on the surface of primary monocytes, even in healthy controls [192]. Previous work from our research group demonstrated that surface ANCA expression was highest in the intermediate monocyte subset, consistent with the increase in proportion of this subset [203]. This finding was not replicated by Tarzi *et al.* [223], who did not find any significant differences across monocyte subsets. This cohort was smaller and had more MPO-ANCA patients, with additional differences in clinical readouts. They did confirm that MPO expression was highest in the intermediate subset, but PR3 was expressed at a greater level in classical monocytes in this healthy control cohort [223]. Increased PR3 and MPO gene transcription in AAV patient monocytes may contribute to this increased surface expression [228, 229], but precise mechanisms have yet to be determined.

Other monocyte surface markers may also contribute to their dysfunction in AAV. Recent work from Zeisbrich *et al.* [230] found reduced expression of the immunoinhibitory checkpoint programmed cell death ligand-1 (PD-L1) on AAV patient monocytes, consistent with ANCA titres. These PD-L1$^{lo}$ monocytes induced greater CD4 T cell proliferation and activation. Adhesion molecules facilitate extravasation of immune cells during disease flare. Monocyte subsets express different levels of adhesion molecules, which facilitates their interaction with activated endothelial cells. AAV patient monocytes have generally shown higher integrin expression (CX3CR1, CD29, CD18, CD11a, CD11b) than those of healthy controls [225, 231-234]. GPA patient monocytes have demonstrated increased expression of CD63 (a marker of degranulation) and CD64 (the high-affinity Fc receptor for IgG)[235]. CD18 (Integrin beta chain-2) expression was increased on monocytes [225] following ANCA stimulation, but CD62L (L-selectin) was decreased [231]. This downregulation of CD62L was however disputed in findings from Johansson *et al.* [236] and some other studies have not noted any significant

changes [232, 237]. These inconsistencies may be a result of differential experimental techniques, or these adhesion molecules may be involved in more complex inflammatory signalling in AAV monocytes. We have demonstrated increased glucose uptake in ANCA-stimulated monocytes [238]. This presumably occurs through the major glucose transporter GLUT-1. While there is evidence linking increased glucose uptake with GLUT-1 expression in HIV [135], the role of this (and other nutrient receptors) and transporters in AAV monocytes should be a focus of future investigations.

#### 1.4.2.5 Cytokine & Chemokine Production

As detailed above, monocytes express ANCA antigens on their cell surface and can thus be readily activated by ANCA. Monocytes activated by ANCA (or primed by other circulating cytokines [183, 239]) adopt a pro-inflammatory phenotype. ANCA-stimulated monocytes showed increased production of IL-1β, IL-6, IL-8, and TNF-α [197, 203, 226, 238, 240]. These cytokines drive vascular inflammation and tissue damage. The IL-1β response to anti-MPO is particularly notable. IL-1β inhibition protected mice from an anti-MPO induced necrotizing crescentic glomerulonephritis [218]. In this model IL-1β production was shown to be dependent on the activity of neutrophil serine proteases – cathepsin G, neutrophil elastase, and proteinase 3. In humans serum IL-1β showed no correlation with ANCA antibody titre, thus it's pro-inflammatory effect may be contained to disease sites [241].

MCP-1 levels increase following ANCA stimulation, and urinary MCP-1 levels also rise during active renal vasculitis [190, 242, 243]. Previous work from our group showed increased secretion of CXCL5 from primary monocytes following anti-MPO stimulation [244]. This is a neutrophil chemoattractant which may contribute (along with other chemokines) to a positive feedback loop for infiltrating innate immune cells. Interestingly, anti-MPO stimulation of primary monocytes reduced secretion of CXCL10/IP-10. This is a surprising anti-inflammatory response but has been previously reported in primary monocytes [197]. Further, AAV was recently revealed not to be an interferonopathy [245], adding further intrigue to the role of this chemokine in monocyte responses. ROS are also released following ANCA stimulation [192, 227], however AAV monocytes have reduced ROS-producing capacity compared to healthy controls [236]. Overall, the cytokine storm triggered in monocytes following ANCA stimulation drives disease pathogenesis.

### 1.4.3 Monocyte Metabolism in AAV

Investigations of cellular metabolism in vasculitis have been scarce and mostly limited to discoveries in T cells. CD28 signalling controls glycolytic activity of T cells in a mouse model of vasculitis [246]. Inhibiting this receptor's activity abrogated vasculitis symptoms and reduced T cell infiltration. CD28 antagonism disrupted T cell's ability to utilise glucose – expression of glycolytic enzymes and surface GLUT1 were abrogated. Monocytes have been implicated in the pathophysiology of other vasculidities [208, 247], however there is currently little evidence of immunometabolic effects.

Recent work from our laboratory demonstrated increases in both oxidative phosphorylation (OXPHOS) and glycolysis in ANCA-stimulated monocytes (see Figure 1.4.2)[238]. Both extracellular acidification rate (ECAR) and oxygen consumption rate (OCR) – surrogate measures of glycolysis and OXPHOS, respectively – are increased immediately after ANCA stimulation. Similar simultaneous enhancement of both glycolytic and oxidative mitochondrial metabolism in primary monocytes have been triggered by stimulation with *C. albicans*, *Escherichia coli* (*E. coli*), *Mycobacterium tuberculosis* (*M. tb*), Bacillus Calmette–Guérin (BCG), and *Staphylococcus aureus* (*S. aureus*) stimulation [97, 124, 248]. The effects of ANCAs on monocyte metabolism appear to implicate more diverse, synergistic metabolic pathways in manner usually reserved for more complex, whole microorganism models. One exception to this observation is the metabolic reprogramming induced by innate immune training. Beta-glucan training alone activates Warburg metabolism in monocytes, but BCG vaccination resulted in upregulation of both glycolysis and OXPHOS [20, 248] similar to ANCA-stimulation. This adds further intrigue to the metabolic influence of these autoantibodies.

The differential metabolic effects by microbial stimulation of monocytes can also be seen with ANCA. There are disparate metabolic responses to MPO- and PR3-ANCA, summarised in Table 1.4.1 and detailed in our lab's recent publication [238]. ANCA-activated monocytes show an immediate increase in both glycolysis and OXPHOS. This increased OXPHOS is sustained by anti-MPO, whereas anti-PR3 stimulated cells return to baseline shortly after peaking. Anti-MPO increased basal respiration in primary monocytes, as well as maximum and spare respiratory

capacity. Despite this OXPHOS was not essential for IL-1β production. Inhibiting glycolysis on the other hand did abrogate IL-1β levels. Glucose intake and basal glycolysis was increased in both anti-MPO and anti-PR3 stimulated monocytes. These metabolic differences were more pronounced in anti-MPO activated cells. Indeed, monocytes exhibit a stronger inflammatory response to MPO-ANCA than to PR3 [197, 203]. Conversely, Wikman *et al.* found both ANCAs to upregulate monocyte metabolism [231]. This was the case for both monoclonal and polyclonal patient-derived antibodies, but not patient sera. MPA and GPA are genetically distinct syndromes, typically associated with anti-MPO and anti-PR3 antibodies respectively [174, 249, 250]. Different cytokine profiles have also been defined for anti-MPO and anti-PR3 positive disease [183], which may account for the differences in metabolism between the two autoantibodies and the clinical phenotypes. These data point towards a mechanism where monocytes are key to MPO+ disease but not PR3+ AAV. The disparities between the metabolic response to anti-MPO and anti-PR3 will be a major focus of this work.

In order to exert the pathogenic inflammation characteristic in AAV, immune cells migrate to disease sites from the circulation. Macrophages are the most abundant cell infiltrates in pulmonary- [251] and renal-dominant AAV [193] and the majority of these macrophages are derived from circulating monocytes [252]. As shown by PET imaging [253], disease sites in AAV are well perfused to provide ample glucose supply. This supports immune cell activation at areas of ANCA-activated inflammation. Kidney epithelial cells also increase their glucose uptake and usage to fuel the PPP in inflammatory kidney disease, particularly AAV [254]. Further subset analyses predicted that this increase in PPP was also linked to monocyte/macrophage infiltrates. Determining the metabolic perturbations induced by ANCAs and how they impact monocyte function is important to understand the role of these cells in AAV pathogenesis and the core focus of this thesis.

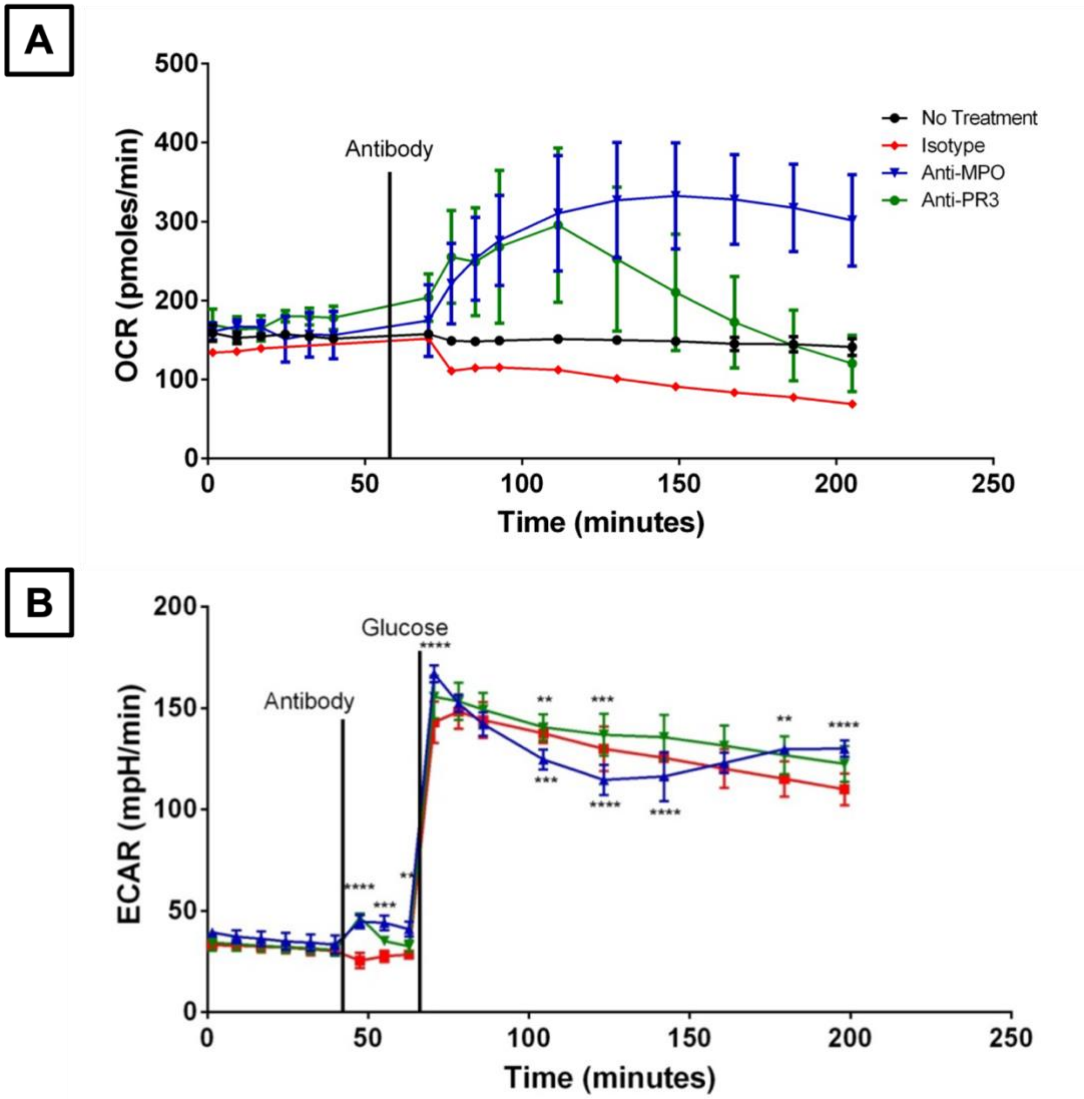


**Figure 1.4.2: Changes in Oxygen Consumption Rate (OCR, A) and Extracellular Acidification Rate (ECAR, B) in ANCA-Stimulated Monocytes.** Adapted from O'Brien *et al.* [238]

| Metabolic Process | anti-MPO | anti-PR3 |
|---|---|---|
| Increased glucose intake | ↑ | ↑ |
| IL-1β production glycolysis-dependent | ↑ | N/A |
| IL-1β production OXPHOS-dependent | No | N/A |
| Increased OXPHOS | ↑ | No |
| Increased mitochondrial mass | No | No |
| Increased glycolysis | ↑↑ | ↑ |
| Immediate increase in OXPHOS | ↑ | ↑ |
| Sustained increase in OXPHOS | ↑ | No |
| Rotenone inhibits increased OXPHOS | ↑ | ↑ |
| Immediate increase in glycolysis | ↑ | ↑ |
| Increased mitochondrial ROS | ↑ | No |
| IL-1β production mitoROS-dependent | ↑ | N/A |

**Table 1.4.1: Summary of Disparate Metabolic Effects of anti-MPO and anti-PR3 ANCAs in Primary Monocytes [238].** Note: IL-1β is not produced by anti-PR3 stimulated monocytes.

### 1.4.4 Metabolic Perturbations in AAV

Serum metabolomics has revealed diagnostic biomarkers for other vasculidities [255-257] and there have been some serum metabolomics investigations in AAV. Misra *et al*. used NMR spectroscopy to profile the metabolome of AAV patients and delineate it from those with Takayasu's arteritis (TAK) and systemic lupus erythematosus (SLE) [258]. They found that AAV sera was characterized by increased levels of N-acetyl-glycoproteins, and lipid metabolites including polyunsaturated fatty acids (PUFAs), choline and glycerophosphocholine. A similar investigation from Najem *et al*. [259] profiled AAV patient plasma (and faeces) by LC-MS to differentiate acute and chronic AAV. Patients with chronic AAV in remission had higher plasma phenylalanine, tyrosine and taurolithocholic bile acid compared to newly diagnosed patients. Plasma glycholic and glycodeoxycholic acids were strongly associated with active disease in this cohort. Recent work from Geetha *et al*. profiled serum and urine from a small cohort of AAV patients in active

disease and remission [260]. This preliminary study found increases in serum amino acids, and compounds of carbohydrate and nucleotide synthesis metabolism during active disease. Citrate and isocitrate were both decreased in urine and serum in active disease compared to remission. Almost all other TCA cycle metabolites were increased in serum during active disease, with the exception of oxaloacetate. The lack of a control group and the small sample size make it difficult to draw solid conclusions from this study. Further, none of these works have provided full details of metabolomic methods or analysis as suggested by minimum required reporting guidelines [29]. Ideally peer-reviewed publication of these works should include raw metabolomics data to allow further interrogation and analysis.

Several urinary protein biomarkers have been discovered in AAV [190, 195], and these types of studies can be useful for revealing disease-specific phenomena in renal vasculitis. Previous work from our group [261] examined the urine metabolome of an MPO-ANCA rat model and its relevance to human AAV patients. Longitudinal profiling by NMR identified distinct metabolite profiles during peak disease (day 56) and remission. Acute disease was defined by alterations in trimethylamine N-oxide (TMAO), α-ketoglutarate (αKG), and citrate, and combining these with existing clinical readouts improved discrimination between disease and control animals. TMAO, αKG and succinate were also predicative of glomerular injury at sacrifice. These findings were used to develop a targeted LC-MS assay to profile human AAV patient urine. Here *myo*-inositol, citrate, maltose, and succinate differentiated patients with active renal vasculitis from those in remission, with the *myo*-inositol:citric acid ratio proving the strongest biomarker of active disease. ANCA specificity (PR3 vs. MPO) did not affect predictive capacity. These findings demonstrate the utility for urine metabolomics as an indicator of renal health and disease. Whether these urinary metabolite changes are derived from inflammatory or epithelial cells should be a focus of future work [254].

#### 1.4.4.1 Metabolic Therapies/Metabolites as Potential Treatments for AAV

Metabolic inhibition has been suggested as a method of regulating immune responses in autoimmunity [262-264]. Antimetabolite drugs such as azathioprine and methotrexate are commonly used in the treatment of autoimmune diseases and cancer. These types of treatments should ideally be cell-specific to avoid unwanted

systemic side effects. Targeting the appropriate immune cell subset at the appropriate disease site [265] will be key to the success of any potential metabolic therapeutic. Therefore, a better understanding of the metabolic pathways involved in the pathogenesis and maintenance of inflammation in AAV is crucial in identifying actionable targets for prospective treatments.

One metabolic manipulator in widespread clinical use is metformin – a hypoglycaemic drug used in the treatment of type 2 diabetes. Metformin has also been proposed as a treatment for diseases of ageing, including autoimmune conditions [266]. This drug can alter phagocytosis, chemotaxis and the rolling neutrophil phenotype [267], as well as reducing NFκB, TNF-α and MPO activity at disease sites [268, 269]. Metformin treatment can limit monocyte migration and differentiation, with additional anti-inflammatory effects on macrophages [270]. MTORC1 inhibition by metformin or sirolimus can limit AAV activity both *in vitro* and *in vivo* [271, 272], but these treatments have not yet seen widespread use in the AAV clinic.

Statins are cholesterol lowering drugs which inhibit the enzyme hydroxymethylglutaryl-CoA (HMG-CoA) reductase to prevent cardiovascular disease. In monocytes statins inhibited the induction of trained immunity, reducing TNF-α production by preventing epigenetic reprogramming [21]. This effect was salvaged with the addition of mevalonate, the product of HMG-CoA. However, mevalonate was unable to reverse the inhibitory effects of respiratory burst by statins in ANCA-stimulated neutrophils [216]. Statins could inhibit respiratory burst in ANCA-stimulated neutrophils by disrupting ERK-mediated MPO and PR3 translocation to the plasma membrane [216]. This is the key physiologic process identified in priming investigations. A recent retrospective cohort study from Japan [273] showed that statin use was associated with reduced relapse risk (HR 0.41; 95% CI=0.18–0.92; P=0.031) in AAV patients. A case study of a GPA patient found that statins significantly reduced proteinuria [274]. Studies of statin use in medium/large-vessel vasculitis found inconsistent effects on disease suppression. In TAK repression of Th1 activation and IFN-γ expression was mediated by statins [275], and these drugs have been proposed as a treatment for Kawasaki Disease (KD). A Phase I/IIa trial of atorvastatin [276] found a lower percentage of circulating

CD8+ T cells in KD patients who received the drug and with no serious adverse events. In the case of AAV, statins limited ANCA activity *in vitro* [216] and may abrogate disease induction with routine use *in vivo*. These systemic and disease-site-specific effects make these drugs attractive candidates for adjunctive AAV therapy.

Other potential metabolic targets such as nuclear factor E2-related factor 2 (Nrf2) [277] and sphingosine 1-phosphate (S1P)[278, 279] represent metabolism-led targets which may hold therapeutic value for autoimmune diseases such as AAV. However, none of these treatments have yet been tested in *in vivo* disease models. Leflunomide is an immunomodulator used for treatment of RA which inhibits the mitochondrial enzyme dihydroorotate dehydrogenase [280]. This drug was recently shown to be an effective and safe therapeutic option for MPA and GPA particularly after previous treatment failure [281]. The glucose analogue 2-deoxy-D-glucose (2-DG) can inhibit the first step of glycolysis, thus limiting the potential for cells to utilise products of glycolysis. *In vitro*, 2-DG abrogates IL-1β production in anti-MPO stimulated monocytes with increased glucose uptake [244]. This drug has shown promising efficacy in a mouse model of polycystic kidney disease [282], and has been used in human trials of several cancers [283, 284]. Glucose transport inhibition is also an appealing potential treatment strategy for AAV, as both anti-MPO and anti-PR3 treated monocytes show increased uptake and utilisation [244].

## 1.5 Project Hypothesis & Aims

The hypothesis of this thesis is that monocytes contribute to the pathogenic effects seen in AAV, and that these inflammatory outputs are facilitated by intracellular metabolism in these cells. The aims of this study were:

1. To optimise LC-MS methods for metabolomic profiling of monocytes and parallel inflammatory and metabolic analyses;
2. Characterise the early metabolic and metabolomic responses to anti-MPO and anti-PR3 stimulation in monocytes;
3. Identify metabolic pathways susceptible to modification to limit the pro-inflammatory monocyte response to ANCA.

# Chapter 2: Materials & Methods

## 2.1 Materials Tables

| Name | Product Code | Company |
|---|---|---|
| Acetonitrile | CC34851-2.5L-F | Honeywell |
| Amino acid standards | A9906 | Sigma |
| β-Nicotinamide | 47865 | Sigma |
| BD FACS Lyse | 349202 | BD Biosciences |
| Bovine Serum Albumin | 12877172 | Fisher BioReagents™ |
| CD14 MicroBeads, human | 130-050-201 | Miltenyi Biotech |
| Cell-Tak | 10317081 | Thermo Fisher |
| Comp Beads | 01-1111-42 | Thermo Fisher |
| CytoTox 96® Non-Radioactive Cytotoxicity Assay | G1780 | Promega |
| Dextran | 31392 | Sigma |
| D-Glucose 6-phosphate sodium salt | G7879 | Sigma |
| dNTPs | R0181 | Thermo Fisher |
| DPBS | 14190-094 | Thermo |
| Fluorescent DNA Quantitation Kit | 1B1558-KIT | VWR Life Science |
| Geimsa | 48900 | Sigma |
| Human CXCL10/IP-10 DuoSet ELISA | DY266 | R&D Systems |
| Human IL-1β/IL-1F2 DuoSet ELISA kit | DY201 | R&D Systems |
| Human IL-6 DuoSet ELISA | DY206 | R&D Systems |
| Human TNF-alpha DuoSet ELISA | DY210 | R&D Systems |
| Inosine 5′-monophosphate disodium salt hydrate | 57510 | Sigma |
| L-(+)-Lactic acid | 46937 | Sigma |
| LC-MS Grade Methanol | 10607221 | Acros Organics |
| LC-MS Grade Water | 10434902 | Fisher Chemical |
| L-glutamine | 25030-024 | Gibco |
| Lipopolysaccharide | L5418 | Sigma |
| Lymphoprep | 07851 | StemCell |
| M-MLV Buffer | M531A | Promega |
| M-MLV RT | M170B | Promega |

| | | |
|---|---|---|
| Medronic Acid Deactivator Additive | 5191-4506 | Agilent Technologies |
| Molecular Grade Methanol | 326950010 | Acros Organics |
| Molecular-Grade Ethanol | E7023 | Sigma |
| Monoclonal anti-MPO | H87207M | Meridian BioSciences |
| Monoclonal anti-PR3 | MABT340 | Merck Life Science |
| *myo*-Inositol | Y0000485 | Sigma |
| Paraformaldehyde | sc-281692 | Santa Cruz |
| Pierce™ BCA Protein Assay | 23227 | Thermo Scientific |
| Random Hexamer | SO142 | Thermo Fisher |
| RNaseOUT™ | 10777019 | Invitrogen |
| RNaseZAP™ | R2020 | Sigma |
| Roche High Pure RNA Isolation Kit | 11828665001 | Roche |
| Seahorse XFe24 FluxPak | 102340-100 | Agilent |
| Sodium Bicarbonate | S5761 | Sigma |
| Sodium Hydroxide | S5881 | Sigma |
| Sodium Pyruvate | 11360-039 | Gibco |
| SYBR™ Green | A25742 | Thermo Fisher |
| TCA Cycle Metabolite Library | ML0010 | Sigma |
| TMB | T0440 | Sigma |
| Trimethylamine N-oxide | 317594 | Sigma |
| Tween-20 | 11417160 | MP Biomedicals |
| XF calibrant solution | 100840-000 | Agilent |

**Table 2.1.1: Reagents Used in this Work**

| Buffer | Components |
|---|---|
| 1% BSA | 1mg/ml BSA in PBS |
| 2% Dextran | 2mg/ml dextran in |
| Blocking Buffer | PBS + 20% FCS |
| cRPMI | RPMI + 10%FCS + 100U/ml streptomycin + 1mg/ml penicillin |

| | |
|---|---|
| ELISA Wash Buffer | PBS + 0.05% Tween-20 |
| FACS Buffer | PBS + 0.1% sodium azide + 3% FCS |
| MACS Buffer | PBS + 2mM EDTA + 0.5% BSA |
| Phosophoproteomics Lysis Buffer | 0.2ml $NA_2CO_3$, 1.8ml $H_2O$, 0.4ml sodium pervanedate, 80µl protease inhibitor, 0.2ml phosphatase inhibitor) |
| RNAse-ZAP Alternative Buffer | 0.1% NaOH solution with 1% triton X-100 and 0.5% SDS |
| XF+++ Media | XF media + 5.5mM D-Glucose + 4mM L-glutamine + 1mM sodium pyruvate |

**Table 2.1.2: Buffers Used in this Work**

| Name | Product Code | Clone | Company |
|---|---|---|---|
| Anti-MPO mAb | H87207M | B3147M | Meridian |
| Anti-PR3 mAb | MABT340 | MCPR3-2 | Merck |
| Isotype mAb | CBL610 | 1E2.2 | Merck |

**Table 2.1.3: Antibodies Used in this Work**

| Target Antigen | Fluorochrome | Clone | Species Targeted | Product Code | Company |
|---|---|---|---|---|---|
| CD14 | PE-Vio770 | TÜK4 | Human | 130-096-628 | Miltenyi Biotec |
| MPO | PE | 2C7 | Human | MCA1757PE | Bio-Rad Laboratories Inc |
| PR3 | FITC | PR3G-2 | Human | ab65255 | Abcam |
| Fixable Viability Dye | eFluor450 | N/A | Human | 65-0863-14 | eBioscience™ |
| CD16 | AlexaFluor 488 | 3G8 | Human | 302019 | BioLegend, Inc. |
| CD54 | APC | REA266 | Human | 130-103-910 | Miltenyi Biotec |

**Table 2.1.4: Flow Cytometry Antibodies Used in this Work**

| Gene | Sense Primer 5'-3' | Antisense Primer 5'-3' |
|---|---|---|
| CXCL5 | TGGACGGTGGAAACAAGG | CTTCCCTGGGTTCAGAGAC |
| CXCL10 | GAAGCTAGCATGAATCAAACTGC CATTCTGATT | GACGAATTCTTAAGGAGATCTTTT AGACCTTTCC |
| OSM | CTCGAAAGAGTACCGCGTG | TCAGTTTAGGAACATCCAGGC |
| IL10RA | GCCGAAAGAAGCTACCCAGTGT | GGTCCAAGTTCTTCAGCTCTGG |
| IL-1β | GAGCAACAAGTGGTGTTCTCC | AACACGCAGGACAGGTACAG |

| | | |
|---|---|---|
| NLRP3 | AAGGGCCATGGACTATTTCC | GACTCCACCCGATGACAGTT |
| ASC | CGCGAGGGTCACAAACGT | TGCTCATCCGTCAGGACCTT |
| 18S | CTACCACATCCAAGGAAGCA | TTTTTCGTCACTACCTCCCCG |

**Table 2.1.5: Primer Sequences used in RT-qPCR Experiments**

| Software | Version | Manufacturer |
|---|---|---|
| Excel | 16.43 | Microsoft |
| FACSDiva™ | 8.0.2 | BD BioSciences |
| G*Power | 3.1.9.6 | Heinrich-Heine-Universität Düsseldorf |
| GraphPad Prism | 9.0.0 | GraphPad Software LLC |
| ImageJ | 1.53c | National Institutes of Health, USA |
| Kaluza | 2.1 | Beckman Coulter, Inc. |
| MassHunter Mass Profiler Professional | 15.1 | Agilent Technologies, Inc. |
| MassHunter ProFinder | 10.0 | Agilent Technologies, Inc. |
| MassHunter Qualitative Analysis | 10.0 | Agilent Technologies, Inc. |
| ND-8000 Software | 1.0.3 | Coleman Technologies, Inc for NanoDrop Technologies |
| Pathways to PCDL | B.08.00 | Agilent Technologies, Inc. |
| PCDL Manager | B.08.00 | Agilent Technologies, Inc. |
| Gen5™ Microplate Reader and Imaging Software | N/A | BioTek Instruments, Inc. |
| SoftMax® Pro | 5.4.1 | Molecular Devices |
| QuantStudio™ Real-Time PCR Software | 1.3 | Applied Biosystems by Thermo Fisher Scientific |
| Wave | 2.6.1.53 | Agilent Technologies, Inc. |

**Table 2.1.6: Software Used in this Work**

## 2.2 Isolation and Stimulation of Primary Monocytes from Peripheral Blood

### 2.2.1 Blood Collection

Blood samples were routinely obtained from two primary sources: buffy coats, and haemochromatosis whole blood donations. Buffy coat samples were obtained through the Irish Blood Transfusion Service (IBTS) with the appropriate clinical indemnity approval. No personal or clinical information about donors is available from these samples. Patients attending the outpatient's haemochromatosis clinic in St. James' Hospital were asked to donate samples with the appropriate ethic approvals. Whole blood donations were collected in CPDA-1 anti-coagulant bags (Fannin Scientific, MSE6500L) from consenting donors who were free from known infections and disclosed their age and sex.

### 2.2.2 Peripheral Blood Mononuclear Cell (PBMC) Preparation

PBMCs were isolated by density gradient centrifugation [285]. For buffy coat samples blood was diluted 1:1 with phosphate buffered saline (PBS) before layering over Lymphoprep™ (StemCell Technologies, 07851) at a ratio of 1:2 Lymphoprep:diluted blood. For haemochromatosis donors, blood was added to 2% dextran (20mg/ml in PBS), mixed thoroughly, and incubated for 30 mins at room temperature. The supernatant layer then was removed and layered onto Lymphoprep™ at a 1:3 ratio. Layered bloods were spun at 400g for 25 mins with minimal acceleration and no brakes. The plasma layer was aspirated and discarded, and the PBMC layer was aspirated and transferred to a new 50ml falcon tube. These tubes were filled to 50ml with PBS and centrifuged at 800g for 5 mins. Supernatant was discarded and cells were again washed with 50ml PBS before being spun at 400g for 10 mins. Supernatant was again removed, and cells were transferred to a new 15ml falcon. Cold MACS buffer (PBS + 2mM EDTA + 0.5% BSA) was added up to 15ml and tube spun at 400g for 7 mins.

### 2.2.3 Monocyte Isolation

Monocytes were isolated from PBMCs by CD14+ magnetic bead isolation [286]. After the final centrifugation step for PBMC isolation supernatant was removed and cells were resuspended in 2.9ml MACS buffer. 100µl of anti-CD14 microbeads (Miltenyi Biotec,130-050-201) were added and cells were incubated for 15 min at 4°C, mixing once. 1ml MACS buffer was added and cells were spun for at 400g for 7 min. PBMCs were resuspended in 3ml MACS buffer and CD14+ cells were

isolated using an LS column (Miltenyi Biotec, 130-042-401) and pre-separation filter (Miltenyi Biotech, 130-041-407) on a quadroMACS separator (Miltenyi Biotec, 130-090-976). The column and filter were washed with 3ml of MACS buffer before and after adding PBMCs. The column was removed from the separator and bound cells were eluted in 5ml MACS buffer. Cells were counted by Trypan blue exclusion and concentration adjusted to $1x10^6$/ml in complete RPMI (RPMI + 10% FCS + 100U/ml streptomycin + 1mg/ml penicillin) or appropriate buffer.

### 2.2.4 Monocyte Stimulation

Monocytes were seeded at $1x10^6$ cells/ml in either 96- or 24-well formats with 200µl or 1ml of cell suspension respectively. Cells were left to rest for at least 30 mins before stimulation at 37°C with 5% $CO_2$. Cells were stimulated with 5µg/ml of anti-MPO (Meridian BioSciences, H87207M) or anti-PR3 (Merck, MABT340). Negative controls were stimulated with serum-free RPMI (No Stimulation) and positive controls with 200ng/ml LPS (Sigma, L5418). Each stimulant was measured at least in triplicate and cells were stimulated for 4 hours (unless otherwise stated) at 37°C with 5% $CO_2$. At the end of the stimulation plates were spun at 400g for 7 mins and supernatants removed for cytokine or LDH analysis as described in Sections 2.3 and 2.4 respectively. Cells were processed for either RT-qPCR or metabolomic analysis as described in Sections 2.6 and 2.9 respectively.

## 2.3 Enzyme-Linked Immunosorbent Assay (ELISA)

DuoSet ELISA kits (R&D Systems) were used to measure cytokine production in supernatants from ANCA-stimulated monocytes. Each kit contained capture antibody, recombinant cytokine standard, biotinylated detection antibody, and streptavidin-horseradish peroxidase (HRP) solution. Stock reagents were diluted based on the manufacturer's instructions in PBS or distilled water ($H_2O$).

Flat-bottomed high binding 96 well plates (VWR, 655061) were coated with 50µl per well of diluted capture antibody, covered, and incubated overnight at 4°C. The ELISA wash step consisted of submersion in ELISA wash buffer (PBS + 0.05% Tween-20 [MP Biomedicals, 11417160]) and quick removal of buffer into a waste sink a minimum of three times. Plates were then dried completely on blotting paper. Plates were blocked with 200µl fresh 1% BSA (1mg/ml BSA in PBS) for 2 hours at room temperature, then washed. Recombinant cytokine standards were serially

diluted in 1% BSA to develop a 7-point standard curve with a negative blank. Supernatants were diluted 1:5, 1:25, and 1:50 for TNF-α (DY210), IL-1β (DY201), and IL-6 (DY206) respectively and undiluted for IP-10 (DY266) assays. 50µl standards, samples or blanks were added to the plate in duplicate/triplicate. Plates were covered and incubated overnight at 4°C. After washing, 50µl diluted detection antibody was added to each well and plates were covered and incubated at room temperature for 2 hours. After washing, 50µl diluted HRP solution was added to each well and plates were incubated for 20min in the dark at room temperature. Plates were washed and 40µl 3,3',5,5' – tetramethylbenzidine (TMB, Sigma, T0440) was added to each well. Plates were incubated in the dark until appropriate colour development in the standard curve (minimum 20 mins). The assay was stopped by adding 25µl 2M $H_2SO_4$ to each well. Absorbances from each well were immediately read at 450nm using a VersaMax™ Microplate Reader (Molecular Devices). Standard curves were interpolated to determine unknown sample concentrations and graphed using GraphPad prism software (Version 9.0, GraphPad Inc.).

## 2.4 Lactate Dehydrogenase (LDH) Cytotoxicity Assay

Quantification of LDH in post-stimulation cell supernatants was performed using the CytoTox 96® Non-Radioactive Cytotoxicity Assay (Promega, G1780). Assay Buffer was thawed and warmed to room temperature in a water bath. Reagent Buffer was prepared by adding 12ml Assay Buffer to a new vial of Substrate Mix and vortexing thoroughly until dissolved completely. LDH Positive Control and cell-free cRPMI acted as positive and negative controls for this assay, respectively. Tubes containing cell supernatants were thawed, vortexed, and centrifuged at 2,000g for 5 mins. 40µl of supernatant (in duplicate) was mixed with 40µl of Reagent Buffer in a 96-well plate. The plate was rocked gently for 5-10 mins at room temperature until colour developed fully in the LDH Positive Control. 40µl of stop solution was added to each well and the assay plate was spun at 2,000g for 5 mins before being read at 490nm with a VersaMax™ Microplate Reader (Molecular Devices). Results were reported as percent (%) cytotoxicity. The percentage of cytotoxicity was calculated by considering the OD value for the negative control as 0% and the OD value for the positive control as 100% across all assay plates. A two-point, straight-line standard curve was drawn, and results were interpolated for each sample taking the mean of duplicate values.

## 2.5 Analysis of Protein Concentrations using Pierce™ Bicinchoninic Acid (BCA) Protein Assay

Protein levels in metabolite fraction and cell pellets were measured using the Pierce™ BCA Protein Assay (Thermo Scientific, 23227). Standards were prepared by serial dilution of bovine serum albumin (BSA) in 80% American Chemical Society (ACS) reagent grade MeOH (Acros Organics, 10607221) with a top standard of 200µg/ml BSA (300nM) and a negative blank. BCA Working Reagent was prepared by diluting BCA Reagent B 1:50 with BCA Reagent A. 9.6ml of Working Reagent is required for a single 96-well plate, and so 200µl of BCA Reagent B was mixed with 9.8ml of BCA Reagent A in a 15ml falcon tube to allow sufficient volume. Residual protein from metabolite extractions was resolubilised with vigorous vortexing in 1X Fluorescent DNA Assay Buffer (see Section 2.10) and dissolved overnight in a heat block @37°C. 12.5µl of each sample was added to the relevant wells of a 96-well plate in duplicate/triplicate. 100µl of BCA Working Reagent was added to each well and the plate was mixed briefly on a plate shaker. The plate was sealed tightly with parafilm and left to incubate at 37°C for 18 hours. After cooling to room temperature, the absorbance was measured at 562nm and 595nm with an Epoch™ Microplate Spectrophotometer (BioTek Instruments, Inc.).

## 2.6 Analysis of Gene Expression by Real-Time Quantitative Reverse Transcription PCR (RT-qPCR)

### 2.6.1 RNA Extraction

RNA was extracted from cells using the Roche High Pure RNA Isolation Kit (Roche, 11828665001). The kit contents are lysis/binding buffer, recombinant DNase I, DNase incubation buffer, wash buffer I & II, elution buffer, high pure filter tubes, and collection tubes. Before the first use of each kit, DNase I was dissolved in 550µl of elution buffer and vortexed. Wash buffers I and II were mixed with 20ml and 40ml of molecular-grade ethanol, respectively, and mixed well. Before beginning the experiment, all surfaces and materials were sprayed thoroughly with RNaseZAP™ (Sigma, R2020) and all materials were DNase and RNAse free.

Approximately $9x10^5$ monocytes were used for 24-well plate stimulations and $2x10^5$ cells for 96-well stimulations. Cells were stored in Eppendorfs for 24-well stimulations or in the stimulation plate in the case of 96-well experiments. High pure filter tubes were inserted into collection tubes and both components (tube units)

labelled appropriately. Cells were resuspended in 200µl PBS and transferred to the correspondingly labelled tubes. 200µl lysis/binding buffer was added to each high pure filter tube and vortexed. Tube units were centrifuged at 8,000g for 15 seconds and waste collected in the bottom of the collection tube discarded. For each sample 10µl of DNase I was added to 90µl of DNase incubation buffer in a sterile tube. 100µl of the solution was gently pipetted onto the glass filter fleece of the upper tube reservoir of each tube unit and vortexed. Tube units were incubated for 15 mins at room temperature then washed with 500µl of wash buffer I and centrifuged at 8,000g for 15 seconds. Waste was discarded and the wash step repeated. 200µl of wash buffer II was added to the upper tube reservoir of each tube unit and tube units were centrifuged at 13,000g for 2 mins. The collection tube was removed and replaced with a sterile 1.7ml RNase & DNase-Free microcentrifuge tube. 75µl of elution buffer was added to the upper reservoir of the filter tube and tube assemblies were centrifuged at 8,000g for 1 minute. Eluted RNA was immediately assessed for purity and used to generate cDNA, or stored at −80°C.

### 2.6.2 RNA Concentration and Purity Analysis

RNA concentration in each sample was measured using the NanoDrop™ 8000 Spectrophotometer with ND-8000 Software Version 1.0 (Thermo Fisher Scientific). 1µl of extracted RNA was pipetted onto the sample loading dock and sample concentration measured at 260 and 280nm. Samples were diluted with sterile distilled water (SDW) to the lowest concentrated sample in the cohort. The 260nm/280nm absorbance ratio was measured to assess purity of RNA with a threshold of ≥1.9 considered acceptable.

### 2.6.3 cDNA Synthesis

Before beginning the experiment, all surfaces and materials were sprayed thoroughly with RNaseZAP™ and all materials were DNase and RNAse free. Ice cold reagents were added to 200µl PCR tubes as per the template in Table 2.6.1 below for a total of 10µl cDNA (sufficient for 6 experiments). Cells were vortexed and spun briefly before being added to a PCR Thermocycler (MJ Research PTC-200). Tubes were heated to 25ºC for 10mins, 42ºC for 60mins, 95ºC for 3mins, and held at 4ºC until use. cDNA samples were diluted 1:1 with SDW and vortexed before storage at -20ºC.

| Reagent | Stock Concentration | Volume (µl) | Final Concentration |
|---|---|---|---|
| RNA Template | Variable | 5.00 | ~2.5µg |
| M-MLV Buffer (Promega, M531A) | 5X | 2.00 | 1X |
| dNTPs (R0181, Thermo Fisher) | 10mM | 2.00 | 2mM |
| Random Hexamer (SO142, Thermo Fisher) | 100µM | 0.50 | 5µM |
| RNaseOUT™ (Invitrogen, 10777019) | 40U/µL | 0.25 | 1U |
| M-MLV RT (Promega M170B) | 200U/µL | 0.25 | 5U |

**Table 2.6.1: Template of reagents for cDNA synthesis**

### 2.6.4 RT-qPCR Primer Design

Primer sequences for RT-qPCR were identified using the U.S. National Library of Medicine, National Centre for Biotechnology Information (NCBI) Gene Database [287]. Primers were designed based on guidelines described by Thornton & Basu [288]. PCR product size was set to 80-150 base pairs (bp), and primers had to span an exon/exon junction. Primer melting temperatures (Tm) were set to 63-64°C where possible and expanded to 59-68°C with a maximum Tm difference of 1°C between forward and reverse where no results were available. Primer length was limited to 18-24bp and GC clamp (maximum $\Delta G$ of the 5 bases from the 5′ end of the primers) limited to <2. Results were reviewed and primers with fewer similar entities (excluding isoforms) were prioritised. Other favourable primer characteristics included a maximum of 4 dinucleotides and 4 runs, annealing temperature between 59 and 60°C, and a Mg2+ concentration between 3-6mM $MgCl_2$. Primers were synthesised by Integrated DNA Technologies, Inc., diluted with SDW upon receipt and stored at -20°C. A list of forward and reverse primers used in the course of this work can be found in Table 2.1.5.

### 2.6.5 RT-qPCR Protocol

Before beginning the experiment, all surfaces and materials were sprayed thoroughly with RNaseZAP™ and all materials were DNase and RNAse free. 2µl of diluted cDNA samples were added to the appropriate wells of a 384-well PCR plate (Fisher scientific, AB1384) and the plate was centrifuged briefly to pool liquid at the bottom of the well. 4µl of SYBR™ Green (Thermo Fisher, A25742) and 3µl SDW was added to each well, and 1µl of the relevant diluted forward and reverse primers

added to the appropriate wells. The plate was covered with an adhesive PCR plate seal and centrifuged briefly. Samples were run on an Applied Biosystems™ 384-well QuantStudio™ 5 Real-Time PCR System in Standard run mode. The method was set as follows:

- Hold Stage
    - Step 1: 50ºC for 2mins, 1.6ºC/sec
    - Step 2: 95ºC for 2mins, 1.6ºC/sec
- PCR Stage – 40 cycles
    - Step 1: 95ºC for 15sec, 1.6ºC/sec
    - Step 2: 60ºC for 1min, 1.6ºC/sec, Data Collection on
- Melt Curve Stage – Continuous
    - Step 1: 95ºC for 15sec, 1.6ºC/sec
    - Step 2: 60ºC for 1min, 1.6ºC/sec
    - Step 3: 95ºC for 15sec, 0.015ºC/sec, Data Collection on

The expression of mRNA was calculated using $2^{-\Delta\Delta CT}$ method [289] using 18S as a reference control gene. Briefly, the difference between the target gene expression and 18S rRNA expression was used to calculate the ΔCt and normalise for variation in cDNA concentrations between samples. The expression of each target gene in the negative control (unstimulated) group was then compared to the treatment groups to determine ΔΔCt. The log-transformed fold change of this value (i.e., $2^{-\Delta\Delta CT}$) was then calculated.

## 2.7 Preparation of Histopathology Cell Slides

### 2.7.1 Cytospin Protocol

Cytospins were carried out on dextran sediment (mixed cell population), freshly isolated monocytes (T0), and stimulated monocytes after 4 hours (T4; No Stimulation, LPS, anti-MPO, anti-PR3). Labelled slides were loaded onto clips and aligned with filter paper and funnels. 100µl of cells were loaded into the relevant funnels and spun for 2 mins at 700rpm in a Shandon Cytospin 3 Centrifuge (Thermo Scientific). Slides were removed and air dried on a rack before staining.

### 2.7.2 Giemsa Staining

Once dry slides were fixed by emersion in molecular biology grade MeOH (Acros Organics, 326950010) for 10 mins and again air dried. Giemsa solution (Sigma, 48900) was diluted 1:20 in $dH_2O$ and cells were completely covered in diluted

Giemsa solution for 45 mins. Slides were carefully rinsed with distilled water and dried. A small drop of mounting solution (Sigma, 06522) was added over the cells and a coverslip carefully lowered over it. Slides were set at room temperature overnight and stored at 4°C before analysis.

### 2.7.3 Cell Size Analysis Using ImageJ

Slides were photographed using a Nikon Eclipse E200 microscope with a OptixCam Summit Series camera attachment. Photographs were taken using the PhotoView software (Version 7) at 10X and 40X magnification. Cell clumps were defined as a group of >5 cells where each cell is in direct contact with at least one other cell in the clump. Clumps were counted in three separate, distinct slide sections and totalled. For each treatment per biological replicate. Clumps were correlated with cytokine production and intracellular metabolite levels

## 2.8 Flow Cytometry Analysis of Cell Surface Markers

### 2.8.1 Staining of Cell Surface Markers on Immune Cells

Fluorochrome-conjugated monoclonal antibodies (mAb) specific for human CD14, CD16, CD54, MPO, and PR3 were used in various experiments. Various live/dead cell markers were also incorporated as specified. A full list of mAbs used for flow cytometry are available in Table 2.1.4. Controls incorporated into flow cytometry experiments included unstained controls, fluorescence-minus-one (FMO) controls, and live/dead controls. Unstained controls include no fluorochrome antibodies, FMO controls involve omitting a specific fluorochrome from the antibody panel from the specified sample, and live dead controls include a population of dead cells stained with the appropriate live/dead marker. Cells were killed by exposing to high temperatures (>60 °C) in a heatblock or water bath for up to 10 mins. Cells were acquired on a FACSCanto II flow cytometer using BD FACSDiva™ software, and results analysed using Kaluza software (Version 2.1, Beckman Coulter, Inc.). Cells were analysed immediately after staining where possible and always within 48 hours.

### 2.8.2 Mixed Cell Analysis

For analysis of mixed blood cell populations whole blood or dextran isolated cells (see Section 2.2) were used as specified. 100µl of whole blood or dextran was added to relevant FACS tubes. Cells were stained in the appropriate fluorescent antibody cocktail for 30 mins in the dark. Red blood cells were lysed with 1ml of

diluted BD lysis buffer (1X diluted in water, 349202, BD Biosciences), vortexed and left to rest for 10 mins. Cells were washed by adding 500µl FACS Buffer, vortexing briefly, centrifuging at 400g for 5 mins, and removing supernatant. This wash procedure was completed a total of 3 times. Where a live/dead stain was used in experiments, PBS was used in place of FACS buffer as specified. Cells were resuspended in 100-200µl PBS/FACS Buffer or 2% paraformaldehyde (PFA, Santa Cruz, sc-281692) for delayed analysis. Where cells had been preserved in 2% PFA they were washed twice before being resuspended in 100-200µl PBS/FACS Buffer.

### 2.8.3 Isolated Monocyte Analysis

Isolated monocytes were analysed for purity, viability, and surface marker expression. $1x10^6$ isolated monocytes in 1ml of cRPMI were added to relevant FACS tubes. Cells were washed by adding 500µl FACS Buffer, vortexing briefly, centrifuging at 400g for 5 mins, and removing supernatant. This wash procedure was completed a total of 3 times before cell staining. Cells were stained in the appropriate fluorescent antibody cocktail for 30 mins in the dark. Where a live/dead stain was used in experiments, PBS was used in place of FACS buffer as specified. After the staining procedure cells were washed 3 times and resuspended in 100-200µl PBS/FACS Buffer or 2% paraformaldehyde (PFA, Santa Cruz, sc-281692) for delayed analysis. Where cells had been preserved in 2% PFA they were washed twice before being resuspended in 100-200µl PBS/FACS Buffer.

### 2.8.4 Flow Cytometry Analysis

Cells were acquired on a FACSCanto II flow cytometer using BD FACSDiva™ software. Compensation controls were included in all experiments with appropriately stained OneComp eBeads™ (01-1111-42, Thermo Fisher). After acquisition .FCS files were imported into Kaluza software for analysis. Getting strategies are reported in the relevant results sections. Results are reported as cell percentages (%) and median fluorescence intensity (MFI) as specified.

## 2.9 LC-MS Metabolomics

### 2.9.1 Principles of Mass Spectrometry

The primary technology applied for metabolomic profiling of ANCA-stimulated monocytes in this work is liquid chromatography-mass spectrometry (LC-MS). LC-MS is a highly sensitive, specific, and reproducible technique for metabolomic analyses. The basic principle of mass spectrometry (MS) is to generate charged ions, and to detect these ions (and their fragments) based on their mass-to-charge ratio (*m/z*). In this work we have employed quadropole time-of-flight (Q-ToF) MS, which accelerates ions through a high voltage, with their velocity dependant on their *m/z* value. Ions are generated using an electrospray ionisation source, well-suited for metabolomic analyses [290]. Modern Q-ToF analysers can detect compounds across five orders of magnitude down to the picomolar range, while also allowing effective identification of molecular formula.

Coupling mass spectrometry to a liquid (see Figure 1.2.1) or gas chromatography system allows improved separation of ion species, more reliable identification of compounds, and rigorous quantification (as the method allows). Metabolite abundances are quantified by measuring the area underneath a chromatographic peak, and peak shape can be optimised by careful manipulation of mobile phases, flow rates, and column choice [24]. Improving chromatographic resolution with a mobile phase gradient also can allow effective separation of isomers.

Metabolites are a chemically and structurally diverse set of compounds, and because of this diversity, there is no single LC-MS method to completely account for all metabolites present in a biological system. Thus, methods must be appropriately developed and optimised for the specific application with consideration for the experimental design and aims, starting material, metabolites of interest, and desired outputs (qualitative/quantitative).

### 2.9.2 LC-MS Sample Preparation

An optimised LC-MS sample preparation method was developed for metabolite extraction of ANCA-stimulated monocytes. Additional validation of optimised sample preparation methods was completed in a cohort of ANCA-stimulated monocytes and PBMCs. All reagents were ACS Reagent Grade suitable for HPLC analysis

Experiments detailing the process for determining optimum metabolite extraction are described fully in Chapter 3.

Following cell stimulation (see Section 2.2), 5 million treated monocytes were centrifuged in 1.5ml Eppendorf tubes at 400g for 7 mins. Supernatants were removed completely, and samples were quenched on dry ice. 100µl of ice cold 80% ACS reagent-grade MeOH (Acros Organics, 10607221) was added, and cells were vortexed for 30secs, then sonicated in an ice bath for 1min, and vortexed for another 30secs. Samples were centrifuged at 16,000g for 10 mins at 4°C and the metabolite fraction (supernatant) removed for LC-MS analysis. The extraction procedure was repeated twice for a final metabolite fraction volume of approximately 200µl. Samples were stored at -80°C until analysis. All reagents used for LC-MS experiments were ACS reagent-grade.

#### 2.9.2.1 Pooled Quality Control Sample Preparation

Pooled Quality Control (PooledQC) samples are a type of control measure for LC-MS experiments whereby small aliquots of each biological sample to be studied are combined [64]. In these metabolomic profiling experiments, 5µl of metabolite fraction for each sample was added to an Eppendorf tube immediately after metabolite extraction. Samples were stored at -80°C until analysis.

#### 2.9.2.2 Synthetic Standard Sample Preparation

Synthetic chemical standards are used for definitive identification of metabolites using parallel analysis of mass, retention time and fragmentation mass spectra. A synthetic standard mix containing amino acids (A9906, Sigma), TCA cycle intermediates (ML0010, Sigma), and other metabolites of interest at a concentration of 50µM was formulated as outlined in Table 2.9.1.

| Name | Product Code | Molecular Weight | Stock Concentration (mg/ml) |
|---|---|---|---|
| L-(+)-Lactic acid | 46937 | 90.08 | 100.00 |
| B-Nicotinamide | 47865 | 662.42 | 25.30 |
| Inosine 5'-Monophosphate | 57510 | 410.19 | 35.10 |
| Trimethylamine N-oxide | 317594 | 75.11 | 52.10 |
| 1-Methyl-L-histidine | A9906 | 169.18 | 500µM |
| 3-Methyl-L-histidine | | 169.18 | |
| Cystathionine | | 222.26 | |
| DL-β-Aminoisobutryic acid | | 103.12 | |
| Ethanolamine | | 61.08 | |
| Glycine | | 75.07 | |
| Hydroxy-L-proline | | 131.13 | |
| L-Alanine | | 89.09 | |
| L-Anserine | | 240.26 | |
| L-Arginine | | 174.20 | |
| L-Aspartic acid | | 133.11 | |
| L-Carnosine | | 226.23 | |
| L-Citrulline | | 175.20 | |
| L-Creatinine | | 113.12 | |
| L-Cystine | | 240.30 | |
| L-Glutamic acid | | 147.13 | |
| L-Histidine | | 155.15 | |
| L-Homocystine | | 135.18 | |
| L-Isoleucine | | 131.17 | |
| L-Leucine | | 131.17 | |
| L-Lysine | | 146.19 | |
| L-Methionine | | 149.21 | |
| L-Ornithine | | 132.16 | |
| L-Phenylalanine | | 165.19 | |
| L-Proline | | 115.13 | |

| | | | |
|---|---|---|---|
| L-Serine | | 105.09 | |
| L-Threonine | | 119.12 | |
| L-Tryptophan | | 204.23 | |
| L-Tyrosine | | 181.19 | |
| L-Valine | | 117.15 | |
| L-α-Amino-n-butyric acid | | 103.12 | |
| Sarcosine | | 89.09 | |
| Taurine | | 125.15 | |
| Urea | | 60.06 | |
| β-Alanine | | 89.09 | |
| γ-Amino-n-butyric acid | | 103.06 | |
| δ-Hydroxylysine | | 162.19 | |
| Glucose 6-Phosphate | G7879 | 282.12 | 30.10 |
| Acetyl coenzyme A sodium salt | ML0010 | 809.57 | 10.00 |
| Citric acid monohydrate | | 210.14 | |
| DL-Isocitric acid trisodium salt hydrate | | 258.07 | |
| L-(−)-Malic acid | | 134.09 | |
| Oxaloacetic acid | | 132.07 | |
| Sodium fumarate dibasic | | 160.04 | |
| Sodium pyruvate | | 110.04 | |
| Sodium succinate dibasic hexahydrate | | 270.14 | |
| Succinyl coenzyme A sodium salt | | 867.61 | |
| α-Ketoglutaric acid disodium salt hydrate | | 190.06 | |
| *myo*-inositol | Y0000485 | 180.16 | 30.60 |

**Table 2.9.1: Contents of Synthetic Standard Mixture used for Quality Control Across MS Experiments.** All metabolites were adjusted to a concentration of 50µM.

### 2.9.3 LC-MS Metabolomic Profiling of ANCA-Stimulated Monocytes

A number of LC-MS methods were tested throughout the course of this work. A summary of the LC and MS parameters used in various experiments is provided in Tables 2.9.2 and 2.9.3, respectively, and described in additional detail in the corresponding results sections. The core LC-MS metabolomics method used is described by Hsiao *et al.* [42] and detailed below.

ANCA-stimulated monocytes were stimulated as described in Section 2.2 and processed as described above (Section 2.9.2). Samples were analysed on an Agilent 6546 Q-TOF (G6546A) paired with an Agilent 1290 Infinity LC. A 150mm × 2.1mm InfinityLab Poroshell 120 HILIC-Z column (683775-924, Agilent Technologies) was used and column temperature maintained at 25°C. Mobile phase A consisted of 10 mM ammonium acetate, pH 9.0 in water plus 5µM deactivator additive (medronic acid, 5191-4506, Agilent); and mobile phase B was 10 mM ammonium acetate, pH 9.0 in 90% ACN for ESI-. Medronic acid was included in Mobile phase B for the Primary Profiling cohort, but omitted for the Validation (see Section 5.2.3.1) For the positive ionisation mode ammonium acetate was replaced with 0.1% formic acid and pH was adjusted to 3.0. Flow rate was 0.25 mL/min and an injection volume of 2µl was used. After sample injection, the column was held at 90% solvent B for 2min before the solvent A gradient with was applied. The gradient elution profile was from 90 to 60% B for 10min followed by washing with 60% B for 3min. The column was then allowed to re-equilibrate with 90% B for 8min prior to subsequent analysis. MS data were acquired with a mass range of 40−1000*m/z* and an acquisition rate of 2 spectra per second. The instrument was operated in negative mode and positive mode on back-to-back runs under the same source conditions. Full details of MS conditions for the metabolomic profiling can be found in Table 2.9.3. Both sample runs included PooledQC samples, synthetic metabolite standards for amino acids (A9906, Sigma), TCA cycle metabolites (ML0010, Sigma), lactic acid (46937, Sigma), *myo*-inositol (Y0000485, Sigma) and trimethylamine N-oxide (TMAO, 317594, Sigma), and extraction blanks. A slightly modified version of this LC-MS method was applied to the Secondary cohort (n=24). Here the medronic acid deactivator additive was omitted from Mobile Phase B and only added to Mobile Phase A in the Secondary cohort. The gradient was also

modified slightly as shown in Figure 4.3.8. Additionally, all other source conditions were identical and both methods performed comparably.

### 2.9.4 LC-MS Data Analysis

The core LC-MS analysis technologies employed for this work were from the Agilent MassHunter suite from Agilent Technologies, Inc (Figure 2.9.1). The primary pre-processing software was Agilent MassHunter ProFinder (B.10.0), which was used for targeted and untargeted feature finding. Additional analyses of chromatography and mass spectra were completed using Agilent MassHunter Qualitative Analysis (B.10.0). For targeted analyses, personal compound database libraries (PCDLs) were built using PCDL Manager (B.08.00). Metabolite information was obtained from the Agilent MassHunter METLIN Metabolomics Database and Library. This is a highly curated and comprehensive collection of over 250,000 metabolites, lipids, and related compounds derived from the METLIN MS database [68]. This custom PCDL contains accurate, high-resolution MS spectral and isotopic data acquired using an Agilent Q-TOF MS. PCDLs for targeted analyses were updated with retention times (RTs) calculated from the appropriate metabolite standards. Metabolite identification, data visualisation, and statistical analyses (see Section 2.9.10) was carried out using Mass Profiler Professional (MPP, Agilent Technologies Version 15.1). Full details of data analysis workflows are provided in the appropriate results sections.

| Method ID | Column | Mobile Phase A | Mobile Phase B | Flow Rate (mL/min) | Gradient (Time, %Mobile A / %Mobile B) | Column Temp (°C) | Injection Volume (µl) |
|---|---|---|---|---|---|---|---|
| SPO C18 ESI+ | Agilent ZORBAX RRHD Eclipse Plus C18, 95Å, 2.1 x 150 mm, 1.8 µm (PN959759-902) | $H_2O$ + 5mM PFPA | 50% ACN + 50% $H_2O$ | 0.40 | 0.5min 97.0/3.0%<br>10.0min 35.0/65.0%<br>10.1min 10.0/90.0%<br>12.0min 10.0/90.0%<br>12.1min 50.0/50.0%<br>14.0min 50.0/50.0%<br>14.1min 97.0/3.0%<br>18.0min 97.0/3.0% | 50 | 5 |
| SPO C18 ESI- | Agilent ZORBAX RRHD Eclipse Plus C18, 95Å, 2.1 x 150 mm, 1.8 µm (PN959759-902) | $H_2O$ + 5mM PFPA | 50% ACN + 50% $H_2O$ | 0.40 | 0.5min 97.0/3.0%<br>10.0min 35.0/65.0%<br>10.1min 10.0/90.0%<br>12.0min 10.0/90.0%<br>12.1min 50.0/50.0%<br>14.0min 50.0/50.0%<br>14.1min 97.0/3.0%<br>18.0min 97.0/3.0% | 50 | 5 |
| SPO HILIC ESI- | Agilent InfinityLab Poroshell 120 HILIC-Z, 2.1 x 100, 2.7 µm, PEEK-lined (PN675775-924) | $H_2O$ + 10mM $C_2H_7NO_2$ + 5µM medronic acid, pH 9.0 | 90% ACN + 10mM $C_2H_7NO_2$ + 5µM medronic acid, pH 9.0 | 0.25 | 2.0min 10.0/90.0%<br>12.0min 60.0/40.0%<br>13.0min 80.0/20.0%<br>16.0min 80.0/20.0%<br>17.0min 10.0/90.0%<br>25.0min 10.0/90.0% | 30 | 5 |

| | | | | | | | |
|---|---|---|---|---|---|---|---|
| Primary Cohort HILIC ESI+ | Agilent InfinityLab Poroshell 120 HILIC-Z, 2.1 x 100, 2.7 µm, PEEK-lined (PN675775-924) | $H_2O$ + 0.1% formic acid + 5µM medronic acid, pH 3.0 | 90% ACN + 0.1% formic acid + 5µM medronic acid, pH 3.0 | 0.25 | 2.0min 10.0/90.0%<br>12.0min 60.0/40.0%<br>13.0min 80.0/20.0%<br>16.0min 80.0/20.0%<br>17.0min 10.0/90.0%<br>25.0min 10.0/90.0% | 30 | 5 |
| Primary Cohort HILIC ESI- | Agilent InfinityLab Poroshell 120 HILIC-Z, 2.1 x 100, 2.7 µm, PEEK-lined (PN675775-924) | $H_2O$ + 10mM $C_2H_7NO_2$ + 5µM medronic acid, pH 9.0 | 90% ACN + 10mM $C_2H_7NO_2$ + 5µM medronic acid, pH 9.0 | 0.25 | 2.0min 10.0/90.0%<br>12.0min 60.0/40.0%<br>13.0min 80.0/20.0%<br>16.0min 80.0/20.0%<br>17.0min 10.0/90.0%<br>25.0min 10.0/90.0% | 30 | 5 |
| Secondary Cohort HILIC ESI- | Agilent InfinityLab Poroshell 120 HILIC-Z, 2.1 x 150 mm, 2.7 µm (PN 683775-924) | $H_2O$ + 10mM $C_2H_7NO_2$ + 5µM medronic acid, pH 9.0 | 90% ACN + 10mM $C_2H_7NO_2$ pH 9.0 | 0.50 | 11.5min 30.0/70.0%<br>12.0min 0.0/100.0%<br>15.0min 0.0/100.0% | 30 | 2 |
| Secondary Cohort HILIC ESI+ | Agilent InfinityLab Poroshell 120 HILIC-Z, 2.1 x 150 mm, 2.7 µm (PN 683775-924) | $H_2O$ + 0.1% formic acid, pH 3.0 | 90% ACN + 0.1% formic acid, pH 3.0 | 0.80 | 11.5min 30.0/70.0%<br>12.0min 0.0/100.0%<br>15.0min 0.0/100.0% | 30 left / 20 right | 2 |

**Table 2.9.2: Summary of Liquid Chromatography Parameters used in LC-MS Experiments.**

| | | Sample Preparation Optimisation | | Primary Cohort | | Secondary Cohort | |
|---|---|---|---|---|---|---|---|
| **Method ID** | **C18 ESI+** | **C18 ESI-** | **HILIC ESI-** | **HILIC ESI+** | **HILIC ESI-** | **HILIC ESI-** | **HILIC ESI+** |
| **MS System** | Agilent 6545 LC/Q-TOF (G6545B) | Agilent 6545 LC/Q-TOF (G6545B) | Agilent 6545 LC/Q-TOF (G6545B) | 6546 LC/Q-TOF (G6546A) | Agilent 6545 LC/Q-TOF (G6545B) | 6546 LC/Q-TOF (G6546A) | 6546 LC/Q-TOF (G6546A) |
| **Ionization Mode** | Dual AJS ESI | Dual AJS ESI | Dual AJS ESI | Dual AJS ESI | Dual AJS ESI | Dual AJS ESI | Dual AJS ESI |
| **Ionization Polarity** | Positive | Negative | Negative | Positive | Negative | Negative | Positive |
| **Gas Temperature** | 200°C | 200°C | 200°C | 200°C | 200°C | 200°C | 200°C |
| **Drying Gas** | 10L/min | 10L/min | 10L/min | 10L/min | 10L/min | 10L/min | 10L/min |
| **Nebulizer Pressure** | 40psi | 40psi | 40psi | 40psi | 40psi | 40psi | 40psi |
| **Sheath Gas Temperature** | 300°C | 300°C | 300°C | 300°C | 300°C | 300°C | 300°C |
| **Sheath Gas Flow** | 12L/min | 12L/min | 12L/min | 12L/min | 12L/min | 12L/min | 12L/min |
| **Capillary Voltage** | 3000V | 3000V | 3000V | 3000V | 3000V | 3000V | 3000V |
| **Nozzle Voltage** | 0V | 2000/0V | 0V | 0V | 0V | 0V | 0V |
| **Fragmentor** | 120V | 120V | 125V | 115V | 125V | 115V | 115V |
| **Skimmer** | 65V | 65V | 65V | 65V | 65V | 65V | 65V |
| **Octopole 1 RF Voltage** | 750V | 750V | 750V | 750V | 750V | 750V | 750V |
| **Acquisition Range** | 50-1000*m/z* | 50-1000*m/z* | 50-1000*m/z* | 40-1000*m/z* | 50-1000*m/z* | 40-1000*m/z* | 40-1000*m/z* |
| **MS Acquisition Rate** | 5 spectra/sec | 5 spectra/sec | 3 spectra/sec | 1 spectrum/sec | 3 spectra/sec | 1 spectrum/sec | 1 spectrum/sec |
| **Reference Masses (*m/z*)** | 121.0509, 922.0098 | 68.9958, 119.0363, 1033.9881 | 68.9958, 119.0363, 980.0164 | 121.0509, 922.0098 | 68.9958, 119.0363, 980.0164 | 68.9958, 119.0363, 980.0164 | 121.0509, 922.0098 |

**Table 2.9.3: Summary of Mass Spectrometry Parameters used in LC-MS Experiments**

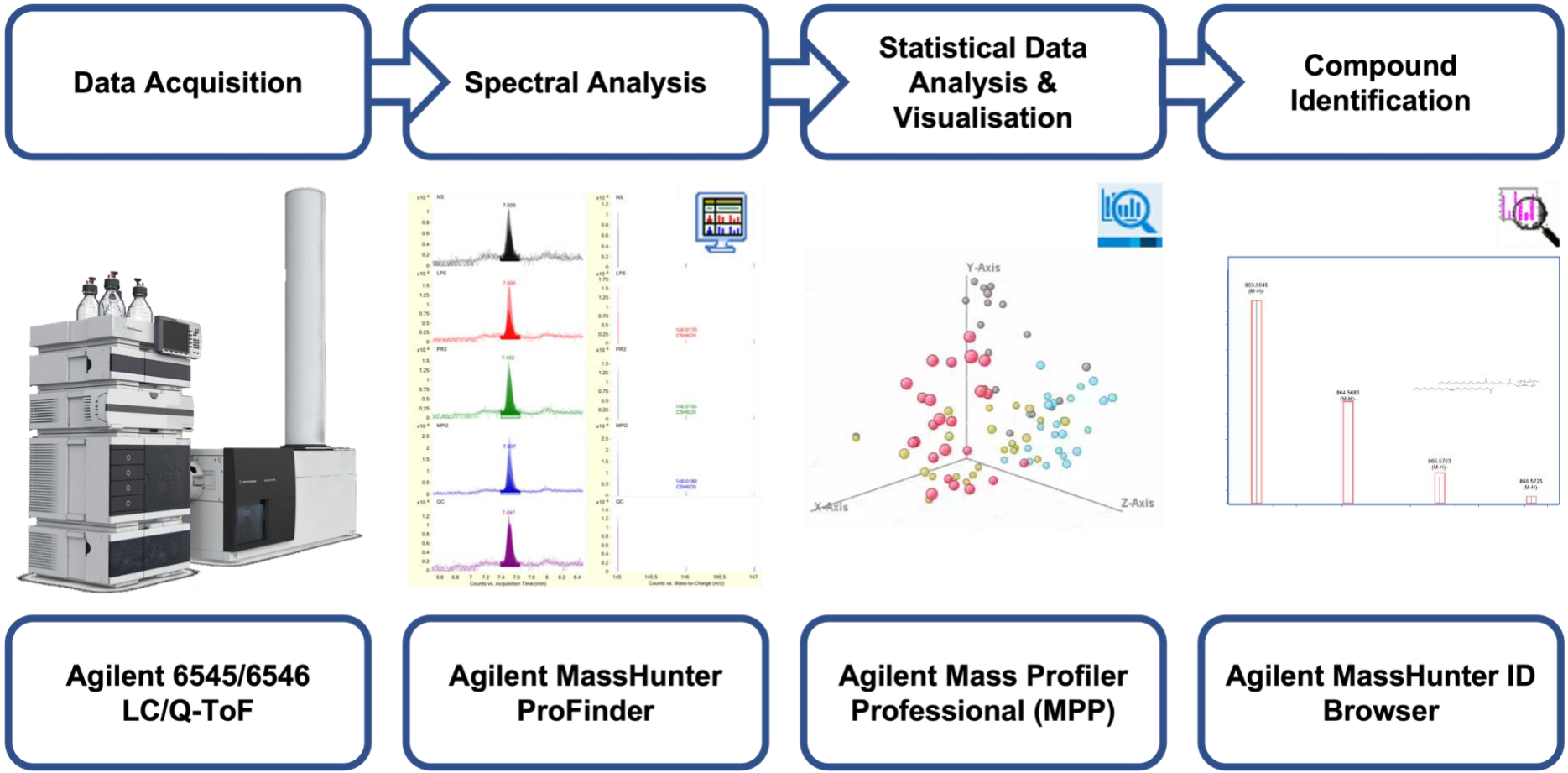


**Figure 2.9.1: Summary of Software Used for Various Stages of LC-MS Data Analysis.** Full details of software versions are shown in Table 2.1.6. LC/Q-ToF: Liquid Chromatography Quadropole Time-of-Flight Mass Spectrometry; *MPP:* Mass Profiler Professional.

### 2.9.5 Pre-Processing – Targeted Analysis

Results files (.d format) for samples, synthetic standards, and PooledQC samples were analysed using Agilent MassHunter ProFinder. For targeted analyses data was analysed using the Batch Targeted Feature Extraction (TFE) wizard. Criteria and parameters for batch TFE are summarised in Figure 2.9.2 and detailed below. A custom PCDL containing the 53 metabolites included in the synthetic standard metabolite mixture (Metabomix) was built from the Agilent MassHunter METLIN Metabolomics Database and Library. A summary of the Metabomix PCDL contents used for targeted analyses is included in Table 2.9.4. Synthetic standards were analysed, and retention times were determined for ESI+ and ESI- modes. Metabolites from the target list were identified in the PooledQC samples. Certain metabolites were detected in both negative and positive modes of ionisation. To choose which mode to use for the detection the following criteria were considered: manual review of chromatography, %CV of area thought the run, and RT drift across the runs.

### 2.9.6 Targeted Feature Extraction Analysis

Mass and retention time matching was required for targeted analysis: tolerances were confined to ±10ppm + 2mDa, and ±0.00 % + 0.5min, respectively. Formula targets were limited to Positive H+ and Negative H- ion species. Charge states were limited to a range of 1-2 and the isotope model assigned to common organic (no halogens) to allow for metabolite analysis. Contributions to matching scores were; Mass Score 100, Isotope abundance score 60, Isotope spacing score 50, and Retention time score 50. Expected data variation was maintained at default levels (MS mass 2mDa + 5.6ppm; MS isotope abundance 7.5%; MS/MS mass 5.0mDa + 7.5ppm; Retention time 0.115min). Overall scores below 75 and single ion predicted abundances below 50 were flagged for manual review. Extracted ion chromatograms were integrated using Agile 2 methods and smoothed by Gaussian function (function width 9 points, Gaussian width 5 points) prior to integration. Peaks were saved in both centroid and profile formats were possible, with preferences for centroid. Maximum spike width was 2 and required valley 0.70 for centroiding peak location. Spectra were included at the apex of the peak and excluded if above 20% of saturation. Find-by-Formula scores above 50 were required and compounds had to satisfy conditions in at least 33% of files in at least 1 sample group. Chromatography was manually reviewed, and compounds present in blank samples

removed from analyses. Results were exported in Compound Exchange Format (.CEF) and subsequently imported and visualised in MPP as described in Section 2.9.10.

### 2.9.7 Pre-Processing – Untargeted Analysis

For untargeted analysis, results files (.d format) for samples and blanks were imported into Agilent MassHunter ProFinder and analysed using the Batch Recursive Feature Extraction (RFE) wizard. Criteria and parameters for batch RFE are summarised in Figure 2.9.3 and detailed below. Chromatography was manually reviewed, and compounds present in blank samples removed from analyses. Results were exported in Compound Exchange Format (.CEF) and subsequently imported and visualised in MPP as described in Section 2.9.10. Tentative metabolite IDs were assigned using ID browser based on 1) score and 2) literature review.

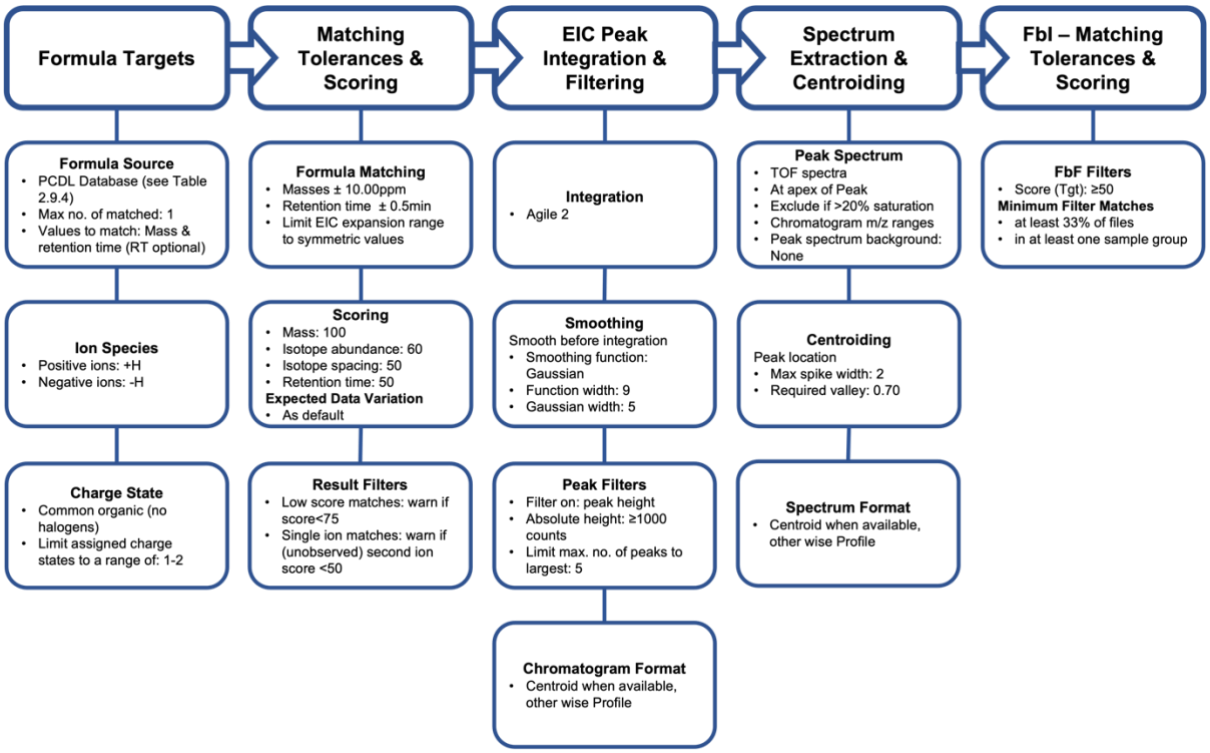


**Figure 2.9.2: Summary of Steps and Parameters for Targeted Feature Extraction (TFE) in (semi-) Targeted Metabolomic Analyses.** See Section 2.9.6 for full details

| Name | Formula | Mass | CAS | METLIN | KEGG ID | n Spectra |
|---|---|---|---|---|---|---|
| 1-Methyl-L-Histidine | $C_7H_{11}N_3O_2$ | 169.0851 | 332-80-9 | 3741 | C01152 | 0 |
| 3-Methyl-L-Histidine | $C_7H_{11}N_3O_2$ | 169.0851 | 368-16-1 | 3293 | C01152 | 0 |
| 4-Hydroxy-L-Proline | $C_5H_9NO_3$ | 131.0582 | 30724-02-8 | 58354 | C01015 | 0 |
| Acetyl-CoA | $C_{23}H_{38}N_7O_{17}P_3S$ | 809.1258 | N/A | N/A | C00024 | 3 |
| alpha-Ketoglutaric Acid | $C_5H_6O_5$ | 146.0215 | 328-50-7 | 119 | C00026 | 3 |
| β-Alanine | $C_3H_7NO_2$ | 89.0477 | 107-95-9 | 36 | C00099 | 3 |
| Carnosine | $C_9H_{14}N_4O_3$ | 226.1066 | 305-84-0 | 38 | C00386 | 5 |
| Citric Acid | $C_6H_8O_7$ | 192.0270 | 77-92-9 | 124 | C00158 | 6 |
| Citrulline | $C_6H_{13}N_3O_3$ | 175.0957 | 372-75-8 | 16 | C00327 | 3 |
| Creatinine | $C_4H_7N_3O$ | 113.0589 | 60-27-5 | 8 | C00791 | 6 |
| delta-Hydroxylysine | $C_6H_{14}N_2O_3$ | 162.1004 | 13204-98-3 | 47 | C01211 | 0 |
| D-Glucose 6-Phosphate | $C_6H_{13}O_9P$ | 260.0297 | 56-73-5 | 145 | C00092 | 3 |
| DL-3-Amino-Isobutanoic Acid | $C_4H_9NO_2$ | 103.0633 | 144-90-1 | 480 | C05145 | 3 |
| Ethanolamine | $C_2H_7NO$ | 61.0528 | 141-43-5 | 3207 | C00189 | 3 |
| Fumaric acid | $C_4H_4O_4$ | 116.0110 | 110-17-8 | 3242 | C00122 | 1 |
| gamma-Aminobutryic Acid | $C_4H_9NO_2$ | 103.0633 | 56-12-2 | 279 | C00334 | 4 |
| Glycine | $C_2H_5NO_2$ | 75.0320 | 56-40-6 | 20 | C00037 | 5 |
| Homocystine | $C_8H_{16}N_2O_4S_2$ | 268.0551 | 462-10-2 | 4189 | C01817 | 0 |
| Inosine 5'-monophosphate (IMP) | $C_{10}H_{13}N_4O_8P$ | 348.0471 | 131-99-7 | 3490 | C00130 | 6 |

| | | | | | | |
|---|---|---|---|---|---|---|
| Isocitrate | $C_6H_8O_7$ | 192.0270 | 320-77-4 | 3328 | C00311 | 2 |
| Lactic acid | $C_3H_6O_3$ | 90.0317 | 50-21-5 | 116 | C01432 | 0 |
| L-Alanine | $C_3H_7NO_2$ | 89.0477 | 56-41-7 | 11 | C00041 | 4 |
| L-alpha-Aminobutyric acid | $C_4H_9NO_2$ | 103.0633 | 1492-24-6 | 35945 | C02356 | 0 |
| L-Anserine | $C_{10}H_{16}N_4O_3$ | 240.1222 | N/A | 4195 | C01262 | 0 |
| L-Arginine | $C_6H_{14}N_4O_2$ | 174.1117 | 74-79-3 | 13 | C00062 | 5 |
| L-Aspartic Acid | $C_4H_7NO_4$ | 133.0375 | 56-84-8 | 15 | C00049 | 4 |
| L-Cystathionine | $C_7H_{14}N_2O_4S$ | 222.0674 | 56-88-2 | 39 | C02291 | 1 |
| L-Cystine | $C_6H_{12}N_2O_4S_2$ | 240.0238 | 56-89-3 | 17 | C00491 | 3 |
| L-Glutamate | $C_5H_9NO_4$ | 147.0532 | 56-86-0 | 19 | C00025 | 8 |
| L-Histidine | $C_6H_9N_3O_2$ | 155.0695 | 71-00-1 | 21 | C00135 | 5 |
| L-Isoleucine | $C_6H_{13}NO_2$ | 131.0946 | 73-32-5 | 23 | C00407 | 4 |
| L-Leucine | $C_6H_{13}NO_2$ | 131.0946 | 61-90-5 | 24 | C00123 | 4 |
| L-Lysine | $C_6H_{14}N_2O_2$ | 146.1055 | 56-87-1 | 25 | C00047 | 3 |
| L-Malic acid | $C_4H_6O_5$ | 134.0215 | N/A | 45931 | C00149 | 3 |
| L-Methionine | $C_5H_{11}NO_2S$ | 149.0510 | 63-68-3 | 26 | C00073 | 6 |
| L-Ornithine | $C_5H_{12}N_2O_2$ | 132.0899 | 3184-13-2 | 45121 | C00077 | 3 |
| L-Phenylalanine | $C_9H_{11}NO_2$ | 165.0790 | 63-91-2 | 28 | C00079 | 5 |
| L-Proline | $C_5H_9NO_2$ | 115.0633 | 147-85-3 | 29 | C00148 | 5 |

| | | | | | | |
|---|---|---|---|---|---|---|
| L-Serine | $C_3H_7NO_3$ | 105.0426 | 56-45-1 | 30 | C00065 | 5 |
| L-Threonine | $C_4H_9NO_3$ | 119.0582 | 72-19-5 | 32 | C00188 | 5 |
| L-Tryptophan | $C_{11}H_{12}N_2O_2$ | 204.0899 | 73-22-3 | 33 | C00078 | 6 |
| L-Tyrosine | $C_9H_{11}NO_3$ | 181.0739 | 60-18-4 | 34 | C00082 | 5 |
| L-Valine | $C_5H_{11}NO_2$ | 117.0790 | 72-18-4 | 35 | C00183 | 4 |
| *myo*-Inositol | $C_6H_{12}O_6$ | 180.0634 | 87-9-8 | 144 | C00137 | 5 |
| Nicotinamide adenine dinucleotide (NAD) | $C_{21}H_{28}N_7O_{14}P_2$ | 664.1169 | 53-84-9 | 101 | C00003 | 0 |
| Oxaloacetate | $C_4H_4O_5$ | 132.0059 | 328-42-7 | 123 | C00036 | 1 |
| Pyruvic acid | $C_3H_4O_3$ | 88.0160 | 127-17-3 | 117 | C00022 | 2 |
| Sarcosine | $C_3H_7NO_2$ | 89.0477 | 107-97-1 | 51 | C00213 | 3 |
| Succinic acid | $C_4H_6O_4$ | 118.0266 | 110-15-6 | 114 | C00042 | 4 |
| Succinyl-CoA | $C_{25}H_{40}N_7O_{19}P_3S$ | 867.1313 | 604-98-8 | 444 | C00091 | 3 |
| Taurine | $C_2H_7NO_3S$ | 125.0147 | 107-35-7 | 31 | C00245 | 3 |
| Trimethylamine N-oxide (TMAO) | $C_3H_9NO$ | 75.0684 | 1184-78-7 | 3773 | C01104 | 0 |
| Urea | $CH_4N_2O$ | 60.0324 | 57-13-6 | 6 | C00086 | 0 |

**Table 2.9.4: Summary of Metabomix PCDL Contents for Targeted Analysis.** See Section 2.9.6 for full details.

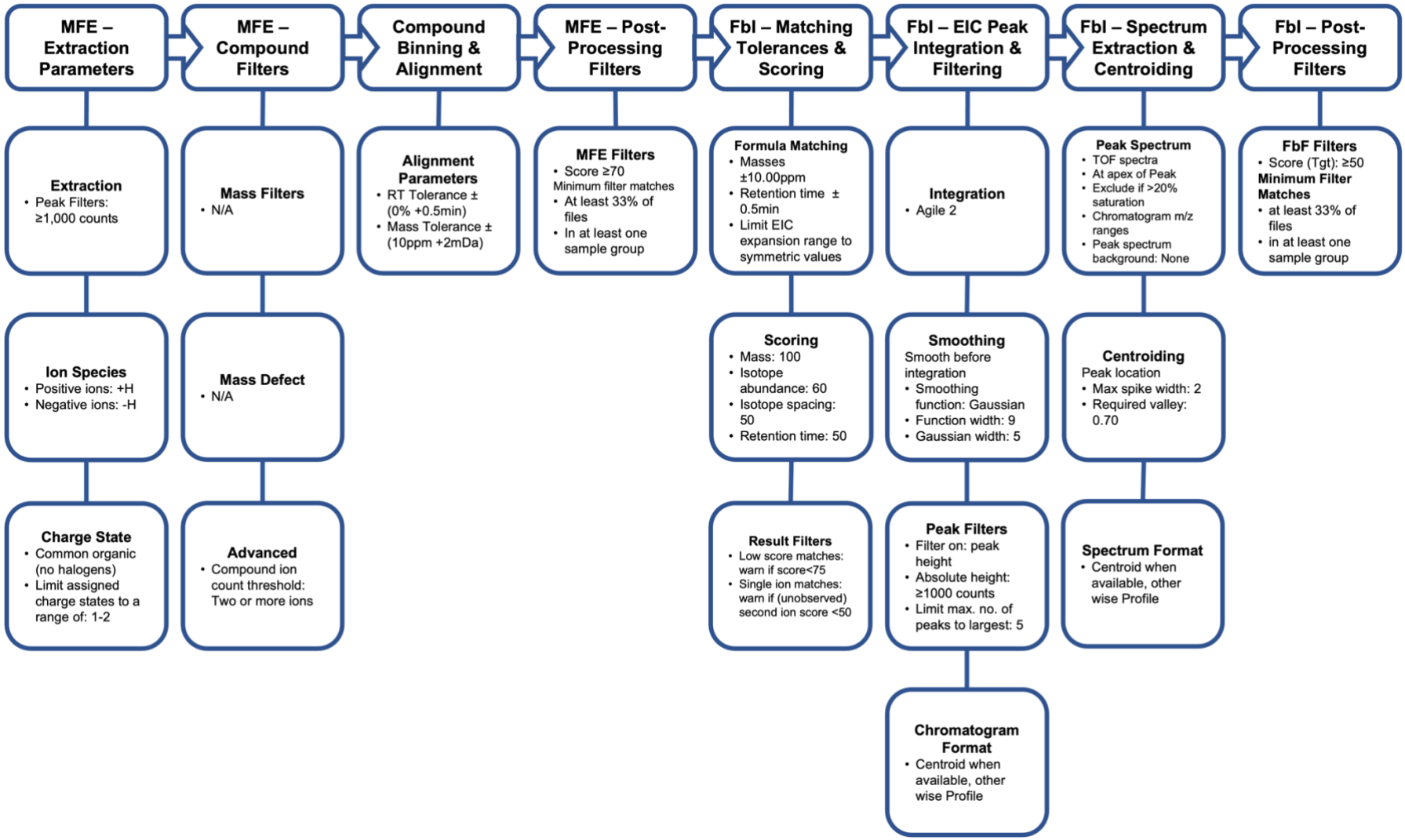


**Figure 2.9.3: Summary of Steps and Parameters for Recursive Feature Extraction (RFE) in Untargeted Metabolomic Analyses.** See Section 2.9.8 for full details.

### 2.9.8 Untargeted Recursive Feature Extraction Method

Extraction parameters were limited to Positive H+ and Negative H- ion species and peaks with (centroid) height above 1,000 counts. Charge states were limited to a range of 1-2 and the isotope model assigned to common organic (no halogens) to allow for metabolite analysis. The compound ion count threshold was limited to ≥2 ions to improve identification efficacy. RT and mass tolerances were confined to ±0.00 % + 0.5min and ±10ppm + 2mDa, respectively. Molecular feature extraction (MFE) scores above 70 were required and compounds had to satisfy MFE conditions in at least 2/6 files in at least 1 sample group and were flagged if they fell below this. Contributions to overall score were as follows; Mass Score 100, Isotope abundance score 60, Isotope spacing score 50, Retention time score 0. Expected data variation was maintained at default levels (MS mass 2mDa + 5.6ppm; MS isotope abundance 7.5%; MS/MS mass 5.0mDa + 7.5ppm; Retention time 0.115min). Matching tolerances were ±10ppm and ±0.5mins for mass and RT, respectively. Chromatograms were smoothed using a Gaussian function width of 9 points and a Gaussian width of 5 points. Chromatograms were extracted in both centroid and profile format (with centroid preferred) and absolute heights below 1,000 at peak apex were excluded. The maximum centroid spike width was 2 and the required valley 0.70. Spectra above 20% saturation were excluded. Target ion scores below 50 were excluded and as for MFE compounds had to satisfy Find by Ion conditions in at least 2/6 files in at least 1 sample group.

### 2.9.9 Metabolite Annotation

Following statistical analysis (see Section 2.9.10), significantly altered metabolites were imported into MPP ID Browser. Tentative metabolite IDs [25] were assigned using the Agilent MassHunter METLIN Metabolomics Database. Compounds were annotated in the first instance by Library/Database search, and by formula generation when there were no Library/Database hits. For formula generation positive and negative hydrogen ions were the assumed charge carriers. A minimum of 3 and max of 60 carbon atoms were permitted. Additional limits of 120, 30, 30, 5 and 3 were set for hydrogen, oxygen, nitrogen, sulphur and phosphorous, respectively. LC/MS tolerances for precursor ion *m/z* were ± 10ppm + 2mDa and for fragment ion *m/z* ±15ppm + 5mDa. Search criteria were not limited by instrument type, ionisation mode, or collision energy. Identification parameter (DB search, MFG score, library search score, BioConfirm) score weights were all evenly set to 40.

Search results were limited to the 10 best hits per compound and minimum overall scores set to 35. Metabolite IDs with scores above 70 were considered reliable. Features were annotated with tentative metabolite IDs assigned based on 1) score and 2) brief literature review. Where scores were equal IDs were assigned by brief literature review to determine likelihood of metabolite's impact on monocyte function. Endogenous metabolites (as listed in HMDB) were preferred.

### 2.9.10 Statistical Metabolomic Analysis

Initial statistical analysis was completed in MPP. Data was imported as .CEF files and treatment groups assigned as parameters. All available RT and mass data was used and all charge states were permitted. A number of different normalisation strategies were applied to metabolomic data of ANCA stimulated monocytes and are described in Chapter 3. Residual protein concentration measured by Pierce™ BCA assay (as described in Section 2.5) was deemed the most appropriate method for data normalisation. Samples were normalised by applying the protein value (measured in OD@595nm or µg/ml, as specified) as an external scalar value. Significantly altered metabolites (relative to unstimulated cells) were highlighted in MPP by filtering on volcano plot using a moderated t-test and a Benjamini-Hochberg false discovery rate (FDR) correction. Clustering analysis on significantly altered metabolites was completed with Euclidean distance metric and median linkage rule. Four-point Principal Component Analysis (PCA) plots were generated on conditions with various entity (metabolite loadings). Subsequent statistical analysis was completed in GraphPad Prism (Version 9.0, GraphPad Software LLC) as specified.

## 2.10 Fluorescent DNA Quantitation Assay

All materials used for DNA quantitation assay were DNase and RNAse free. A frozen Fluorescent DNA Standard (1mg/ml) was thawed in a 50°C water bath for 10mins. The high concentration DNA standard solution was prepared by combining 100µl Fluorescent DNA Standard, 100µl 10X Fluorescent DNA Assay Buffer, and 800µl $dH_2O$ in a sterile 1.5ml Eppendorf tube. This 100µg/mL DNA Standard is serially diluted to create a 7-point standard curve with an additional negative blank. Fluorescent DNA Dye consists of 1µg/mL bisbenzimide H33258 Solution. High concentration Fluorescent DNA Dye solution was prepared by combining 1ml 10X Fluorescent DNA Assay Buffer, 9ml $dH_2O$, and 10µl Fluorescent DNA Dye in a 15ml falcon. This volume is sufficient for a single 96-well plate. Turn on fluorimeter and

allow to warm up for 15-20 mins prior to use. Add 100µl Fluorescent DNA Dye solution to appropriate wells of 96-well plate. Add 0.5µl each sample and standard to appropriate wells (in duplicate/triplicate). Set excitation and emission wavelengths to 360nm and 460nm, respectively and read plate. Unknown values were interpolated from the standard curve and results analysed using GraphPad Prism (Version 9.0.0).

## 2.11 Real-Time Analysis of Cellular Metabolism with Seahorse Extracellular Flux Technology

### 2.11.1 Seahorse Assay Plate Preparation

The day prior to a Seahorse experiment FluxPaks cartridges were hydrated by emersion in XF Calibrant Solution (100840-000, Agilent Technologies) overnight at 37°C in a CO2-free incubator. Non-adherent monocytes were immobilised onto the base of the XF24 cell culture plate with Cell-Tak (10317081, Thermo Fisher). Stock CellTak was diluted to 2.85µg/ml with 0.1M sodium bicarbonate (pH 8.0) and 2mM sodium hydroxide. Immediately after dilution, 200µl Cell-Tak solution was added to each well of the XF24 well cell culture plate and left to absorb for 30 mins at room temperature. Wells were washed twice with 500µl sterile $H_2O$ and the plate was left to air dry.

Once dry and at room temp $1x10^6$ freshly isolated monocytes were plated in each well in 100µl XF Media (Agilent Technologies, 102365-100) supplemented with 5.5mM D-Glucose (Sigma, G7021), 4mM L-glutamine (Gibco, 25030-024), and 1mM sodium pyruvate (Gibco, 11360-039). This media is hereby referred to as XF+ media. Plates were centrifuged up to 40g with acceleration = 4 and no brake. The plate was then turned 180° and centrifuged up to 80g with acceleration = 4 and no brake to allow even coating of cells. Plates were incubated at 37°C with 5% CO2 for 30min and an additional 200µl XF+ Media was then added to each well.

### 2.11.2 Measurement of Real Time Metabolic Changes by Seahorse

The appropriate stimulants were added to the relevant ports of a pre-prepared XFe24 FluxPak (Agilent Technologies, 102340-100). The loaded FluxPak was left to equilibrate for 10 min at 37°C in a $CO_2$-free incubator before being placed in the Seahorse XFe24 analyser for calibration. The plate containing adhered monocytes was then added to the analyser. Each measurement cycle consisted of 2 mins Mix,

2 mins Wait, 3 mins Measure. Four initial basal measurements were performed followed by injection of stimulants from port A.

### 2.11.3 Seahorse Assay Analysis

Results were analysed initially using Wave (Version 2.6.1.53, Agilent Technologies Inc.) and subsequently with Microsoft Excel (Version 16.43, Microsoft) and GraphPad Prism (9.0.0, GraphPad Software LLC). Results are reported as readings of extracellular acidification rate (ECAR) and oxygen consumption rate (OCR), which are used as correlates of glycolytic activity and oxidative phosphorylation respectively.

## 2.12 Statistical Analysis

Unless otherwise stated, all results are compared to equivalent values in unstimulated cells. Statistical analysis was performed in GraphPad Prism (Version 9.0, GraphPad Software LLC). Fold change (FC) was calculated by dividing results by the corresponding value for unstimulated cells. Specific statistical tests used are indicated in relevant figure legends. A detailed description of statistical methods employed for metabolomics analysis of monocytes is provided in Section 2.9.10. Significance levels are reported compared to unstimulated controls unless otherwise specified. Data are presented as mean ± (SEM). Significance labels in figures are indicated as follows: * = $p<0.05$; ** = $p<0.01$; *** = $p<0.001$; **** = $p<0.0001$. Non-significant findings are not labelled unless otherwise specified.

# Chapter 3: Optimisation of Parallel Immunologic Readouts for Metabolomic Profiling of Primary Monocytes

## 3.1 Introduction

To date, investigations of monocyte metabolism by LC-MS have been limited. In immunometabolic research, CD14+ cells are typically differentiated into macrophages (or DCs). Because primary monocytes have not received as much attention as their macrophage counterparts, less is known about their immunological or metabolic relevance in autoimmune disease. This project is designed to build on previous work from our group investigating monocytes in AAV [203, 238, 244]. Here CD14+ magnetic activated cell sorting (MACS) was chosen as the optimum monocyte isolation protocol in terms of cell purity and viability [244]. Monocyte isolation procedures are susceptible to functional and phenotypic variations [291, 292]. Cell sorting by flow cytometry can also alter the metabolic phenotype of cells [293]. These changes in monocyte physiology pose a challenge for measuring metabolic function. The lack of an appropriate monocyte cell model for AAV research further complicates these investigations [294]. Thus, the experimental protocols and relevant readouts to be incorporated must be carefully considered.

The power of high-quality metabolomics data increases massively when it can be integrated with additional biological readouts. Given the dynamic nature of metabolism, it is crucial to validate the findings of untargeted metabolomic investigations. A recent review [26] recommended coupling LC-MS metabolomics with multiple functional readouts. Sample readouts include cytokine production by ELISA, monitoring gene expression by transcriptomics or qRT-PCR, quantitative fluorescence- or luminescence-based measurements with metabolite assay kits, or flow cytometry/CyToF to assess changes in cell phenotype and function. Metabolomic sample preparation strategies that preserve DNA, RNA, and protein after metabolite extraction have also been developed to permit these subsequent analyses [295, 296]. Inhibition or synthesis gene knock-out of a specific metabolite and monitoring the changes in immune function can verify the importance of a given pathway. These experiments can be carried out *in vitro* or with appropriate animal models.

In this work our key immunological readout was cytokine production - primarily IL-1β secretion. This is a pro-inflammatory cytokine primarily produced by monocyte-lineage cells which has shown to be increased in autoimmune disease [297]. In

contrast to their macrophage counterparts, primary monocytes can release IL-1β following activation from a single signal using an alternative inflammasome pathway [121, 298]. Anti-MPO is one such stimulus that can induce IL-1β release from monocytes, an effect which was dependent on access to glucose [203, 238]. Further, IL-1β is a critical inflammatory mediator in murine AAV, and IL-1 receptor blocking protected these animals from severe glomerulonephritis [218]. Other key inflammatory cytokines produced by monocytes in response to ANCA include IL-6 and TNF-α. In macrophages cytokine production is closely linked to metabolism [7, 299]. The mechanisms surrounding cytokine production and release by ANCA are currently unknown and are beyond the scope of this work, but we do theorise them to be intimately linked to metabolism. Pro-inflammatory cytokine production is rapidly induced in ANCA-stimulated monocytes, with significant upregulation seen as early as 4 hours [226, 238, 240]. We theorise that early (and potentially pre-emptive) changes in metabolism are facilitating these pro-inflammatory responses.

Measuring rates of glycolysis and OXPHOS using Seahorse is a good 'litmus test' for the metabolic phenotype of immune cells. However, there are thousands of endogenous human metabolites which feed from these into more diverse and interconnected metabolic pathways. Many preliminary investigations of immune cell metabolism utilise the Seahorse analyser. This device measures real-time changes in oxygen consumption and extracellular acidification of live cells in real time [300]. These readouts are effectively surrogates for oxidative phosphorylation (OXPHOS) and glycolysis, respectively, two key pathways for immune cell metabolism [11]. Determining the metabolic preference of a given immune cell under specific conditions can give clues to their functional relevance. In the context of AAV, anti-MPO immediately increased rates of both OXPHOS and glycolysis in primary monocytes [238]. PR3-ANCA also increased cell metabolism through these pathways, but there were substantial kinetic differences to anti-MPO (see Figure 1.4.2). These metabolic disparities may account for the differences in inflammatory cytokine production between the two ANCA subtypes [203].

Seahorse-based analysis calls for specific experimental conditions which may create discordance with linked parallel experiments. A specific buffer-free media formulation is required for Seahorse experiments, and FBS cannot be added as it

can interfere with the accuracy of readouts. Cellular metabolomic investigations are sensitive to differences in cell media [301], and this may confound findings. In addition, suspension cells need to be adhered to the Seahorse plates, which significantly alters the cell matrix and requirements for metabolite extraction. To date, there have been no reports of sequential LC-MS analysis of cells measured using Seahorse. Silva *et al.* [88] showed slight differences in protein levels from directly extracted cells compared to those plated for experimental use. Availability of sufficient cell numbers, utility of parallel experiments, and the feasibility of measuring multiple physiological readouts simultaneously, must be carefully considered during experimental design. LC-MS analysis to profile the monocyte metabolome in response to ANCA stimulation is a logical next step to discern the specific metabolic pathways implicated. The aim of this chapter was to optimise immunological experiment protocols in ANCA stimulation, to ensure their compatibility with metabolomic analyses.

## 3.2 Aims & Methods

I. To define optimum cell culture conditions and experimental protocols for ANCA stimulation of primary monocytes.

II. To investigate pilot immunologic readouts in ANCA-stimulated monocytes.

III. To optimise additional immunologic and metabolic experimental readouts for parallel analysis with LC-MS.

### 3.2.1 Experimental Methods

The experiments described in this chapter follow the general paradigm of monocyte isolation and stimulation described in Section 2.2. Modifications to this protocol were trialled including the use of priming agents, polyclonal IgGs, donor blood sources, and metabolic/immunologic inhibitors. Attempts to combine immunological and metabolic/metabolomic experiments are also described. Antibodies used for flow cytometry experiments in Sections 3.3.12 and 3.3.13/14 are shown in Tables 3.2.1 and 3.2.2, respectively. Precise details of these alterations are described in the appropriate sections and figure legends.

| Target Antigen | Fluorochrome | Clone | Species Targeted | Product Code | Company |
|---|---|---|---|---|---|
| CD14 | PE-Vio770 | TÜK4 | Human | 130-096-628 | Miltenyi Biotec |
| MPO | PE | 2C7 | Human | MCA1757PE | Bio-Rad Laboratories Inc |
| PR3 | FITC | PR3G-2 | Human | ab65255 | Abcam |
| Fixable Viability Dye | eFluor450 | N/A | Human | 65-0863-14 | eBioscience™ |

**Table 3.2.1: Flow Cytometry Antibodies used for Monocyte Staining in the Secondary Metabolomic Profiling Cohort.** See Section 3.3.12.

| Target Antigen | Fluorochrome | Clone | Species Targeted | Product Code | Company |
|---|---|---|---|---|---|
| CD14 | PE-Vio770 | TÜK4 | Human | 130-096-628 | Miltenyi Biotec |
| MPO | PE | 2C7 | Human | MCA1757PE | Bio-Rad Laboratories Inc |
| CD54 | APC | REA266 | Human | 130-103-910 | Miltenyi Biotec |

**Table 3.2.2: Flow Cytometry Antibodies used for Monocyte Surface Staining for Assessment of MPO Expression and IL-1β Production and CD54 Expression.** See Sections 3.3.13 & 3.3.14.

## 3.3 Results

### 3.3.1 Monocyte Source can Affect Inflammatory Effector Functions

Interpersonal variation can affect biological readouts, as can blood collection and storage protocols. We compared the functionality of primary monocytes isolated from two sources: IBTS buffy coats and fresh blood from haemochromatosis patients attending St. James' Hospital. Fresh blood monocytes produced more IL-1β in response to anti-MPO stimulation than buffy coats (Figure 3.3.1). This effect was seen at both 4- and 18-hours post-stimulation. Surprisingly, LPS did not induce significant changes in IL-1β production at either timepoint. After 4 hours of stimulation the blood source was a small (6.06%) but significant source of variation ($p=0.0356$). This effect was lost at 18 hours, but an interaction between blood source and treatment did emerge (10.91% of variation, $p=0.0493$). Given the enhanced inflammatory response to anti-MPO and the other logistical benefits, fresh blood was selected as the blood source for metabolomic profiling experiments.

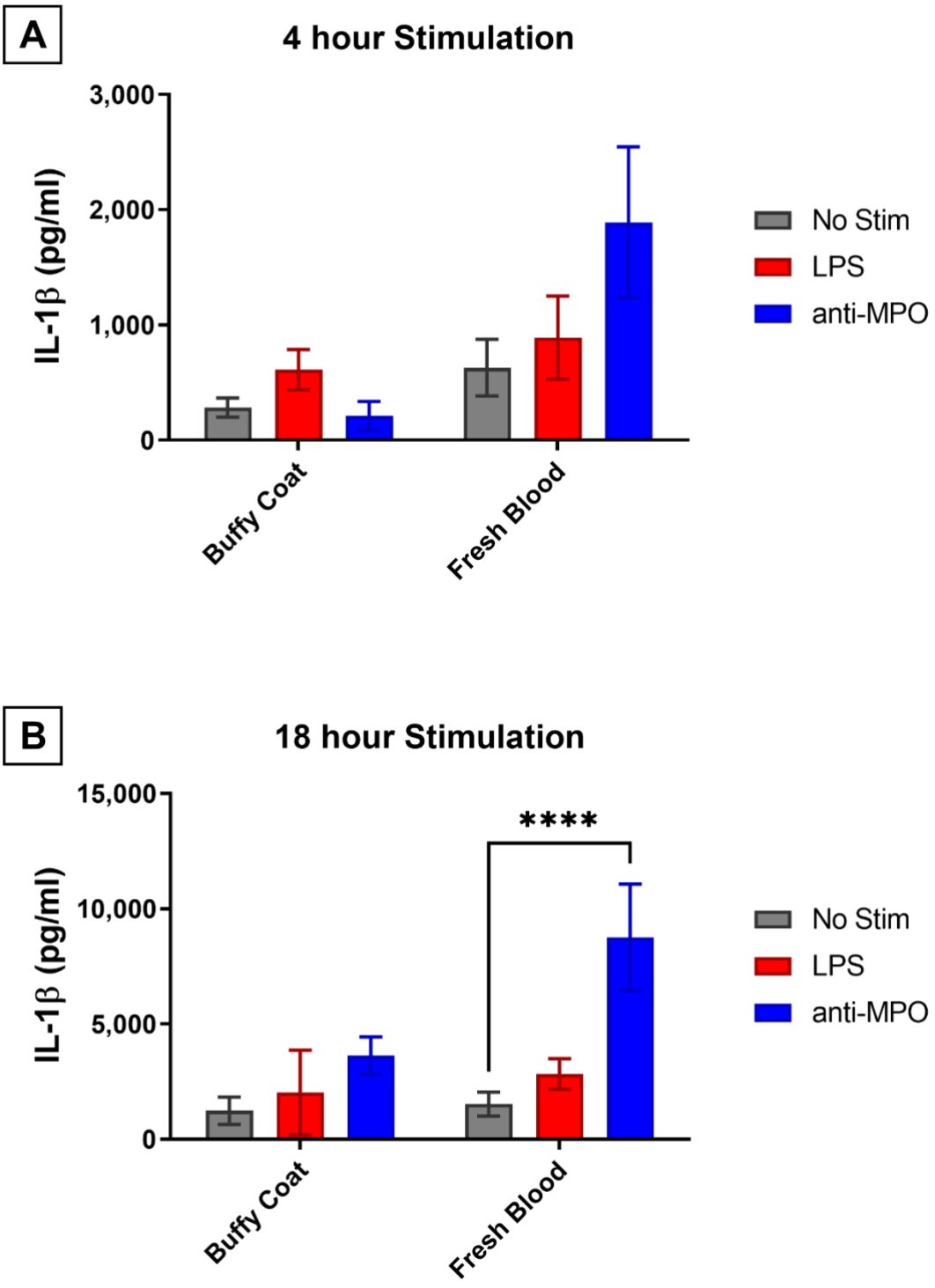


**Figure 3.3.1: Comparison of Buffy Coat and Fresh Blood Monocyte IL-1β Production after 4- and 18-hour Stimulation.** CD14+ monocytes were isolated from PBMCs by MACS separation using blood collected from buffy coats (n=8) or haemochromatosis patients (fresh blood, n=13). Cells were plated and stimulated @37°C for 4 (A) or 18 hours (B) with 5µg/ml monoclonal anti-MPO or 200ng/ml LPS. IL-1β production was measured in the supernatant by ELISA. Results from each timepoint were analysed by 2-way ANOVA and Dunnett's multiple comparisons test. Results are plotted as mean ± standard error of the mean (SEM).

### 3.3.2 Optimising Conditions for CD14+ MACS Monocyte Isolation

Previous work from our group compared different isolation techniques for assessing primary monocytes function upon ANCA stimulation [244]. CD14+ positive magnetic activated cell sorting (MACS) isolation was determined to be the superior technique based on cell purity and viability. Manufacturer's instructions recommend resuspending thrice-washed PBMCs in 80µl of buffer per $10^7$ total cells and adding 20µL of CD14 MicroBeads per $10^7$ total cells. Given the large cell volumes available from buffy coats and fresh blood samples, these recommendations can be incredibly wasteful. We sought to determine an optimum ratio of magnetic beads to cell buffer suspension for maximised CD14+ monocyte yield. We determined that a lower volume of magnetic beads was required when the ratio of magnetic beads to cell buffer suspension was high (Figure 3.3.2). The volume of cell suspension did not influence cell yield. Reducing the volume of magnetic beads used also allows for additional replicates to be completed. We determined that a 1:30 ratio of magnetic beads to cell buffer suspension was optimal. Full details of the cell isolation protocol can be found in Section 2.2.3

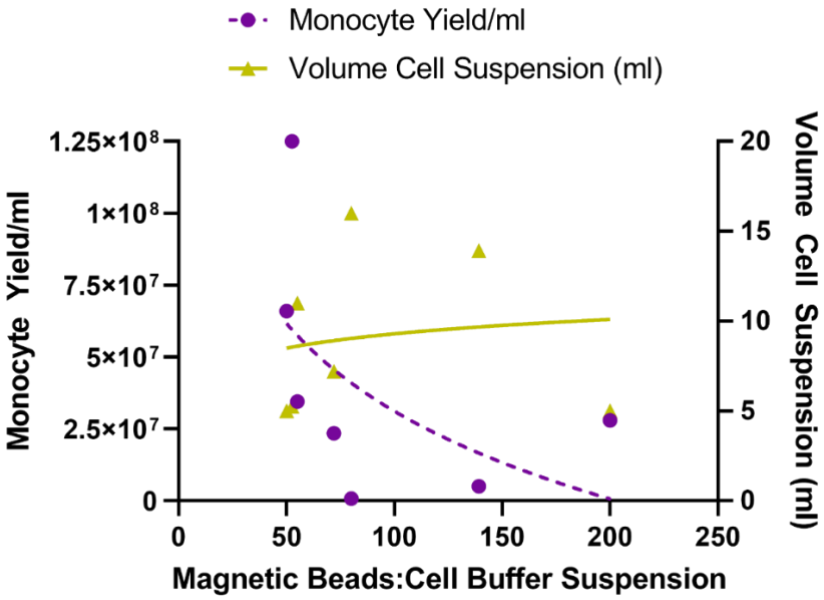


**Figure 3.3.2: Optimising Conditions for CD14+ MACS Monocyte Isolation.** PBMCs were isolated from buffy coats using CD14+ positive magnetic activated cell sorting (MACS) isolation. Different CD14 magnetic bead:cell buffer suspension ratios were trialled to maximise monocyte yield. Monocyte yield is plotted on the left Y axis (purple) and the total volume of cell suspension on the right Y axis (gold). More concentrated ratios improved monocyte yield regardless of total cell suspension volume. Best-fit lines were plotted by simple linear regression with a semi-log line.

### 3.3.3 Comparison of 6- and 24-Well Plates for Monocyte Stimulation and Metabolomic Analysis

A higher cell number is an advantage in cellular metabolomic analyses as it increases the levels of low abundance metabolites that can be detected above background. To achieve the required cell numbers for metabolomic analysis the 96-well format needed to be scaled up. Keeping the concentration of $1x10^6$ cells per ml consistent we compared the utility of 6- and 24-well plates using 5ml and 1ml of cells, respectively (Figure 3.3.3). Overall, there were significant differences between treatment conditions (p=0.0181). Unstimulated cells in the 6-well plate had higher background IL-1β production than 24-well. Activation of these monocytes with LPS did not induce the expected increase in IL-1β, likely due to this high background. As is common with investigations of primary cells there was a high degree of interpersonal variation between donors. Despite the 24-well format also not returning significant results with LPS activation, the lower background makes this configuration preferable. Both plate formats were adaptable to the optimised metabolite extraction protocol (see Section 2.9.2 and Chapter 3). Given the activated baseline microenvironment apparent in the 6-well format we opted to use the 24-well format for metabolomic profiling experiments.

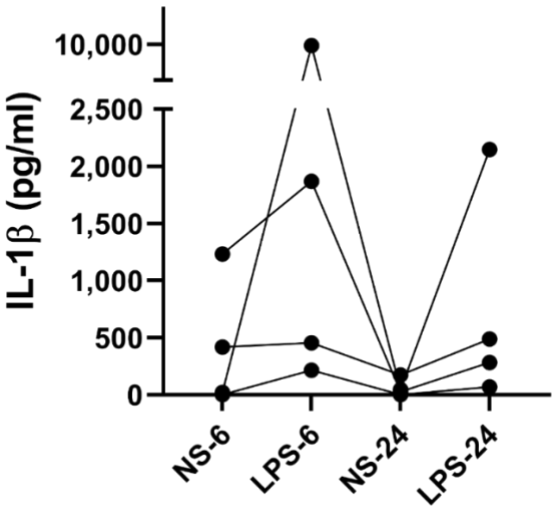


**Figure 3.3.3: Comparison of 6- and 24-Well Plates for Monocyte Stimulation and Metabolomic Analysis.** CD14+ monocytes (n=4) were isolated from the PBMCs of healthy controls by MACS separation. Primary monocytes were plated in 6- and 24-well plates in 5ml or 1ml RPMI at a concentration of $1x10^6$/ml. Cells were stimulated for 4 hours with 200ng/ml LPS and IL-1β production was measured in cell supernatants by ELISA. Results for individual donors are plotted under different conditions and linked by a straight line. Differences between conditions were compared using Friedman's test.

### 3.3.4 Polyclonal IgG Preparations from AAV Patients do not Induce Pro-Inflammatory Cytokine Production as Commercial Monoclonals do

Many investigations of the effects of ANCAs on innate immune cells use polyclonal IgG preparations from AAV patients. We investigated the use of an in-house prepared cohort of IgG preparations; four ANCA negative or anti anti-glomerular basement membrane (GBM), four MPO-ANCA, and four PR3-ANCA. First comparing 25 and 250μg/ml IgG stimulations (Figure 3.3.4A), we found no significant difference between either concentration in terms of IL-1β production. 250μg/ml IgG is more frequently used in the literature and was used in subsequent stimulations to maintain consistency with these peer-reviewed protocols. Next, we examined the utility of TNF-α priming for polyclonal IgG stimulation. TNF-α priming did not enhance IL-1β production in IgG-stimulated primary monocytes after 4- or 18-hour stimulation (Figures 3.3.4B and C, respectively). In many cases TNF-α actually limited IL-1β production, in both monoclonal and polyclonal stimulations. There was no significant increase in IL-1β production at either timepoint, for MPO-ANCA or PR3-ANCA, with or without TNF-α, though there was for monoclonal anti-MPO stimulation. Given these findings we opted to continue our investigations using monoclonal ANCA antibodies without TNF-α priming.

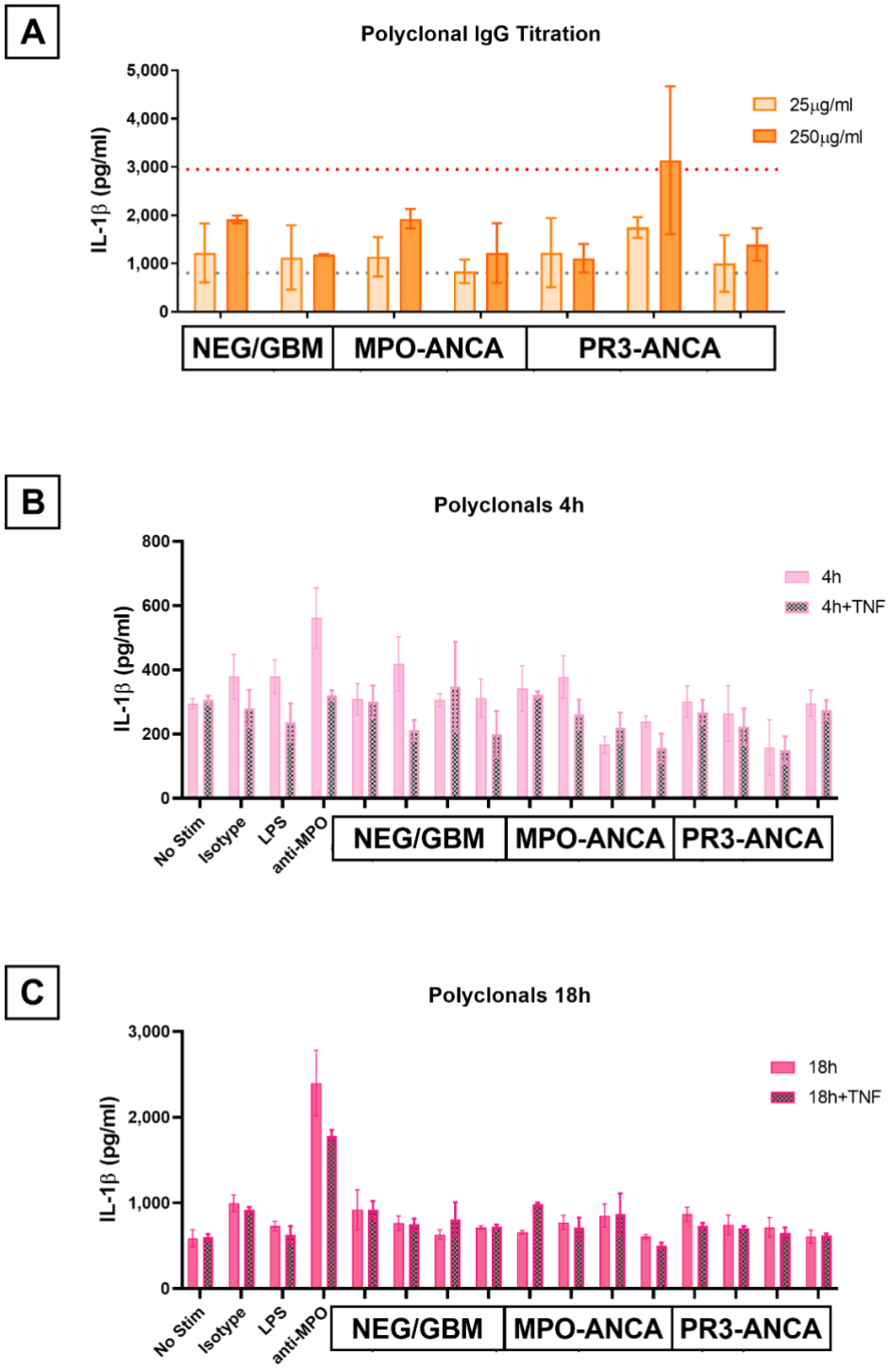


**Figure 3.3.4: IL-1β Production from Polyclonal AAV Patient IgG Preparations.** CD14+ monocytes were isolated from the PBMCs of healthy controls by MACS separation. Primary monocytes were stimulated with 5μg/ml monoclonal anti-MPO or polyclonal IgG preparations from AAV patients (MPO- and PR3-ANCA). 25 and 250μg/ml IgG stimulations were compared to unstimulated (grey dotted line) and LPS-stimulated cells (red dotted line, A). 250μg/ml IgG stimulation was examined with and without 2ng/ml TNF-α priming for 4 (B) or 18 hours (C). IL-1β production was measured in cell supernatants by ELISA and compared to unstimulated cells. Results are plotted as mean ± standard error of the mean (SEM).

### 3.3.5 LPS Priming Enhances IL-1β Production in anti-MPO-Activated Monocytes

Investigations of ANCA function in neutrophils typically adopt a TNF-α priming step. However, previous work from our group (and in Section 3.3.4 above) has shown that this does not enhance pro-inflammatory cytokine production in monocytes [244]. We hypothesised that LPS would be a better priming agent for these cells, given its well-defined role in pro-inflammatory monocyte responses. Indeed, when monocytes were primed with a low dose of LPS (2ng/ml – the concentration of TNF-α traditionally used for neutrophils) prior to ANCA stimulation, the levels of secreted IL-1β surpassed that of high-dose LPS alone (Figure 3.3.5). This effect was only seen with anti-MPO stimulation, and not with anti-PR3. The majority of IL-1β production from primed PR3-treated cells came from the priming LPS (pLPS). We also did not see any increase in IL-1β secretion using TNF-α for cell priming. This synergistic effect of LPS and anti-MPO may explain why ANCA flares typically occur after bacterial infections. Further work is needed to discern the contributions of these two stimuli independently to determine their role in ANCA-induced inflammation.

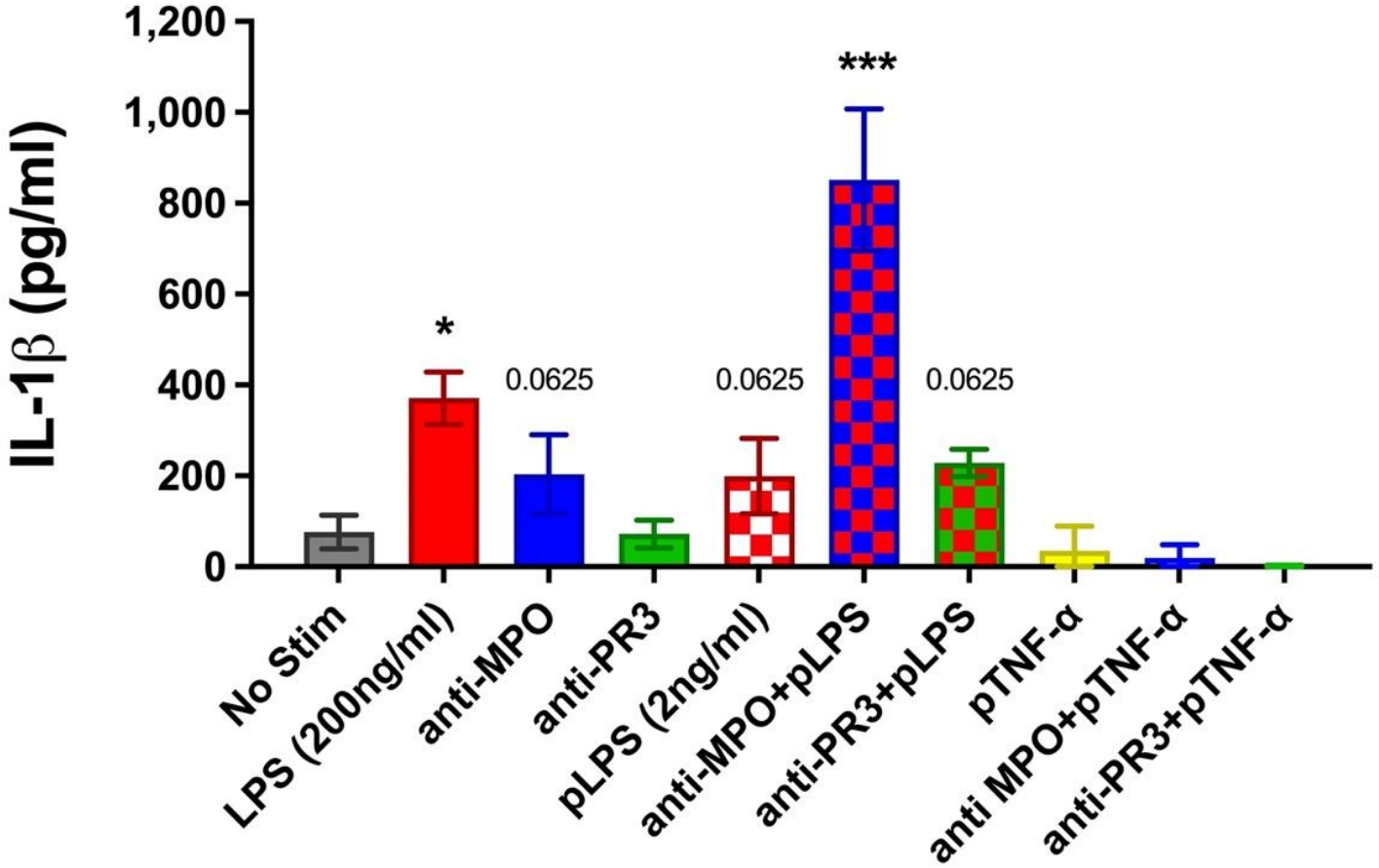


**Figure 3.3.5: Effects of LPS and TNF-α Priming on IL-1β Production in ANCA-Stimulated Monocytes.** CD14+ monocytes were isolated from the PBMCs of healthy controls (n=6) by MACS separation. Primary monocytes were pre-treated with 2ng/ml LPS (pLPS) or 2ng/ml TNF-α (pTNF-α) as indicated for 30 mins before being stimulated with 5μg/ml monoclonal antibody (mAb) directed against MPO or PR3 for 4 hours. IL-1β production was measured in cell supernatants by ELISA and compared to unstimulated cells. Results are plotted as mean ± standard error of the mean (SEM) and analysed by Friedman's ANOVA.

### 3.3.6 Sodium Azide ($NaN_3$) Does Not Affect Inflammatory Responses in Primary Monocytes at Low Concentrations

Sodium azide ($NaN_3$) is a chemical preservative used to prevent bacterial contamination in aqueous laboratory reagents. Our monoclonal anti-MPO and anti-PR3 antibodies are stored in 0.09% and 0.05% $NaN_3$, respectively. Sodium azide has been shown to influence monocyte function at high concentrations (≥10mM). To confirm that this is not the case in this work and that we are preserving the ANCA-specific effects in our results we assessed the impact of $NaN_3$ on IL-1β production. $NaN_3$ preparations of various concentrations were prepared using PBS and used to stimulated primary monocytes (n=3). None of the $NaN_3$ preparations significantly altered IL-1β levels (Figure 3.3.6A). Addition of $NaN_3$ to the experimental system did have a small net negative effect on IL-1β production. Furthermore IL-1β production did not correlate with concentrations of $NaN_3$ (Figure 3.3.6B). We can conclude that the concentration of $NaN_3$ consequentially found in our experiments does not significantly influence inflammatory responses in primary monocytes. Additional experiments with LPS stimulation may confirm this.

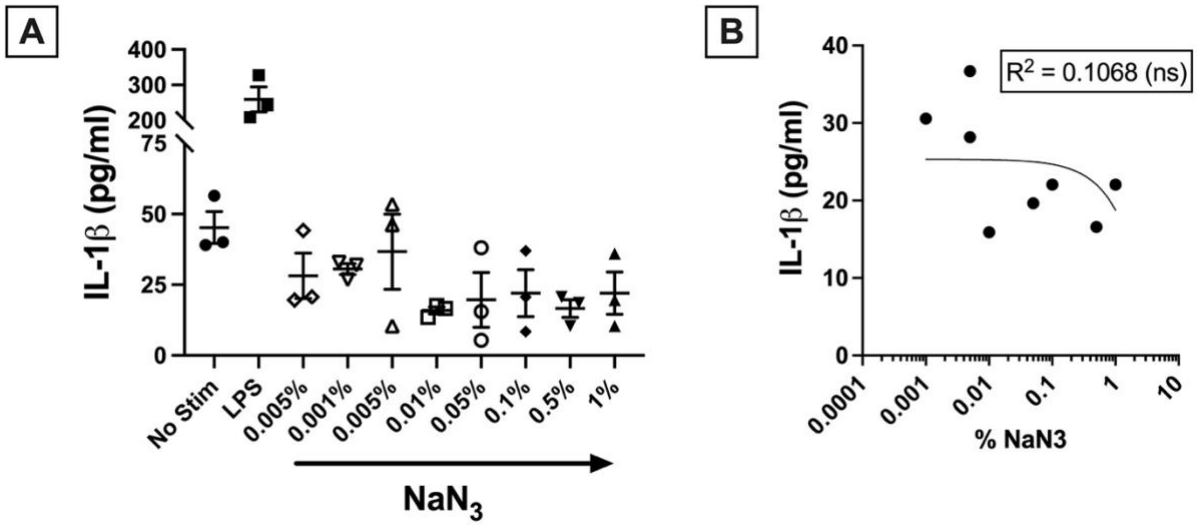


**Figure 3.3.6: Sodium Azide ($NaN_3$) Does Not Affect Inflammatory Responses in Primary Monocytes at Low Concentrations.** CD14+ monocytes (n=3) were isolated from the PBMCs of healthy controls by MACS separation. Primary monocytes were stimulated with various concentrations of sodium azide ($NaN_3$) for 4 hours and IL-1β production was measured in cell supernatants by ELISA (A). Results are plotted as mean ± standard error of the mean (SEM). IL-1β production was compared to $NaN_3$ concentration and a titration curve prepared by Pearson correlation (B).

### 3.3.7 Metabolomic Differences Between ANCA- and LPS-Stimulated Monocytes are Limited at 24h in a Pilot Analysis

The number of peer-reviewed publications investigating monocyte metabolomics is limited, however the majority involve a 24-hour stimulation [96, 97, 124, 302]. Targeted analysis of metabolites included in the synthetic standard mix (see Section 2.9.2.2) was carried out on ANCA- and LPS- treated monocytes in a small cohort (n=3) as described in Section 2.9.5. 32 of the 53 metabolites in the mixture were detected in experimental and PooledQC replicates. Statistical analysis was performed after normalising of the data to residual protein content as outlined in Chapter 4. Using these 32 metabolites, Principal Component Analysis (PCA) plots were generated for the four treatment groups – unstimulated cells (NS, negative control), LPS (positive control) anti-MPO and anti-PR3 – and PooledQC samples. There was moderate separation of treatment groups evident from the PCA plot (Figure 3.3.7A). Unstimulated (grey) and LPS-treated (red) monocytes clustered together and separately from one another, but still overlapped with other treatment groups. The anti-PR3 group (green) clustered relatively well, but the anti-MPO stimulated cells (blue) were more variable. PooledQC samples did cluster very well together off-centre of the PCA plot (purple), indicating good intra-run consistency. Normalised metabolite abundances are plotted in Figure 3.3.7B. There are no uniform alterations evident in any one treatment group, likely owing to the small sample size. Metabolites highlighted in red – 4-hydroxy-L-proline, serine, threonine, and tyrosine – were significantly altered across treatment groups as measured by ANOVA. These results should be considered with caution as the small sample size may not be entirely reflective of ANCA-induced metabolism. To maintain consistency with previously established protocols [238] we opted to profile monocyte metabolism at 4 hours for future experiments. There have been some metabolic changes detected in monocytes at this early timepoint [85], but this work would address a substantial gap in the knowledge base of monocyte metabolism and allow us to explore the inchoate metabolic changes that drive the rapid and diverse inflammatory responses in these cells.

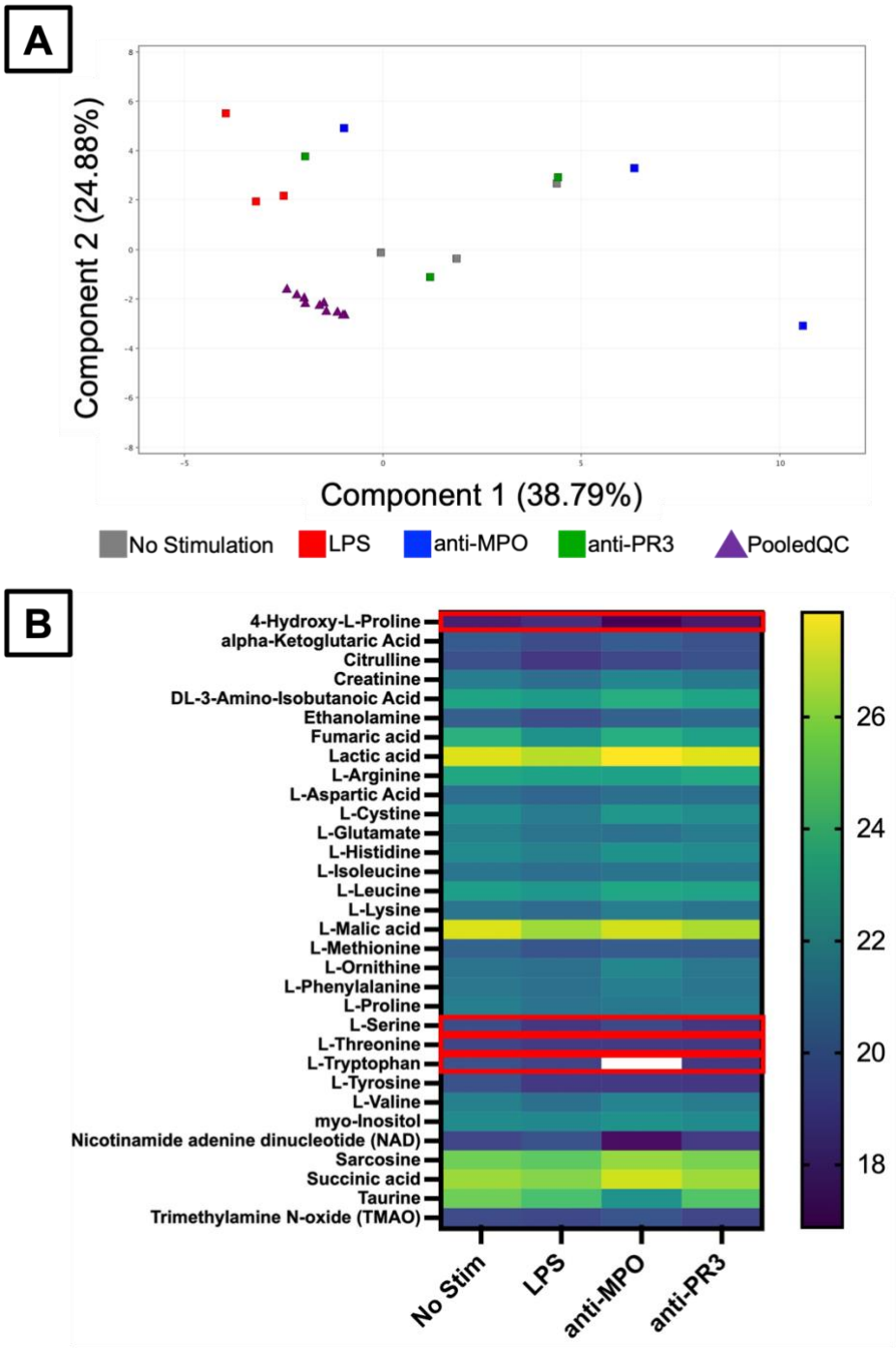


**Figure 3.3.7: Pilot Metabolomic Heatmap Analysis of Targeted Metabolites in ANCA- and LPS-Stimulated Monocytes.** CD14+ monocytes (n=3) were isolated from PBMCs of healthy controls by MACS separation (n=3). Cells were plated and stimulated @37°C for 24 hours with 5µg/ml monoclonal antibody (mAb) directed against MPO, PR3, or 200ng/ml LPS. ANCA- and LPS-stimulated monocytes were analysed by LC-MS and targeted metabolomic analysis of 53 metabolites was completed. 32 of the 53 metabolites were detected in experiment samples. Principal Component Analysis (PCA) plots were generated for the four treatment groups (NS, LPS, anti-MPO, and anti-PR3) and PooledQC samples (A). Median intergroup values are displayed as BCA and $\log_2$ normalised AUCs (B).

### 3.3.8 Increased Rates of Glycolysis Correlate with Increases in Intracellular Amino Acids

In a pilot metabolomics investigation, we stimulated primary monocytes with ANCA and measured intracellular amino acid content by LC-MS. The stimulated cells were also analysed in a parallel Seahorse experiment using a Seahorse XF Glycolysis Stress Test (Figure 3.3.8A). This assay quantifies glycolytic function in cells by measuring the extracellular acidification rate (ECAR). Fold change in glycolysis/ECAR was calculated by dividing the average ECAR after addition of glucose (measurements 4-6) by the average ECAR from the basal state (measurements 1-3), then dividing results for treatment groups by the paired unstimulated cells (NoStim). A number of amino acids were significantly increased in lysates of ANCA-stimulated monocytes. The concentrations of these metabolites were analysed for potential correlations with the average rates of glycolysis in treated cells. Twelve amino acids were reliably detected by LC-MS methods, and intracellular concentrations of several of them correlated with the increased rates of glycolysis in the corresponding treatment groups (Figure 3.3.8B). In each instance, anti-MPO treated cells showed the highest rates of glycolysis, followed by anti-PR3 and isotype control. Serine showed the strongest linear correlation with an $R^2$ of 0.9904 (p=0.0048). Threonine ($R^2$=0.9261, p=0.0377) and phenylalanine ($R^2$=0.9477, p=0.0265) levels also significantly correlated with glycolysis although these associations better suited a hyperbolic trajectory. L-arginine also showed a slightly more modest hyperbolic correlation of 0.8939 which approached significance (p=0.0545). These findings suggest that the increase in glycolysis drives serine, threonine, and phenylalanine anabolism. These metabolites did not correlate with increases in cytokine production (data not shown), thus their role in driving ANCA-induced inflammation remains to be determined.

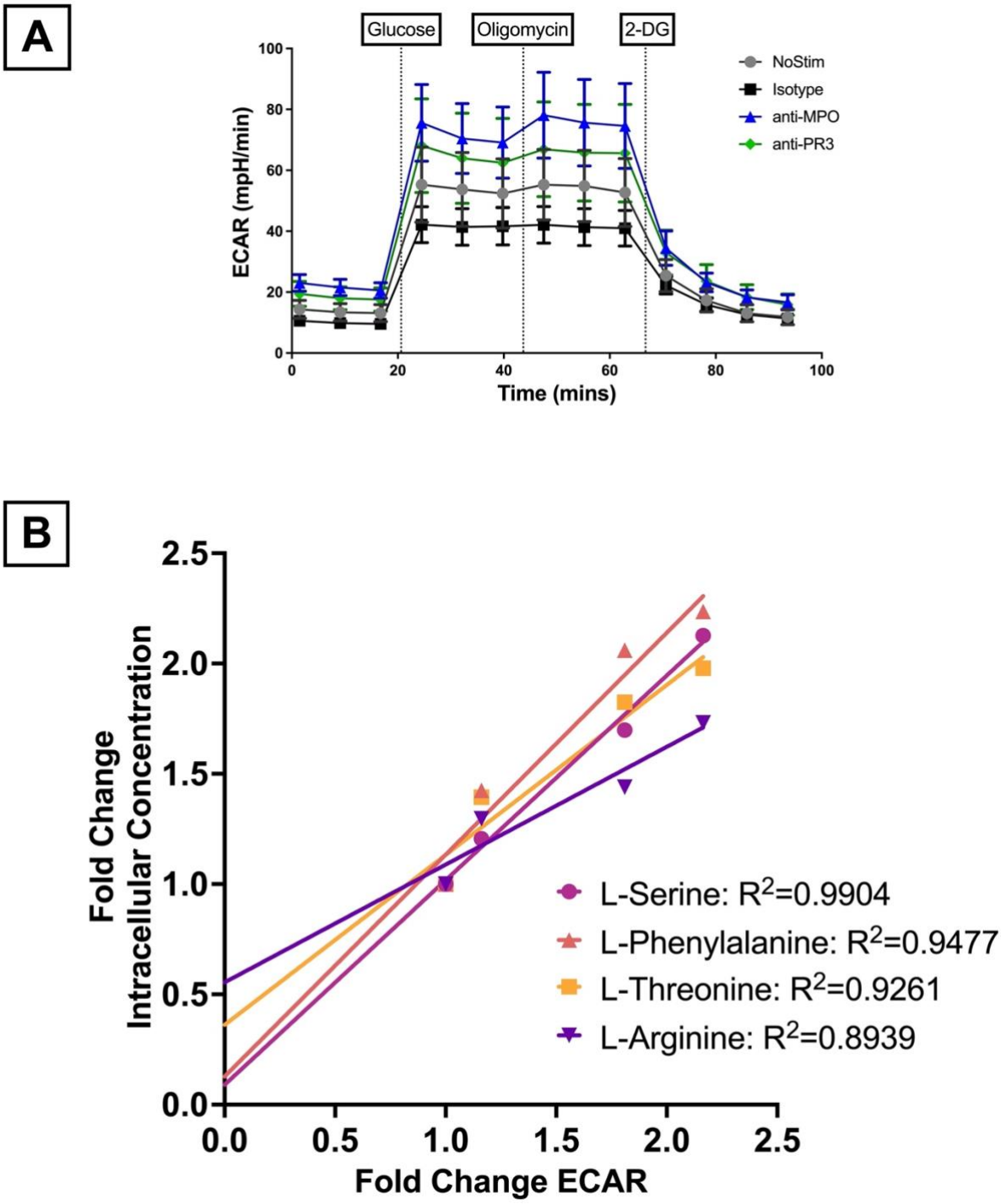


**Figure 3.3.8: Correlations of Intracellular Amino Acid Levels with Rates of Glycolysis in ANCA-Stimulated Monocytes.** CD14+ monocytes (n=3) were isolated from the PBMCs of healthy controls by MACS separation. Cells were plated and stimulated @37°C for 4 hours with 5µg/ml monoclonal antibody (mAb) directed against MPO, PR3, or IgG isotype control. Glycolysis (ECAR) was measured by Seahorse XF Glycolysis Stress Test (A), and intracellular amino acid concentrations were measured in a parallel experiment by LC-MS. Fold changes were calculated relative to unstimulated cells and relationships assessed by Pearson correlation and linear regression (B).

### 3.3.9 Inhibition of Serine Production Abrogates IL-1β Production in Primary Monocytes

Given the relationship between serine production and glycolysis in ANCA-stimulated monocytes we next investigated if this was linked to IL-1β production. CBR-5884 inhibits 3-phosphoglycerate dehydrogenase (PHGDH) – the first step of the *de novo* serine synthesis pathway which directly branches off from glycolysis [303]. We first determined which concentration of CBR-5884 most effectively inhibited IL-1β production in monocytes. Primary monocytes isolated from healthy blood were pre-treated with CBR-5884 of varying concentrations and incubated for 4.5 hours. IL-1β production was inhibited in a dose-dependent manner down to 50μM (Figure 3.3.9A). At lower concentrations the inhibition effect was inconsistent. All inhibitory effects of CBR-5884 were lost when cells were incubated for 18 hours (Figure 3.3.9B). When cells were stimulated with and without serine inhibition, the effect of CBR-5884 became even more apparent. Inhibiting serine production with CBR-5884 for 30 mins prior to (4h) stimulation completely abrogated IL-1β production (Figure 3.3.9C). In this small cohort anti-MPO did not induce a significant increase in IL-1β levels as was shown previously. These data suggest that CBR-5884 can inhibit IL-1β production by limiting serine synthesis.

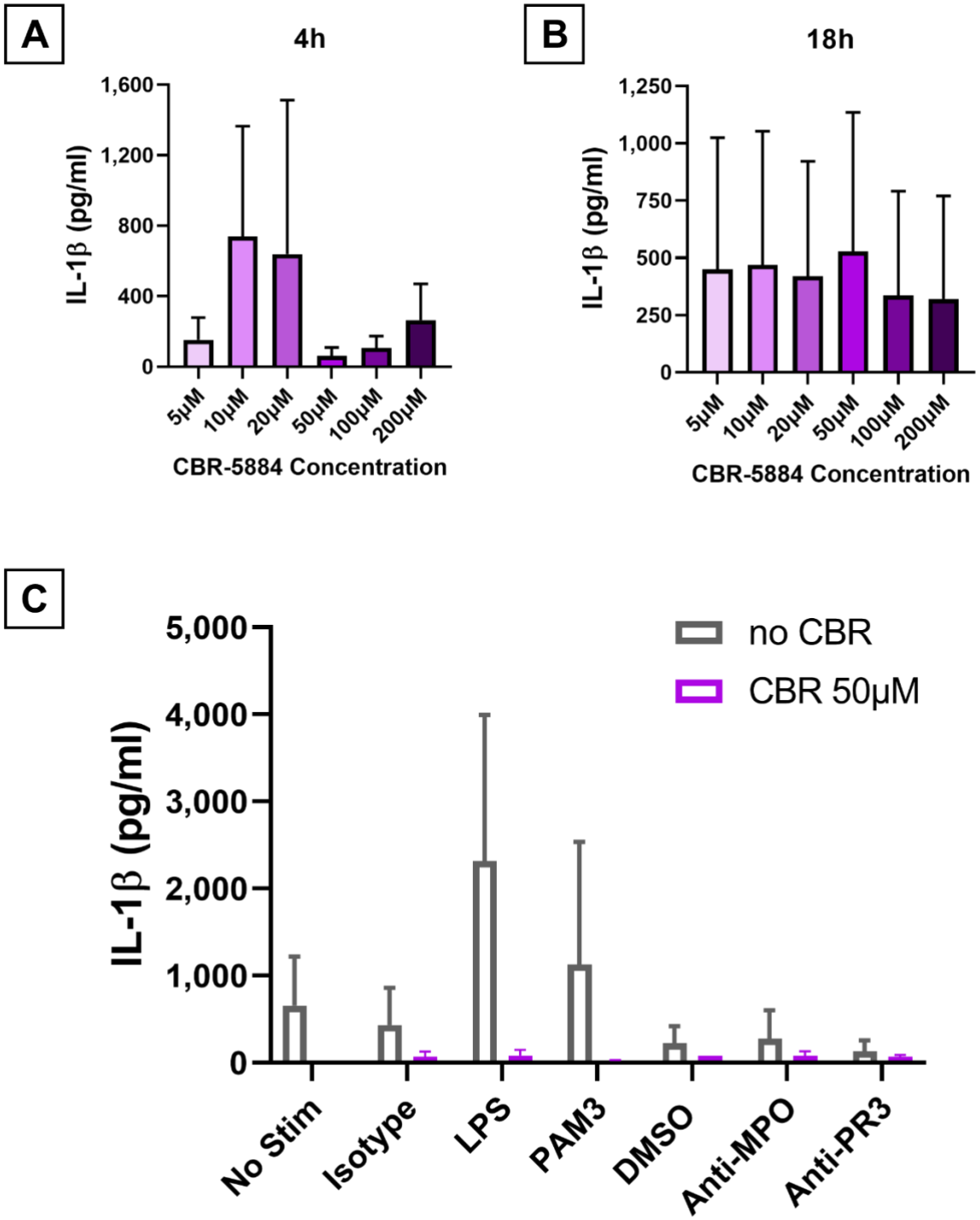


**Figure 3.3.9: Effects of Serine Synthesis Pathway Inhibition on IL-1β production in ANCA-Stimulated Monocytes.** CD14+ monocytes were isolated from the PBMCs of healthy controls by MACS separation. Primary monocytes were pre-treated with CBR-5884 of varying concentrations for 30 mins before being stimulated with 200ng/ml LPS for 4 (A) or 18 hours (B). IL-1β production was measured in cell supernatants by ELISA. IL-1β secretion was compared for cells pre-treated with (and without) 50μM CBR-5884 for 30 mins and stimulated for 4 hours with 200ng/ml LPS, or 5μg/ml monoclonal antibody (mAb) directed against MPO or PR3 (n=3, C). Results are plotted as mean ± standard error of the mean (SEM).

### 3.3.10 Attempted Recovery of Primary Monocytes from Seahorse Assay Plates for Subsequent Metabolomic Analysis

Seahorse analysis measures metabolic changes in real-time, while cellular metabolomics provides a deeper snapshot of the metabolic state of the cell at a fixed point in time. To complement our primary LC-MS metabolomic profiling experiments, we attempted to extract metabolites from Seahorse assay plates after stimulation. Seahorse plates were prepared and analysed as described in Section 2.11 and stimulated for 4 hours with different concentrations of LPS as indicated. Immediately following Seahorse analysis, cells were placed on wet ice and 100µl 80% MeOH @-20ºC was added to each well. Cells were gently scraped and removed with gentle pipetting. Replicates were combined for a total of $3x10^6$ cells per condition. Cells were subjected to the optimised metabolite extraction protocol described in Section 2.9.2 and residual protein content of the metabolite fraction (MF) measured by BCA as outlined in Section 2.5. Protein levels were compared to those in the metabolite fraction of PBMCs from experiments described in Section 4.2.3. Using this modified extraction protocol, we measured protein content in metabolite (Figure 3.3.10A) and cell pellet fractions (Figure 3.3.10B) to see if concentrations were consistent with expected levels. The metabolite fraction levels were above those expected for the same cell numbers measured by direct extraction (dotted line) but were similar to the blank samples. Conversely cell pellet protein measurements fell far below expected values and were lower than those of the metabolite fraction. For both fractions (particularly MF) the blank readings were on par with treated cells, which may indicate contamination coming from the Cell-Tak. Further optimisation of cell recovery from Seahorse plates is needed if these samples are to be viable for any subsequent analyses.

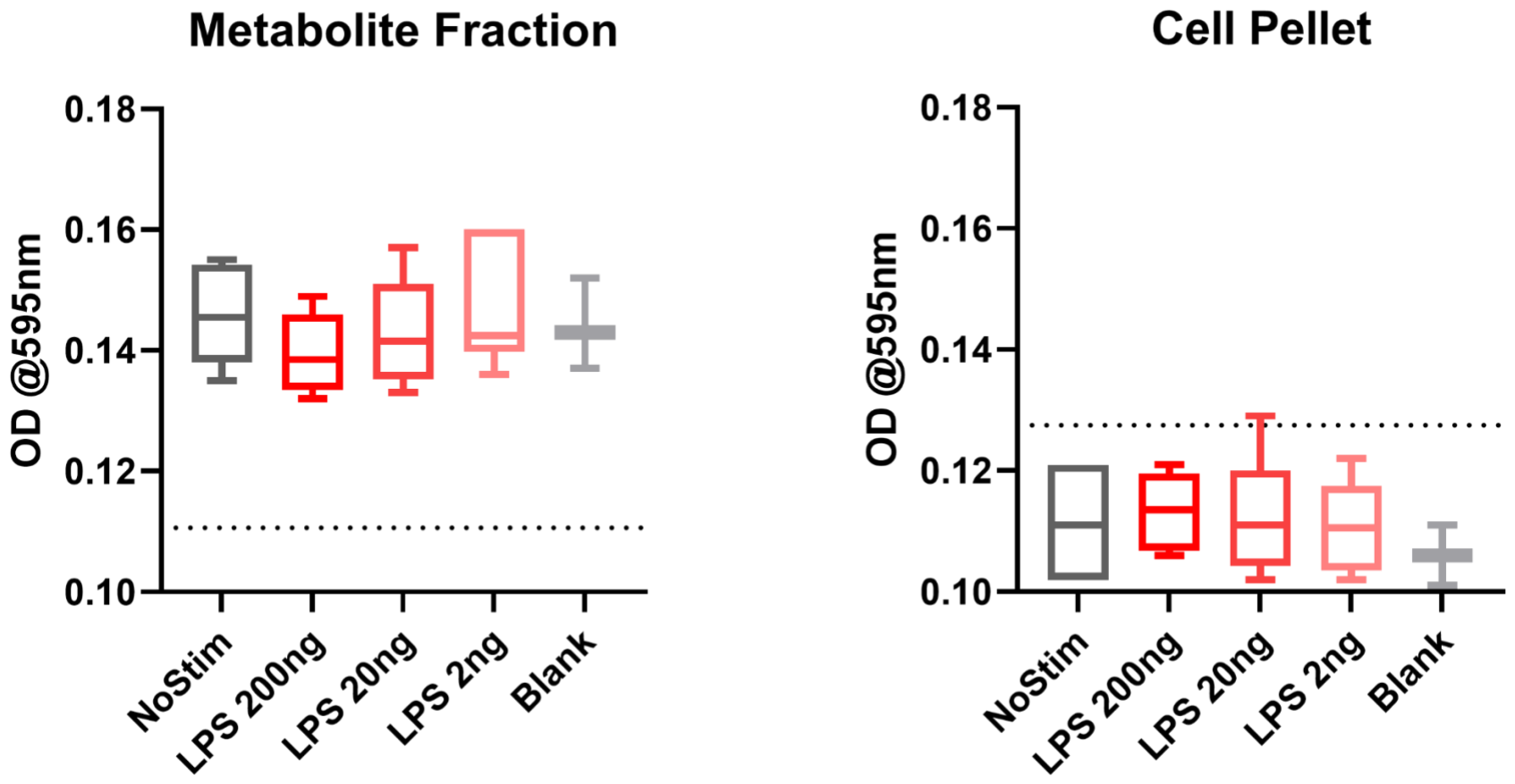


**Figure 3.3.10: BCA Analysis of Primary Monocytes Recovered from Seahorse Assay Plate.** CD14+ monocytes (n=6) were isolated from healthy donors and analysed by stimulated with varying concentrations of LPS for 4 hours in a Seahorse analyser. 80% MeOH was added directly to assay plates and combined replicates were centrifuged to separate metabolite fraction (A) and cell pellet (B). Both fractions were analysed by BCA assay to determine protein content as compared to $3x10^6$ directly extracted cells.

### 3.3.11 Investigation of Effects of MPO inhibition on Cytokine Production in Primary Monocytes

Inhibition of MPO activity has been proposed as an anti-inflammatory treatment strategy for AAV [197, 304]. We investigated the use of the MPO inhibitor 4-aminobenzoic acid hydrazide (4-ABAH) on ANCA-induced IL-1β production. Despite inconsistent results, 100μM brought about the greatest reduction in IL-1β levels, despite not reaching significance (Figure 3.3.11A). This is well above the IC50 value of 0.3μM, but consistent with concentrations used *in vitro* [305]. When cells were stimulated with and without MPO inhibition we see that 4-ABAH completely abrogates the effects of LPS- and (to a lesser extent) anti-MPO-induced IL-1β secretion (Figure 3.3.11B). In this small pilot experiment anti-MPO did not induce a significant increase in IL-1β as was shown previously. These data suggest that inhibition of MPO activity with 4-ABAH can limit IL-1β production in LPS-stimulated monocytes. Additional experimental replicates are needed to confirm if this is the case for ANCA-induced cytokine production.

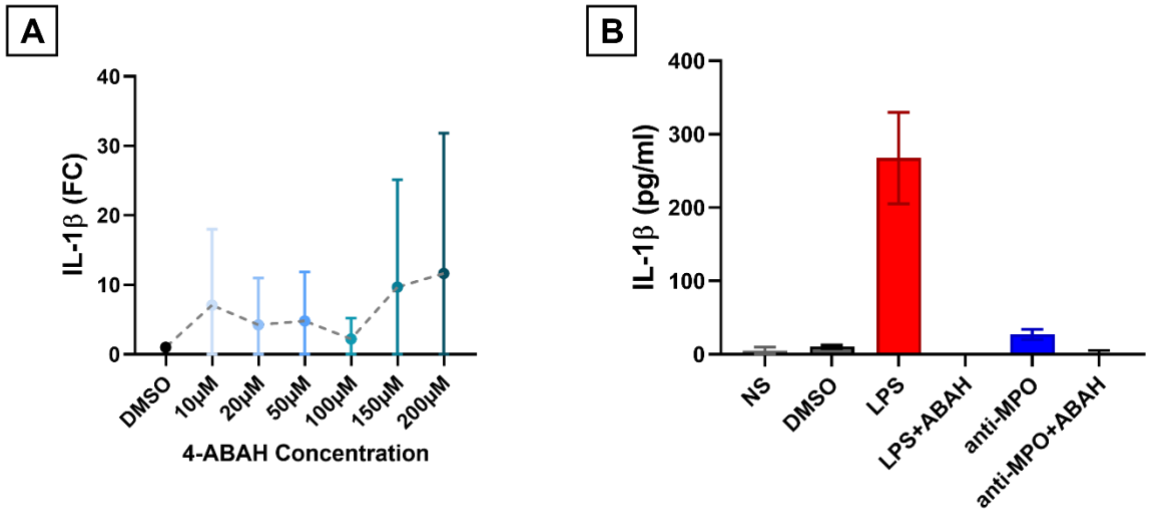


**Figure 3.3.11: Effects of MPO Inhibition on IL-1β production in Activated Monocytes**. CD14+ monocytes (n=3) were isolated from the PBMCs of healthy controls by MACS separation. Primary monocytes were treated with varying concentrations of the MPO inhibitor 4-Aminobenzoic Acid Hydrazide (4-ABAH) for 4 hours (A). IL-1β production was measured in cell supernatants by ELISA. Cells were subsequently pre-treated with 100μM 4-ABAH for 30 mins before being stimulated for 4 hours with 200ng/ml LPS, or 5μg/ml monoclonal antibody (mAb) directed against MPO or PR3 (n=3, B).

### 3.3.12 MPO and PR3 are Differentially Expressed in Mixed Leukocyte Populations and Isolated Monocytes and Correlate with Donor Age

In the Secondary metabolomic profiling cohort (see Chapter 5) additional flow cytometry experiments were carried out on dextran sedimented cells and isolated monocytes. The dextran sedimented cells are a mixed population of leukocytes – including neutrophils – deplete of red blood cells, and are representative of whole blood. Cells were prepared and stained as described in Section 2.8 and fluorochromes used are shown in Table 3.2.1. The percentage of MPO+ and PR3+ cells were calculated using fluorescence-minus-one controls for the dextran and monocyte fractions respectively (Figure 3.3.12A and 3.3.12B). CD14+ cells were identified from dextran fractions and represented 5.79% (±1.83%) of total dextran cells. There was substantial variation in MPO and PR3 expression among donors, accounting for 54.80% and 28.13% of total variation in the dextran and monocyte fractions, respectively. There was no significant difference in MPO and PR3 expression in the dextran fraction. Isolated monocytes however showed significantly higher PR3 expression than MPO (Figure 3.3.12B) with >95% PR3+ cells in all donors. The percentages of both MPO+ and PR3+ monocytes increased after monocyte isolation (Figure 3.3.12C and 3.3.12D). This increase was much more pronounced in PR3+ cells. Of note, three groups emerge in the isolated monocyte in terms of MPO surface expression: high, medium, and low (Figure 3.3.12B).

We also assessed the influence of age and sex on surface ANCA expression. CD14+ monocytes in the dextran sediment had a small but significant inverse association with age for MPO expression only (Figure 3.3.13A). This effect was however lost after MACS isolation (Figure 3.3.13B). PR3 expression showed no association with age in neither the dextran monocytes nor the MACS isolated monocytes. Only 3 of the 24 donors in this cohort were female, and there were no detectable associations of sex with surface ANCA expression (data not shown). From these results we can conclude that the process of monocyte isolation increases surface ANCA antigen expression, and that there appears to be a vague association between age and ANCA surface expression.

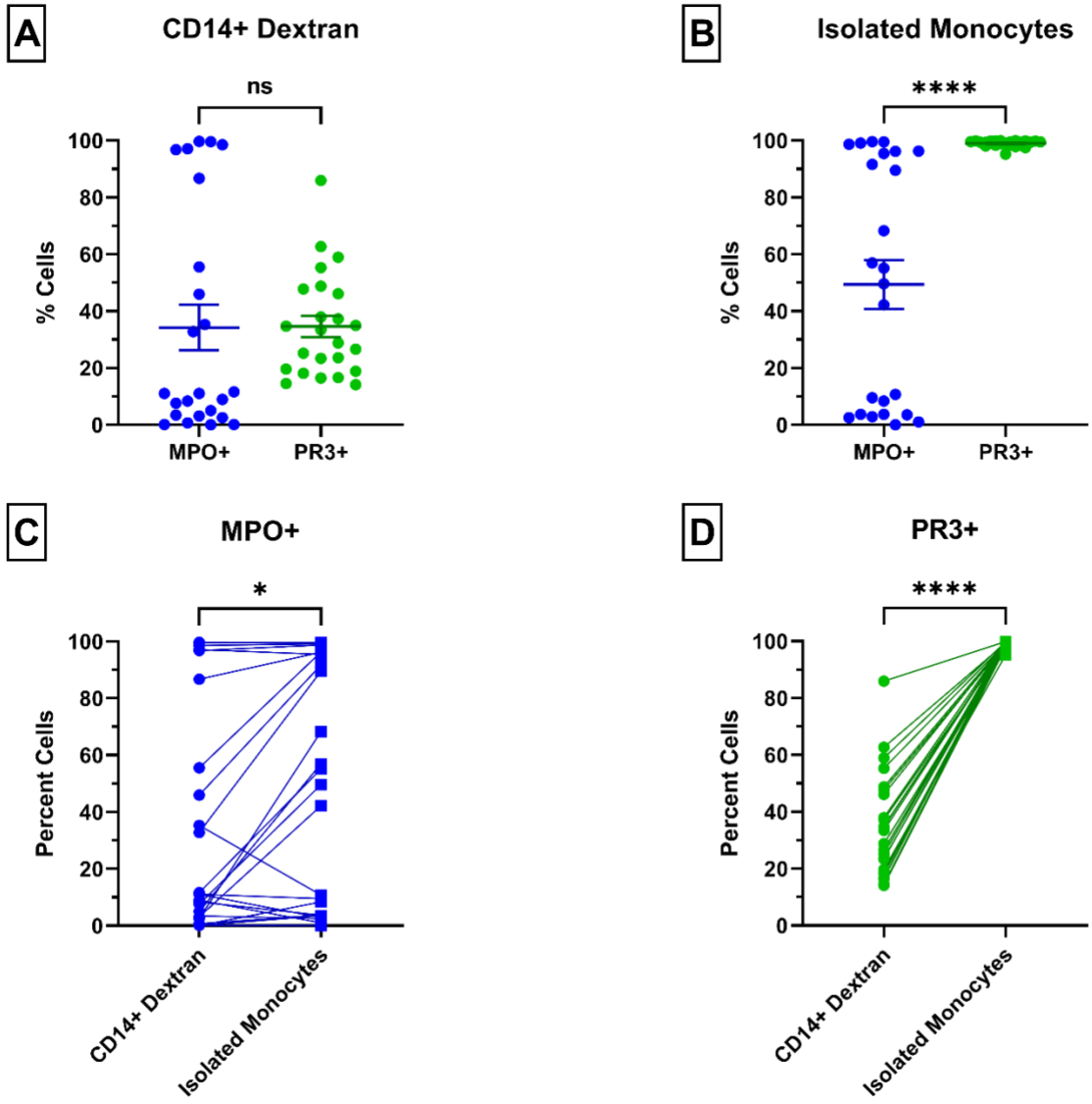


**Figure 3.3.12: MPO and PR3 Expression on Surface of Monocytes in Dextran Sediment (Whole Blood) and after CD14+ MACS Isolation.** CD14+ monocytes were isolated from the PBMCs of healthy controls by MACS separation. Freshly isolated monocytes were stained for flow cytometry with antibodies directed against CD14, MPO, PR3, and a cell viability stain. Monocytes and dextran sediment (representative of whole blood) were analysed by flow cytometry and live CD14+ cells assessed for MPO and PR3 surface expression. Percentages of MPO and PR3 positive cells in dextran (A) and post-MACS isolation (B). Changes in MPO (C) and PR3 (D) expression during cell isolation.

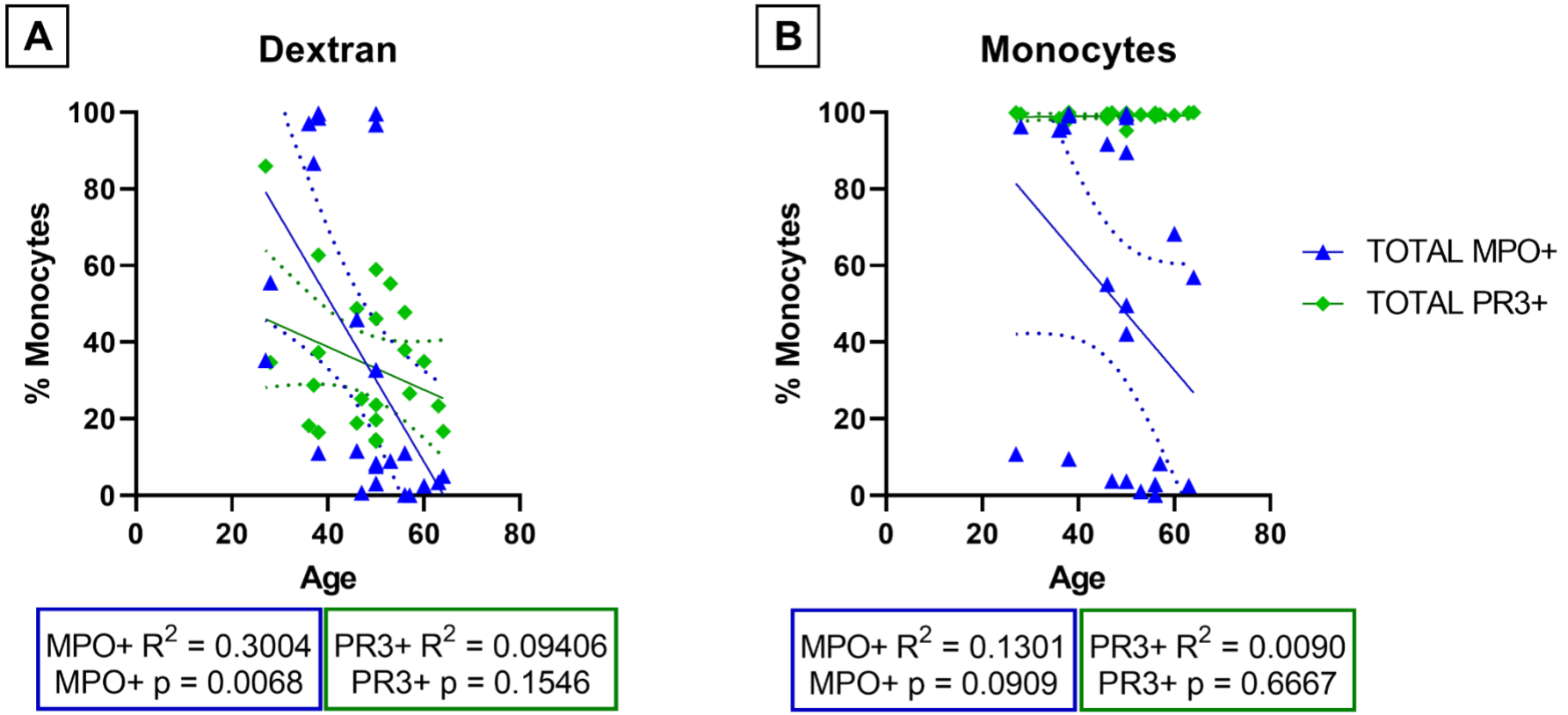


**Figure 3.3.13: Correlation of MPO and PR3 Expression on Surface of Monocytes in Dextran Sediment (Whole Blood) or after CD14+ MACS Isolation with Donor Age.** CD14+ monocytes were isolated from the PBMCs of healthy controls by MACS separation. Freshly isolated monocytes were stained for flow cytometry with antibodies directed against CD14, MPO, PR3, and a cell viability stain. Monocytes and dextran sediment (representative of whole blood) were analysed by flow cytometry and live CD14+ cells assessed for MPO and PR3 surface expression. The percentages of MPO+ and PR3+ cells in the dextran sediment (A) and after MACS isolation (B) were correlated with donor age using Pearson correlation. Simple linear correlation was used to calculate best fit lines for MPO (blue) and PR3 (green) and are plotted with 95% confidence intervals (dotted line).

### 3.3.13 MPO Surface Expression Determines Extent of IL-1β Production in anti-MPO Stimulated Monocytes

Interpersonal variation appears to influence LPS- and anti-MPO-induced IL-1β production from primary monocytes. We hypothesised that these disparities could be accounted for by differences in MPO surface expression. Cells were prepared and stained as described in Section 2.8 and fluorochromes used are shown in Table 3.2.2. Assessing MPO surface expression pre-stimulation, we found a strong correlation between the percentage of MPO+ monocytes and subsequent IL-1β production upon MPO-ANCA stimulation ($R^2$=0.9503, p=0.0048, Figure 3.3.14A). This effect was only seen in anti-MPO-treated cells despite higher IL-1β production by LPS stimulation ($R^2$=0.2063, p=0.4423, Figure 3.3.14A). A similar pattern was observed when assessing median fluorescence intensity (MFI), however this effect was not significant (Figure 3.3.14B). However, this may be due to low MFI reported in these cells. These findings point to a physiological mechanism of monocyte activation by anti-MPO.

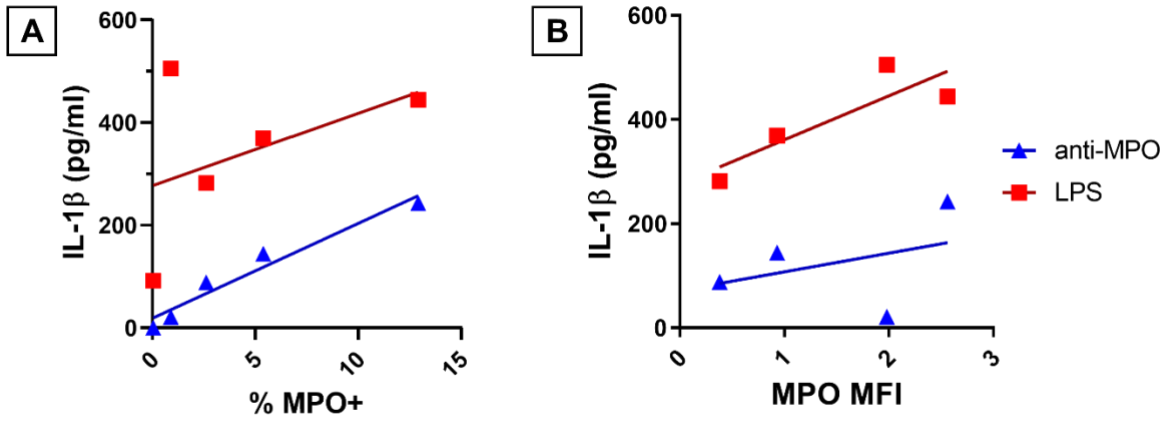


**Figure 3.3.14: Correlation of Baseline MPO Surface Expression with IL-1β Production in Stimulated Primary Monocytes.** CD14+ monocytes were isolated from buffy coat PBMCs by MACS separation. Surface expression of MPO was measured immediately after isolation by flow cytometry. Cells were plated and stimulated @37°C for four hours with 5μg/ml monoclonal antibody (mAb) directed against MPO or 200ng/ml LPS. IL-1β production was measured in the supernatant by ELISA. The relationship between IL-1β production and the percentage (%) of MPO positive live CD14+ monocytes (A) and the median fluorescence intensity (MFI, panel ) of MPO was assessed by Pearson correlation.

### 3.3.14 Monocyte CD54 Expression is Increased During MACS Isolation

Sample processing can affect outcomes in cellular metabolomics investigations. We have shown that the process of monocyte isolation increases surface ANCA antigen expression (Figure 3.3.12). We next assessed if the process of MACS monocyte isolation altered the cell's function/phenotype using CD54/Intercellular Adhesion Molecule-1 (ICAM-1) as a marker of monocyte activation. Cells were prepared and stained as described in Section 2.8 and fluorochromes used are shown in Table 3.2.2. CD54 expression was increased in isolated primary monocytes compared to whole blood (Figure 3.3.15A). A smaller increase in MPO surface expression was also noted. The percentage of CD54+ or MPO+ cells did not change during the course of MACS monocyte isolation (Figure 3.3.15B). This finding suggests that changes in monocyte phenotype occur during the course of isolation. Whether these changes affect the outcomes of immunological and metabolic readouts remains to be seen.

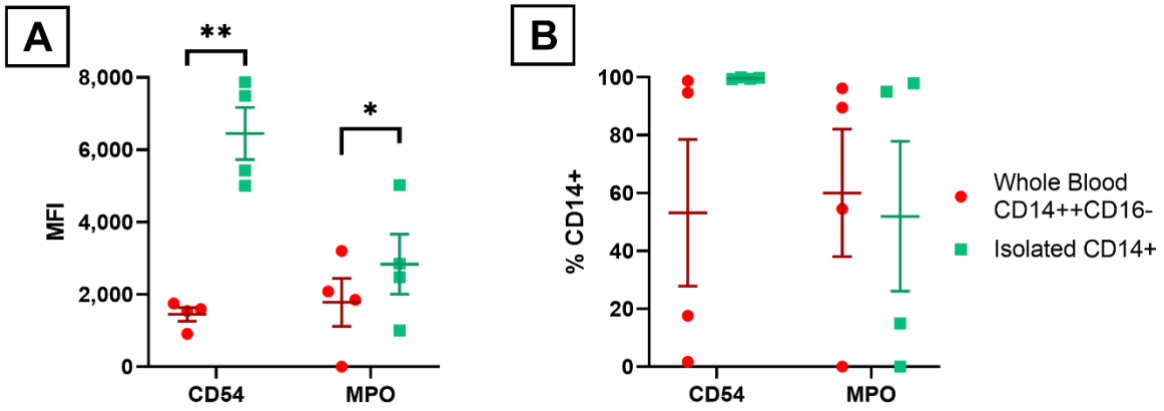


**Figure 3.3.15: Changes in Surface Expression of CD54 and MPO on Primary Monocytes in Whole Blood and after MACS Isolation.** CD14+ monocytes were isolated from the PBMCs of healthy controls by MACS separation. Cells were stained for flow cytometry with antibodies directed against CD14, MPO, CD54, and a cell viability stain. Surface expression of CD54 and MPO in CD14+ monocytes was measured in whole blood and after MACS isolation using flow cytometry. MFI (A) and the percentage of positive cells (B) was determined for both markers. Results for each marker were analysed by paired t-test and Holm-Šídák's multiple comparisons test. Results are plotted as mean ± standard error of the mean (SEM).

### 3.3.15 Anti-MPO Stimulation Alters Chemokine Release at a Transcriptional Level

Previous work from our lab profiled ANCA-stimulated monocyte supernatants using the OLINK inflammation panel [244]. This panel measures 92 inflammation-related proteins, of which 55 were detectable in monocyte supernatants. Significant alterations were found in a number of protein biomarkers in anti-MPO treated monocyte supernatants with a less pronounced response in anti-PR3 stimulated. A selection of these biomarkers altered by anti-MPO stimulation were chosen to be analysed by quantitative reverse transcription PCR (RT-qPCR, see Section 2.6). Of those which were consistently detected by qPCR, anti-MPO was found to significantly increase C-X-C motif chemokine ligand (CXCL)-5 and decrease CXCL10 expression (Figure 3.3.16) when compared to isotype controls. Anti-MPO did not alter expression of IL-10 receptor subunit alpha (RA) or oncostatin M (OSM), suggesting that secretion of these proteins is regulated at a post-transcriptional level. There were no significant differences in LPS-stimulated cells for any of the measured genes. These results show that the alterations in CXCL5 and CXCL10 release occur at the transcriptional level.

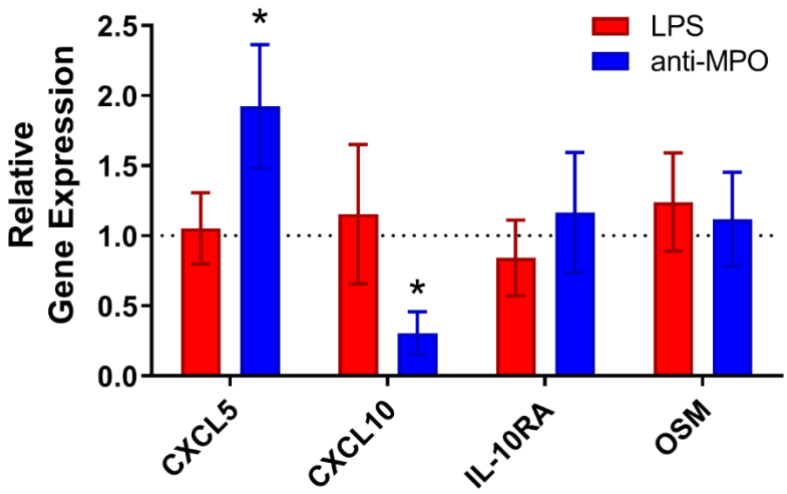


**Figure 3.3.16 Changes in Relative Gene Expression of Inflammatory Proteins with Altered Secretion Following ANCA Stimulation.** CD14+ monocytes (n=5) were isolated from the PBMCs of healthy controls by MACS separation. Cells were plated and stimulated @37°C for 4 hours with 200ng/ml LPS, 5µg/ml monoclonal antibody (mAb) directed against MPO or 200ng/ml LPS (n=5). RNA was isolated and changes in gene expression measured by qPCR (see Section 2.6). Fold change was calculated relative to unstimulated cells (grey dotted line) and statistical analysis performed using t-test compared to isotype controls. CXCL: C-X-C motif chemokine ligand; IL-10RA: Interleukin 10 Receptor Subunit Alpha; OSM: Oncostatin M.

### 3.3.16 Cell Clumping is Increased in ANCA-Stimulated Cells

Through routine microscopy inspection of cell stimulation plates, we observed slight morphological changes in monocytes after stimulation. LPS- (and to a lesser extent, ANCA-) stimulated cells appear to cluster or “clump” together whereas unstimulated cells remained distanced from one another and remain consistent in appearance after plating. To investigate this, we prepared cytopsin slides and stained and imaged as described in Section 2.7. The total number of clumps was defined for each treatment group for each biological replicate. Due to processing errors two replicates were excluded form analysis for a total n=22. The total number of clumps was significantly increased in anti-PR3 stimulated monocytes compared to unstimulated cells (Figure 3.3.17). Clumping for LPS- and anti-MPO-treated cells was also increased but did not reach statistical significance (p=0.0889 and p=0.745 for LPS and anti-MPO, respectively). These statistical effects are likely confounded by the high level of zero values, as many slides showed no evidence of clumping in any treatment groups. Clumps in LPS-treated cells were generally larger, perhaps indicating a greater degree of cellular activation. The precise effects of this cell clumping phenomenon and its relation to inflammatory and metabolic outputs are not clear.

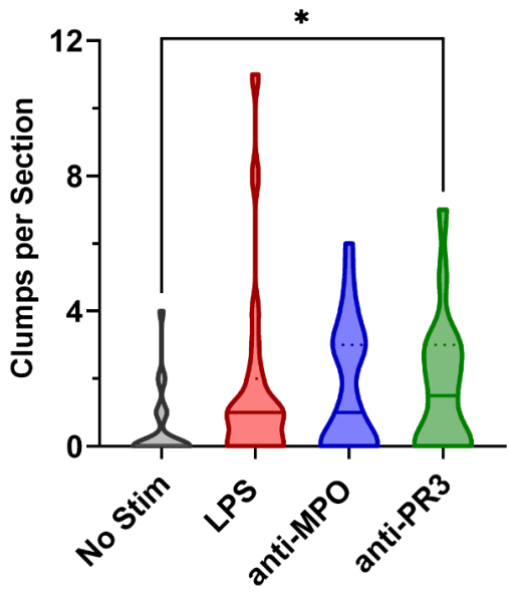


**Figure 3.3.17: Effects of ANCA Stimulation on Cell Clumping in Primary Monocytes.** CD14+ monocytes (n=22) were isolated from the PBMCs of healthy controls by MACS separation. Primary monocytes were stimulated with 5µg/ml monoclonal antibody (mAb) directed against MPO or PR3, or 200ng/ml LPS for 4 hours. Cytospin slides were prepared and stained as described in Section 2.7 and clumps of cells quantified using light microscopy. Median (solid lines) and interquartile values (dotted lines) are plotted for each treatment group as truncated violin plots.

## 3.4 Discussion

### 3.4.1 Optimising Cell Culture Conditions & Experimental Protocols

This project is designed to build on previous work from our group investigating monocytes in AAV [203, 238, 244]. There were only slight improvements to be made to these experimental protocols – namely blood source (Figure 3.3.1), monocyte isolation protocol (Figure 3.3.2), and adaptations for metabolomic analysis. These assays were easily scalable to larger plate formats (Figure 3.3.3) and preferable for metabolite extraction protocols (see Chapter 4 for full details). Buffy coats (BC) are routinely used in immunological investigations as a source of healthy leukocytes. In our experience however BC monocytes have had highly variable results, and high background production of inflammatory cytokines (Figure 3.3.1). Differences in cytokine production at baseline and after LPS stimulation have been noted in BC preparations compared to fresh blood samples, with additional decreases in monocyte recovery in BCs [306]. We speculate that this may be due to the extended storage times of BCs. The sample storage conditions and time since acquisition of IBTS BCs are not specified. Sample aging can have profound effects on cytokine release by monocytes [307]. Classical CD14++CD16- monocytes have a lifespan of roughly 24 hours [308, 309], and the higher IL-1β production in haemochromatosis monocytes is likely a result of the shorter time *ex vivo*, despite some variation between donors (Figure 3.3.1).

Haemochromatosis blood also comes with additional advantages: it is fresh, a high volume of blood is available, and it allows collection of basic demographic info (age and sex) from donors. Blood donation from people with haemochromatosis is safe, tolerated, and accessible [310]. For these reasons we have chosen to use fresh blood for our monocyte metabolomic profiling experiments. Use of blood from people with high iron levels does come with caveats. To date there have been no metabolomics investigations comparing haemochromatosis patients to healthy controls. One study compared metabolic syndrome patients with and without hyperferritinaemia to healthy controls, revealing differences in some amino acid and long chain FAs between the two patient groups [311]. This group concluded that hyperferritinaemia is linked to impaired glucose homeostasis among people with metabolic syndrome. They also note a trend toward increased inflammation with iron overload in these patients. Dysfunctional iron metabolism can affect immune

cell function and monocyte differentiation [312]. Ultimately the goal of this work is to generate hypotheses that can be validated in the relevant patient cohorts. We would aim to validate these findings in AAV patients and a suitable age- and sex-matched cohort of (relatively) healthy controls to confirm true metabolic associations.

Much of the AAV literature focusses on functional work in neutrophils. These experiments typically use polyclonal IgG antibodies derived from AAV patients to stimulate cells. Indeed, polyclonal antibodies have increased pro-inflammatory cytokine production in ANCA-stimulated monocytes [197, 203]. Despite these findings, none of the polyclonal IgG preparations we tested increased IL-1β production in primary monocytes (Figure 3.3.4). TNF-α priming also had no effect on IL-1β levels. While this is in contrast to what is seen in the literature, we would argue against the use of patient polyclonal antibodies altogether. Patient-derived IgG preparations are not sustainable, isolation protocols are neither standardised nor well documented, and in our experience have not been reproducible. These antibodies are highly patient-specific, though have not been well characterised to define pathogenic epitopes. To overcome this and define a more standardised and reproducible approach to ANCA stimulation we have opted to use monoclonal antibodies (mAbs) in our experiments.

Investigations of ANCA function in neutrophils typically adopt a TNF-α priming step. Previous work from our group has shown that this does not enhance pro-inflammatory cytokine production in ANCA-stimulated monocytes [244]. We further confirmed this using polyclonal IgG preparations (Figure 3.3.4) and mAbs (Figure 3.3.5). TNF-α also has notable effects on cellular metabolism. In neutrophils, lactate and phosphocholine levels are increased by low dose TNF-α [313], and lipid mediators can suppress cytokine production and dysregulate cell death programs in TNF-α primed macrophages [314]. Hypoxia-inducible factor (HIF)-1α is induced by TNF-α to promote expression of lactate dehydrogenase (LDH) and pyruvate dehydrogenase kinase (PDK) [315], supporting increased glycolysis in activated immune cells [316, 317]. TNF-α stimulation can alter glucose, lipid, and adipocytokine levels in arthritic murine joints [318], and is also crucial for insulin resistance development in obese mice [319]. Given these metabolic disturbances

the inclusion of a TNF-α priming step could confound any ANCA-specific effects on monocyte metabolism, and was not considered in any further stimulation protocols.

We investigated the use of LPS as a novel priming agent and find it to synergistically increase IL-1β when paired with anti-MPO (Figure 3.3.5). Infection often precedes onset of AAV; the consequent systemic alterations in leukocyte metabolism caused by bacterial endotoxins may thus facilitate (pre-)activation of neutrophils and monocytes by ANCA [210, 320]. This may explain the upregulated TLR4 expression on AAV patient monocytes [223-226] and suggests an *in vivo* mechanism where LPS primes monocytes to enhance responses to ANCA. There is ample evidence of metabolic manipulation of immune cells by LPS. Succinate and itaconate have pro- and anti-inflammatory roles in LPS-stimulated macrophages respectively [321]. LPS stimulation alters intracellular metabolite levels in macrophages with a concurrent shift from OXPHOS to glycolysis [322]. As well as decreasing OXPHOS in monocytes [97], LPS can increase ROS production and neutrophil-mediated tissue damage [323]. These findings are physiologically relevant in the context of AAV, however, introducing LPS to the experimental system will also mask any ANCA-specific effects. Given these potentially confounding effects, we have opted to exclude any cell priming steps from our metabolomic profiling protocol. Precise unravelling of the synergistic LPS/anti-MPO relationship should be a priority of future investigations of monocytes in AAV.

One concern with using mAbs was that the presence of sodium azide ($NaN_3$) in these antibodies could impact our results. $NaN_3$ is a chemical preservative used to prevent bacterial contamination in aqueous laboratory reagents, but can also induce apoptosis by altering mitochondrial respiration via cytochrome oxidase inhibition [324]. $NaN_3$ is also a potent MPO inhibitor and has also been shown to affect monocyte function. Pre-treatment of THP-1 cells with $NaN_3$ inhibited MCP-1 release and transcription, and limited LPS-induced CXCL10 and IL-6 production [325]. $NaN_3$ increases phagocytosis [326] and limits chemotaxis (polarisation) by inhibiting oxidative metabolism [327] in primary monocytes. Investigations in foetal cell lines [328] confirmed decreased respiratory after $NaN_3$ treatment. However, these investigations were carried out at higher concentrations than those found in our experimental model. After dilution in experimental assay plates the concentrations

of $NaN_3$ were 68.625µM and 38.125µM for anti-MPO and anti-PR3 stimulated cells, respectively. At these concentrations (Figure 3.3.6) we did not find any $NaN_3$-induced functional inconsistencies in primary monocytes. Thus, monoclonal antibodies are suitable for use in metabolic profiling experiments in primary immune cells.

### 3.4.2 Pilot Immunologic Readouts: LC-MS, Flow Cytometry, and Functional Inhibition

Previous experiments from our group have profiled monocyte metabolism after four hours of ANCA stimulation. However, most peer-reviewed publications investigating monocyte metabolomics are in timepoints ≥24 hours [96, 97, 124, 302]. Zhu *et al.* comprehensively profiled the monocytic THP1 cell line to replicate a sepsis model monitoring acute inflammation to resolution [96]. This detailed the switch from anabolic energy consumption during early immune activation (0-8h), to a catabolic energy-conserving process during immune deactivation (24-48h), before re-establishing energy homeostasis during resolution (48-96h). During this time course however, monocytes would begin to differentiate into macrophages and alter their functionality. This is also true for *in vitro* investigations of innate immune metabolism, which are initiated in monocytes, but the subsequent epigenetic changes and surges in cytokine production occur in polarized macrophages [20, 21, 329, 330]. One metabolomic analysis of primary monocytes did detect increases in intracellular lactate upon LPS stimulation as early as 1 hour post stimulation, confirming a rapid increase in glycolysis in these cells [85]. We have also found ANCAs to rapidly increase glycolysis immediately after stimulation, an effect that was maintained up to 4h with anti-MPO stimulation [238]. Our pilot analysis of monocyte metabolomics at 24h did find significant increases in some amino acids, including serine (Figure 3.3.7). Future experiments will examine the more premature changes in ANCA-induced metabolism at 4 hours.

Another pilot LC-MS analysis was carried out in a cohort of cells due to an abundance of linked data. Here we uncovered correlations of intracellular amino acids with rates of glycolysis in ANCA-treated monocytes (Figure 3.3.8). Unfortunately, we were only able to reliably detect amino acids (with the help of synthetic standards) given the low cell number. Although these samples were useful for preliminary results the number of detectable metabolites were limited as cells

were stored in a phosphoproteomic buffer (0.2ml 1M $Na_2CO_3$,1.8ml $H_2O$, 0.2ml 10X phosphatase inhibitor, 80µl 25X protease inhibitor, 0.4ml 100mM sodium pervanedate) and further diluted with extraction buffer before MS analysis. Despite this these samples were useful to optimise a number of MS conditions, including preliminary extraction solvent comparisons, injection volumes, MS vial inserts, gradients, flow rates, column types, and mobile phases.

Our two pilot LC-MS analyses identified serine as a potential metabolic marker of ANCA activation in primary monocytes (Figure 3.3.7 and 3.3.8). Serine is an important fuel for cancer metabolism [331-333], and small molecule inhibitors of serine synthesis [334] have been developed as potential therapies. One such inhibitor is CBR-5884 which targets 3-phosphoglycerate dehydrogenase to limit serine production via the *de novo* serine synthesis pathway directly branching from glycolysis [303]. We found that inhibiting serine synthesis completely abrogated LPS-induced IL-1β production (Figure 3.3.9). That IL-1β production recovered by 18 hours indicated that these cells replenish serine levels via alternate metabolic pathways, demonstrating the metabolic plasticity of primary monocytes. Serine synthesis was shown to be essential for IL-1β and TNF-α production in murine macrophages [335]. This may be the first metabolite found to regulate cytokine production in AAV. However, there was high background in both this and our MPO inhibition experiments (see Figure 3.3.11), which may influence the utility of these assays. The concentration of CBR-5884 used was also above the IC50 (33µM), and cell viability may have been affected by limiting serine anabolism. Similar issues were evident in our MPO inhibition experiment. MPO-ANCA can influence MPO oxidation activity and maybe associated with more severe disease [336, 337]. As such, inhibition of MPO activity has been proposed as an anti-inflammatory treatment strategy for AAV [197, 304]. In addition these inhibitors may have off-target effects contributing to these outcomes. While our results were promising, low n numbers have limited the interpretability of these results. Furthermore, these investigations used a novel MPO inhibitor different to our 4-ABAH compound, further limiting comparisons between these works. These experiments should be repeated and expanded in larger cohorts with additional MPO and serine synthesis inhibitor candidates.

Monocyte MPO and PR3 surface expression is dysregulated in AAV [192, 203, 223] and can be altered by other inflammatory stimuli [227]. Indeed, we found inconsistencies in ANCA antigen surface expression in our monocyte cohort. Both MPO and PR3 expression are increased during CD14+ isolation (Figure 3.3.12). This effect was much more pronounced in PR3+ cells, an interesting outcome given that monocytes typically do not produce IL-1β (or other inflammatory cytokines) in response to anti-PR3 stimulation. A correlation between age and MPO surface expression in whole blood (dextran) monocytes was also revealed (Figure 3.3.13), but this did not maintain significance after monocyte isolation. As whole blood represents the immune environment in its most natural form, we can reason that this correlation is accurate. Finally, the percentage of MPO+ monocytes at baseline was strongly predictive of IL-1β production upon subsequent anti-MPO stimulation (Figure 3.3.14). ANCA antigens are constitutively expressed on AAV patient [192] and HC monocytes [203]. Whether this is a true effect or a result of technical alterations to cell phenotype remains to be seen. These effects should be further examined in whole blood and in larger patient cohorts.

Monocyte surface markers including CD14 ,PD-L1, CD63, CD64, and various integrins are dysregulated in AAV [1, 187]. Adhesion molecules are increased on AAV patient monocytes and after ANCA stimulation (see Section 1.4.2.4). In attempting to examine the extent of CD54 expression on primed monocytes we found that the process of CD14+ isolation significantly increases CD54 MFI (Figure 3.3.14). Far from a novel finding, this phenomenon was first described in by Stent *et al.* in 1997 [338]. Changes in immune cell surface markers during isolation can affect findings in cell phenotype investigations. As a result there is a push to use whole blood to limit inevitable technical variation related to sample preparation in immunologic investigations [339].

### 3.4.3 Combining Metabolomic & Immunological Readouts

These experiments allow for a multitude of parallel immunological and metabolic readouts. We used RT-qPCR to validate the findings of a previous proteomic screen of monocyte supernatants [244]. We did confirm that the modest increase in CXCL5 and the decrease in CXCL10 release by anti-MPO stimulation occurs at the transcriptional level (Figure 3.3.16). CXCL5 can be induced by a range of pro-inflammatory cytokines and is a prominent neutrophil activator. Its expression is NF-

κB dependent and can be activated by IL-1β [340]. Transcripts are also highly upregulated in kidneys of AAV patients with crescentic glomerulonephritis [341]. Conversely, CXCL10 (also known as IP-10) showed a marked decrease in expression in anti-MPO stimulated cells. These results could not be validated by ELISA as CXCL10 expression was undetectable in any of the treatment groups (data not shown). This chemokine is secreted in response to IFN-γ and is a biomarker and therapeutic target for several autoimmune diseases [342]. Inhibition of IFN-γ reduced CXCL10 expression and macrophage infiltration in a type of large-vessel vasculitis [343]. The decreased expression in ANCA-stimulated monocytes is unexpected. This phenomenon may represent a negative feedback loop to prevent prolonged inflammation. Recent work from our group exposed that AAV is not in fact an interferonopathy as once theorised [245]. One incidental finding from this work was that serum CXCL10 was increased in treatment-naïve AAV patients with active disease but was lowered after treatment and into remission. Whether or not these changes in gene expression are metabolically regulated will be a focus of future experiments. Berti *et al.* characterized distinct circulating cytokine profiles for MPO- and PR3-AAV [183] and found unique signatures for clinical and molecular subgroups of AAV. However, none of the indicated cytokines were implicated in our analysis of monocyte supernatants. One reason for this is that our analysis reflects ANCA-driven inflammation at a cellular level rather than systemically. It may also be the case that monocytes are not involved in the pathogenesis of PR3-AAV and are sensitive only to activation by MPO antibodies. Additional work is needed to confirm if these genes are related to monocyte metabolism.

Metabolomic sample preparation protocols have been optimised not just for metabolomics, but also with potential for subsequent integrated multi-omics experiments. Proteins contained in the cell lysate pellet can be isolated and quantified by Western blot. Our BCA data that also shows high levels of protein preserved in the cell lysis pellet (see Chapter 4), where cell lysates preserve protein contents after metabolite extraction. This protein could potentially be used in Western blot experiments. This would provide a fuller understanding of biological changes taking place resulting in alterations to the monocyte metabolome. Extraction methods may also conserve RNA for subsequent extraction and parallel analysis [56, 344].

The Mito- and Gluco-Stress tests are commonly used to measure rates of OXPHOS and glycolysis, respectively. Direct injection of stimuli to Seahorse assay plates can also be used to measure simultaneous, real time changes in OCR and ECAR [300] and has been used to assess real-time metabolic effects of ANCA stimulation [238]. Attempts to aid concomitant experiments by using the same ANCA stimulated monocytes analysed by Seahorse for subsequent metabolomic analysis, have not yet been successful. Immobilisation of suspension cells is an essential step for Seahorse analysis. Using previously optimised Seahorse conditions [244], this was achieved using a commercially available adhesive protein mixture: Cell-Tak™. To account for this, we modified our optimised sample preparation protocol to suit adherent cells by taking inspiration from work by Fei *et al*. in macrophages [322, 345]. This combined quenching/extraction protocol was developed with additional considerations for these now adherent monocytes, but was unable to extract sufficient intracellular content using the previously optimised readout of protein levels in metabolite and cell pellet fraction (Figure 3.3.10). Acidified extraction buffer has been suggested for extraction of metabolites from mammalian cells and can even improve quenching efficiency [27]. Acidifying the 80% MeOH with formic acid may disrupt the efficiency of the Cell-Tak™ and allow improved removal of cells from Seahorse plates.

Even if removal of cells from Seahorse plates for metabolomic analysis was a feasible option, differences in Seahorse media and other commercial media formulations may confound findings of parallel experiments [98, 301, 346]. The Seahorse XF media is a proprietary formulation and thus direct comparisons of metabolic effects are not easily accounted for. Furthermore, FBS is not added to the Seahorse media as it can interfere with the sensitivity of the probes and effectiveness of the Cell-Tak adhesive. This omission could also affect metabolomic readouts, as FBS is a source of nutrients and essential for cell viability [301]. Finally, the use of Cell-Tak to adhere monocytes for Seahorse analysis may interfere with normalisation of metabolic flux data [347]. These findings mean that cells used for Seahorse experiments will likely not be compatible for subsequent metabolomic analysis. These experiments should be carried out in parallel where appropriate.

The optimised experimental outline for metabolomic profiling of primary monocytes is shown in Figure 3.4.1.

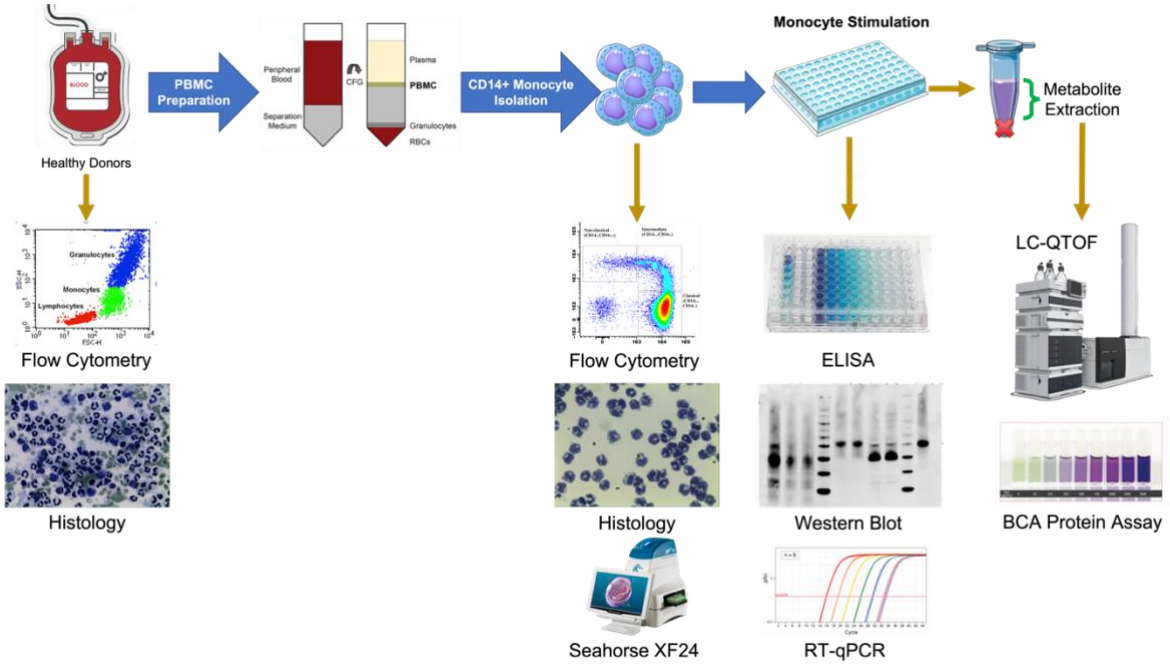


**Figure 3.4.1: Optimised Experimental Outline for Metabolomic Profiling of Primary Monocytes.** Monocytes are isolated from healthy blood by CD14+ MACS separation and stimulated for 4 hours with 5µg/ml monoclonal anti-MPO or anti-PR3 for 4 hours. Supernatants are separated from cells and used for ELISA, and metabolites are extracted from cell pellets for analysis by LC-MS. Additional RT-qPCR and Western blot experiments can be carried out on cell pellets. Parallel Seahorse, flow cytometry, and histology experiments allow simultaneous measurement of multiple cellular processes.

# Chapter 4: Optimisation of LC-MS Metabolomic Profiling of Primary Monocytes

## 4.1 Introduction

Preparing a metabolomic profiling investigation requires careful consideration. The steps involved in the design and execution of such an experiment are summarised in Figure 4.1.1 (adopted from [50]). A non-exhaustive collection of potential variables for consideration are also shown for each step. Experimental design must be carefully considered to allow protocols to be adapted for metabolomic profiling. Biofluids are commonly used in these types of investigations to measure systemic physiological effects in health and disease. Serum, plasma, and urine can be easily and routinely obtained, and established processing protocols are highly reproducible even in large-scale population studies [64, 348-350]. Sample preparation protocols for metabolomic analysis of yeasts and bacteria are also well-established. However, these findings will not be universally applicable to primary human cells because of substantial, inherent biochemical differences in eukaryotic and prokaryotic cells.

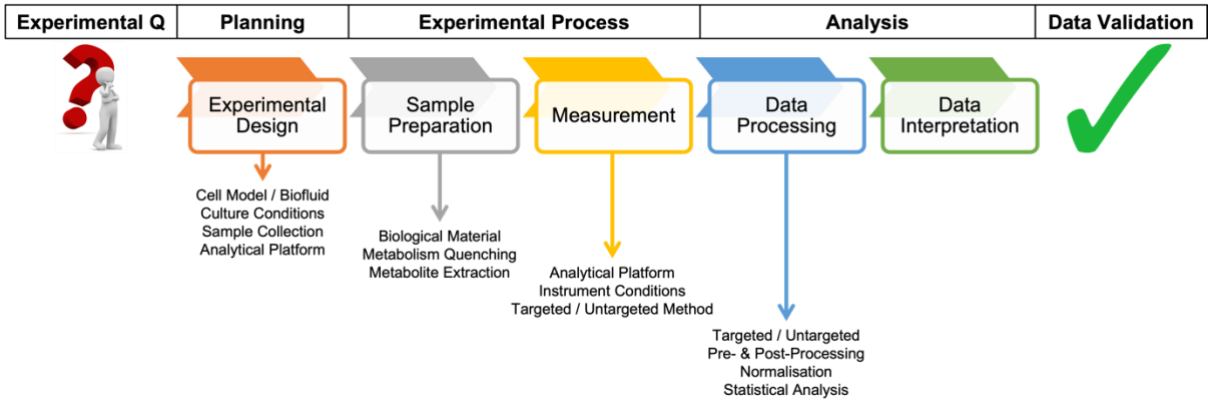


**Figure 4.1.1: Summary Overview of the LC-MS Experiment Optimisation Pipeline.** Some potential sources of variation/additional considerations are linked below the experimental stages. Adapted from Leon *et al.* [50].

Pre-analytical factors and even transport and storage conditions [351] can introduce variation in blood and urinary metabolomics [348]. Cellular metabolomics – although more specific in application and focus – introduces several additional variables into the experimental protocol. Cell culture conditions [301], cell number [352, 353], media formulations [98, 301, 346], incubation time/temperature [301], and harvesting method [71], can all affect results of metabolomics investigations. Cellular metabolomics in primary human cells combines the complexities of cellular metabolomics with the multi-faceted interpersonal variability of the human

metabolome [47, 354, 355]. This underlies the requirement for optimised sample preparation protocols and LC-MS methods for cellular metabolomic profiling.

Subtle changes in mobile phases, chromatography columns, or extraction protocols can drastically alter the recovery of metabolite classes [46]. The response of the metabolites to LC-MS is further influenced by the properties of the compound, eluent composition, and instrument [356]. Quantitative measurement can also be a challenge, as different compounds ionize to different extents in an electrospray (ESI) source. LC-MS methods must be tailored to the experimental design with the target compounds in mind. Despite these challenges LC-MS remains the gold standard for untargeted metabolomic profiling, and is the primary analytical platform used here for metabolomic analysis of ANCA-stimulated monocytes.

The LC-MS data analysis pipeline is another crucial step in untargeted metabolomic analysis requiring careful consideration and optimization. This process can be strengthened with appropriate quality and experimental controls [63, 64]. Given the many sources of variability cellular metabolomics studies, data normalization is an essential step. As with sample preparation, there is no single superior normalisation method universally applicable to untargeted metabolomics. Several sample- and data-based normalization approaches are outlined in Section 1.2.2.1. To date these methods have not been examined for their relevance to primary human cell metabolomics.

Preserving the biological phenotype while ensuring metabolites are accurately and appropriately measured is key for metabolomics investigations. In this work, we have adapted established experimental methods [203, 238] and optimised parallel functional readouts (see Chapter 3) to further characterise the role of monocyte metabolism in AAV. Sample collection protocols and culture conditions were optimised for study of early changes in monocyte metabolism in response to ANCA stimulation. The process of optimising LC-MS methods and sample processing to complement these findings and develop a metabolomic workflow are described in this chapter.

## 4.2 Experiment Description

### 4.2.1 Aims

I. To optimise sample preparation and LC-MS methods for metabolomic profiling of primary human monocytes.

II. To optimise LC-MS data analysis workflows for untargeted metabolomic analysis of primary human monocytes.

### 4.2.2 Experiment Outline

This chapter describes the optimisation of LC-MS profiling and analysis methods to facilitate metabolomic profiling of primary human monocytes. This includes technical details of experimental design, sample preparation, LC-MS methods, data analysis workflows, and metabolomic data normalisation. A high-level overview of the LC-MS optimisation process is outlined in Figure 4.1.1. Conditions for monocyte culture and stimulation utilised in this work are described in Section 2.2. The optimised methods described here are used to characterise the metabolomic response of CD14+ monocytes to LPS and ANCA as described in Chapter 4.

### 4.2.3 Methods

#### 4.2.3.1 Sample Preparation Optimisation

To optimise sample preparation for LC-MS metabolomics, three commonly used extraction solvents and lysis protocols we compared: methanol (MeOH), acetonitrile (ACN), and a mix of ACN, MeOH and water (ACN:MeOH:$H_2O$, 2:2:1). Monocytes (n=3) were isolated from healthy controls as described in Section 2.2. Unstimulated, freshly isolated monocytes ($1x10^6$) were aliquoted into Eppendorf tubes, centrifuged at 400g for 7 mins at 4ºC, and supernatants removed. Cells were rapidly quenched on dry ice and stored on wet ice for the duration of the experiment. Cells were resuspended in 1ml of the relevant extraction solvent (-20ºC) and stored on ice throughout the protocol. Cells were subjected to one of three lysis protocols: sonication, freeze-thaw, or vortexing. For sonication, cells were sonicated in an ice bath sonicator (Ultrawave QS3, F00239) for 10 min. For freeze-thawing, cells were placed on dry ice for 30 seconds then immediately into a 37ºC water bath for 90 seconds. This freeze-thaw cycle was repeated three times. For vortexing, cell tubes were vortexed for 15 seconds and returned to dry ice. This vortexing cycle was repeated three times. All cells were returned to dry ice after lysis and centrifuged at 12,000g for 15mins at 4°C. The metabolite fraction was stored at -80°C until

analysis. The experimental outline for this sample preparation experiment is outlined in Figure 4.2.1.

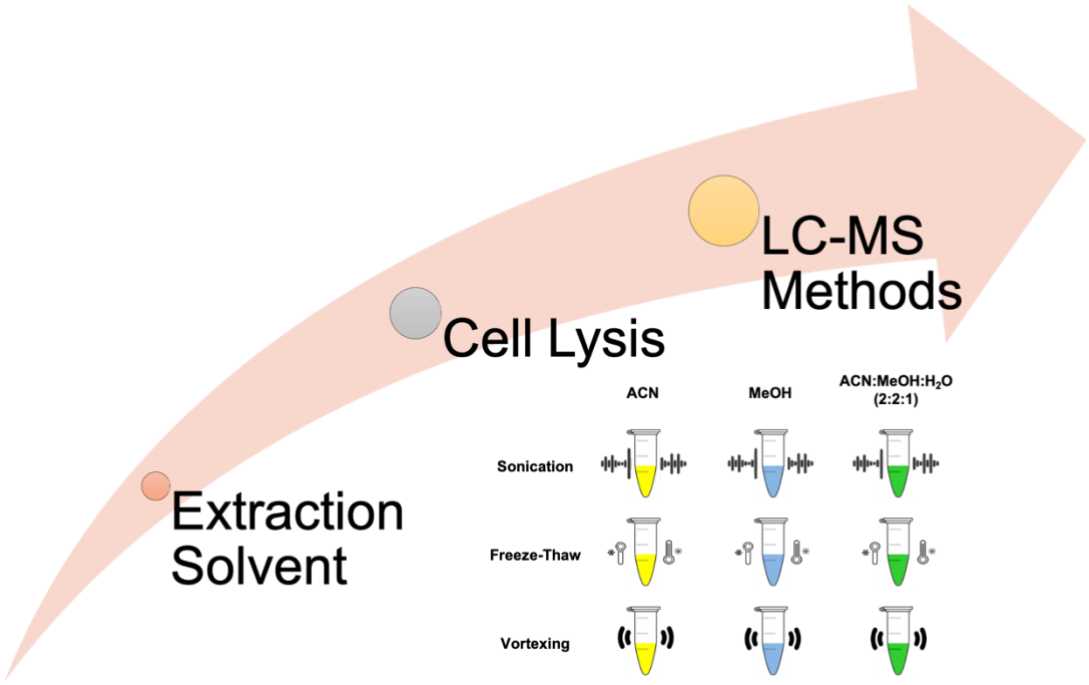


**Figure 4.2.1: Experimental Outline of Sample Preparation Optimisation Experiment.** CD14+ monocytes were isolated from PBMCs of healthy controls by MACS separation (n=3). Metabolites were extracted using one of three extraction solvents and one of three lysis methods as described in Section 4.2.3.1.

### 4.2.3.2 Sample Preparation Optimisation – LC-MS Analysis

A comprehensive literature review was carried out to identify methods capturing a broad range of metabolite (and lipid) classes. Several LC-MS methods were trialled in pilot experiments, modifying mobile phases, gradients, and columns. Two key LC-MS methods were used in the course of this optimisation work and are modelled on those used by Metabolon. The first was a reverse phase (RP) method using a C18 column based on work from Meissen *et al.* [357] and referred to henceforth as "C18". Samples were analysed in both ESI+ and ESI- using this method. The second LC-MS method used a hydrophilic interaction chromatography (HILIC) method using a zwitterionic HILIC phase (HILIC-Z) column and is described in detail by Hsaio *et al.* [42]. For these experiments this method was run only in ESI- (see Section 4.3.1 and 4.4.2). Full details of the LC and MS conditions for these methods are shown in Tables 4.2.1 and 4.2.2, respectively. Samples were randomised and analysed using both LC-MS methods.

| | C18 ESI+ | C18 ESI- | HILIC ESI- |
|---|---|---|---|
| **LC System** | Agilent 1290 Infinity LC, G7110B Iso Pump, G7120A Binary Pump | Agilent 1290 Infinity LC, G7110B Iso Pump, G7120A Binary Pump | Agilent 1290 Infinity LC, G7110B Iso Pump, G7120A Binary Pump |
| **Column** | Agilent ZORBAX RRHD Eclipse Plus C18, 95Å, 2.1 x 150 mm, 1.8 µm (PN959759-902) | Agilent ZORBAX RRHD Eclipse Plus C18, 95Å, 2.1 x 150 mm, 1.8 µm (PN959759-902) | Agilent InfinityLab Poroshell 120 HILIC-Z, 2.1 x 100, 2.7 µm, PEEK-lined (PN675775-924) |
| **Mobile Phase A** | $H_2O$ + 5mM PFPA | $H_2O$ + 5mM PFPA | $H_2O$ + 10mM $C_2H_7NO_2$ pH9 + 5uM additive |
| **Mobile Phase B** | 50% ACN + 50% $H_2O$ | 50% ACN + 50% $H_2O$ | 90% ACN + 10mM $C_2H_7NO_2$ pH9 + 5uM additive |
| **Flow Rate (ml/min)** | 0.40 | 0.40 | 0.25 |
| **Gradient (Timepoint, %Mobile A / %Mobile B)** | 0.5min 97.0/3.0%<br>10.0min 35.0/65.0%<br>10.1min 10.0/90.0%<br>12.0min 10.0/90.0%<br>12.1min 50.0/50.0%<br>14.0min 50.0/50.0%<br>14.1min 97.0/3.0%<br>18.0min 97.0/3.0% | 0.5min 97.0/3.0%<br>10.0min 35.0/65.0%<br>10.1min 10.0/90.0%<br>12.0min 10.0/90.0%<br>12.1min 50.0/50.0%<br>14.0min 50.0/50.0%<br>14.1min 97.0/3.0%<br>18.0min 97.0/3.0% | 2.0min 10.0/90.0%<br>12.0min 60.0/40.0%<br>13.0min 80.0/20.0%<br>16.0min 80.0/20.0%<br>17.0min 10.0/90.0%<br>25.0min 10.0/90.0% |
| **Column Temperature ( °C)** | 50 | 50 | 30 |
| **Injection Volume (µL)** | 5 | 5 | 5 |
| **Autosampler Temperature (°C)** | 4 | 4 | 4 |

**Table 4.2.1: Liquid Chromatography (LC) Conditions for LC-MS Methods Used in Sample Preparation Optimisation Experiments.**

| | C18 ESI+ | C18 ESI- | HILIC ESI- |
|---|---|---|---|
| **MS System** | Agilent 6545 LC/Q-TOF (G6545B) | Agilent 6545 LC/Q-TOF (G6545B) | Agilent 6545 LC/Q-TOF (G6545B) |
| **Ionization Mode** | Dual AJS ESI | Dual AJS ESI | Dual AJS ESI |
| **Ionization Polarity** | Positive | Negative | Negative |
| **Gas Temperature (°C)** | 200 | 200 | 200 |
| **Drying Gas (L/min)** | 10 | 10 | 10 |
| **Nebulizer Pressure (psi)** | 40 | 40 | 40 |
| **Sheath Gas Temperature (°C)** | 300 | 300 | 300 |
| **Sheath gas Flow (L/min)** | 12 | 12 | 12 |
| **Capillary Voltage (V)** | 3000 | 3000 | 3000 |
| **Nozzle Voltage (V)** | 0 | 2000/0 | 0 |
| **Fragmentor (V)** | 120 | 120 | 125 |
| **Skimmer (V)** | 65 | 65 | 65 |
| **Octopole 1 RF Voltage (V)** | 750 | 750 | 750 |
| **Acquisition Range (*m/z*)** | 50-1000 | 50-1000 | 50-1000 |
| **MS Acquisition Rate** | 5 spectra/sec | 5 spectra/sec | 3 spectra/sec |
| **Reference Mass(es) (*m/z*)** | 121.0509, 922.0098 | 68.9958, 119.0363, 1033.9881 | 68.9958, 119.0363, 980.0164 |

**Table 4.2.2: Mass Spectrometry (MS) Conditions for LC-MS Methods Used in Sample Preparation Optimisation Experiments.**

#### 4.2.3.3 Sample Preparation Validation

To validate the optimised sample preparation and LC-MS methods, PBMCs and monocytes were isolated from healthy donors (n=3) as described in Section 2.2. $5x10^6$ cells were plated in 6 well plates and stimulated with 5µg/ml of isotype control, (5µg/ml Mouse IgG1, Merck, CBL610), monoclonal anti-MPO (Meridian, H87207M) or monoclonal anti-PR3 (Merck, MABT340) for 4 hours. Cells were gently pipetted and spun at 400g for 7mins at room temperature. Supernatant was removed and cells were quenched on dry ice. 300µl of 80% MeOH was added to each tube and cells were vortexed for 30 seconds. Cells were then sonicated in an ice bath for 1 minute before vortexing for another 30 seconds. Samples were spun at 4,000g for 20 mins at 4ºC and the metabolite fraction was removed to a new Eppendorf tube. 2µl of each sample was combined into a PooledQC sample and was run three times at the beginning and the end of the run. Samples were kept on dry ice between extraction steps and stored at -80ºC before processing. Samples were run using the HILIC-Z method described in Section 4.2.3.2.

#### 4.2.3.4 Normalisation Assessment

Refined data analysis workflows were developed for targeted and untargeted analysis using the Agilent MassHunter software suite and are described in Section 2.9. To account for the biological variation inherent in primary human cells, a multitude of normalisation techniques were applied. These included both sample- and data-based methods and are outlined in Figure 4.2.2. A total of 41 normalisation strategies were assessed. Targeted data from the primary metabolomic profiling experiment (see Section 5.3 and Figure 5.2.1) was used to test the efficacy of normalisation methods. This included six biological replicates stimulated for four hours with 200ng/ml LPS, 5µg/ml anti-MPO, and 5µg/ml anti-PR3. Metabolites were extracted using the optimised extraction protocol (See Section 2.9.2) and analysed by LC-MS as described in Section 2.9.3. Data was primarily analysed using Mass Profiler Professional (MPP, Agilent Technologies, Version 15.1) where raw AUC data from the targeted analysis (see Section 2.9.5 & 2.9.6) was imported in .csv format from MassHunter ProFinder (Agilent Technologies, B.10.0). The MPP data import wizard integrates a $\log_2$ transformation step and all subsequent normalisation results are compared to $\log_2$ transformation alone.

A number of criteria were used to assess the quality of different normalised data based on those applied by NOREVA [102]. Intragroup variation was assessed by calculating %CV and median absolute deviation (MAD) for the PooledQC and unstimulated (NS) cells. Principal Component Analysis (PCA) plots were generated to visualise the degree of separation between treatment groups using LPS as a positive control and comparing to the NS group. Receiver operating curves (ROCs) for these metabolites were generated for each of the normalisation methods to determine the efficacy of separation between the LPS and NS groups with the curve's AUC used as a performance metric. All criteria were graded and assessed for the 41 normalisation techniques. Results for the top-performing normalisation strategies are shown in Table 4.3.1.

#### 4.2.3.4.1 NOREVA Normalisation

The online NOREVA 1.0 platform (http://idrblab.cn/noreva2017/, [102]) was used for additional *in silico* normalisation. Raw AUC data for samples and PooledQCs were uploaded and pre-processed using the default settings. NOREVA completes a QC-based signal correction step as standard by robust LOESS signal correction (QC-RLSC). This corrects for intra-run variability on a per-metabolite basis. The default settings specify a local polynomial fit with a filter criterion and bias-variance trade-off of 0.8 and 0.75, respectively. Missing values were imputed using the k-nearest neighbour (KNN) algorithm. Data was normalised using the appropriate methods outlined in Figure 4.2.2. Normalised data were exported in .csv format for subsequent analysis in MPP. The NOREVA workflow does not specify a log transformation step as standard, and the $\log_2$ transformation was not applied to these data during import.

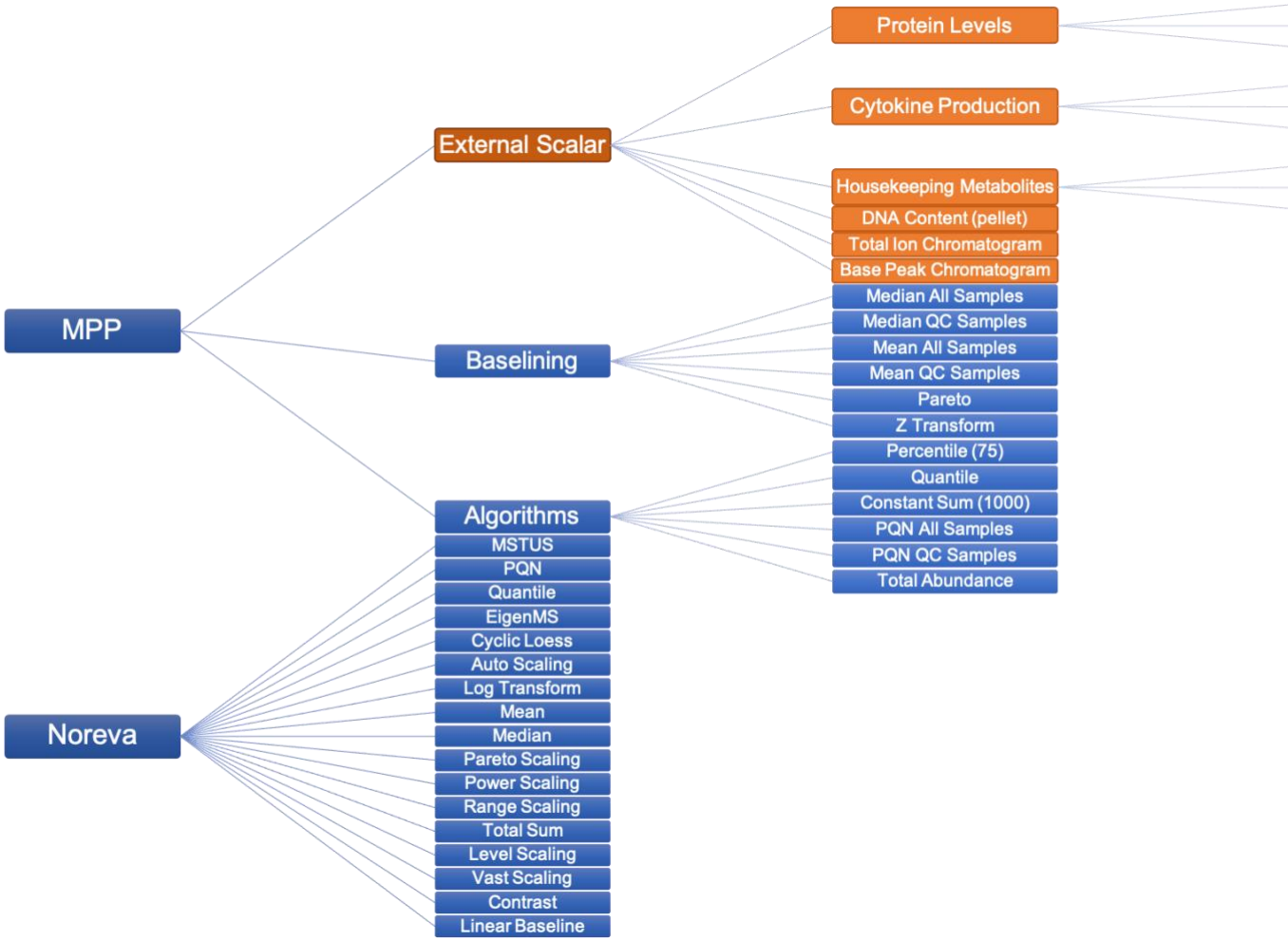


**Figure 4.2.2: Summary of Normalisation Techniques Applied to Metabolomic Data from Stimulated Primary Monocytes.** The primary software used for normalisation was Agilent MassProfiler Professional (MPP, Agilent Technologies, Version 15.1) and the online NOREVA platform [102]. External Scalar values were primarily sample-based methods, while baselining, MPP Algorithms, and NOREVA were data-based. Statistical normalisation methods are shown in blue and biological normalisation techniques in orange.

#### 4.2.3.4.2 BCA Assay Optimisation with PBMCs

To account for the low protein levels in the metabolite fraction and to test the compatibility of the extraction solvent (80% MeOH) with the BCA assay, a number of pilot experiments were carried out. First, standard curves ranging from 400-6.25µg/ml BSA were prepared using MeOH and PBS. Solutions were gently heated and vortexed until completely dissolved. Protein levels in these standards were measured using the Pierce™ BCA Protein Assay (Thermo Scientific, 23227), as per the manufacturer's standard test tube protocol.

To assess the efficacy of using metabolite fraction protein levels as a surrogate for cell number, PBMCs were isolated from healthy buffy coat samples as described in Section 2.2.2. Cells were counted and spun down in Eppendorf tubes ranging from 1-10x$10^6$ cells per tube. Metabolites were extracted using the optimised extraction method described above (see also Section 2.9.2) and protein levels measured by BCA assay. Here 12.5µl of metabolite fraction was added to a flat-bottom 96-well plate. Working reagent was freshly prepared and 100µl added to wells and mixed. Plates were sealed tightly with parafilm and left to incubate at 37°C for 30 mins. After cooling to room temperature, the absorbance was measured at 562nm and 595nm with an Epoch™ Microplate Spectrophotometer (BioTek Instruments, Inc.). The plate was again covered and returned to the incubator and a second reading was taken after 18 hours of incubation.

The protein pellet was dried down on low setting using a SpeedVac (Savant DNA Speed Vac® DNA110). The pellet was then reconstituted in 1ml of warm PBS and heated in a 37°C heatblock until completely dissolved. Protein levels were measured by BCA as described above. Protein levels were also assessed using a NanoDrop™ 8000 Spectrophotometer with the Protein A280 and UV-VIS modules in ND-8000 Software Version 1.0 (Thermo Fisher Scientific). DNA concentrations in the pellet fraction were measured as described in Section 2.10. This optimised BCA protocol has been applied to the primary and validation monocytes profiling cohorts and is described in full in Section 2.5.

## 4.3 Results

### 4.3.1 Comparison of Solvent and Lysis Metabolite Extraction Strategies for Primary Monocytes

Three extraction solvents and three lysis protocols were compared for their effectiveness in extracting useful metabolomic data from freshly isolated, unstimulated primary monocytes (see Figure 4.2.1). Samples were analysed using three LC-MS methods; a reverse phase method on a C18 column in ESI+ and ESI-, and a HILIC method in ESI-. Total ion chromatograms for the three LC-MS methods are shown in Figure 4.3.1. The C18 ESI+ method (Figure 4.3.1A) provided good separation of multiple peaks across the entire run. ACN-extracted samples (black, blue, and bright green) showed some peak broadening between 2 and 3 mins, and again segregated from the other techniques at 8.5-10.5mins. There was minimal variation between lysis methods for all three solvents. The C18 ESI- method (Figure 4.3.1B) had a remarkably high baseline and very little differentiation between extraction or lysis methods. There were very few distinguishable peaks, which may indicate a low number of detectable compounds. The HILIC method (Figure 4.3.1C) again showed good separation peaks throughout. The large peaks early in the method point to a high number of compounds eluting in the void volume. As with C18 ESI+ there was very little to distinguish the different extraction and lysis protocols. Vortexed ACN (bright green) and MeOH (cyan) did show some incongruity throughout the run. Ultimately extracted ion chromatograms will be needed to assess the effectiveness of the different sample preparation protocols. Examples of extracted features for solvent and lysis protocols measured by the three LC-MS methods are shown in Figures 4.3.1D-F.

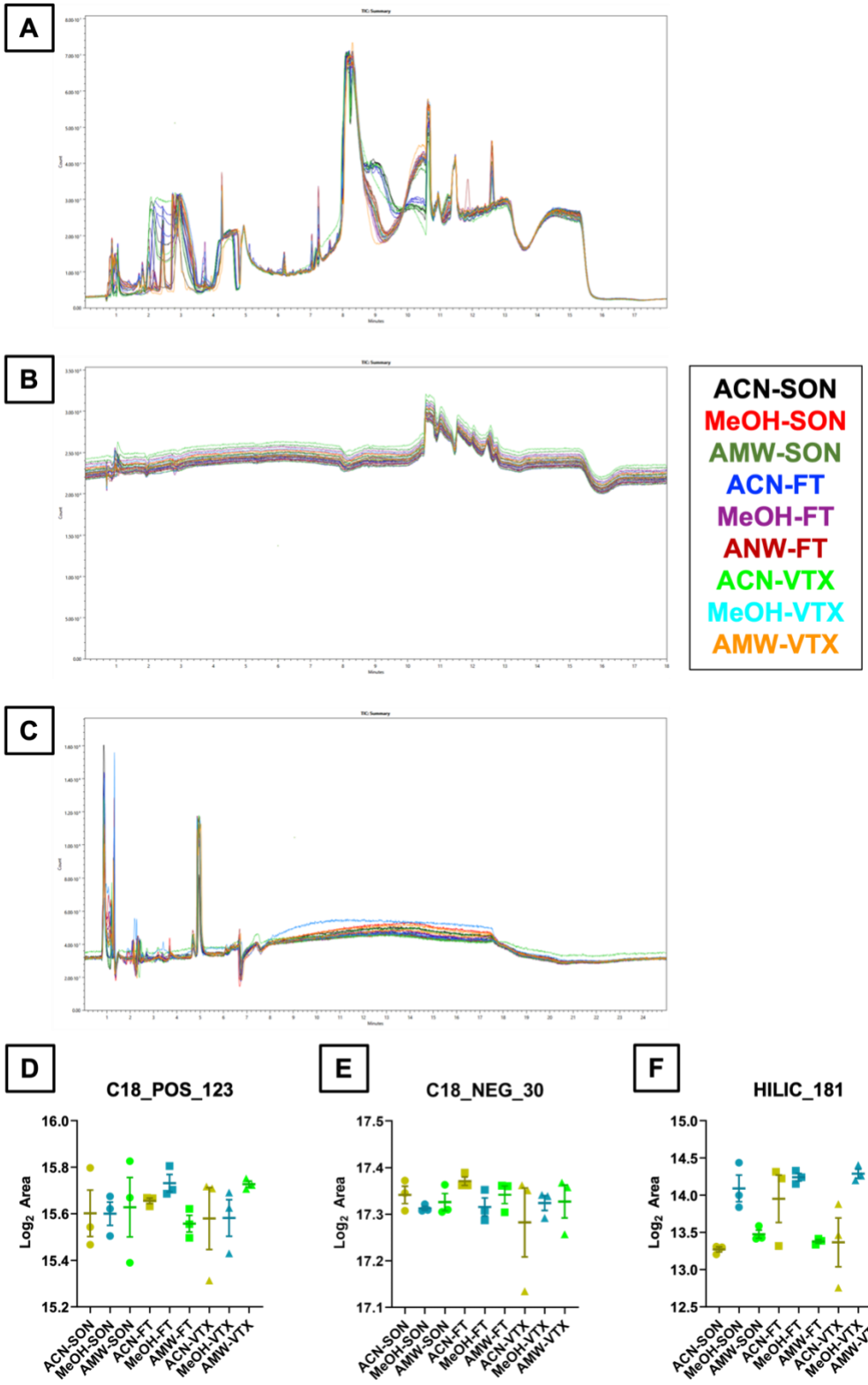


**Figure 4.3.1: Total Ion Chromatograms (TICs) for Sample Preparation Optimisation Experiment.** TICs of 1x10$^6$ primary monocytes isolated from healthy blood and metabolites extracted with either acetonitrile (ACN), methanol (MeOH), or ACN:MeOH:$H_2O$ (AMW, 2:2:1) and lysed by either sonication (SON), freeze-thaw (FT), or vortexing (VTX). Samples were analysed by LC-MS with reverse-phase C18 in ESI+ (A), ESI- (B), and HILIC ESI- (C). Example metabolite levels for solvent and lysis protocols measured by C18 in ESI+ (D), ESI- (E), and HILIC ESI- (F) are plotted as mean ± standard error of the mean (SEM).

Next, looking at the different extraction methods in an unbiased approach untargeted analysis of extracted monocytes was carried out as described in Sections 2.9.7 and 2.9.8. There were 146, 96 and 205 unique features detectable in all samples from the C18 ESI+, C18 ESI-, and HILIC ESI- respectively (Figure 4.3.2A). The low number of detectable features in C18 ESI- was predictable given the high baseline and lack of distinguishable peaks in the TIC (Figure 4.3.1B). The combined detectable features were used to generate PCA plots comparing extraction solvents and lysis methods (colour-coded in Figures 4.3.2B & 4.3.2C). Methanol- and ACN:MeOH:$H_2O$-extracted samples clustered closely together, and ACN-extracted samples were separate from these and one another (Figure 4.3.2B). This separation is likely coming from variance in metabolites detected in the C18 ESI+ method as predicted from the TIC. In contrast, lysis methods did not readily cluster together or apart from one another and were not particularly distinct (Figure 4.3.2C).

Next, the combined features (n=447) from the three LC-MS methods were used to determine the combined peak area, and the variation in peak areas across replicates was measured by percent coefficient of variation (%CV). A number of methods showed consistently high total peak area with limited variation between replicates. In particular, the freeze-thaw lysis method returned consistently high total peak area (Figure 4.3.3A) and had the lowest %CV between replicates (Figure 4.3.3B). Methanol extractions with all three lysis methods also performed well. There was substantial variation in total peak area with ACN extractions, which indicates that ACN may not be an appropriate extraction solvent for larger cohorts. The ACN:MeOH:$H_2O$ blend did however show impressive peak areas and %CV, particularly with freeze-thaw and vortexing lysis protocols.

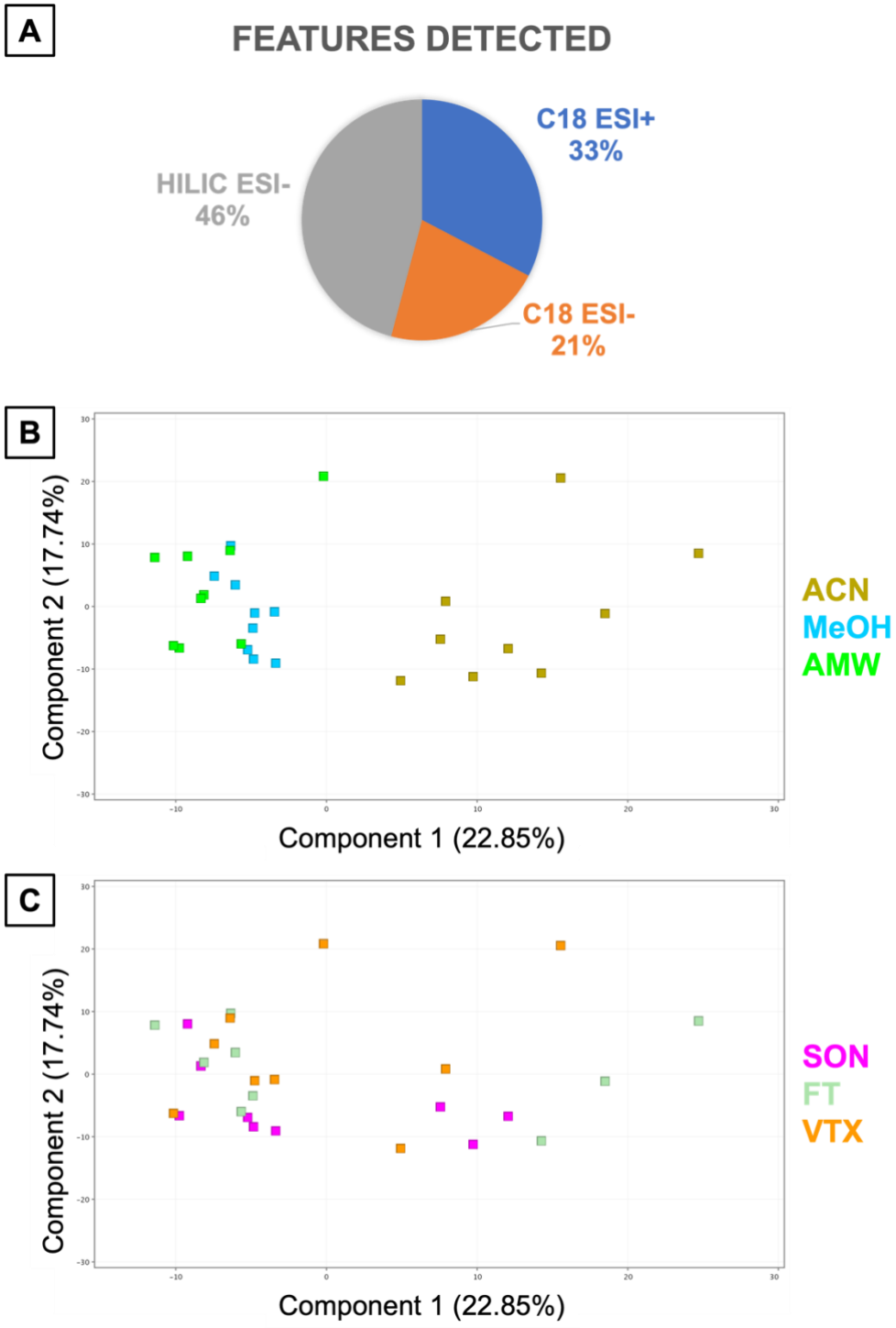


**Figure 4.3.2: Principal Component Analyses of Solvent and Lysis Strategies for Primary Monocyte Metabolite Extraction.** $1x10^6$ primary monocytes were isolated from healthy blood and metabolites extracted with monocytes extracted with either acetonitrile (ACN), methanol (MeOH), or ACN:MeOH:Water (AMW, 2:2:1) and lysed by either sonication (SON), freeze-thaw (FT), or vortexing (VTX). Samples were analysed by LC-MS with reverse-phase C18 in ESI+, C18 ESI-, and HILIC ESI- and untargeted analysis carried out using MassHunter ProFinder. There were 146, 96 and 205 features from the C18 ESI+, C18 ESI-, and HILIC ESI- respectively (A). Features identified in all variable groups from the three LC-MS methods (n=447) were combined and principal component analysis (PCA) was carried out to investigate clustering by solvent (B) and lysis method (C).

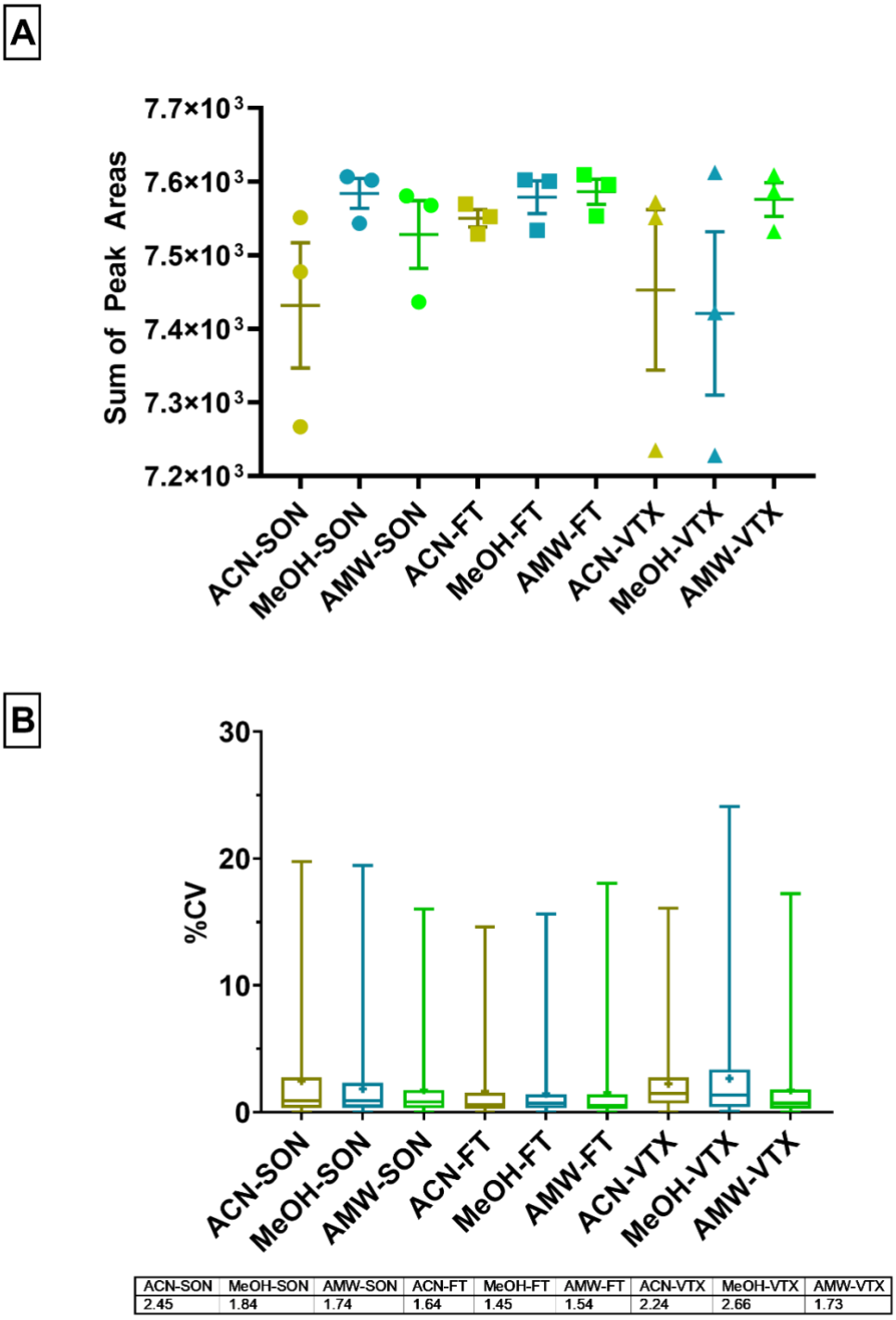


| ACN-SON | MeOH-SON | AMW-SON | ACN-FT | MeOH-FT | AMW-FT | ACN-VTX | MeOH-VTX | AMW-VTX |
|---|---|---|---|---|---|---|---|---|
| 2.45 | 1.84 | 1.74 | 1.64 | 1.45 | 1.54 | 2.24 | 2.66 | 1.73 |

**Figure 4.3.3: Peak Areas and %CVs Comparison of Solvent and Lysis Strategies for Primary Monocyte Metabolite Extraction.** Primary monocytes ($1x10^6$) were isolated from healthy blood and metabolites extracted with monocytes extracted with either acetonitrile (ACN), methanol (MeOH), or ACN:MeOH:Water (AMW, 2:2:1) and lysed by either sonication (SON), freeze-thaw (FT), or vortexing (VTX). Samples were analysed by LC-MS with reverse-phase C18 in ESI+, C18 ESI-, and HILIC ESI- and untargeted analysis carried out using MassHunter ProFinder. The sum of peak areas (A) and %CVs (B) for the 447 features detected across all sample preparation protocols are compared for the different methods. Peak areas (A) are plotted as mean ± standard error of the mean (SEM) and %CVs are plotted as maximum and minimum with the mean highlighted with a "+".

Correlation analysis of the combined feature peak areas (n=447) was carried out to compare consistency across extraction protocols (Figures 4.3.4 and 4.3.5). All extractions correlated well with one another, and the lowest Pearson r value was 0.876 (MeOH-FT vs ACN-SON). The ACN-SON extraction had the lowest correlation coefficients of all the extraction methods and ACN extractions also had lower r values than the other extractions. ACN does not appear to be as effective as MeOH or the ACN:MeOH:$H_2O$ blend, but there is little to separate the latter two in terms of extraction efficacy. The blend slightly outperformed MeOH slightly in terms of Pearson r and other readouts.

Untargeted analysis was carried out on individual extraction-lysis protocols to measure the total numbers of metabolite features detectable for each technique. These are plotted in Figure 4.3.6 separated by LC-MS method. As with previous analysis there was very little to discriminate between lysis protocols, and the majority of variation came from different extraction solvents. Methanol-based extractions detected the most metabolite features, particularly with the C18 ESI+ and HILIC methods. ACN extractions detected a greater number of metabolites when measured by C18 ESI-, but this method detected the fewest features of the three LC-MS methods overall.

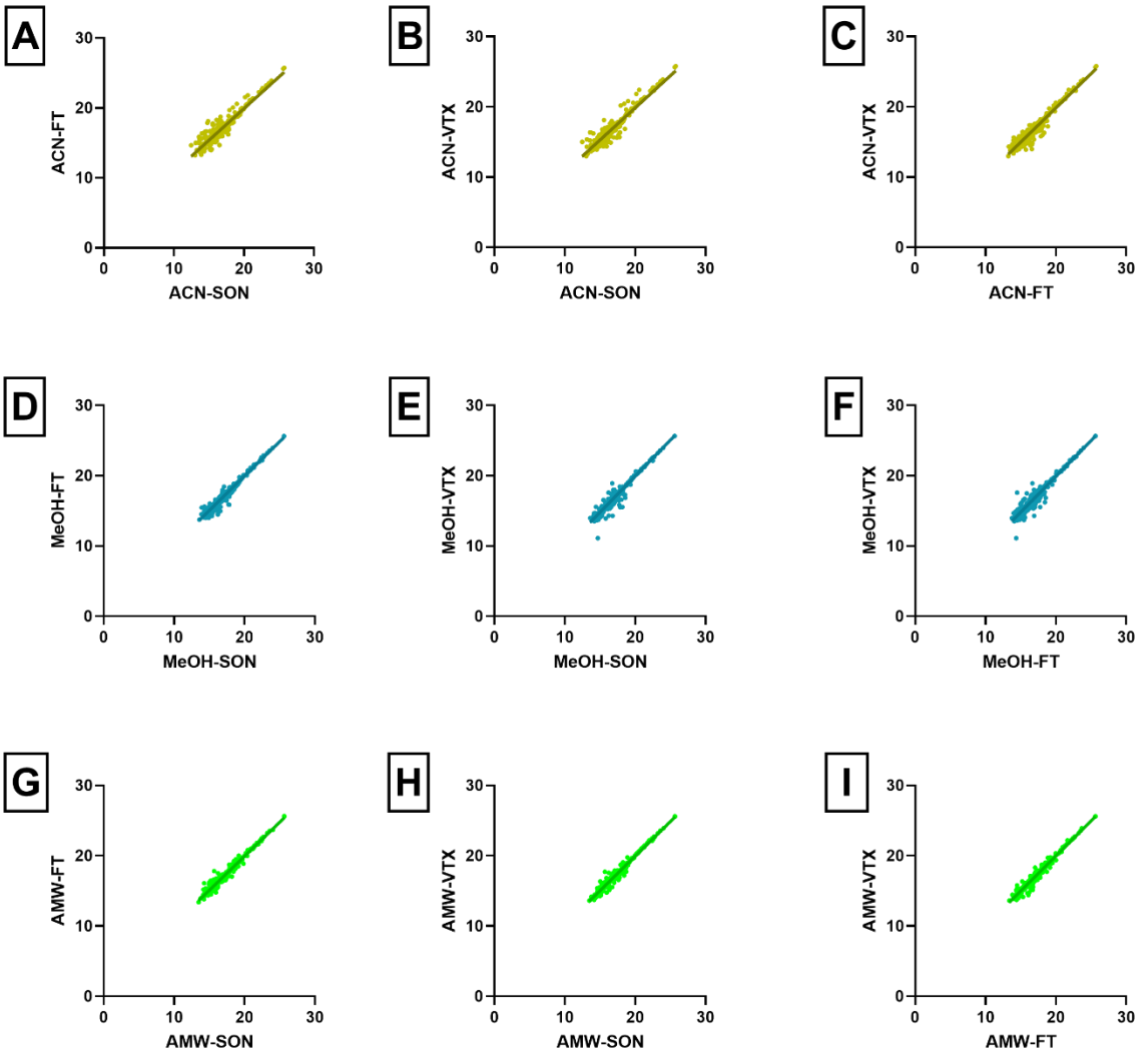


**Figure 4.3.4: Correlations of Peak Areas with Solvent and Lysis Strategies for Primary Monocyte Metabolite Extraction.** Primary monocytes ($1x10^6$) were isolated from healthy blood and metabolites extracted with monocytes extracted with either acetonitrile (ACN), methanol (MeOH), or ACN:MeOH:Water (AMW, 2:2:1) and lysed by either sonication (SON), freeze-thaw (FT), or vortexing (VTX). Samples were analysed by LC-MS with reverse-phase C18 in ESI+, C18 ESI-, and HILIC ESI- and untargeted analysis carried out using MassHunter ProFinder. Correlations of peak areas within solvents are shown in Figures A-I.

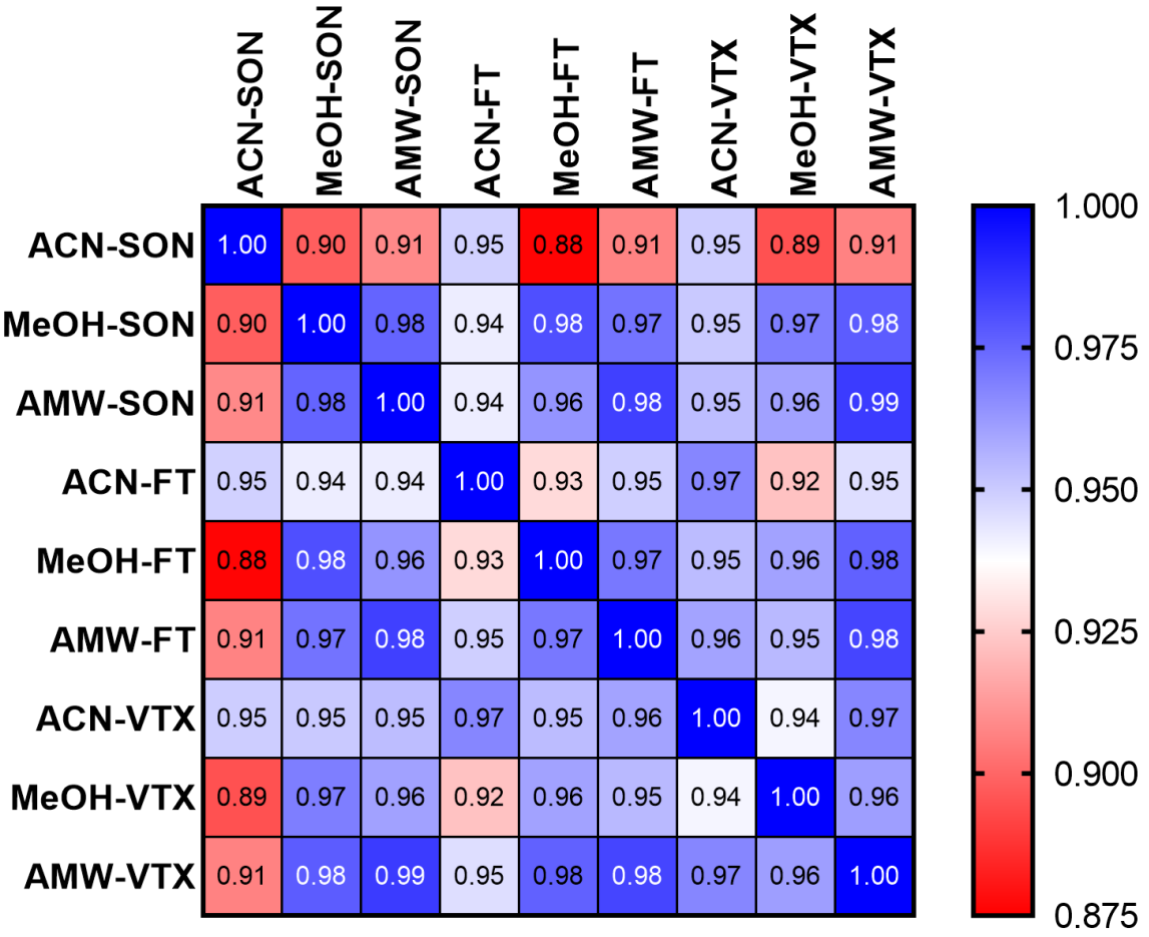


**Figure 4.3.5: Correlation Matrix of Peak Areas with Solvent and Lysis Strategies for Primary Monocyte Metabolite Extraction.** Primary monocytes ($1x10^6$) were isolated from healthy blood and metabolites extracted with monocytes extracted with either acetonitrile (ACN), methanol (MeOH), or ACN:MeOH:Water (AMW, 2:2:1) and lysed by either sonication (SON), freeze-thaw (FT), or vortexing (VTX). Samples were analysed by LC-MS with reverse-phase C18 in ESI+, C18 ESI-, and HILIC ESI- and untargeted analysis carried out using MassHunter ProFinder. The Pearson correlation matrix for all solvent and lysis methods is shown highlighting strong (blue) and weaker correlations (white-red) in paired samples.

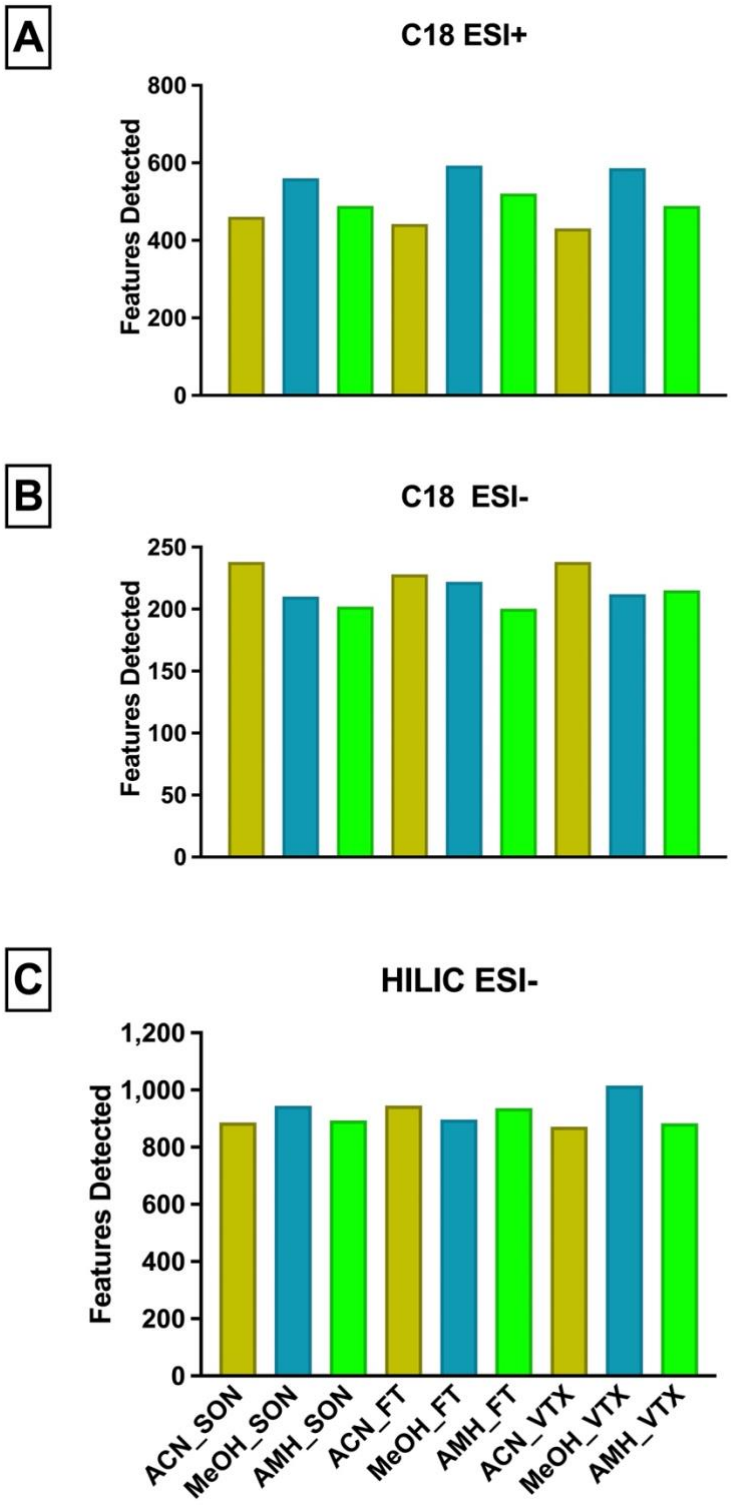


**Figure 4.3.6: Unique Features Detected Across Solvent and Lysis Strategies for Primary Monocyte Metabolite Extraction.** Primary monocytes ($1x10^6$) were isolated from healthy blood and metabolites extracted with monocytes extracted with either acetonitrile (ACN), methanol (MeOH), or ACN:MeOH:Water (AMW, 2:2:1) and lysed by either sonication (SON), freeze-thaw (FT), or vortexing (VTX). Samples were analysed by LC-MS with reverse-phase C18 in ESI+ (A), C18 ESI- (B), and HILIC ESI- (C) and untargeted analysis carried out using MassHunter ProFinder. Numbers of metabolite features detected by different LC-MS methods for nine solvent/lysis strategies are shown.

These results do not point to a clear, superior extraction strategy, and the literature is conflicting in recommendations for single phase extractions. The final choices for the optimised sample preparation protocol are as follows:

- **Solvent**: Some experts recommend a mixture of solvents with different polarities (e.g. ACN:MeOH:$H_2O$) for extensive metabolome coverage [47]. The most common extraction protocol for mammalian cell metabolomics is 80% MeOH in water [58]. The high performance of the ACN:MeOH:$H_2O$ may come from the addition of water [358]. Based on these results (high numbers of features detected, low %CV) and recommendations from literature review, we opted to use 80% MeOH as our extraction solvent for metabolomic profiling.
- **Lysis.** Overall, there was very little variation between lysis protocols. Freeze-thaw (FT) protocols had lower inter-replicate variation regardless of extraction solvent. However vigorous lysis protocols such as these are typically only required for cell types with rigid membranes such as yeasts and bacteria. We opted to combine the sonication and vortexing protocols and the full optimised sample preparation protocol is detailed in Section 2.9.2.
- RP and HILIC chromatography are traditionally used together used as complimentary techniques to improve metabolome coverage. However, due to the lower numbers of features detected with the C18 method plus the requirement for an ion-pairing agent (PFPA) in the mobile phase, this method was not considered appropriate for metabolomic profiling. The HILIC method (run in ESI+ & ESI-) will be the primary LC-MS method for metabolomic profiling experiments. Full details of this method can be found in Section 2.9.3.

### 4.3.2 Validation of Sample Preparation Optimisation in Peripheral Blood Mononuclear Cells (PBMCs) and Monocytes

To validate the sample preparation optimisation results, we stimulated PBMCs and monocytes with ANCA and trialled the optimised extracted protocol (see Section 4.2.3.3). As shown in the PCA plot for the targeted metabolites in Figure 4.3.7 (20/53 and 19/53 detectable in PBMCs and monocytes respectively, cells were differentiated more on the basis of cell type (PBMC vs. monocyte) than treatment (unstimulated, isotype, anti-MPO or anti-PR3). This is to be expected as PBMCs represent a diverse cell population with various metabolic demands, many of which do not respond to ANCA stimulation. From these data, neither cell type could discriminate treatment groups based on metabolism. Due to poor metabolite recovery in monocytes for Donor 2 and PBMCs in Donor 3, these replicates were excluded from the analysis. There were only minor differences in metabolite levels between anti-MPO, anti-PR3, and unstimulated cells (Figure 4.3.8). Some metabolites which were not detectable in PBMCs were enriched in monocytes – notably aconitic acid and citrate – which are involved in the TCA cycle. A number of amino acids detectable in PBMCs were not found in monocytes (see Figure 4.3.8). Curiously, concentrations of inosine 5-monophosphate (IMP) showed a slight decrease in PBMCs in response to ANCA, but this compound was not detectable in isolated monocytes (Figure 4.3.8B). This metabolite may be involved in the ANCA response in other cell types in the PBMC fraction. However, this small experiment is dramatically underpowered to give meaningful results about ANCA stimulation, and these findings should be considered with caution. We can however confirm that the optimised sample preparation protocol is effective at detective metabolites of interest contained in the synthetic standard mix in primary immune cells.

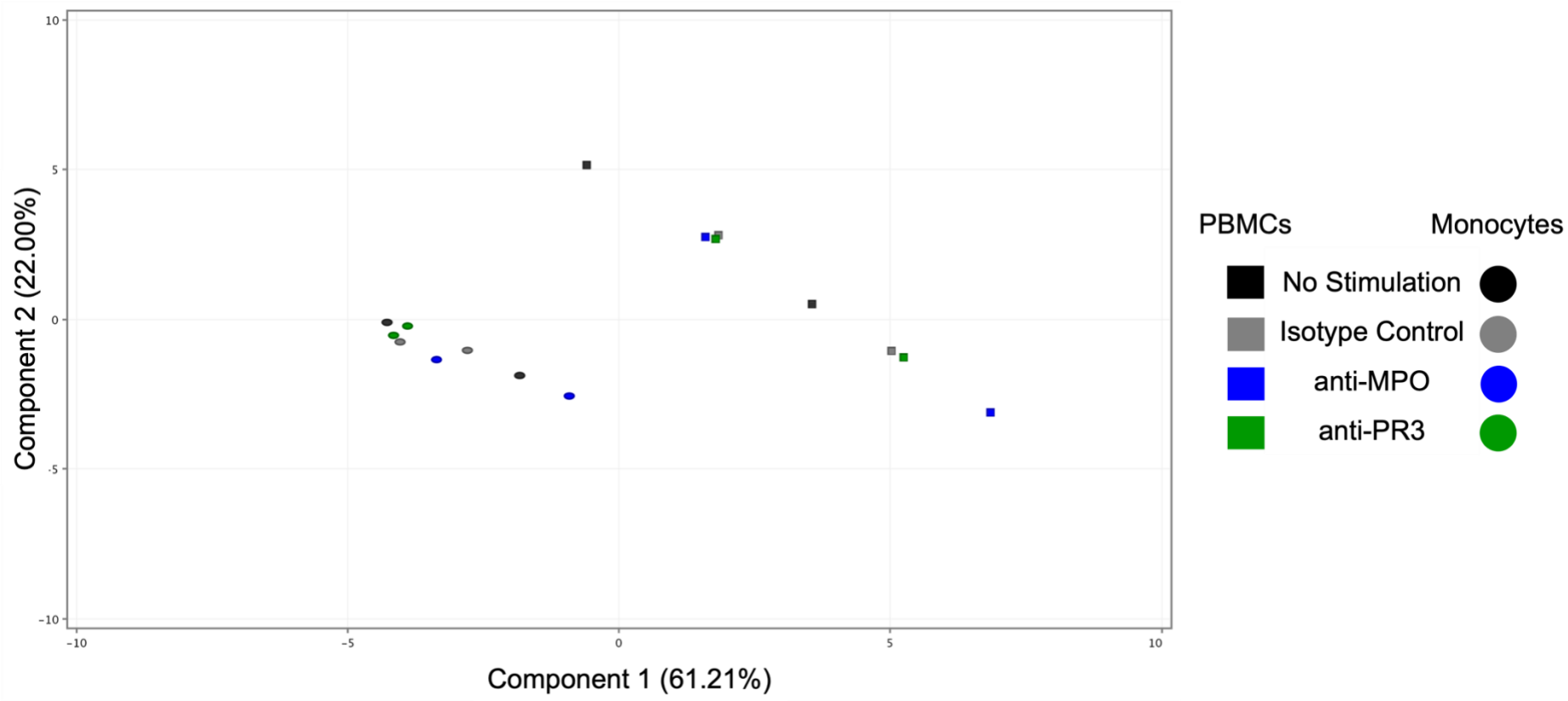


**Figure 4.3.7: Principal Component Analyses of Targeted Analysis of Primary Monocytes and PBMCs for Sample Preparation Validation.** PBMCs (squares) and CD14+ monocytes (circles) were isolated from blood of healthy controls (n=3) and stimulated for 4 hours with 5µg/ml monoclonal antibody (mAb) directed against MPO (blue), PR3 (green), or IgG1 isotype control (light grey). Metabolites were extracted and analysed using optimised sample preparation and LC-MS protocols and targeted metabolite analysis carried out using MassHunter ProFinder. Principal Component Analysis (PCA) plots were generated for the four treatment groups.

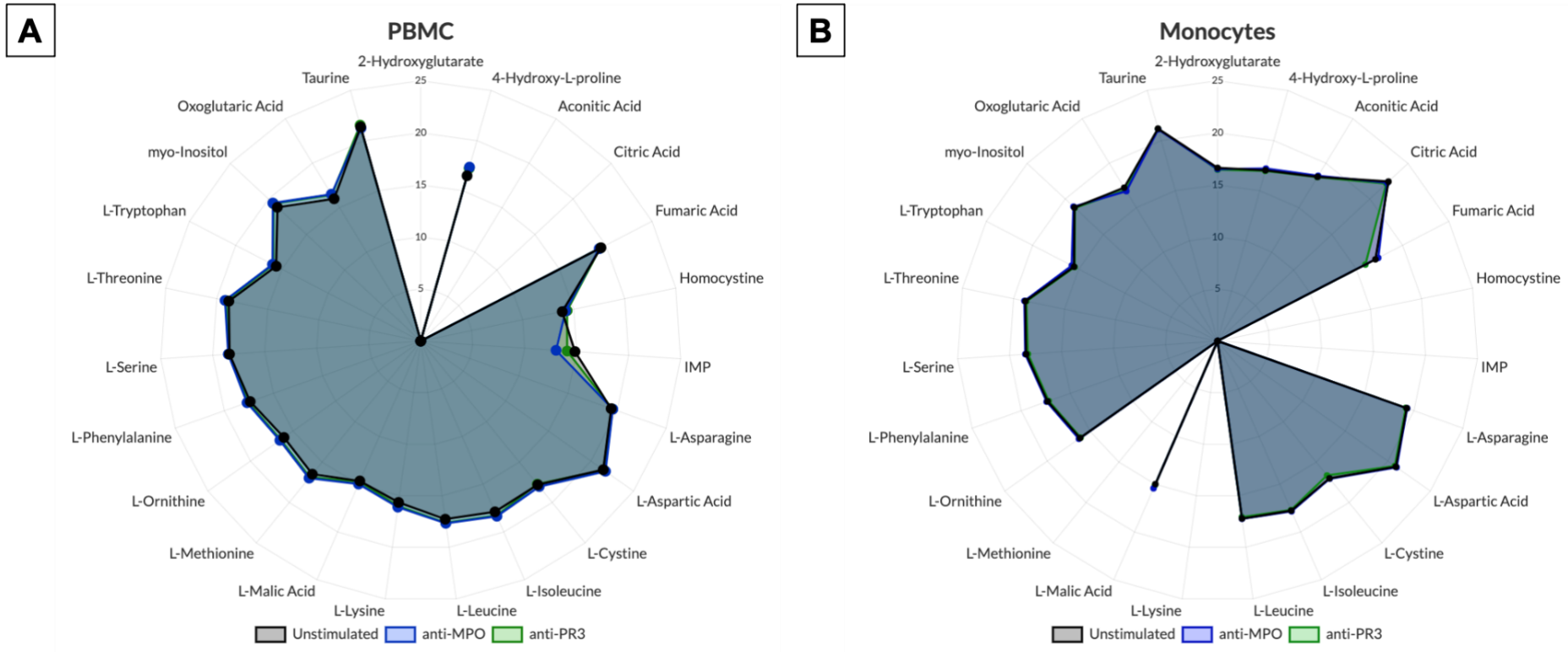


**Figure 4.3.8: Radar Plot Analyses of Targeted Analysis of Primary Monocytes and PBMCs for Sample Preparation Validation.** PBMCs (A) and CD14+ monocytes (B) were isolated from blood of healthy controls and stimulated for 4 hours with 5µg/ml monoclonal antibody (mAb) directed against MPO, PR3, or IgG1 isotype control (n=3). Metabolites were extracted and analysed using optimised sample preparation and LC-MS protocols and targeted metabolite analysis carried out using MassHunter ProFinder. Radar plots of $log_2$-transformed metabolite data of PBMCs (A) and CD14+ monocytes (B) are shown.

The number of detectable metabolite features was assessed and compared to previous experiments (Figure 4.3.9). This sample preparation validation experiment used $5x10^6$ cells per stimulation condition, a fivefold increase on cell numbers from the sample preparation optimisation work. As a result, the number of detectable features would be expected to increase compared to MeOH and AMW extractions. However, there were fewer metabolite features detected in the sample preparation validation than the sample preparation optimisation (Figure 4.3.9). There were 901, 952, and 904 features detected on average in the ACN, MeOH and blended AMW monocyte extractions, respectively. Validation experiments detected just 528 features in monocytes after stimulation, with 874 and 739 in the PBMC and PooledQC groups respectively. These differences are likely a result of insufficient quenching, as the Validation experiments were not cooled after stimulation. Additional sample handling in the post-stimulation cells compared to the freshly isolated, unstimulated monocytes from the optimisation work, may also have affected peak area accuracy. The disparity could also be a result of variation between treatment groups or confounded by higher number of (mismatched) samples. Additional considerations for the optimised protocol will focus on improving removal of cells from plates, sample dry down to concentrate samples, and monitoring consistency in extraction efficacy between replicates.

Finally, the HILIC method was shown to have excellent coverage of metabolites in the synthetic standard mixture. 52 of the 53 metabolites in the synthetic standard preparation were detectable across the positive and negative ionisation modes (see Figure 5.3.8). Urea was the only metabolite not detectable by either ionisation mode. The method was also able to detect 739 features in the PooledQC samples of the sample preparation validation experiment. Additional optimisation of experimental conditions and metabolomic data analysis is needed to precisely determine the role of ANCA stimulation in primary monocytes at this early timepoint.

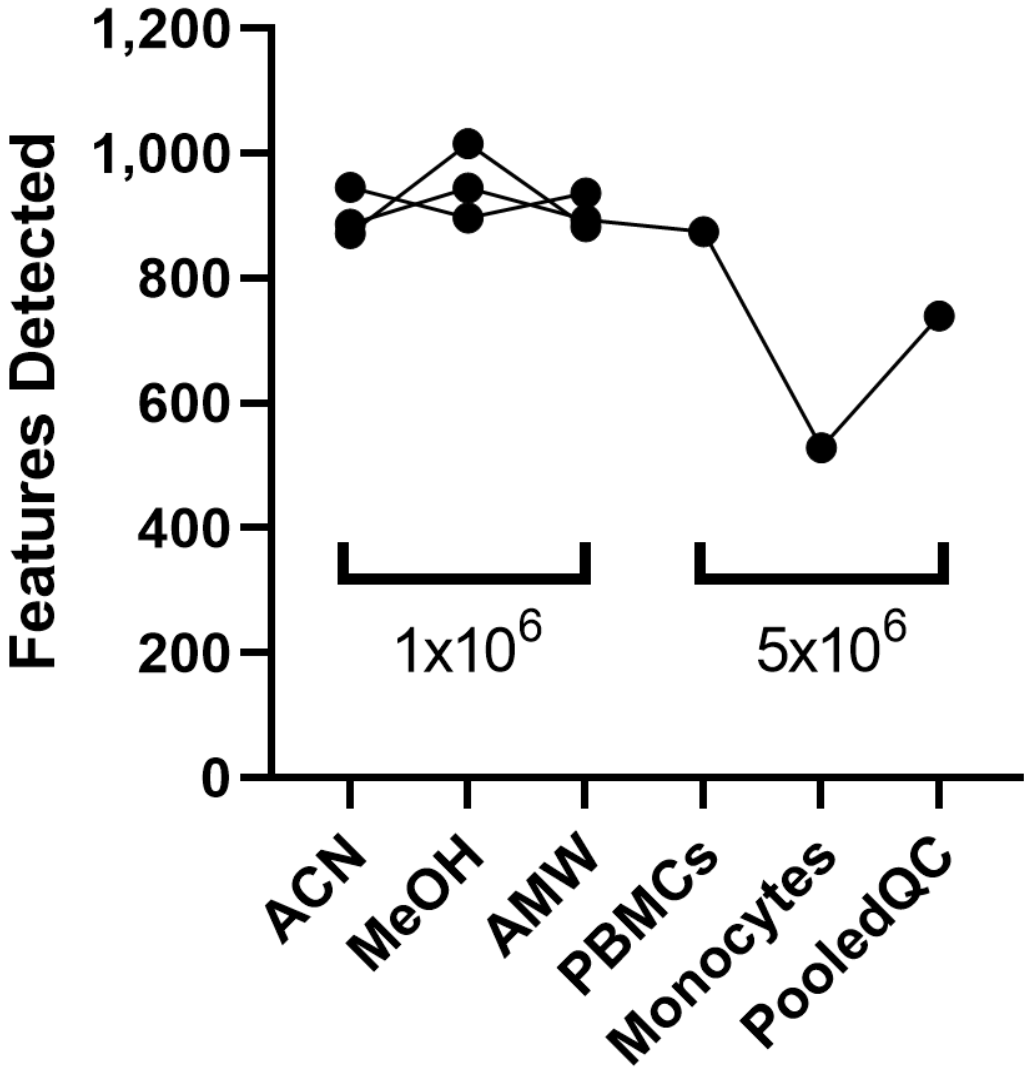


**Figure 4.3.9: Numbers of Detectable Metabolite Features by HILIC ESI- LC-MS across Sample Preparation Optimisation and Validation Experiments.** ACN, MeOH, and AWH represent the numbers of features detectable in the acetonitrile, methanol and ACN:MeOH:Water blend in the sample preparation optimisation experiments, respectively. These experiments were carried out in freshly isolated primary monocytes. Features detected in the Sample Preparation Optimisation PBMCs and Monocytes are plotted (extracted in 80% MeOH), as well as the PooledQC containing both cell types.

### 4.3.3 Log Transformation is an Essential Step for Metabolomic Data Normalisation

Metabolomics data covers several orders of magnitude, and primary cell culture introduces a high degree of inter-replicate variability. Log transformation (to base 10 or base 2) is a routine data analysis procedure which limits the influence of extreme values for subsequent statistical analysis. Normality and lognormality of metabolomic data from the targeted analysis of the Primary monocyte profiling cohort (see Figure 5.2.1) was assessed using four methods: Anderson-Darling, D'Agostino & Pearson, Shapiro-Wilk, and Kolmogorov-Smirnov tests. QQ plots for normal (non-transformed AUC values) and lognormal values are shown in Figure 4.3.10. Actual values do not remotely correlate with the predicted values on the normal QQ plot (Figure 4.3.10A), indicating a high degree of skewness. Conversely, the majority of the lognormal samples align closely with predicted values (Figure 4.3.10B). There is a small amount of kurtosis in some samples, which may represent outliers or may be amenable to data normalisation. From these results, we can conclude that $\log_2$ transformation is an essential step for metabolomic data normalisation. All metabolomic data reported in this work has been $\log_2$ transformed.

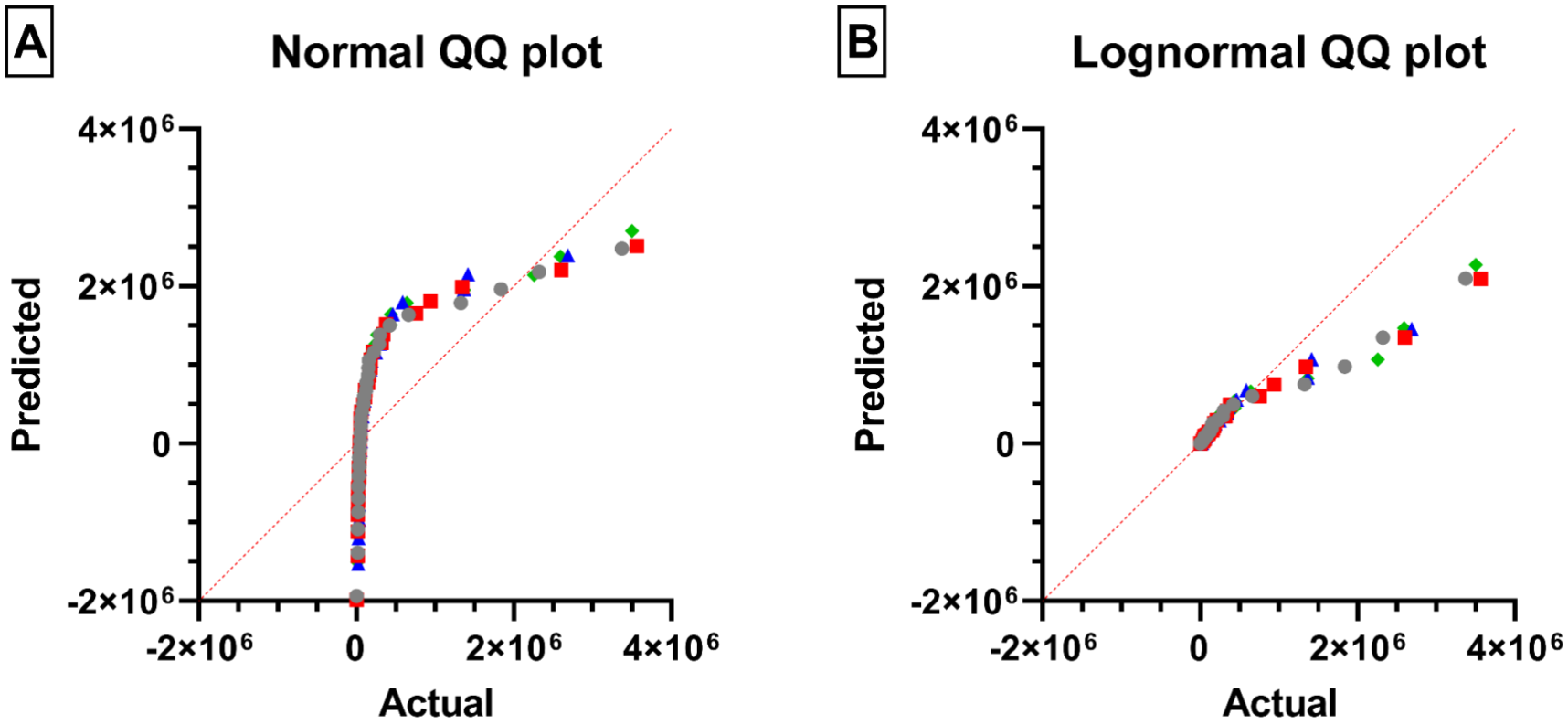


**Figure 4.3.10: Normality Testing Metabolomics Data of Stimulated Primary Monocytes.** CD14+ monocytes were isolated from healthy donors and stimulated (or left unstimulated, grey) @37°C for 4 hours with 5µg/ml monoclonal antibody (mAb) directed against MPO (blue), PR3 (green), or 200ng/ml LPS (red). Metabolites were extracted, analysed by LC-MS, and targeted metabolomic analysis of 53 metabolites was completed. 32 of the 53 metabolites were detected in experimental samples. Normality testing was completed using four methods: Anderson-Darling test, D'agostino & Pearson test, Shapiro-Wilk test, and Kolmogorov-Smirnov test. QQ plots for Normal (A) and Lognormal (B) data were generated.

### 4.3.4 Assessment of Normalisation Strategies for Untargeted Metabolomic Analysis of Primary Monocytes

Given the high degree of variability in cellular metabolomics studies, data normalization is an essential step. Here a total of 41 normalisation methods were applied to the primary monocyte metabolomic profiling data. A summary of the normalisation methods trialled in this work is shown in Figure 4.2.2. The effectiveness of the various normalisation strategies is compared to $log_2$ transformed data alone. These methods were assessed for efficacy using the following criteria:

- Intragroup variance measured by coefficients of variation (%CV) and median absolute deviation (MAD); and
- Intergroup differentiation with principal component analyses (PCA) and receiver operating characteristic (ROC) curves;

These analyses were carried out in PooledQC samples where possible, and also in the negative (unstimulated cells, NS) and positive (LPS) control groups.

Before carrying out these assessments, Pearson correlation analysis was completed to evaluate the similarity of these normalisation methods with one another. Comparing the levels of 32 metabolites in unstimulated cells (n=6, see Figure 5.3.2) we show that several methods correlated very strongly with one another (Figure 4.3.11), indicating an overlap in their methodologies. In particular, biological normalisation methods – which applied additional experimental results (cytokine production, protein content) to samples as an external scalar – showed very high correlations in these unstimulated cells. Certain algorithms (scaling, baselining) were similar in their application. Interestingly, both MPP and the NOREVA [102] platforms offer Pareto Scaling [359], probabilistic quotient normalization (PQN [360]), and quantile [361] normalisation. These methods had r values of 0.86, 0.43, and 0.62 with their relevant counterparts, respectively, indicating differences in application, despite being identical in name. Two protein measurement approaches (A280, BCA) were also considered, and both showed perfect correlation with $log_2$ alone and with one another. An exception to the similarities is the Contrast method, which showed a (minor) negative correlation with almost all methods. This highlights the need for an intimate understanding of input data before application of different normalisation methods.

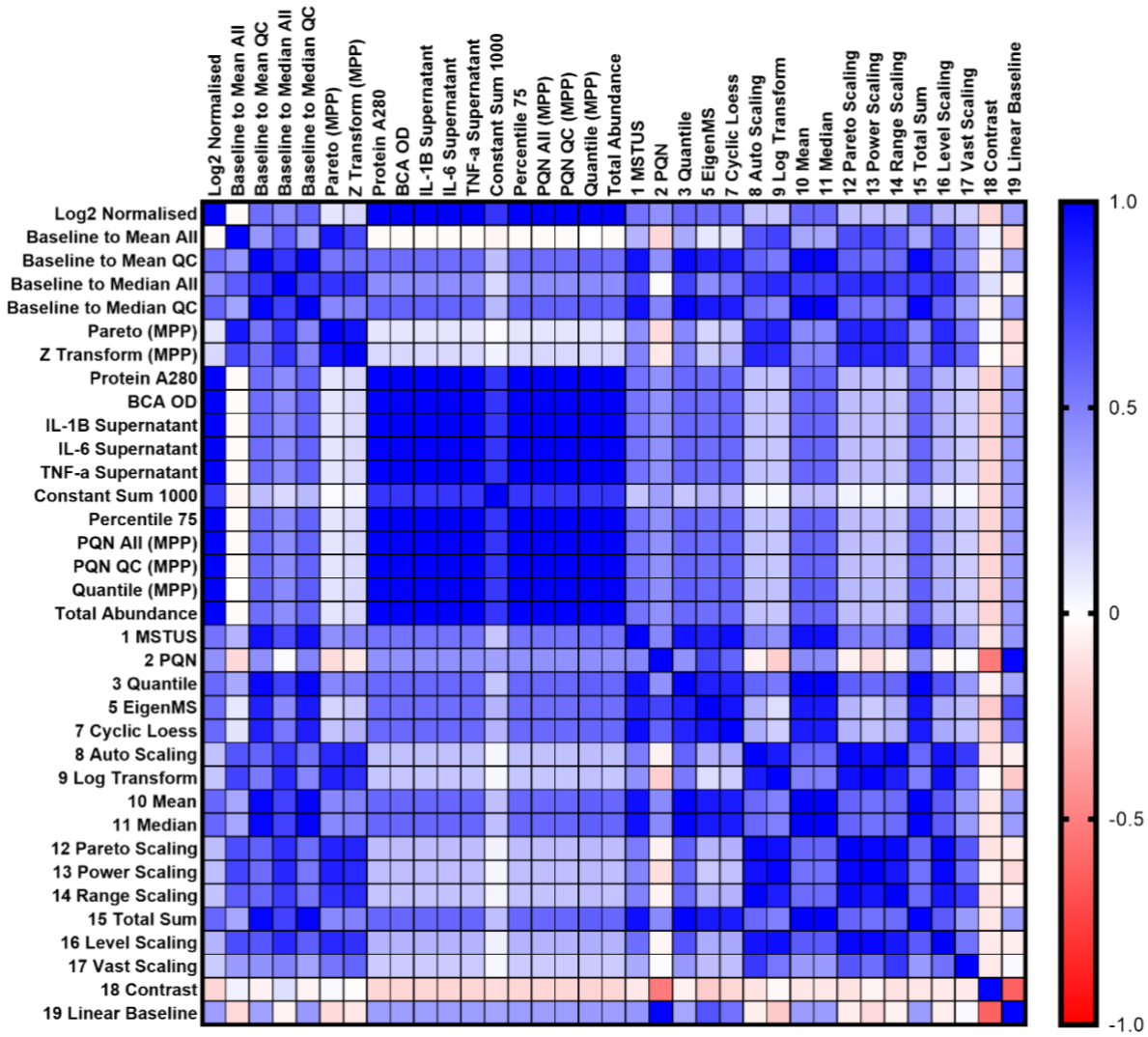


**Figure 4.3.11: Correlation Matrix of Normalisation Methods Applied to Unstimulated Cells.** CD14+ monocytes (n=6) were isolated from healthy donors and stimulated @37°C for 4 hours with unstimulated cells as a negative control. Metabolites were extracted, analysed by LC-MS, and targeted metabolomic analysis of 53 metabolites was completed. 32 of these 53 metabolites were detected and metabolite abundances calculated. Abundance values for unstimulated cells were normalised by 41 different normalisation techniques. Pearson r values for these normalised areas were calculated for each method and plotted here as a correlation matrix.

### 4.3.5 Intragroup Variation Assessment by Normalisation Strategies in PooledQC Samples and Unstimulated Cells

Next, we assessed intragroup variance in the PooledQC (PQC) and negative control (NS) groups. There were 10 PQC measurements throughout the run including a triplicate block at the beginning and end. The NOREVA methods use PQC samples for additional inter-run normalisation by LOESS as standard [102]. Therefore, PQC results for these normalisation strategies are not available and were excluded from this analysis. %CVs for 32 metabolites detectable in PQC samples were calculated for 18 of the 41 normalisation methods and plotted in Figure 4.3.12A. Although %CV is routinely used in LC-MS it is sensitive to negative and zero values, which many of the normalisation methods generate. Median absolute deviation (MAD) was calculated to overcome this shortfall and results are plotted in Figure 4.3.12B.

$Log_2$ transformation alone reduced the median %CV from 10.29 to 0.92 (Figure 4.3.12A) in PQC samples. The protein content measurements (A280 and BCA OD MF) and MPP PQN and Quantile algorithms further improved upon the $log_2$ %CV value. %CV for Total Abundance normalised data is not shown on the plot as it is below zero, and normalised values for the baselining methods were highly exaggerated. Conversely, these methods performed better when assessed by MAD. The MAD values for non-normalised samples are exceptionally high, further emphasising the need for $log_2$ transformation in cellular metabolomic data analysis. Baselining methods had improved/decreased MAD compared to $log_2$ transformation alone. Protein content and cytokine production readouts did not alter MAD values. These two readouts show that different normalisation strategies can improve intragroup variation in PQC samples.

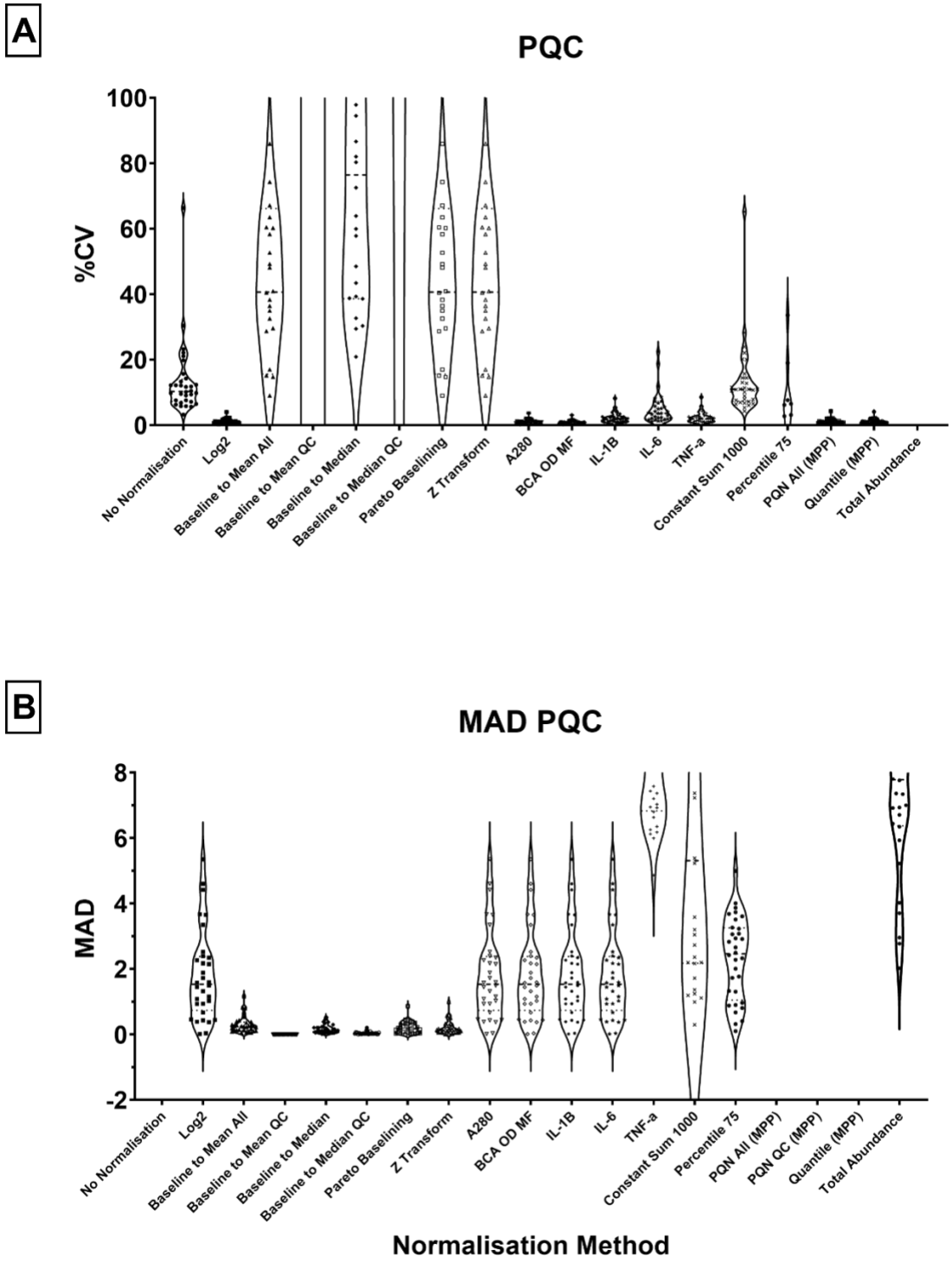


**Figure 4.3.12: Intergroup Variation in PooledQC Samples by Normalisation Method.** CD14+ monocytes (n=6) were isolated from healthy donors and stimulated @37°C for 4 hours with unstimulated cells as a negative control. Metabolites were extracted, analysed by LC-MS, and targeted metabolomic analysis of 53 metabolites was completed. 32 of these 53 metabolites were detected in experimental samples and metabolite abundances calculated. Abundance values for PooledQC samples (n=10) were normalised using 18/41 normalisation techniques that do not utilise PooledQC samples in their methodology. Coefficients of Variation (%CV, A) and median absolute deviation (MAD, B) were calculated for each metabolite with each normalisation method.

Similar results to PQC samples were also evident in unstimulated cells (Figure 4.3.13). %CV and MAD were calculated for all 41 normalisation methods in unstimulated monocytes. It is clear from these graphs that %CV and MAD work differently for different normalisation techniques – external scalars are more effective as measured by %CV and algorithms perform better when assessed by MAD. Several normalisation methods had %CVs well above 100% for all 32 metabolites and some results could not be plotted as the %CV values were negative (TIC, BPC, Total Sum, Sum M32), further emphasising the need for diverse intragroup variation measurements. Similar to PQCs, MAD was excessive for non-normalised data in unstimulated cells. MAD values for the cluster of methods in Figure 4.3.11 were almost unchanged, but show massive improvements in %CV. Many NOREVA normalisation algorithms showed improvements in MAD compared to $\log_2$ transformation alone. Here we have identified a number of normalisation techniques which can improve intragroup variation in primary monocytes. Before we can rule out certain methods, additional effectiveness strategies will be required to determined which of these are the most appropriate for our dataset.

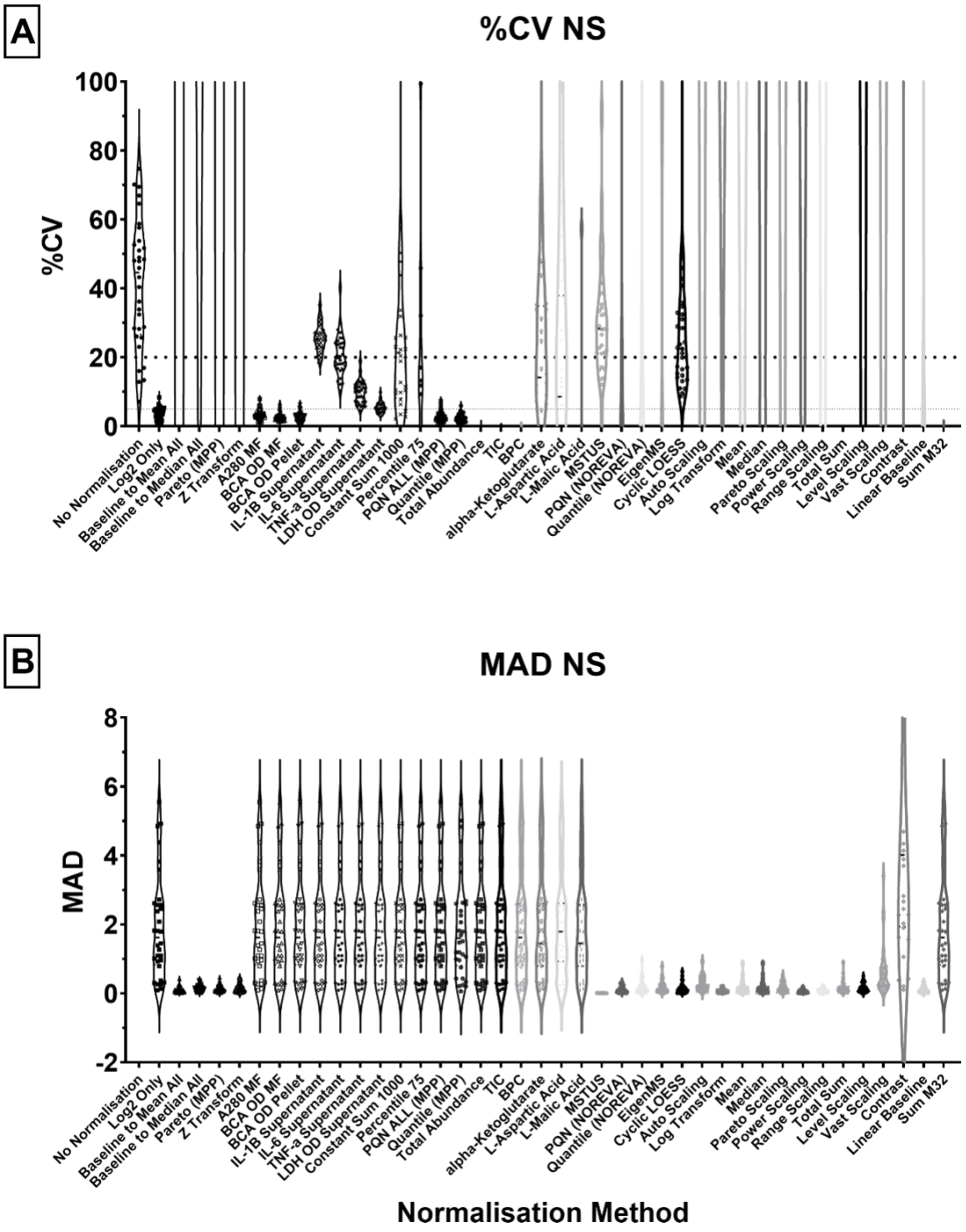


**Figure 4.3.13: Intragroup Variation in Unstimulated Cells by Normalisation Method.** CD14+ monocytes (n=6) were isolated from healthy donors and stimulated @37°C for 4 hours with unstimulated cells as a negative control. Metabolites were extracted, analysed by LC-MS, and targeted metabolomic analysis of 53 metabolites was completed. 32 of these 53 metabolites were detected in experimental samples and metabolite abundances calculated. Abundance values for unstimulated cells (n=6) were normalised by 41 different normalisation techniques. Coefficients of Variation (%CV, A) and median absolute deviation (MAD, B) were calculated for each metabolite with each normalisation method.

### 4.3.6 Intergroup Separation Assessment by Normalisation Strategies

In total, 25 of the 41 normalisation methods had lower %CV and/or MAD compared to $log_2$ transformation alone. A280 metabolite fraction (MF), BCA OD MF, BCA OD Pellet, PQN ALL (MPP) and Quantile (MPP) all lower %CV. MAD improved for Baseline to Mean All, Baseline to Median All, Pareto (MPP), Z Transform, MSTUS, PQN (NOREVA), Quantile (NOREVA), EigenMS, Cyclic LOESS, Auto Scaling, Log Transform, Mean, Median, Pareto Scaling, Power Scaling, Range Scaling, Total Sum, Level Scaling, Vast Scaling, and Linear Baseline. To further interrogate the utility of these normalisation methods, PCA plots for each method were generated to assess separation of the positive (LPS) and negative (unstimulated, NS) controls. These plots were compared to $log_2$ transformation alone. Improved separation of these two groups would indicate effective data normalisation [73]. Normalisation methods which matched $log_2$ %CV (3.66) or MAD (1.92) were not plotted.

The five normalisation methods which showed improvement in intragroup variation in unstimulated cells measured by %CV are displayed in Figure 4.3.14. Normalisation by cell pellet protein (D) was the only method with improved PCA appearance compared to $log_2$ alone (A). Other protein content measurements (A280 [B] or BCA OD MF [C]) showed lesser improvements in intergroup separation, and MPP algorithms (PQN [E] and Quantile[F]) were almost unchanged. Cytokine production as a normalisation method (IL-1β, IL-6 or TNF-α; Figures 4.3.14G, H, & I, respectively) showed a very favourable PCA appearance. However, these results are normalised to an external scalar with (substantial) significant differences between treatment groups. Not only does this scalar become the primary driver of intergroup separation when there are significant differences between groups, this technique can also conceal metabolic links to cytokine production. Thus, these normalisation methods were not considered for further analyses.

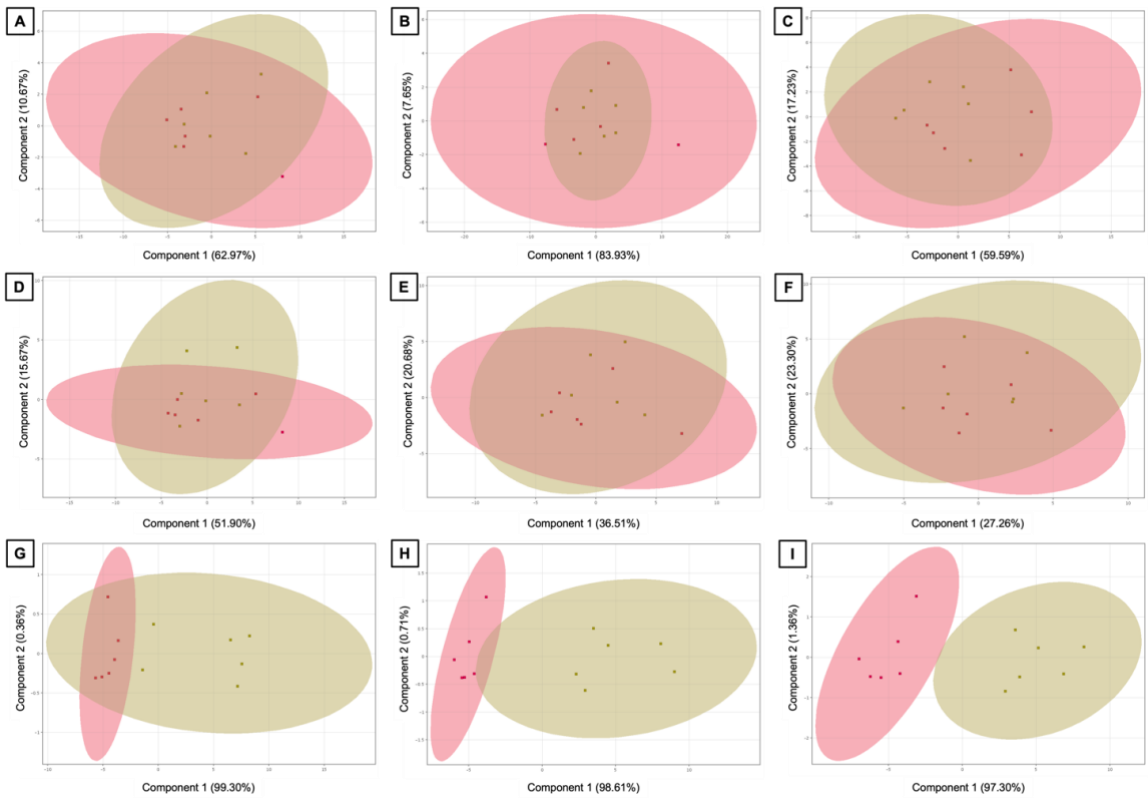


**Figure 4.3.14: Principal Component Analysis Comparison of Normalisation Methods with Improved %CV Relative to $Log_2$ Transformation.** CD14+ monocytes (n=6) were isolated from healthy donors and stimulated @37°C for 4 hours with 200ng/ml LPS (and ANCA) or left unstimulated. Metabolites were extracted, analysed by LC-MS, and targeted metabolomic analysis of 53 metabolites was completed. 32 of these 53 metabolites were detected in experimental samples and metabolite abundances calculated. Abundance values for unstimulated cells were normalised using different methods which improved %CV relative to $log_2$ alone principal component analysis (PCA) plots were created to compare unstimulated (NS, gold) and LPS (red). $Log_2$ transformation alone (A) was compared to normalisation by protein levels measured by A280 of the metabolite fraction (B), BCA of the metabolite fraction (C), BCA of the cell pellet (D), or by probable quotient normalisation (PQN, E) or quantile (F) algorithms. Normalisation to cytokine production (IL-1β [G], IL-6 [H], TNF-α [I]) was also assessed.

PCA plots for all twenty methods which had lower MAD than $log_2$ transformation alone are shown in Figure 4.3.15. The four baselining algorithms (Baseline to Mean All, Baseline to Median All, Pareto [MPP], and Z Transform) had identical PCA plots (B) which were unchanged from $log_2$ alone (A). Several of the NOREVA scaling methods also had very similar PCA plots with limited improvement. Only MSTUS (C), cyclic LOESS (G), mean (J), and (K) median showed improved separation of treatment groups. PQN (D) and linear baseline (R) did show improved clustering of LPS-treated cells, but not of unstimulated cells. Total sum (O) had a unique PCA appearance, but little improvement in separation.

Several normalisation techniques which improve data normalisation in primary monocytes have been explored here, and those perfomring well in multiple categories are listed in Table 4.3.1. Given the positive performance in limiting intragroup variation and improving intergroup separation, metabolite fraction protein content (BCA MF OD) was chosen as the superior normalisation strategy. This will be investigated in additional detail for utility in cellular metabolomic data normalisation.

| Normalisation Method | Category | NOREVA Readouts | | | PCA | Correlation by Sample | Mean %CV | Mean MAD |
|---|---|---|---|---|---|---|---|---|
| | | Sum A2 | Sum PMAD & PEV | Rank D | | | | |
| $Log_2$ Only | N/A | 99.11 | 1.31 | 0.53 | Fair | Good | 3.66 | 1.93 |
| Constant Sum 1000 | MPP Algorithms | N/A | N/A | N/A | Fair | Good | 6.28 | 1.93 |
| Total Abundance | MPP Algorithms | N/A | N/A | N/A | Fair | Good | -7.36 | 1.93 |
| BCA OD MF | Biological | N/A | N/A | N/A | Fair | Good | 2.77 | 1.93 |
| MSTUS | NOREVA Algorithms | 62.53 | 0.02 | 0.28 | Fair | Fair | 31.07 | 0.00 |
| PQN | NOREVA Algorithms | 848.2 | 0.64 | 0.94 | Fair | Fair | -142.88 | 0.11 |
| EigenMS | NOREVA Algorithms | 556.4 | 0.62 | 0.06 | Fair | Good | -135.16 | 0.19 |
| Cyclic LOESS | NOREVA Algorithms | 52.95 | 0.51 | 0.14 | Fair | Fair | 27.06 | 0.14 |

**Table 4.3.1: Summary of Top Performing Normalisation Techniques.** Forty-one normalisation methods were compared for their effectiveness at normalising targeted metabolomic data in unstimulated monocytes. Results are colour-coded as improvements (green fill ) or worsening (red fill) compared to $log_2$ transformation alone. Negative values (red text) were not considered. NOREVA readouts are elaborated in reference [102]. PCA: principal component analysis; MAD: median absolute deviation.

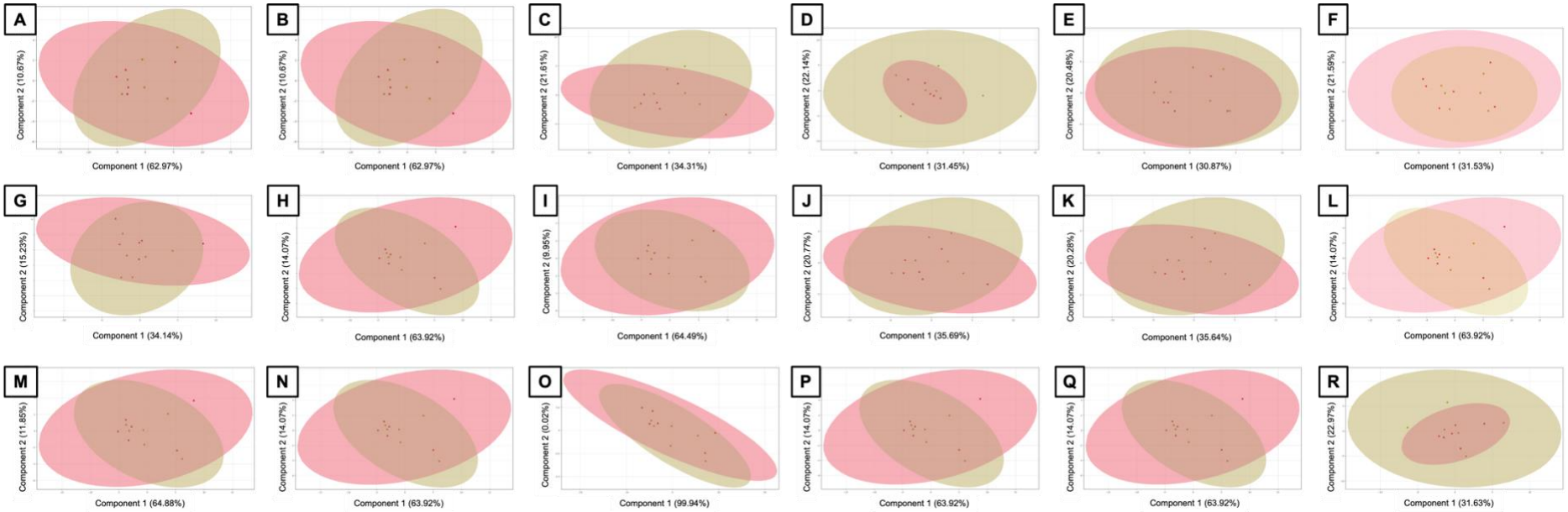


**Figure 4.3.15: Principal Component Analysis Comparison of Normalisation Methods with Improved MAD Relative to $Log_2$ Transformation.** CD14+ monocytes (n=6) were isolated from healthy donors and stimulated @37°C for 4 hours with 200ng/ml LPS (and ANCA) or left unstimulated. Metabolites were extracted, analysed by LC-MS, and targeted metabolomic analysis of 53 metabolites was completed. 32 of these 53 metabolites were detected in experimental samples and metabolite abundances calculated. Abundance values for unstimulated cells were normalised using different methods which improved MAD relative to $log_2$ alone principal component analysis (PCA) plots were created to compare unstimulated (NS, gold) and LPS (red). $Log_2$ transformation alone (A) was compared to normalisation by the four baselining protocols (B), MSTUS (C), PQN (D), Quantile (E), EigenMS (F), Cyclic LOESS (G), Auto Scaling (H), Log Transform (I), Mean (J), Median (K), Pareto Scaling (L), Power Scaling (M), Range Scaling (N), Total Sum (O), Level Scaling (P), Vast Scaling (Q), and Linear Baseline (R).

### 4.3.7 Improving Compatibility of Methanol Extraction Solvent for Protein Measurement with the Pierce™ BCA Assay

BCA was the optimal method for measuring protein content in monocyte extracts and for normalisation of metabolomic data in this cohort. In order to further improve the efficiency of this assay a number of optimisation experiments were performed. First the compatibility of MeOH with the assay was assessed (Figure 4.3.16A). Despite only being listed as compatible below 10%, we found that 80% MeOH performed comparably to PBS, particularly in a plate-based assay. PBS correlated very well will MeOH in both plate- and tube-based assays ($R^2$ = 0.9823, p<0.0001). Methanol was even better at detecting low protein concentrations, which is promising for measurement of metabolite extracts where the majority of proteins have been precipitated during sample preparation. Blank samples with a higher percentage of MeOH also had lower OD values (Figure 4.3.16B), limiting background interference. Finally, different sample volumes were tested across a standard curve. Sample volumes as low as 10µl maintained consistency in protein measurements with this plate-based assay (Figure 4.3.16C). Lower protein contents were better detected with longer incubation times, even up to 18 hours. Overall, the Pierce™ BCA protein assay was compatible with 80% MeOH and suitable for measurement of residual protein content measurements in metabolomic extractions. The optimised BCA assay protocol for protein concentration measurements of extracted metabolite fractions is described in Section 2.5.

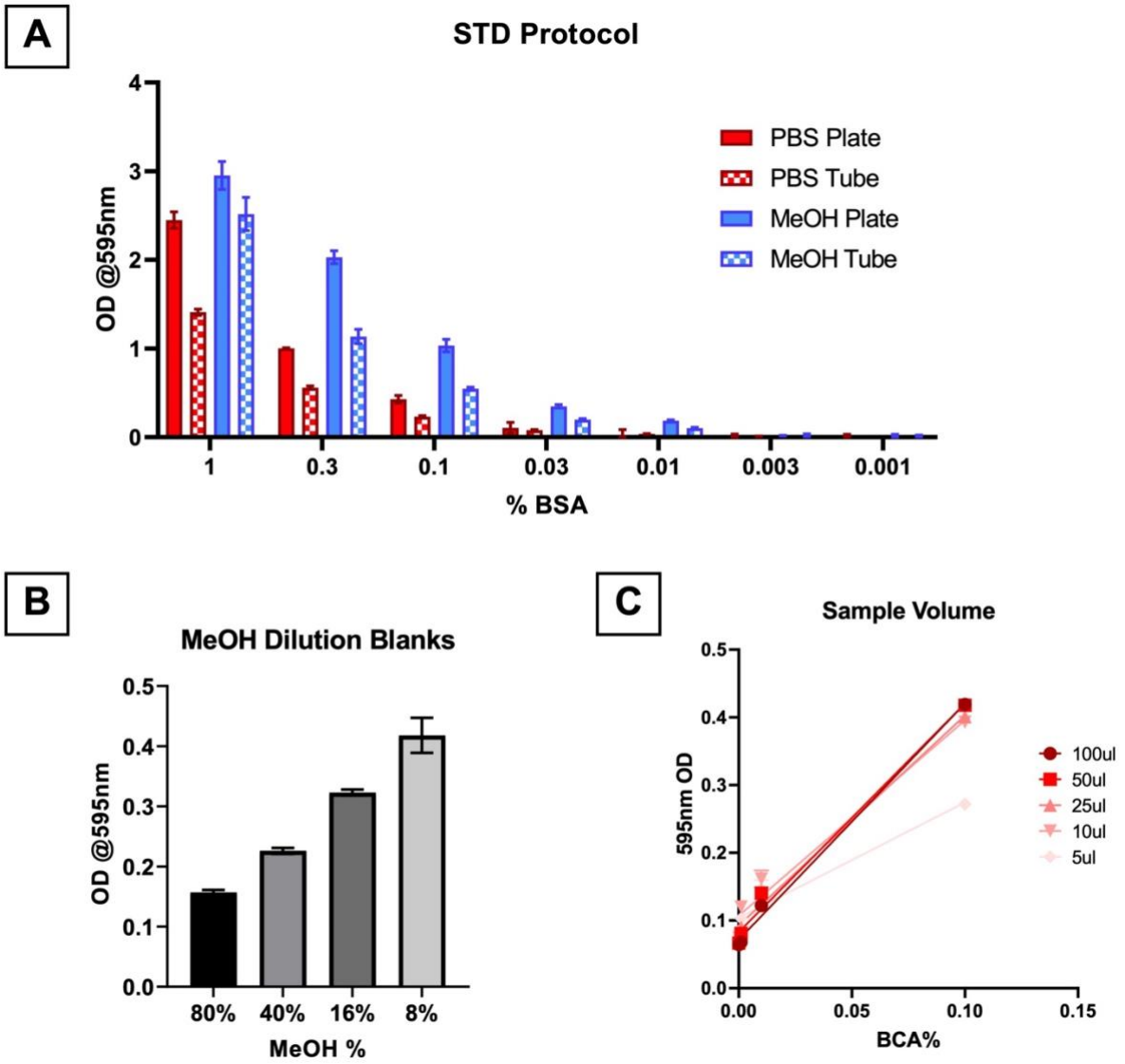


**Figure 4.3.16: Optimisation of BCA Assay with Methanol Extraction Solvent.** The Pierce™ BCA assay protocol was modified to assess compatibility with 80% MeOH extraction solvent. Plate and tube protocols were compared with various concentrations of BSA standards prepared with PBS or MeOH (A). Background error from blank sample interference (B), and different sample loading volume protocols were also trialled (C).

### 4.3.8 Residual Protein in the Metabolite Fraction Shows the Strongest Correlation with Cell Number

Biomass normalisation is commonly used for cellular metabolomic normalisation. We compared three different readouts – metabolite fraction protein content (BCA assay, Section 2.5), cell pellet protein content (BCA assay), and cell pellet DNA content (DNA assay, Section 2.10) – for their utility in determining cell number to correct for technical experimental variation (Figure 4.3.17). All three methods showed a significant correlation with cell number. This association was weakest for the DNA assay, which also had inconsistent readouts. Measuring protein content by BCA assay correlated strongly with cell number for both the metabolite fraction and the cell pellet. These two protein content measurements also strongly correlated with one another ($R^2$= 0.9266, p<0.0001, data not shown). However, protein levels were significantly different between treatment groups in the cell pellet, but not the metabolite fraction (Figure 4.3.17B & 4.3.17C). This indicates that the metabolite fraction would be the preferable option, as technical differences in metabolite levels between groups will not be statistically impacted by the normalisation. Measurement of protein content in the cell pellet was also challenging as it was not entirely soluble in the DNA assay buffer. Compatibility of the DNA assay buffer with the BCA assay was also confirmed in a similar manner to experiments shown in Figure 4.3.16 (data not shown).

Based on the consistent high performance across normalisation assessment criteria, ease and accuracy of measurement, and ability to detect significant metabolite changes between groups without influencing biomarker discovery, residual protein content in the metabolite fraction was determined to be the optimum metabolomic data normalisation technique.

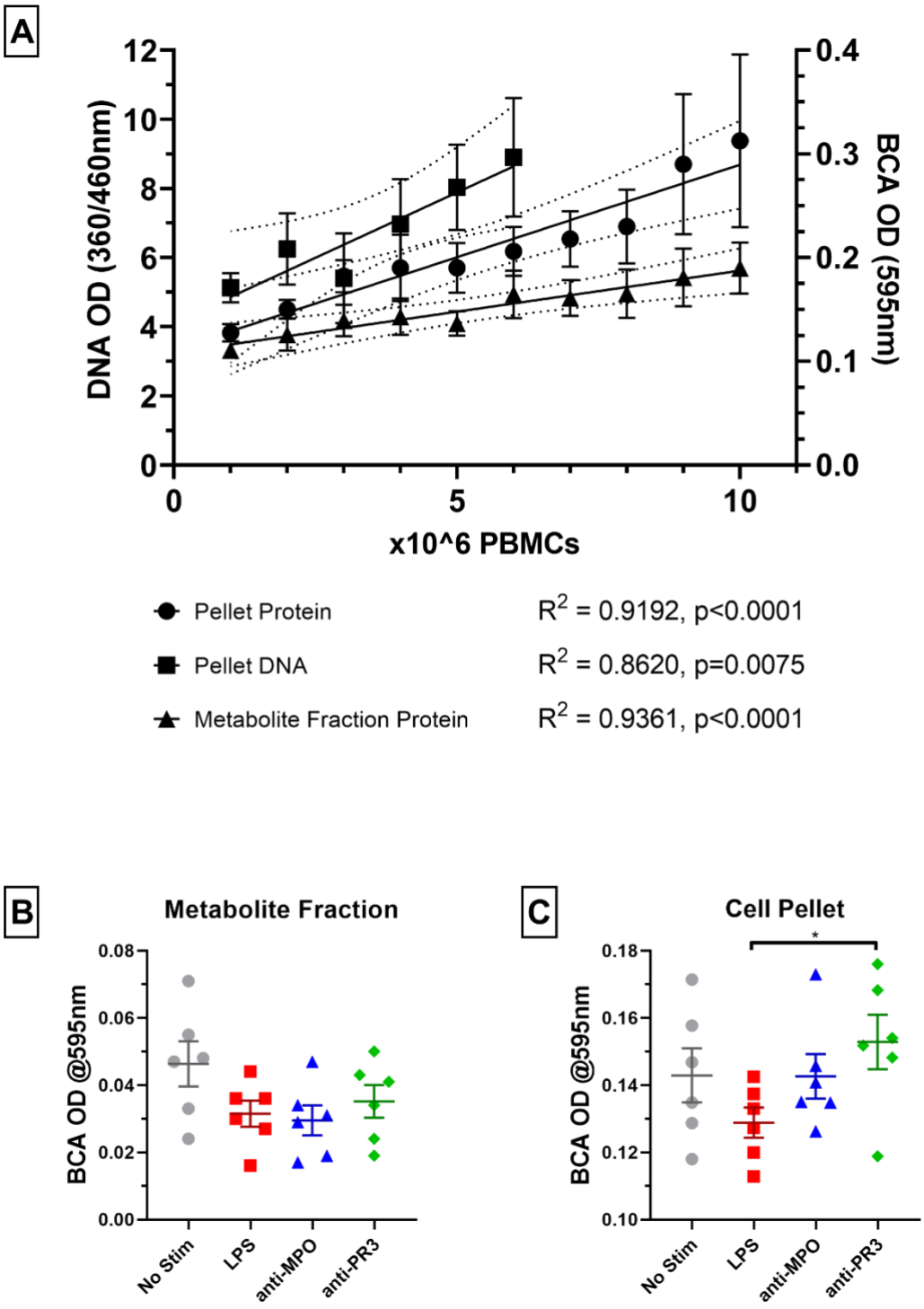


**Figure 4.3.17: Comparison of Biomass Normalisation Methods for Metabolomic Data Normalisation.** PBMCs were isolated from blood of healthy controls (n=5), quantified and fractioned, and metabolites extracted in 80% MeOH. Protein levels in the metabolite and pellet fractions were quantified by BCA assay, and DNA levels in the cell pellet were also measured. Results for each cell fraction were plotted and correlation (Pearson) with cell number was determined (A). Protein levels in the metabolite (B) and pellet (C) fractions were measured in ANCA- and LPS-stimulated monocytes in the Primary monocyte metabolomics cohort. Differences between groups were assessed by ANOVA and compared to unstimulated cells.

## 4.4 Discussion

### 4.4.1 LC-MS Sample Preparation

There are many factors to consider when optimising an untargeted metabolomic experiment. These sample preparation and LC-MS method optimisation experiments focused on extraction solvents, cell lysis, and column/gradient optimisation. For this work, we have combined direct ice-cold extraction buffer with quenching on dry ice to arrest metabolite turnover in primary human monocytes. Extraction solvent choice directly affects metabolome coverage. In our investigations with primary human monocytes, 100% MeOH and a blend of ACN, MeOH, and water (ACN:MeOH:$H_2O$, 2:2:1) both performed well in terms of detectable metabolites and consistency between replicates. Methanol-based extractions have been shown to be effective extraction solvents for adherent cells [362]. The ACN:MeOH:$H_2O$ extraction was used by Rahman *et al.* [94] on a variety of cell lines (and tissues) across a range of LC-MS methods, where it showed excellent coverage of a range of metabolic pathways. Indeed, a mixture of solvents with opposing polarities is recommended for broad metabolome coverage [47]. As such, adding water to the extraction solvent may increase the number of detectable features and improve metabolome coverage and biomarker discovery [358]. The favourable performance of the ACN:MeOH:$H_2O$ blend may be due to its water content, and the same ratio of water with methanol alone (80% MeOH) is commonly used in cellular metabolomics investigations [58]. As such this was used as the extraction solvent for subsequent metabolomics experiments. Dual-phase extractions were not explored in these optimisation works, but may be useful for additional multi-omics experiments to validate our findings. Technical variation can be minimised by completing metabolite extractions on the same day with the same solvent batch. This should be incorporated to the standardised protocol for mammalian cell metabolomics.

Cell lysis is necessary to release intracellular contents for metabolite extraction. Similar to the investigation of adherent SW480 cells by Dettmer *et al.* [362], we did not see a huge influence of different cell lysis techniques on metabolite recovery. The freeze-thaw protocol had the lowest %CVs for metabolite features (Figure 4.3.3) but was the most time-intensive of the three lysis methods trialled. Intensive lysis protocols such as direct probe sonication and bead beating are only necessary

for cell types with rigid membranes such as yeast and gram-negative bacteria. As such a combined ice-bath sonication and vortexing extraction was used in subsequent extractions.

This optimised sample preparation method was validated in PBMCs and monocytes. Despite a higher cell number used in these experiments, there were a similar number of metabolic features detected in this and the sample preparation optimisation work (Figure 4.3.9). Given the number of experimental variables in cellular metabolomics we believe that the additional sample handling involved in the validation work may have impacted metabolite detection [47, 73-75, 88]. Additionally, these cells were only quenched on wet ice, which may not have effectively preserved metabolite integrity, meaning low abundance metabolites were not detected Quenching with ice-cold extraction solvent can be sufficient for cellular metabolomics [50], but additional quenching on dry ice is recommended to fully preserve the cells' phenotype. Through extensive literature review and a number of pilot experiments, additional steps were incorporated into (or omitted from) the final sample preparation protocol. Washing to ensure complete removal of cells from plates and effectively separate cells from supernatant media is one such process. Although suspension cells are less susceptible to metabolite leakage from scraping than their adherent counterparts, the wash step is still important to preserve the intracellular metabolome (and separate it from cell supernatant). Chilled 0.9% sodium chloride (NaCl) was chosen as the wash buffer for this step as it was less likely to contribute to ion suppression than PBS and has been used in similar investigations [62, 363]. Thorough wash steps such as those use in various biotechnology applications [18] were not applicable to this work, and we adapted the method used by Fei *et al.* [345] for metabolomic analysis of macrophages.

To limit sample handling and preserve cellular metabolism, certain sample preparation steps were omitted, notably sample dry down. After sample extraction cells can be dried down to further concentrate the sample for reconstitution in a more a compatible LC-MS solvent. Cell dry down is typically carried out using a lyophiliser, an $N_2$ evaporator, or a SpeedVac. Although a SpeedVac was available, we opted not to include a solvent removal step in the sample preparation protocol for a number of reasons. Firstly, 80% MeOH is a mildly polar extraction solvent and broadly compatible with a number of LC-MS methods. Secondly, the need for

concentration of metabolites was limited by use of a second extraction and high starting cell number. Repeat extractions can improve metabolite recovery [27, 50, 345], and we added a second extraction step to our protocol for the Primary and Validation experiments described in Chapter 5. Further, these optimisation experiments were carried out $1x10^6$ primary monocytes. The availability of a high volume of fresh blood from the haemochromatosis clinic meant that we were able to use $5x10^6$ cells per condition in our monocyte stimulation experiments, limiting the requirement for sample concentration. Although metabolomics can be carried out on much smaller cell numbers [352], this ensured that even lower abundance metabolites would be above our limits of detection. Thirdly, sample concentration using a room temperature SpeedVac can oxidise metabolites during drying [27]. This could impact measurement of oxidised species such as ATP, NADP+ and GSH. Given the increased OXPHOS in ANCA-stimulated monocytes [238] it is important to accurately detect/measure these sensitive metabolites and not introduce artefacts as a result of excessive processing. For these reasons, sample concentration/drying is not considered essential in this sample preparation protocol.

Finally, all sample preparation extraction solvents were stored at -20°C and all samples should be stored on wet ice for the duration of the sample preparation protocol. Cooler temperatures maintain quenching and limit metabolite degradation [27, 50]. In addition, the same batch of solvents should be used for each experimental cohort and extractions should take place on the same day when possible to limit variation. The fully optimised sample preparation protocol is shown in Figure 4.4.1 and described in Section 2.9.2.

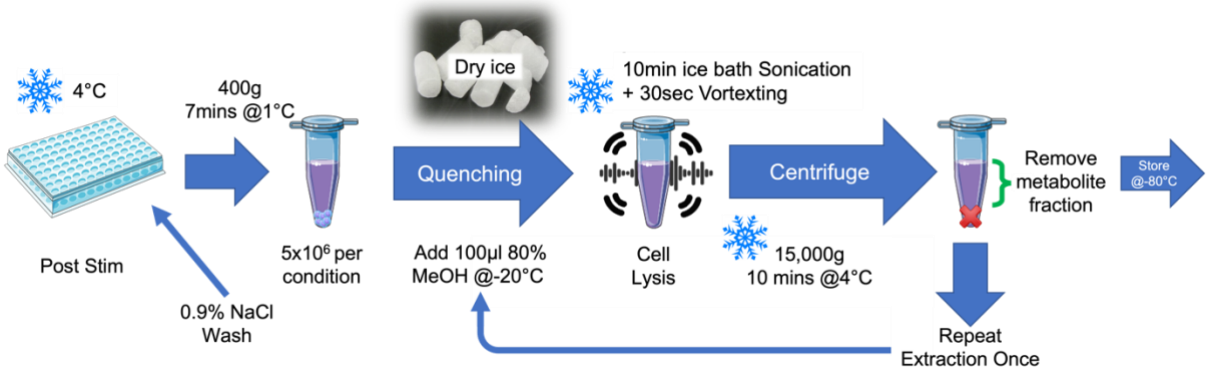


**Figure 4.4.1: Summary of Optimised Sample Preparation Protocol of Primary Monocytes for Metabolomic Analysis by LC-MS.**

### 4.4.2 LC-MS Method Development

The initial LC-MS methods used for sample preparation optimisation were based on those used by Metabolon [28] which combines RP and HILIC chromatography (and GC-MS) to measure four metabolite subfractions. We utilised an RP method ("C18") and a HILIC method which were shown to have impressive metabolome coverage of our metabolites of interest [42, 357]. Of the three methods trialled, the C18 ESI- method had a conspicuously high background in the total ion chromatogram (TIC, Figure 4.3.1). TICs represent the sum of all mass spectral peak intensities across an LC-MS run without quantitation or individual compound detection. Extracted ion chromatograms can then be used to calculate abundances of specific peaks and can be used to track intra- or inter-run variability. Whilst a high background can be caused by a number of issues such as column/LC contamination, the C18 ESI- method also had the lowest number of detectable features across sample methods, and higher inter-replicate variability.

A large number of compounds eluting in the void volume as seen with the HILIC methods (Figure 4.3.1C) may indicate that these compounds be better detected by RP-HPLC-MS. Indeed, RP and HILIC methods should complement each other in their metabolite coverage. However, use of this C18 method is complicated by the PFPA mobile phase additive. This is an ion pairing agent which requires dedicated instrumentation and can induce ion suppression, particularly in positively charged compounds. Despite excellent chromatographic quality, we have decided not to continue with the C18 method and to use HILIC LC-MS as our primary metabolomic profiling technique. Omission of a C18 method may reduce the total numbers of detected metabolites and exclude certain non-polar metabolite classes not detectable by HILIC alone. Ulmer *et al.* [59] described an optimized two-step protocol for metabolite and lipid extraction from Jurkat T cells. A lipid extraction protocol could be applied to cell pellets from our optimisation experiments after the initial MeOH extraction to better measure lipid content, should this be necessary. Blood and urine lipids have shown to be stable for several years when stored at -80°C [348], and given the thorough quenching applied to these samples we could expect the same from these cells. Certain lipid classes have been reliably detected by (HILIC) single phase extraction [345], and the relevance of these compounds to monocyte inflammatory responses should be investigated in profiling experiments.

HILIC methods can detect a larger number of molecular features than RPLC and at higher abundances [54]. With subtle alterations to LC conditions, we can further improve the MS response without the need for a complimentary method. Medronic acid has been shown to significantly improve the peak shapes and metabolite signals for nucleotide, amino acids, and carbohydrates [42]. This novel mobile phase additive can also be easily cleared from the LC/MS system and run in both positive and negative ESI modes. This LC-MS method was recently used to profile the metabolism of activated human T cells with succinate dehydrogenase (SDH) inhibition [364]. SDH inhibition impaired proliferation, cytokine production and activation marker expression, while synchronously increasing glycolytic intermediates. Itaconic acid was also detectable with this method and has been shown to be an important metabolite for modulation of inflammatory responses in macrophages [365].

Ultimately a modified version of the HILIC-based method was adopted (based on work from Hsiao *et al.* [42]) and used to characterise the metabolic response of CD14+ monocytes to LPS and ANCA as described in Chapter 5. Medronic acid was omitted from mobile phase B for both ionisation modes (see Section 5.2.3.1). A thorough description of LC-MS methods can be found in Section 2.9.3, and are summarised in Figure 4.4.2.

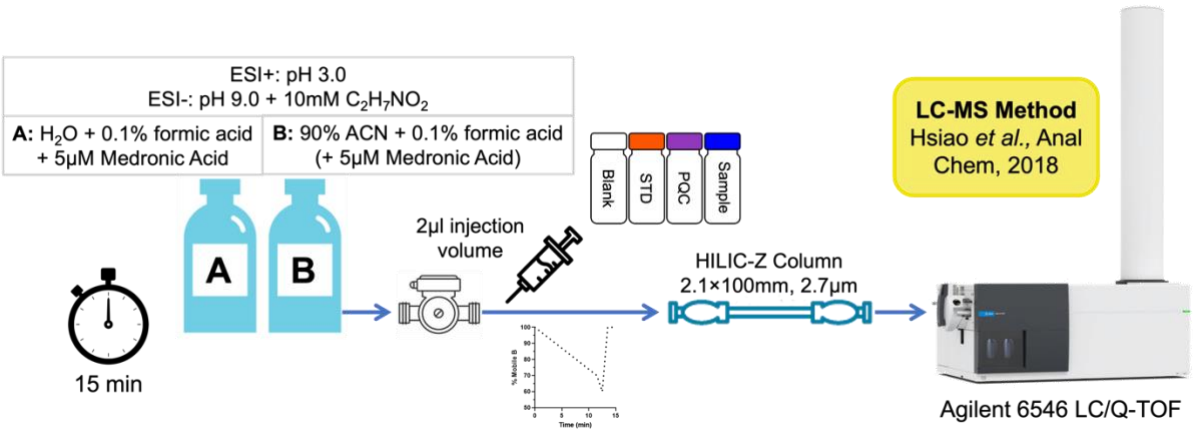


**Figure 4.4.2: Summary of Optimised LC-MS Method for Metabolomic Profiling of Primary Monocytes.** The optimised LC-MS method used in this work was adopted from Hsiao *et al.* [42] and is described in detail in Sections 2.9.3 and 5.2.3.1.

### 4.4.3 Metabolomic Data Normalisation

A key step of the metabolomic data analysis pipeline is data normalisation, which must be appropriately optimised for each application. Log transformation is a routine data analysis step to curtail the influence of extreme values for subsequent statistical analysis [362]. The data from the Primary (and Validation) profiling experiments is not normally distributed – it is lognormal. This was confirmed by Anderson-Darling, D'Agostino & Pearson, Shapiro-Wilk, and Kolmogorov-Smirnov tests (Figure 4.3.10). Additional normalisation strategies were applied to improve data quality and assessed for their improvement over $\log_2$ transformation alone. The NOREVA platform assesses normalisation efficacy as standard using five key criteria: reduction in intragroup variation, effect on differential metabolic analysis, consistency of identified markers among different datasets, classification accuracy, and correspondence to reference data [102, 110]. We adopted and applied these criteria to our data from ANCA- and LPS-stimulated monocytes.

Many of the normalisation techniques applied used similar methodologies as demonstrated by similarity of unstimulated data in the targeted analysis in Figure 4.3.11. For instance, many normalisation approaches are centred around using all available information to calculate total metabolite abundance and correcting individual concentrations around this. Manual calculation with the “Sum M32” method – which summed the abundance values of the 32 detectable synthetic standard metabolites – produced near identical MAD plots to several other similar techniques (Figure 4.3.13B). The MSTUS method (mass spectrometry total useful signal) was developed to improve on this by only using signals present in all samples (except extraction blanks) to calculate the total appropriate signal to normalise around [76]. Indeed, MSTUS was among the lowest MAD values and showed improvements in intergroup separation in the PCA plot (Figure 4.3.15C). Normalisation to cytokine production (via an external scalar) can potentially obscure metabolic links to inflammatory functions. For example, serine was shown to be essential for IL-1β production by murine macrophages, and inhibiting its serine synthesis limited IL-1β production and release [335]. Thus, despite improvements in intergroup separation, normalising to inflammatory readouts is not a viable normalisation strategy.

Overall, the top performing normalisation technique across all readouts was measurement of residual protein content in the metabolite fraction by BCA. This technique outperformed measurement of protein content by UV absorbance at 280nm (“Protein A280”), and once optimised (see Section 4.3.7) became a suitable normalisation strategy effective at reducing intragroup variation in both PooledQC samples and unstimulated cells. Our 80% MeOH extraction solvent was compatible with the standard Pierce™ BCA Protein Assay (23227, Thermo Scientific) and improved results may be obtained with more sensitive BCA iterations. The low OD values measured in this Secondary cohort were improved by increasing the incubation time of the BCA assay. This effect is evidenced in the difference between protein levels in the Primary and Validation metabolomic profiling cohorts (see Figure 5.3.21D). There was no difference in metabolite protein fraction between groups (Figure 4.3.17B) so no potential to obscure significant metabolite biomarkers, and protein levels correlated with almost all detectable metabolites (data not shown). Many cellular metabolomics investigations do normalise to protein content, but without specifying how (or indeed where) this protein is measured. To our knowledge, this is the first detailed report of optimised measurement and validation of metabolite fraction protein content as a normalisation factor for cellular metabolomics.

# Chapter 5: LC-MS Profiling of ANCA-Stimulated Monocytes

## 5.1 Introduction

Activated immune cells require substantial energy consumption to produce proinflammatory cytokines and mediate other host defence mechanisms. Thus, it is unsurprising that cells alter their metabolism after activation. Disruption of nutrient supply can have detrimental effects on the pro-inflammatory monocyte functions, such as phagocytosis, cytokine production, and ROS generation among others.

A range of pro-inflammatory cytokines are produced by monocytes to co-ordinate the innate immune response to pathogens. Inhibition of glycolysis can abrogate cytokine production in monocytes and monocyte-derived cells (DCs [366], macrophages [367] & microglia [368]). Inhibition of glycolysis by 2-deoxy-D-glucose (2-DG) decreased IL-1β, IL-6, and TNF-α in LPS, Pam3, and *C. albicans* stimulated primary monocytes [97, 124]. Glucose-deprived monocytes do not appear functionally impaired, though did suffer at 24h in the absence of sugar [133]. Manipulation of additional metabolic pathways can influence cytokine production. Dimethyl itaconate is a derivative of itaconate, a metabolite with established anti-inflammatory roles in macrophages. Dimethyl itaconate decreased IL-1β, IL-6 and IL-10 levels, without affecting TNF-α or lactate [97]. Inhibition of glycolysis (mTOR), glutaminolysis (glutaminase), or OXPHOS (ATP synthase) abrogated *C. albicans*-induced cytokine production, but FAO and PPP did not play a role [124]. Hypermetabolic RA monocytes use lipid metabolism to fuel CCL20 production in the synovium [86]. Disease- and stimulus-specific cytokine production in monocytes relies on differential metabolic pathways. How these pathways are involved in AAV remains to be discovered.

Monocyte-lineage cells are a major source of IL-1β. Typically IL-1β production and release requires activation of the inflammasome complex by dual stimuli. Monocytes are unique in that they can produce IL-1β in response to a single trigger [121], including anti-MPO (see Section 3.3.5)[203, 238]. Glucose-dependent IL-1β production was initially demonstrated in macrophages and causes specific TCA-cycle “breaks” at succinate dehydrogenase and isocitrate dehydrogenase [8]. Primary human monocytes exhibit a similar dependence on glycolysis for IL-1β production. 2-DG inhibited LPS-induced IL-1β [97, 124], although glucose-deprived monocytes had comparable cytokine production [85]. Modifying glutathione metabolism affected IL-1β production by *Borrelia burgdorferi*, largely at the (post-

)translational level [302]. Blocking FAO increased IL-1β levels by shifting metabolism towards glycolysis [86]. Hypoxia also improved IL-1β release in these cells, presumably through HIF-1α. Monocytes appear to exploit multiple metabolic pathways to preserve IL-1β production, another example of the metabolic plasticity in these cells.

Other monocyte defence functions such as ROS generation and phagocytosis are important in AAV [236, 238, 369, 370] and heavily reliant on manipulating cellular metabolism. Glucose-deprived monocytes had reduced ROS production after LPS stimulation, but had comparable phagocytosis rates to normally cultured cells [85]. Glycolysis and the PPP are crucial for monocyte ROS production by *C. albicans* activation [124]. Neither hypoxia nor 2DG had any impact on phagocytosis rates in LPS-activated cells, but inhibition of OXPHOS by rotenone significantly reduced the phagocytic capacity of Pam3CysSK4 (Pam3)-stimulated monocytes [97]. OXPHOS, but not glycolysis, seems to be an important determinant of the phagocytic capacity of human monocytes. These findings highlight the stimulus determines the metabolic and functional response of monocytes.

To date the number of metabolomic profiling investigations in primary monocytes have been limited to those discussed above (see Figure 1.3.1). Furthermore, these studies have generally involved a 24-hour stimulation timepoint/period. Raulien *et al*. noted broad decreases in metabolite levels after 6 hours of LPS-stimulation [85]. These early-stage decreases were hypothesised to be triggered by AMPK activation which drives the switch to catabolic metabolism. Accumulation of stimulus-specific functional metabolites can then occur. A longer-term investigation of a validated sepsis model in THP1 cells [96] monitored the metabolic flux brought on by LPS. Early (8 hour) metabolic changes during immune activation were defined by increases in a number of lipid species, protein breakdown, nucleotide enrichment, and breaks in the TCA cycle at succinate dehydrogenase (SDH) and aconitase [371]. This metabolic reprogramming tracks a shift from anabolic immune activation during early activation, to catabolic energy-conserving process during immune deactivation, and restoration of energy balance and homeostasis during resolution. These early changes in the monocyte metabolome that precede their inflammatory

outputs further highlight the metabolic flexibility of monocytes and implore more in-depth study.

Metabolites can also exert additional functional effects/modification secondary to their role in energy production [372, 373]. Mitochondrial TCA cycle metabolites contribute to chromatin modifications and DNA methylation to co-ordinate immune responses [374]. In addition to its role in the TCA cycle and FAO, α-ketoglutarate can skew M1/M2 macrophage polarisation and influence trained innate immunity via epigenetic reprogramming and HIF1α degradation, respectively [20, 22]. Succinate accumulation can promote inflammation in macrophages through mitochondrial ROS generation and HIF-1α activation [8, 299]. Even microbial metabolites have been shown to alter immune function and exacerbate autoimmune disease [375-377]. The contributions of metabolites to ANCA-induced monocyte activation (or priming) have not yet been determined. In this chapter we profile the metabolome of ANCA-stimulated monocyte using optimised LC-MS methods, in an effort to see how they relate to pro-inflammatory functions.

## 5.2 Experimental Methods

### 5.2.1 Hypothesis

I. Increases in glycolysis and OXPHOS in ANCA-stimulated monocytes feed into specific, diverse metabolic pathways to trigger unique metabolic responses.

II. These metabolic responses are different in anti-MPO- and anti-PR3-treated cells.

III. Metabolic perturbations are associated with inflammatory outputs in ANCA-stimulated cells.

### 5.2.2 Methods

This chapter describes metabolomic profiling of ANCA- and LPS- stimulated monocytes by LC-MS. The methods used here have been optimised for primary monocytes as explicated in Chapter 4. Figure 5.2.1 summarises the experimental methods used and outline and distinguishes the experimental cohorts for this work. Full details of methods used can be found in the appropriately labelled sections of Chapter 2.

### 5.2.3 Experiment Outline

The methods used to investigate the hypotheses above are summarised in Figure 5.2.1. Two cohorts of stimulated monocytes were analysed: a Primary (n=6), and a Secondary cohort (n=24). In both groups, CD14+ monocytes were isolated from whole blood taken from haemochromatosis patients (see Section 2.2). Monocytes were stimulated for 4 hours with 5µg/ml monoclonal antibody (mAb) directed against MPO or PR3, or 200ng/ml LPS. Cells were prepared for metabolomic analysis (see Section 2.9.2) and analysed by LC-MS (see Section 2.9.3). Residual protein concentrations were measured by Pierce™ BCA assay, and ELISA and LDH assays were carried out on cell supernatants to measure cytokine production and cell death, respectively. Additional flow cytometry experiments were performed on freshly isolated (T0) monocytes in the Secondary cohort. Cytospin slides were also prepared for T0 monocytes and for each of the treatment groups at the end of the 4-hour stimulation in these replicates.

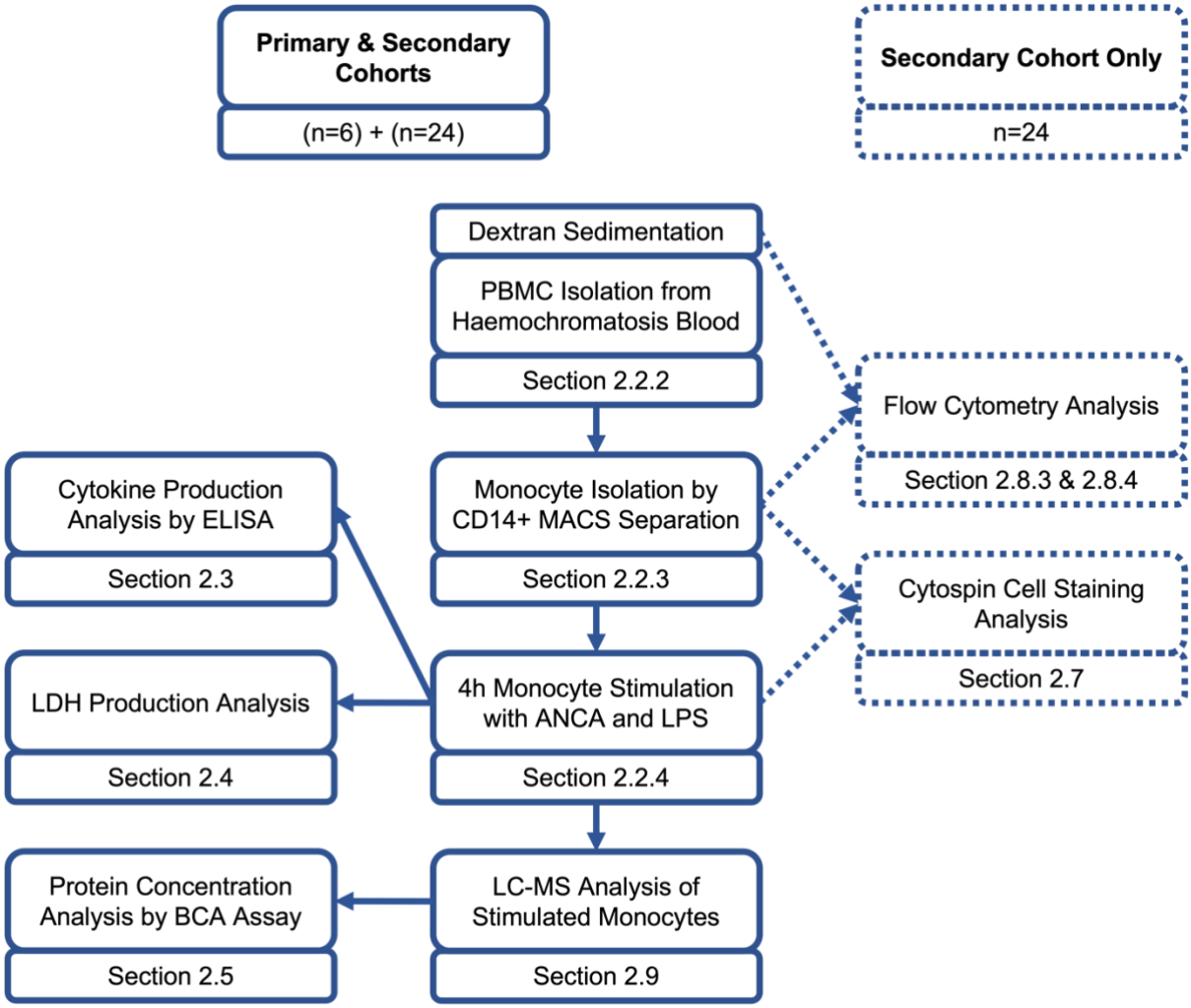


**Figure 5.2.1 Diagrammatic Representation of Techniques Used in Chapter 5.** Overview of experimental plan and techniques used to profile the metabolome of ANCA- (and LPS-) stimulated monocytes.

### 5.2.3.1 LC-MS Method Adjustments between Primary and Secondary Metabolomic Profiling Cohorts

An optimised LC-MS method was adopted for metabolomic profiling of ANCA- and LPS-stimulated monocytes and used in the Primary analysis (n=6). A slight change was made to chromatography conditions in the Secondary experiments (n=24). To reduce the need for inter-run cleaning/passivation, the medronic acid deactivator additive (Agilent Technologies, 5191-4506) was omitted from Mobile Phase B and only included in Mobile Phase A in the Secondary cohort. A slight change to the gradient was made in the Secondary cohort as visualised by the dotted line in Figure 5.2.2. Both methods dropped from 100% to 70% Mobile B at 11.5 mins. The Primary method gradient (dashed line) returned to 100% at 12 mins, but the Secondary method was modified to a lower ratio of Mobile B (60%) at 12.5 mins before returning to 100% at 13.5 mins until the end of the method. This slight modification in the gradient in the ESI- method allowed a better separation for the late eluting features. Post equilibration was also reduced from 5 mins to 2 mins. All other source conditions remained consistent between the pilot and secondary cohorts both methods performed comparably in terms of detectable metabolites (see Figures 5.3.8 & 5.3.9). Experimental conditions were identical for the two cohorts, and additional flow cytometry and Geimsa staining experiments were carried out on the Secondary cohort (see Figure 5.2.1).

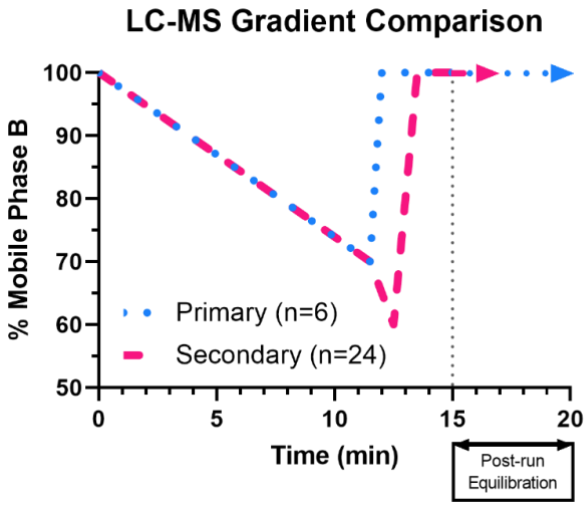


**Figure 5.2.2: Comparison of LC-MS Method Gradients for Metabolomic Profiling Experiments.** An optimised LC-MS method was developed for untargeted metabolomic profiling of ANCA- and LPS-stimulated monocytes. The gradients are visualised here by plotting the percentage (%) of mobile phase B (90% ACN + 10mM ammonium acetate pH9, ±5µM medronic acid) for the Primary (n=6, blue, included medronic acid) and Secondary (n=24, magenta, dotted line) cohorts.

## 5.3 Results

### 5.3.1 Targeted Metabolomic Analysis does not Differentiate ANCA- and LPS-Stimulated Monocytes in a Pilot Primary Analysis

Targeted analysis of metabolites included in the synthetic standard mix was carried out on ANCA- and LPS- treated monocytes in the Primary cohort as described in Section 2.9.5. 32 of the 53 metabolites in the mixture were detected in samples and PooledQC replicates. Statistical analysis was performed after data normalisation to residual protein content in the metabolite fraction as described in Section 2.5. Using these 32 metabolites, a Principal Component Analysis (PCA) plot was generated for the four treatment groups – unstimulated cells (NS), LPS, anti-MPO, anti-PR3 – and PooledQC samples. There was no clear separation of treatment groups evident from the PCA plot (Figure 5.3.1). Both anti-MPO- (blue) and anti-PR3-treated (green) monocytes showed moderate intra-group clustering, yet still overlapped with other treatment groups. PooledQCs (purple) grouped very well at the centre of the plot, indicating that they are a good representation of the sample set as a whole. Further, this means that variations observed between stimulation groups are a result of the stimulus and not the analytical technique. This analysis indicates that ANCA- and LPS-treated monocytes cannot be distinguished based on these 32 compounds alone, and additional analysis is required to determine the contribution of metabolism to ANCA activation in these cells. Reviewing normalised metabolite abundances (Figure 5.3.2) confirms that only subtle differences are evident between treatment groups. There is greater variation between metabolites (89.57%) than treatment (1.32%) as determined by 2-way ANOVA. Despite this there was a significant treatment effect seen in this Primary cohort analysis ($p<0.0001$), indicating that metabolism is distinct between the treatment groups compared to unstimulated cells.

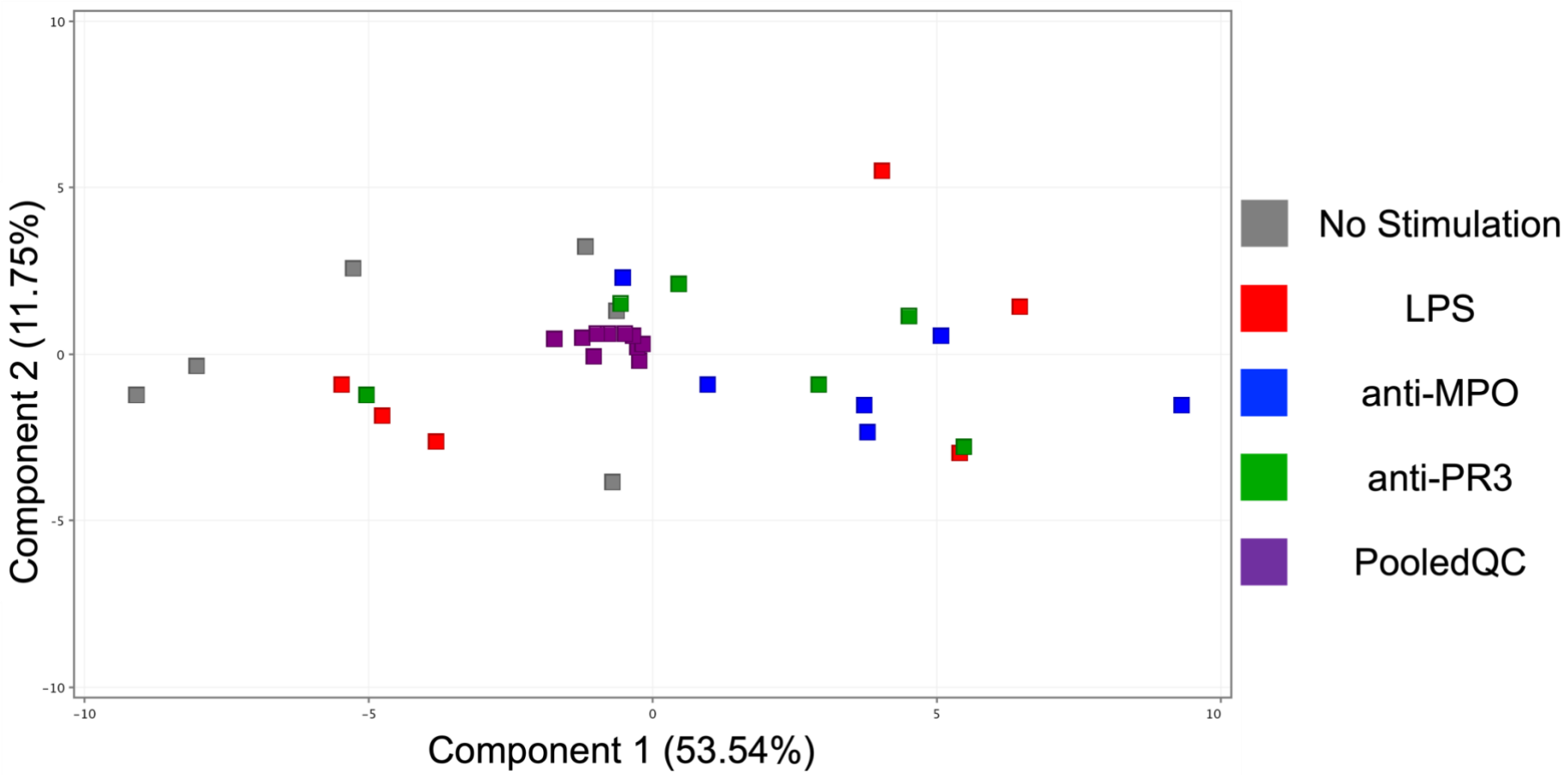


**Figure 5.3.1: Principal Component Analysis of Targeted Metabolites in ANCA- and LPS-Stimulated Monocytes in the Primary Cohort.** CD14+ monocytes were isolated from PBMCs of healthy controls by MACS separation (n=6). Cells were plated and stimulated @37°C for 4 hours with 5µg/ml monoclonal antibody (mAb) directed against MPO, PR3, or 200ng/ml LPS. ANCA- and LPS-stimulated monocytes were analysed by LC-MS and targeted metabolomic analysis of 53 metabolites was completed. Area-under-the curve (AUC) values were normalised by $\log_2$ transformation and to metabolite fraction protein levels (measured by BCA). 32 of the 53 metabolites were detected in the experiment samples. A Principal Component Analysis (PCA) plot was generated for the four treatment groups and Pooled QC samples.

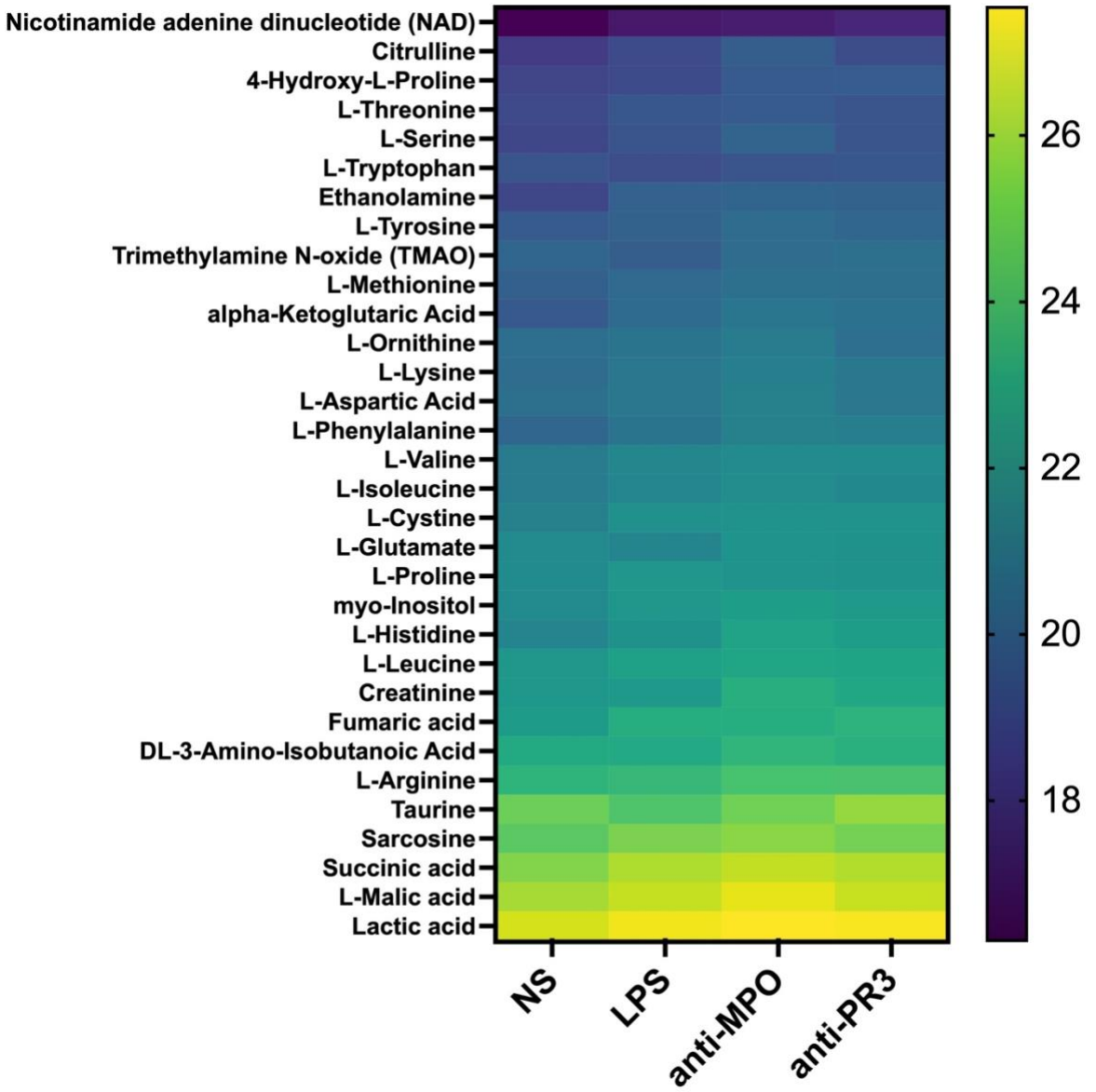


**Figure 5.3.2: Heatmap Analysis of Targeted Metabolites in ANCA- and LPS-Stimulated Monocytes in the Primary Cohort.** CD14+ monocytes were isolated from PBMCs of healthy controls by MACS separation (n=6). Cells were plated and stimulated @37°C for 4 hours with 5µg/ml monoclonal antibody (mAb) directed against MPO, PR3, or 200ng/ml LPS. ANCA- and LPS-stimulated monocytes were analysed by LC-MS and targeted metabolomic analysis of 53 metabolites was completed. 32 of the 53 metabolites were detected in experimental samples. Intergroup values are reported as BCA and $log_2$ normalised AUCs.

### 5.3.2 ANCA Stimulation Upregulates α-Ketoglutarate, Ethanolamine, and L-Histidine Production in Monocytes

Metabolites measured in the targeted analysis were evaluated by ANOVA with Benjamini-Hochberg FDR correction. Three of the 32 metabolites were significantly altered among treatment groups and are displayed as individual dot plots in Figure 5.3.3. Alpha-Ketoglutaric acid, ethanolamine, and histidine were all significantly increased in stimulated cells (Table 5.3.1). Alpha-Ketoglutarate is a TCA cycle intermediate and was significantly upregulated by LPS and ANCA stimulation. Ethanolamine is involved in glycerophospholipid metabolism and was increased by both ANCAs. Anti-PR3 treatment increased the amino acid histidine, with a similar (non-significant) elevation in anti-MPO-stimulated cells. Other metabolites approached statistical significance in individual analyses, but could not be considered, likely due to the small sample size. These increases represent upregulation of diverse metabolic pathways in ANCA stimulated monocytes.

| | α-Ketoglutaric Acid | | Ethanolamine | | L-Histidine | |
|---|---|---|---|---|---|---|
| | FC | P-Value | FC | P-Value | FC | P-Value |
| NS vs. LPS | 1.7729 | 0.0404* | 1.6103 | 0.1475 | 1.7921 | 0.0967 |
| NS vs. anti- MPO | 2.4601 | 0.0025** | 2.1951 | 0.0045** | 3.4005 | 0.0526 |
| NS vs. anti-PR3 | 1.9526 | 0.0010*** | 2.2716 | 0.0066** | 2.0522 | 0.0051** |

**Table 5.3.1: Fold Changes and P Values of Statistically Altered Metabolites as Measured by ANOVA**. ANCA- and LPS-stimulated monocytes (n=6) were analysed by LC-MS and evaluated by ANOVA with Benjamini-Hochberg FDR correction. Fold Change (FC) was calculated relating to unstimulated (NS) cells. NS: No Stimulation; LPS: lipopolysaccharide; MPO: anti-myeloperoxidase; PR3: anti-proteinase 3

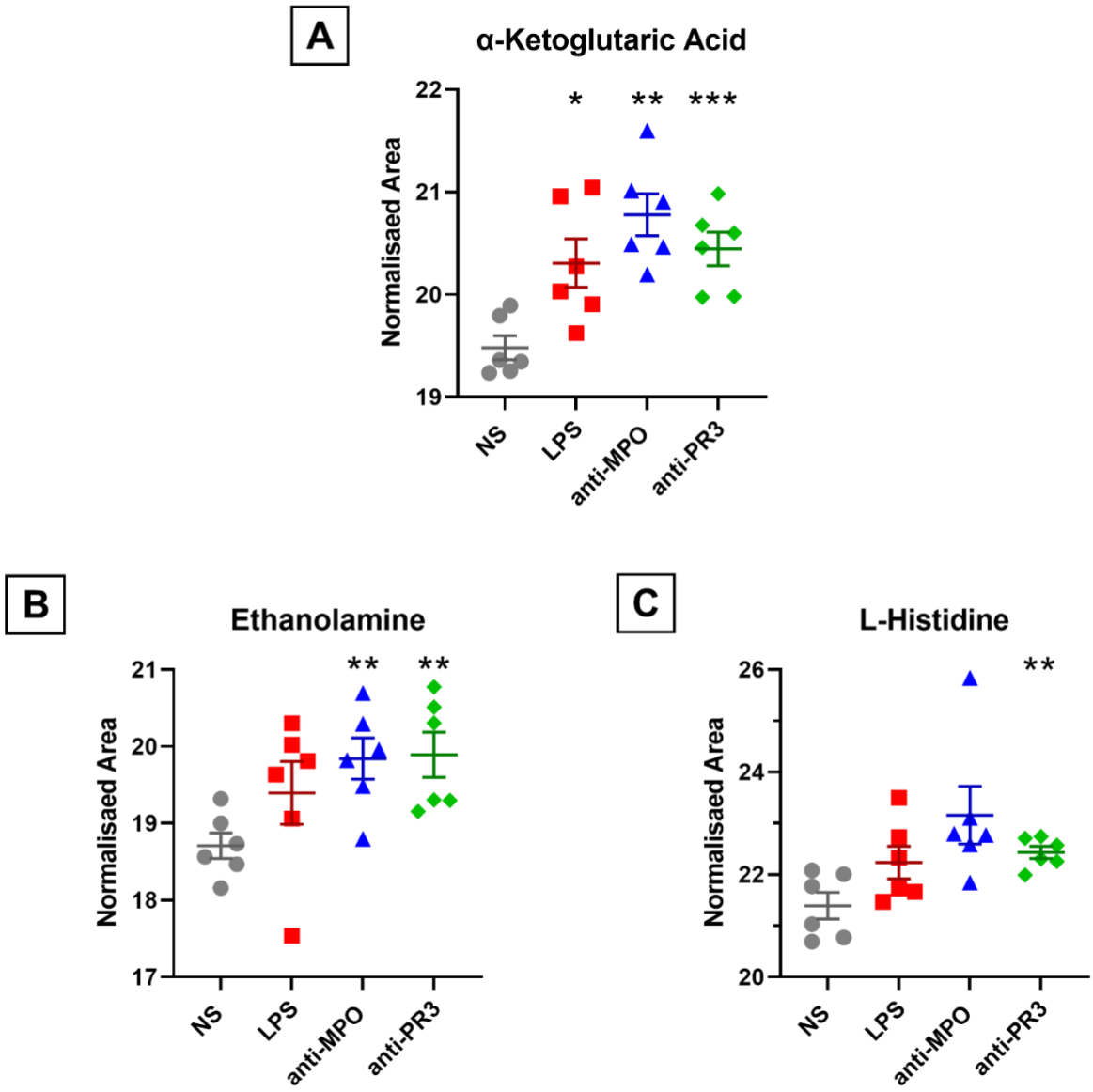


**Figure 5.3.3: Significantly Altered Metabolites in Targeted Analysis of ANCA- and LPS-Stimulated Monocytes in the Primary Cohort (n=6).** CD14+ monocytes were isolated from PBMCs of healthy controls by MACS separation (n=6). Cells were plated and stimulated (or Not Stimulated, NS) @37°C for 4 hours with 5µg/ml monoclonal antibody (mAb) directed against MPO, PR3, or 200ng/ml LPS. ANCA- and LPS-stimulated monocytes were analysed by LC-MS and targeted metabolomic analysis of 53 metabolites was completed. BCA and $\log_2$ normalised AUC values were analysed by 2-way ANOVA with a Benjamini-Hochberg FDR correction comparing to paired unstimulated cells. Results for significantly altered metabolites are displayed as individual dot plots (A-C).

### 5.3.3 Untargeted Analysis Identifies Multiple Significant Metabolic Alterations in anti-MPO-Stimulated Monocytes

Untargeted analysis of ANCA- and LPS-stimulated monocytes was carried out as described in Sections 2.9.7 and 2.9.8. Using the MassHunter ProFinder recursive feature extraction (RFE) algorithm, a total of 8,084 metabolite features were detected – 4,197 in the positive and 3,887 in the negative mode. Extraction blank samples comprising empty tubes which underwent the metabolite extraction process described in Section 2.9.2 were included in LC-MS analysis. Features present in these extraction blank injections were removed from analyses. Following blank removal and manual chromatography review 3,399 features were imported into MPP for further analysis. In order to prioritize high impact compounds in the identification pipeline only metabolites that were present in 100% of samples in all four treatment groups were considered for this initial analysis. This comprised 1,515 compounds in the negative mode and 406 in the positive mode. A summary of the feature extraction workflow and associated peak numbers is provided in Figure 5.3.4A.

Statistically altered compounds in each treatment group were recognised using moderated t-test with a Benjamini-Hochberg FDR correction. Features with fold changes >2 (relative to unstimulated group) and p values below 0.1 were considered. Volcano plots for LPS-, anti-MPO-,and anti-PR3-treated monocytes are displayed in Figures 5.3.4B, C, & D respectively. A total of 194 significantly altered features were found to be significantly altered from the unstimulated cells based on these criteria. The majority (193/194) of these features were in the anti-MPO treated group (Figure 5.3.4C). Of note, all significant features were identified from compounds measured in ESI- ionisation mode. The highly significant feature in the LPS-treated cells had *m/z* 137.8993 and was measured at 8.43min. These results point to a significant metabolic signature in anti-MPO stimulated monocytes.

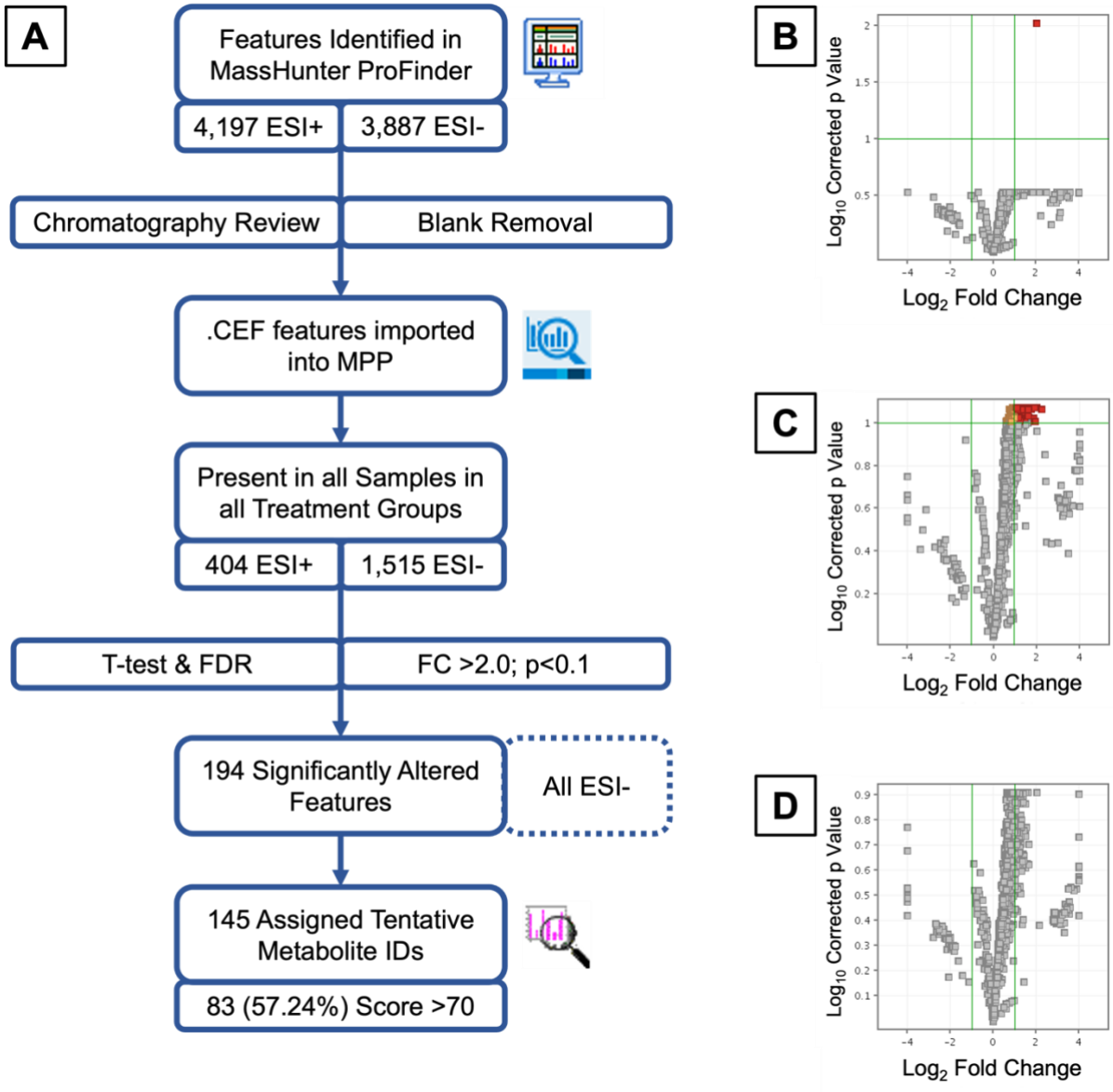


**Figure 5.3.4: Volcano Plot Analysis of Untargeted Metabolites in ANCA- and LPS-Stimulated Monocytes in the Primary Cohort.** CD14+ monocytes were isolated from PBMCs of healthy controls by MACS separation (n=6). Cells were plated and stimulated @37°C for 4 hours with 5µg/ml monoclonal antibody (mAb) directed against MPO, PR3, or 200ng/ml LPS. ANCA- and LPS-stimulated monocytes were analysed by LC-MS and untargeted metabolomic analysis was completed. 4,197 and 3,887 features were initially detected in ESI+ and ESI, respectively (A), and irrelevant peaks removed by manual chromatography review and extraction blank analysis. features present in all samples of all four treatment groups (n=1,921) were analysed by moderated t-test with a Benjamini-Hochberg FDR correction. Treatments were compared to unstimulated cells and features with fold changes >2 and p values <0.1 were considered. Volcano plots for LPS- (B), anti-MPO- (C), and anti-PR3- (D) treated monocytes are shown and significantly altered features are highlighted in red. Fold change and p-value thresholds are shown in green lines on the X and Y axes respectively.

### 5.3.4 Lipid Metabolism is Increased in anti-MPO Stimulated Monocytes.

We attempted to annotate the significantly altered features (all detected in ESI-) as described in Section 2.9.9. 145 of the 194 features imported into ID Browser were assigned tentative IDs. These IDs were assigned based on accurate mass and isotopic distribution obtained from the Agilent MassHunter METLIN Metabolomics Database and represent mid-level confidence in identification (compared to high-level confidence in the targeted analysis)[25]. Eighty-three of these (57.24%) had an identification score above 70. Normalized AUC values for these 83 metabolites are plotted in the heatmap in Figure 5.3.5A, in ascending p value order. A subtle metabolite signature is reflected by increased AUC values evident in anti-MPO-treated cells. Interestingly, almost all of the tentatively assigned metabolite IDs for significantly altered metabolites were lipids and lipid-like molecules (Figure 5.3.5B). Fatty acyls and glycerophospholipids were the most represented metabolite classes among significantly altered metabolites in ANCA-stimulated monocytes.

Individual plots of the most significantly altered compounds with their tentatively assigned IDs are shown in Figure 5.3.6. Differences between treatment groups were further scrutinised by ANOVA with Friedman's post-hoc testing. The most prominent changes were indeed seen in the anti-MPO treated cells. When subjected to these additional statistical tests a number of compounds also appear to be increased in anti-PR3 treated cells. The most significantly altered metabolite was annotated as palmitic (hexadecenoic) acid, which was increased in both anti-MPO- and anti-PR3-stimulated cells. These results reveal an apparent increase in lipid metabolism in ANCA-stimulated cells, particularly anti-MPO.

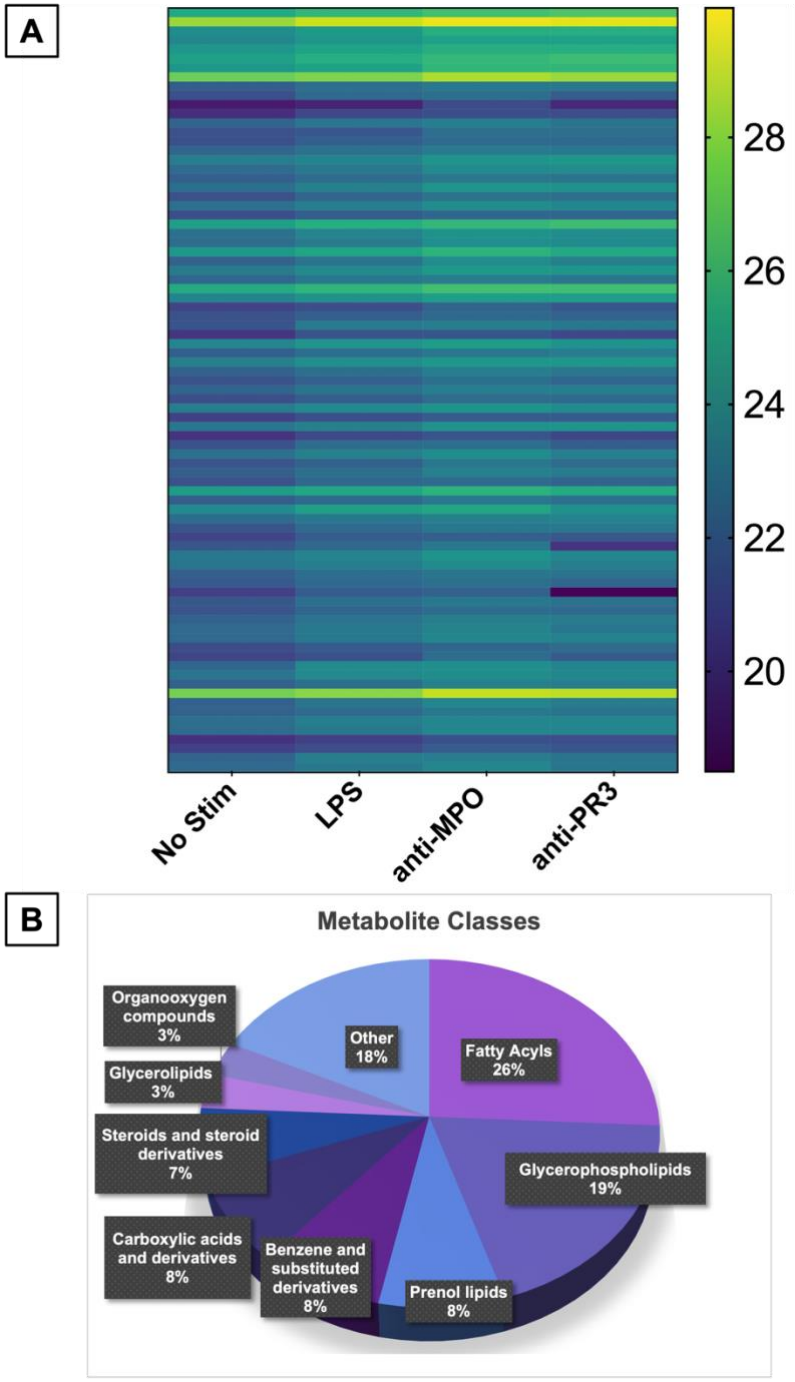


**Figure 5.3.5: Untargeted Metabolite Analysis of ANCA- and LPS-Stimulated Monocytes in the Primary Cohort.** CD14+ monocytes were isolated from PBMCs of healthy controls by MACS separation (n=6). Cells were plated and stimulated @37°C for 4 hours with 5µg/ml monoclonal antibody (mAb) directed against MPO, PR3, or 200ng/ml LPS. ANCA- and LPS-stimulated monocytes were analysed by LC-MS and untargeted metabolomic analysis was completed. Features present in all samples and all four treatment groups (n=1,921) were compared to unstimulated cells using a moderated t-test with a Benjamini-Hochberg FDR correction. 194 significantly altered peaks were imported into IDBrowser and assigned tentative IDs. (A) Heatmap of BCA and $\log_2$ normalised AUC values for metabolites with ID scores >70 (n=83). (B) Metabolites annotated based on accurate Mass and isotopic distribution with scores >70 as classified by the Human Metabolome Database (https://hmdb.ca/classyfication).

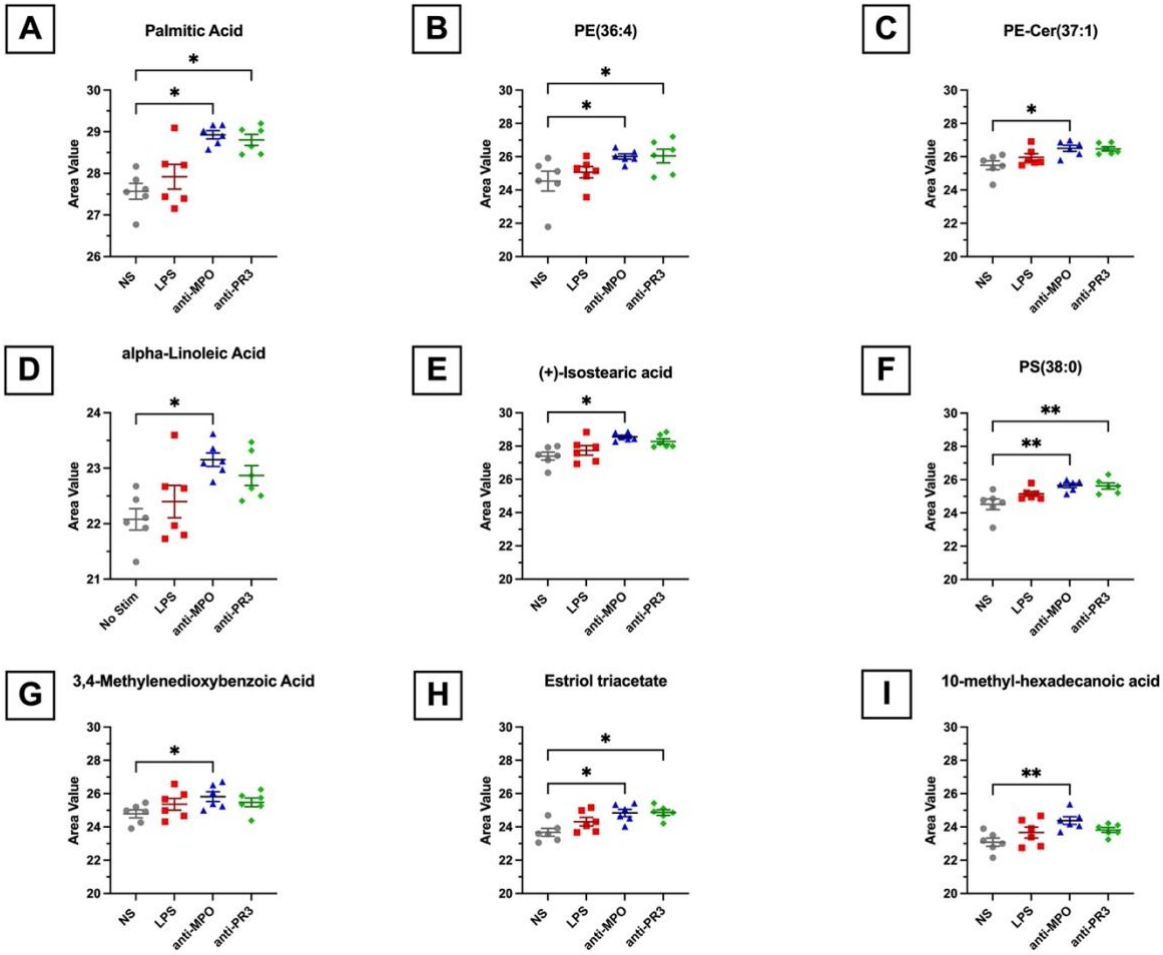


**Figure 5.3.6: Significantly Altered Metabolites in Untargeted Analysis of ANCA- and LPS-Stimulated Monocytes in the Primary Cohort.** CD14+ monocytes were isolated from PBMCs of healthy controls by MACS separation (n=6). Cells were plated and stimulated @37°C for 4 hours with 5µg/ml monoclonal antibody (mAb) directed against MPO, PR3, or 200ng/ml LPS. ANCA- and LPS-stimulated monocytes were analysed by LC-MS and untargeted metabolomic analysis was completed. Significantly altered features present in all samples of all four treatment groups were annotated based on accurate mass and isotopic distribution, ID scores >70 were analysed by 2-way ANOVA with a Benjamini-Hochberg FDR correction. $Log_2$ and BCA-normalised AUC values for significantly altered metabolites are displayed as individual dot plots (A-H).

### 5.3.5 Power Analysis Specifies Biological Replicate Requirements for Subsequent Metabolomic Experiments

Initial findings appear to demonstrate increased lipid metabolism in ANCA-stimulated cells. Additional experiments are required to confirm these findings, and to determine the ideal sample size for such an experiment, power analyses were conducted using results from the Primary cohort targeted analysis. Initial power analysis by G*Power (Version 3.1, Faul *et al*. [378]) calculated mean and median sample size estimates (SSE) for intergroup comparisons on a per metabolite basis (Figure 5.3.7A) using BCA-normalised AUC values for the 32 detectable metabolites included in the synthetic standard mix. Mean values were substantially higher in the LPS and PR3 groups, further demonstrating the variation between metabolites and the relevance (or lack thereof) of these metabolites to ANCA-induced changes. Median SSE values were below 20 for all three treatment groups – a more feasible and manageable sample size for metabolomic validation experiments. Additional analyses with raw AUC values and $\log_2$-normalized data returned much higher SSEs than the BCA-normalized data (data not shown). This further demonstrates the utility of BCA normalization for improving interpersonal variability in metabolomics experiments.

An additional power analysis was carried out using the MetSizeR package [379]. Input settings specified a graduation of eight different sample sizes with 100 datasets simulated for each of these. Desired FDR was set to 0.05 and an expected dataset of 1,000 metabolites was explored of which 5% were estimated to be distinguished between groups. This was a conservative estimate based on the ~10% of statistically altered metabolites in the Primary cohort (see Figure 5.3.4A). Figures 5.3.7B, 5.3.7C, and 5.3.7D show the FDR curves obtained via simulation for comparisons of unstimulated cells versus LPS, anti-MPO and anti-PR3 stimulation, respectively. The solid red curve gives a mean FDR derived from the simulated datasets with dashed lines showing 95% uncertainty bounds. These plots would suggest an additional 23 biological replicates to maintain an FDR below 5%. Combining results of these 2 power analyses, an additional 24 replicates will be used in the subsequent metabolomic profiling experiment.

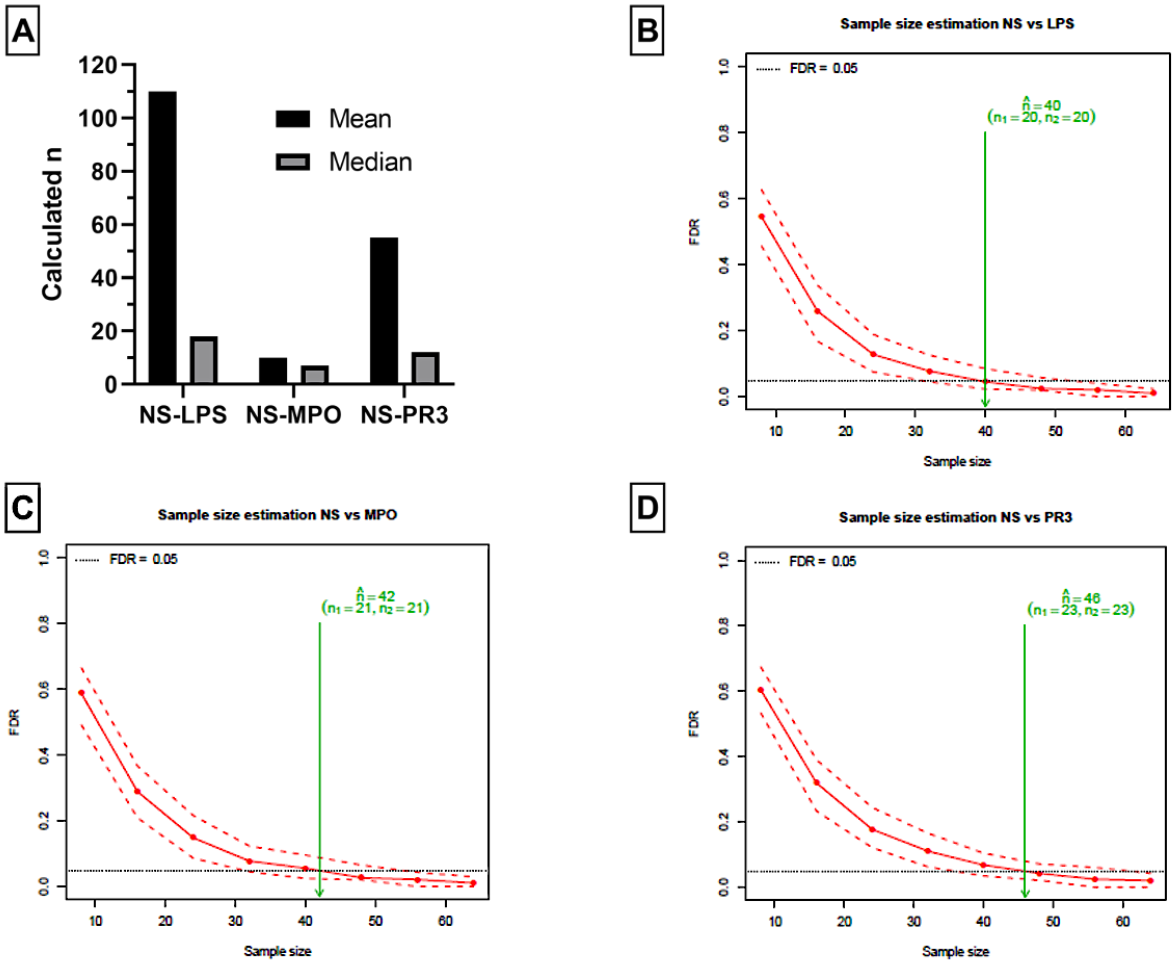


**Figure 5.3.7: Power Analysis of Monocyte Metabolomic Profiling Results for Subsequent Experiments.** Power analysis to determine required sample sizes (n numbers) for experimental validation was carried out using results from targeted metabolomic analysis of the Primary cohort (n=6). Initial G*Power [378] analysis (A) compared mean AUC values of individual BCA-normalised metabolites in each of the 3 treatment groups (LPS, anti-MPO, and anti-PR3) to unstimulated cells (NS) by t-test. Sample sizes for each metabolite were measured and sample size estimated were reported as mean and median for the intergroup comparison. Additional power analyses used methods described by Nyamundanda *et al.* [379] to generate FDR curves for LPS (B), MPO (C) and PR3 (D) versus unstimulated cells. The solid red curve gives a mean FDR while dashed lines show 95% uncertainty bounds for the FDR derived from the simulated datasets. Optimum sample numbers for each data set are highlighted with green lines.

### 5.3.6 Synthetic Standard Formulation Measurements are not Entirely Consistent Between Metabolomic Profiling Cohorts

A synthetic standard formulation was analysed by HILIC-Z LC-MS in both the primary and secondary cohorts (see Section 2.9.2.2). Metabolite abundances for compounds included in this synthetic standard formulation were determined by targeted analysis. 52 of the 53 synthetic standard metabolites were detected by the optimised LC-MS method across the positive and negative ESI modes (Figure 5.3.8A). The same sample was injected for both the primary and secondary experiments and the same 52 metabolites consistently detected across runs. A PCA plot (Figure 5.3.8B) was generated to demonstrate the level of consistency in AUC values for these metabolites across the runs. Metabolites detected in the negative mode (circles) clustered well together for both the primary (blue) and secondary (gold) cohorts. This same degree of clustering was not seen for metabolites the ESI+ (triangles), indicating higher inter-run variance among these compounds. Indeed, when synthetic standard AUC levels were compared across runs (Figure 5.3.8C & 5.3.8D), synthetic standard metabolites measured in ESI+ had a weaker inter-run correlation than ESI- ($R^2$=0.4750 ESI+ vs. $R^2$=0.7058 ESI-, $p<0.0001$). There was also greater intra-run variation in the Secondary cohort for both ionisation modes as measured by standard deviation (data not shown). Despite the same replicates being injected each time, inter- and intra-run variability are evident in the synthetic standards. Without appropriate batch correction these data show that the two monocyte metabolomic profiling cohorts cannot (and thus, will not) be combined in their current forms.

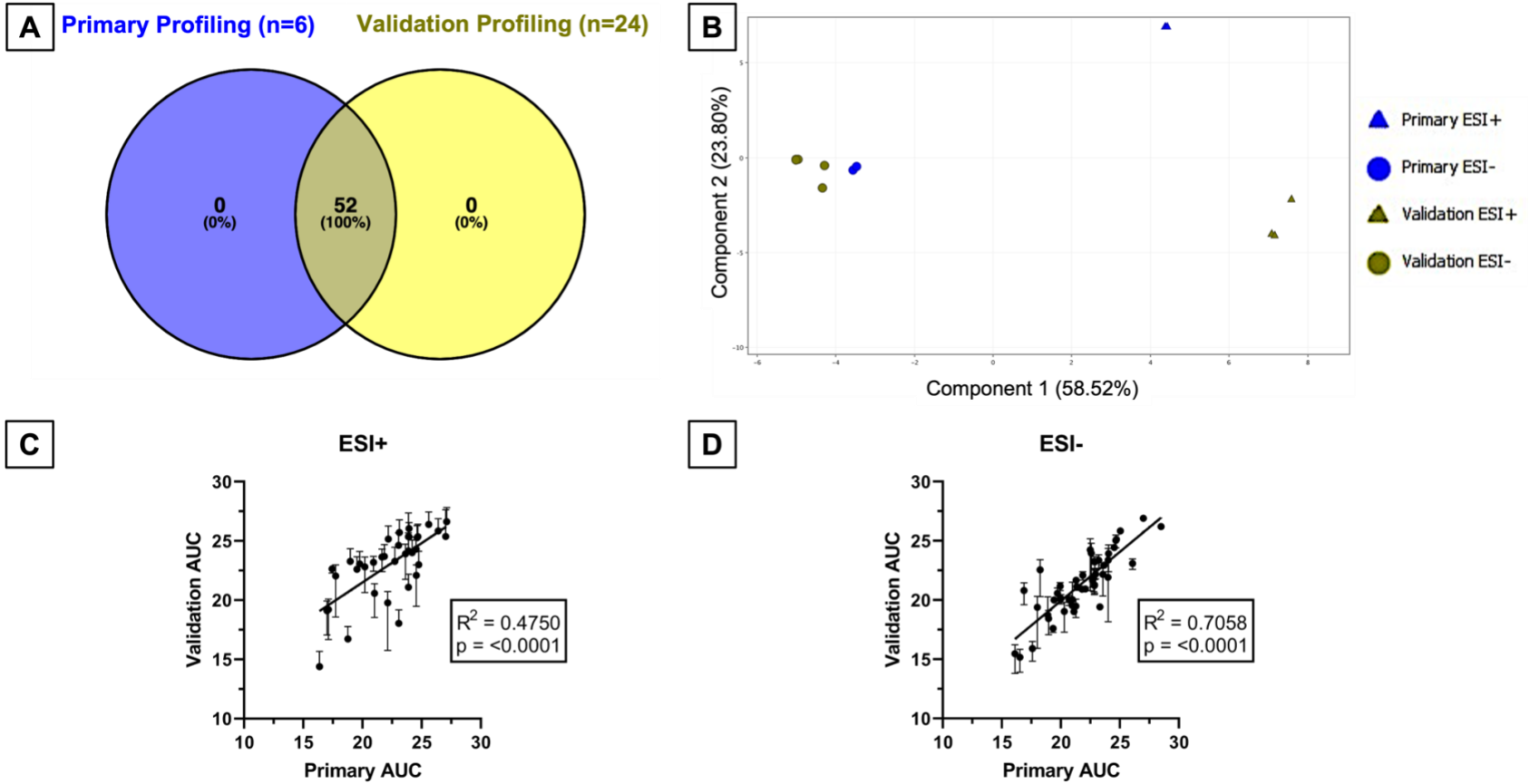


**Figure 5.3.8: Comparison of Synthetic Standard Metabolite Coverage and Consistency Across Metabolomic Profiling Experiments.** The number of synthetic standard metabolites (n=53) detected across both ionisation modes in the synthetic metabolite mixture was compared by Venn Diagram (A)[380]. Principal Component Analysis (PCA) was carried out to detect consistency between the initial metabolomic profiling experiment ("Primary") and the subsequent Secondary cohort ("Secondary") for metabolites detected in ESI+ (n=36) and ESI- (n=47) modes (B). Metabolite AUCs were compared for Primary and Secondary experiments in ESI+ (C) and ESI- (D) ionisation modes. Metabolite values are plotted as mean (and error) of $log_2$-transformed AUC values. Simple linear regression was used to determine best-fit lines for the data and $R^2$ values calculated by Pearson correlation.

### 5.3.7 PooledQC Samples are not Consistent Between Metabolomic Profiling Cohorts

PooledQC samples were prepared (See Section 2.9.2.1) for each of the respective profiling cohorts. These PooledQC samples were analysed by LC-MS and metabolite abundances for compounds included in the synthetic standard formulation were determined. There were 32 and 44 metabolites detected in the Primary and Secondary PooledQC samples, respectively. Two of these compounds were detected in the Primary cohort alone, and 14 were unique to the Secondary cohort (Figure 5.3.9A). There were 30 metabolites common to both cohorts detected in the PooledQC samples. It is very likely that the higher number of biological replicates included in the Secondary experiment (n=24 vs. n=6) drove this increase in detected metabolites as they surpassed minimum height filters. PCA analysis was carried out on common metabolites which were detected in the same ionization mode(s)(n=19). There was a clear divergence of PooledQC samples among the two profiling cohorts (Figure 5.3.9B). This effect persisted even after correcting for the number of biological replicates in the sample, the metabolite fraction BCA OD readout (595nm), and baselining by Z-transformation to correct data from different sources (data not shown). There was further intra-run variability evident in the Secondary cohort (gold). PooledQC samples towards the end of the run showed substantial signal drift, with later injections digressing from the core cluster. Despite these discrepancies area measurements for the Primary and Secondary cohorts, PooledQCs showed a significant (albeit moderate) inter-run correlation (Figure 5.3.9C, $R^2$=0.6159, $p<0.0001$). Only metabolites detected in both experiments and measured in the same ionisation mode (n=19) were included in this analysis. Based on the above results it was determined that the Primary and Secondary experiments could not be combined in their current forms. As such the results for the Secondary cohort will be considered as a separate experimental result.

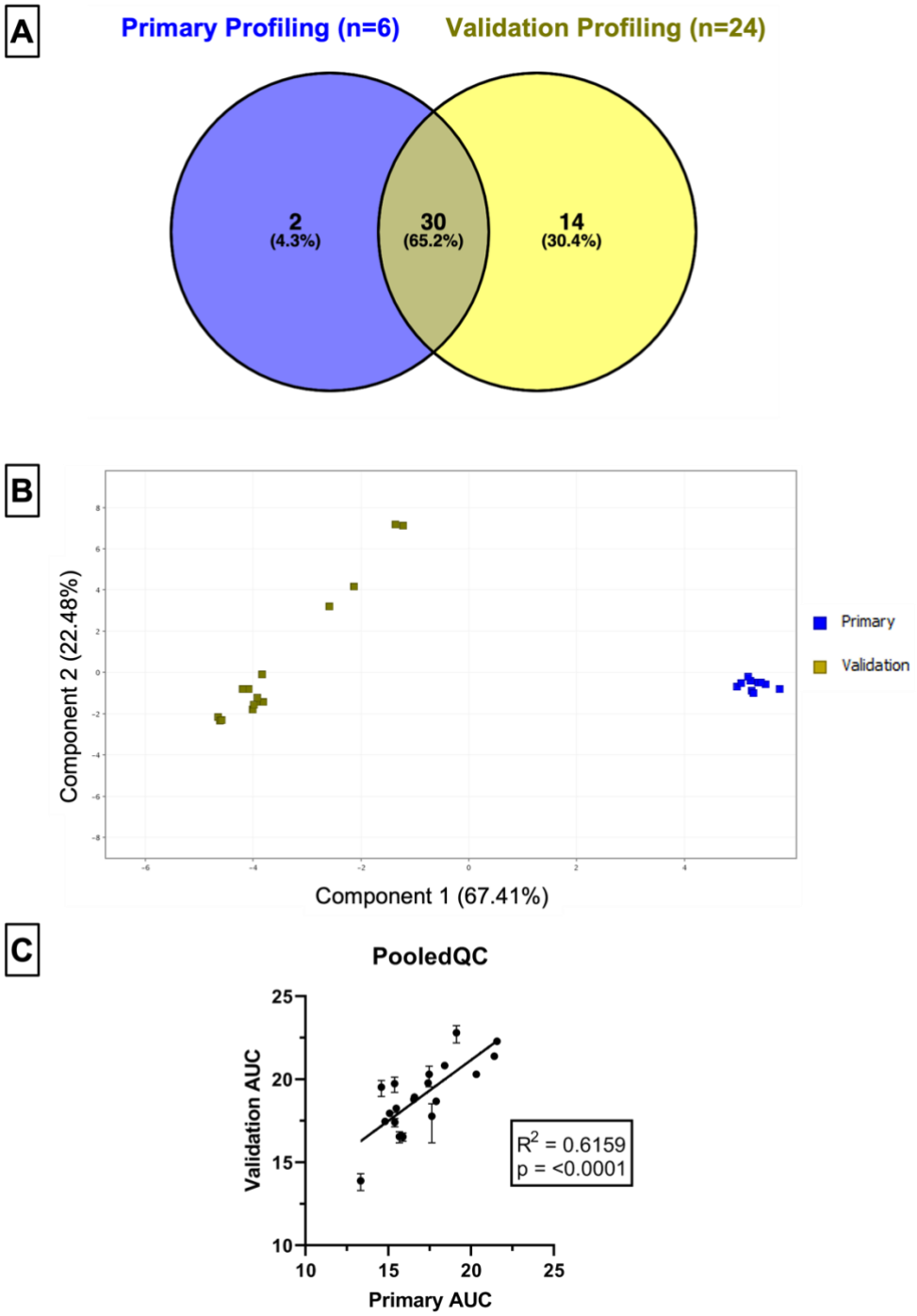


**Figure 5.3.9: Comparison of PooledQC Metabolite Coverage and Consistency Across Metabolomic Profiling Experiments.** The number of metabolites included in the synthetic standard mixture (n=53) detected across both ionisation modes in PooledQC samples was compared by Venn diagram (A)[380]. Principal Component Analysis (PCA) was carried out to detect consistency between the initial metabolomic profiling experiment ("Primary") and the subsequent Secondary cohort ("Secondary") for detected metabolites (B). Metabolite AUCs were compared for Primary and Secondary experiments (C) with metabolite values plotted as $\log_2$ transformed AUC values and error bars representing standard deviation. Simple linear regression was used to determine best-fit lines for the data and $R^2$ values calculated by Pearson correlation. Only metabolites detected in both experiments and measured in the same ionisation mode (n=19) were included in this analysis.

### 5.3.8 Technical Issues in the ESI+ Secondary Cohort LC-MS Experiment Caused Significant Variation in PooledQC Samples

The Secondary cohort PooledQC sample showed substantial variation throughout the ESI+ LC-MS run (see above). Intra-run %CV was higher for metabolites measured in ESI+ (n=9) than ESI- (n=28)(Figure 5.3.10A). 19 metabolites from the synthetic standard mixture were detected by both ionisation modes in the Secondary PooledQC samples (Figure 5.3.10B), and only 4 metabolites were uniquely detected in the positive mode. A PCA plot was generated for the shared metabolites (n=19) to compare variation by ionisation mode (Figure 5.3.10C). The negative mode samples clustered together very well with limited variation (red). Conversely, the same metabolites measured in positive mode (gold) showed substantial variation and drift, particularly towards the end of the run. This was caused by a pressure drop which led to the worklist being reset and the final 25% of samples rerun. Due to the efficient randomisation, affected samples evenly spanned the four treatment groups. Excluding ESI+ samples acquired after the restart (and analysed using an unpaired t-test), of the four metabolites detected in ESI+ alone we see no significant differences in nicotinamide adenine dinucleotide (NAD) or trimethylamine n-oxide (TMAO) between treatment groups (Figure 5.3.11A & 5.3.11B, respectively). The isomers 1- and 3-methyl-L-histidine were only effectively separated in positive mode. AUC values for 3-methyl-L-histidine were significantly lower than 1-methyl-L-histidine (Figure 5.3.11C). Ethanolamine, which was significantly altered in the Primary cohort was not detected in the Secondary sample set. Due to this technical variation and given that all significantly altered metabolites from the primary cohort untargeted analysis were measured in the negative mode (see Figure 5.3.4), only the ESI- LC-MS run was considered in the Secondary cohort analysis. Unless otherwise specified, all subsequent metabolite results for the Secondary cohort have been measured in ESI- only.

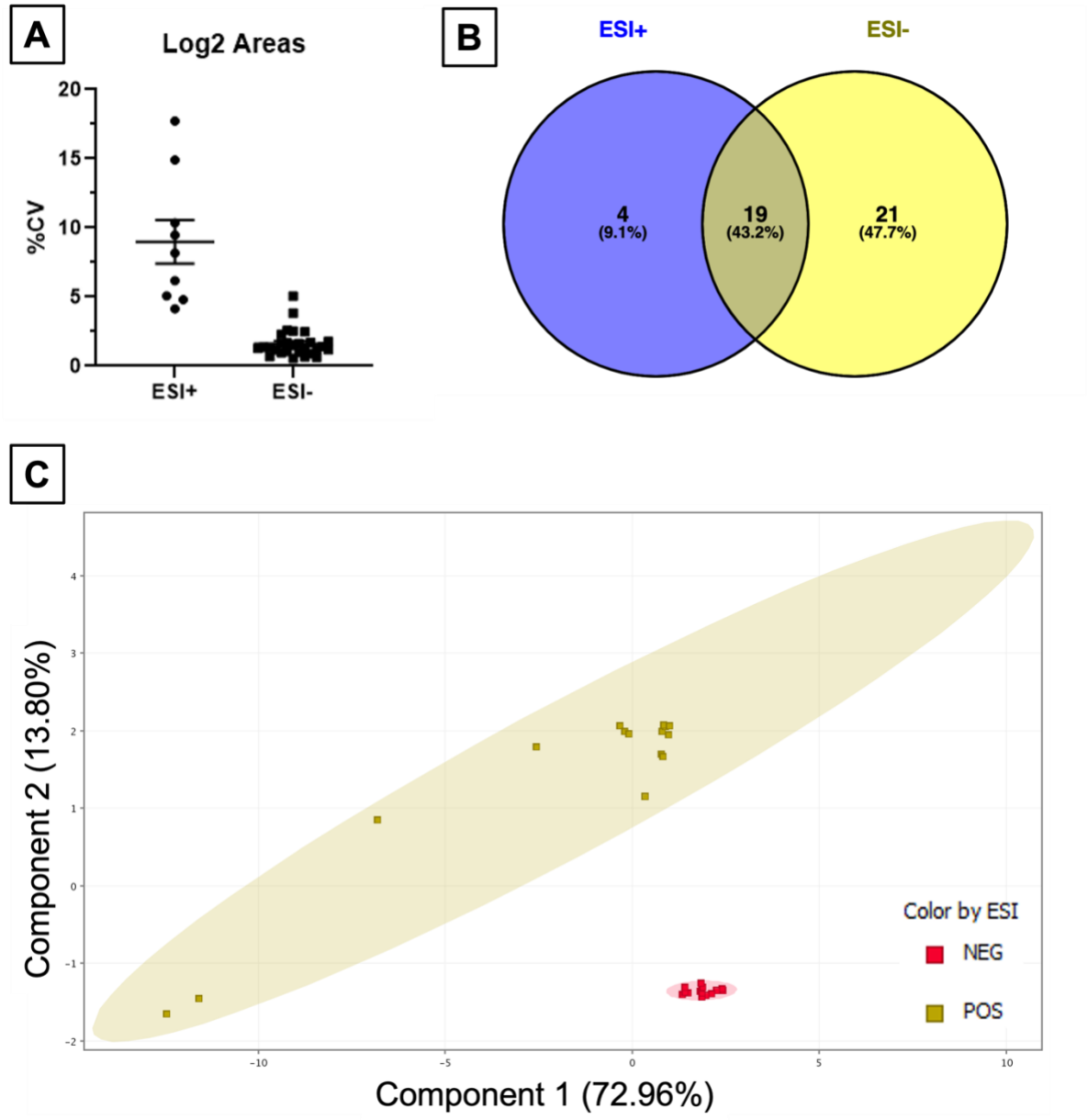


**Figure 5.3.10: Technical Variation in ESI+ Secondary Cohort PooledQC Samples.** The Secondary cohort PooledQC sample showed significant intra-run variation in ESI+ mode. $Log_2$-transformed values for synthetic standard metabolites measured in both ionisation modes were compared (A). Synthetic standard metabolites detected across ionisation modes were compared [380]. A PCA plot was generated for the 19 metabolites detectable across both methods to visualise intra-run variation (C).

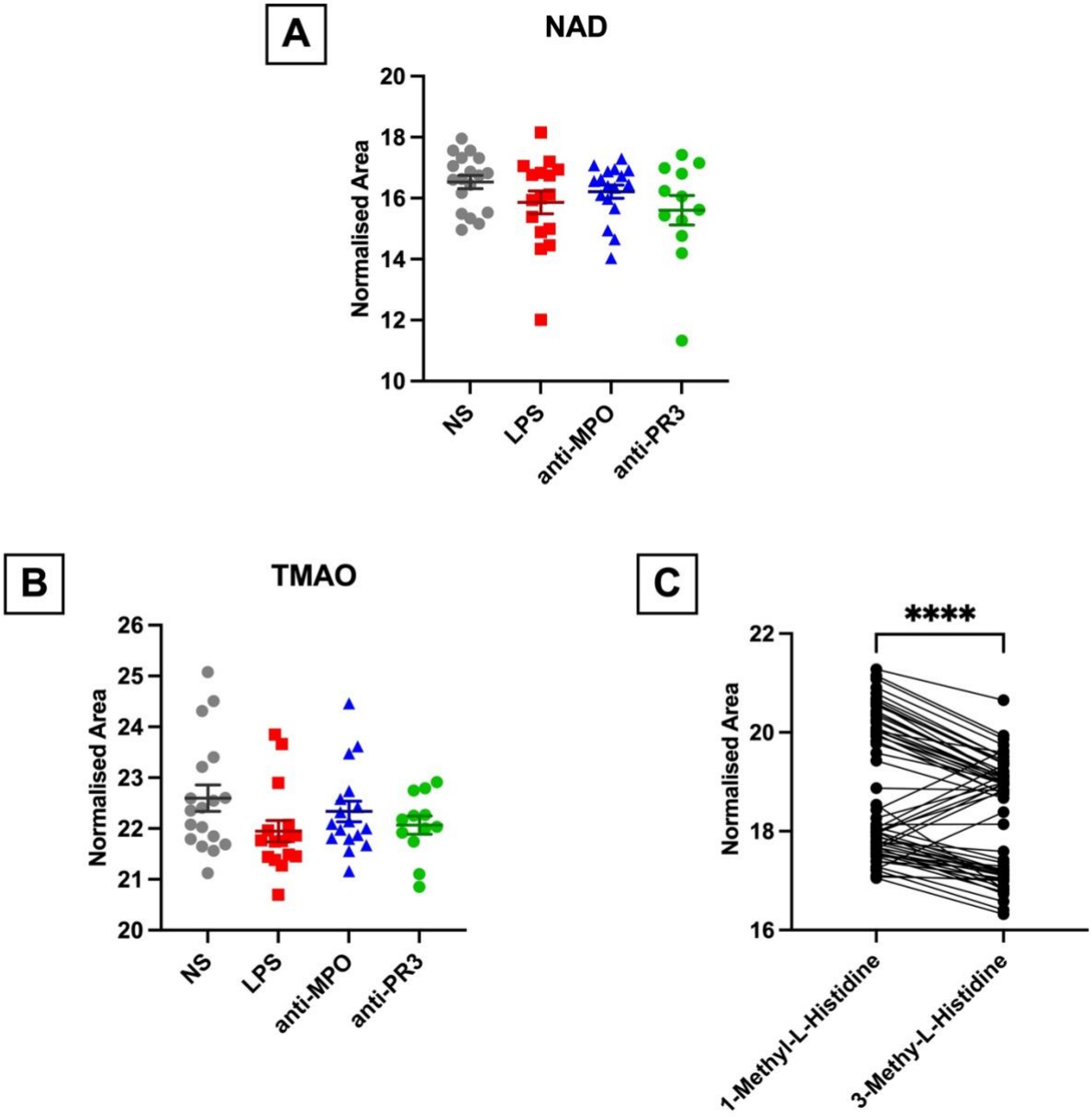


**Figure 5.3.11: ESI+ Unique Metabolites in Pre-Interruption Samples in the Secondary Cohort.** CD14+ monocytes were isolated from PBMCs of healthy controls by MACS separation (n=24). Cells were plated and stimulated @37°C for 4 hours with 5µg/ml monoclonal antibody (mAb) directed against MPO, PR3, or 200ng/ml LPS. ANCA- and LPS-stimulated monocytes were analysed by LC-MS in ESI+ mode and targeted analysis carried out BCA- and $Log_2$-normalised AUCs. Only a portion of samples acquired prior to a technical interruption were analysed. NAD (A), TMAO (B) and 1/3-methyl-L-histidine (C) were uniquely detected in ESI+. Differences between treatment groups were analysed by Kruskal-Wallis test to account for missing values, and 1/3-methyl-L-histidine levels compared by Wilcoxon matched-pairs signed rank test.

### 5.3.9 Targeted Analysis of the Larger Secondary Cohort Reveals Additional Metabolite Alterations in LPS- and ANCA-Stimulated Monocytes.

Considering just ESI- LC-MS run, 29 of the 53 synthetic standard metabolites (40 of which were detectable in PooledQC samples) were detected in experimental samples. This discrepancy is likely due to metabolites falling below minimum height filters in biological replicates. An overlay of the total ion chromatograms (TIC) shows slight shifts between peaks and minimal differences between treatment groups (Figure 5.3.12A). AUC values were $\log_2$ transformed and normalised to metabolite fraction BCA values for each sample. PCA analysis showed treatment groups largely overlapped (Figure 5.3.12B). LPS-treated cells did cluster slightly better than other treatment groups when considering all 29 detected synthetic standard metabolites. A heatmap of BCA-normalised AUC values by treatment group is shown in Figure 5.3.13. Contrary to the anti-MPO signature seen in the Primary cohort, there was a more profound shift in LPS-stimulated metabolite levels. Although this was rather subtle, there were eleven metabolites significantly altered among the three treatment groups (Table 5.3.2). These mostly comprised amino acids, as well as TCA cycle metabolites (fumaric acid, L-malic acid) and nucleotides (inosine 5'-monophosphate [IMP]). Surprisingly none of these significantly altered metabolites overlapped with those discovered in the primary cohort. α-ketoglutaric acid was not found to be significantly altered in the Secondary cohort, and ethanolamine and L-histidine were not detected in ESI-. Metabolites with significant alterations in at least two treatment groups are displayed as individual dot plots in Figure 5.3.14. Considering only the metabolites that were significantly altered in the targeted analysis did not particularly alter the appearance of the PCA plot (data not shown).

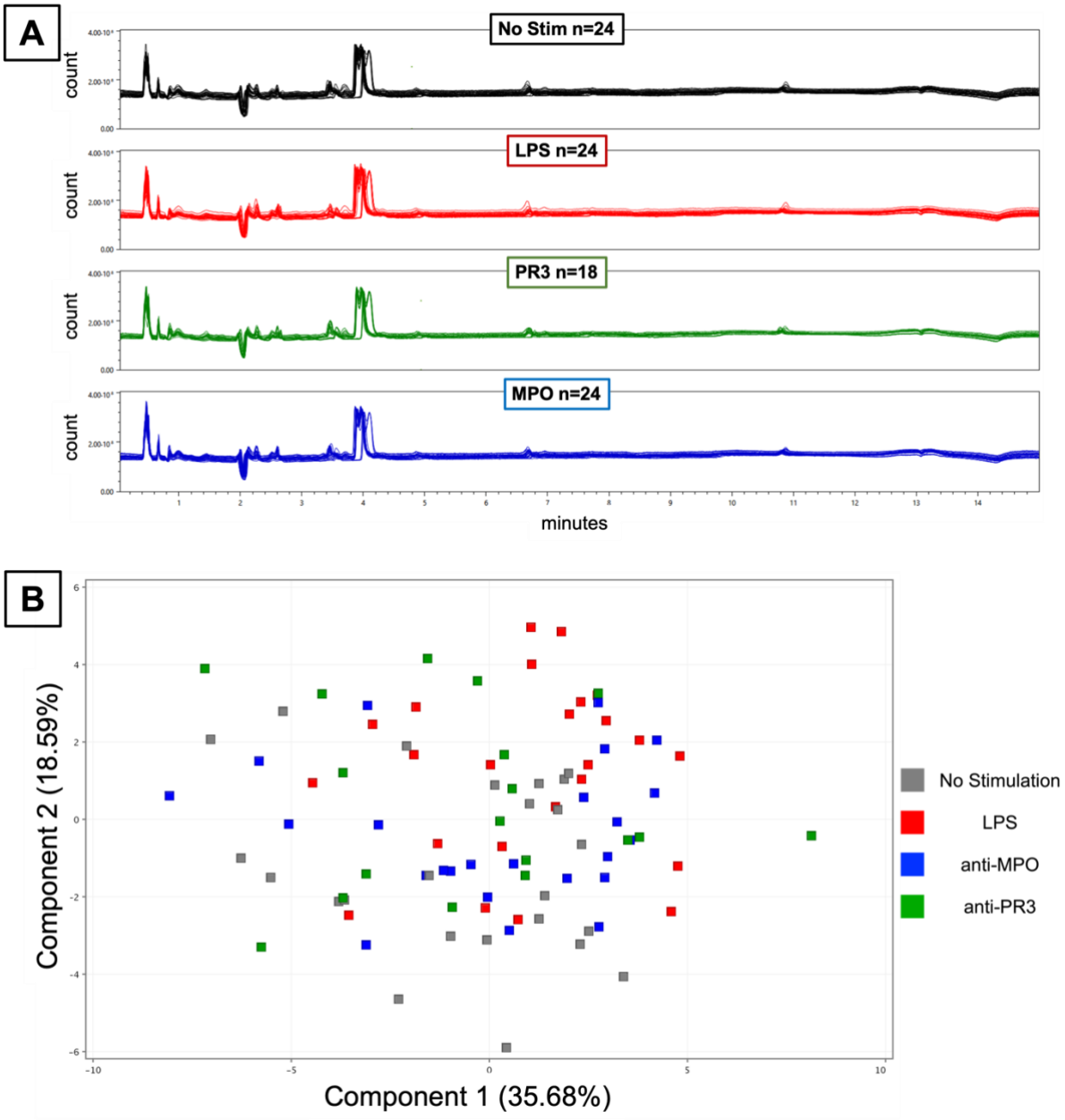


**Figure 5.3.12: Principal Component Analysis and Total Ion Chromatograms of Targeted Metabolites in ANCA- and LPS-Stimulated Monocytes in the Secondary Cohort.** CD14+ monocytes were isolated from PBMCs of healthy controls by MACS separation. Cells were plated and stimulated @37°C for 4 hours with 5µg/ml monoclonal antibody (mAb) directed against MPO, PR3, or 200ng/ml LPS. ANCA- and LPS-stimulated monocytes were analysed by LC-MS and targeted metabolomic analysis of 53 metabolites was completed in ESI-. Overlay of the TIC shows a perfect overlay with the exception of one replicate (A). Area-under-the curve (AUC) values were normalised by $Log_2$ transformation and to metabolite fraction protein levels (measured by BCA). 29 of the 53 metabolites were detected in the experiment samples. Principal Component Analysis (PCA) plots were generated for the four treatment groups – NS (blue), LPS (red), MPO (gold), PR3 (grey), and Pooled QC samples.

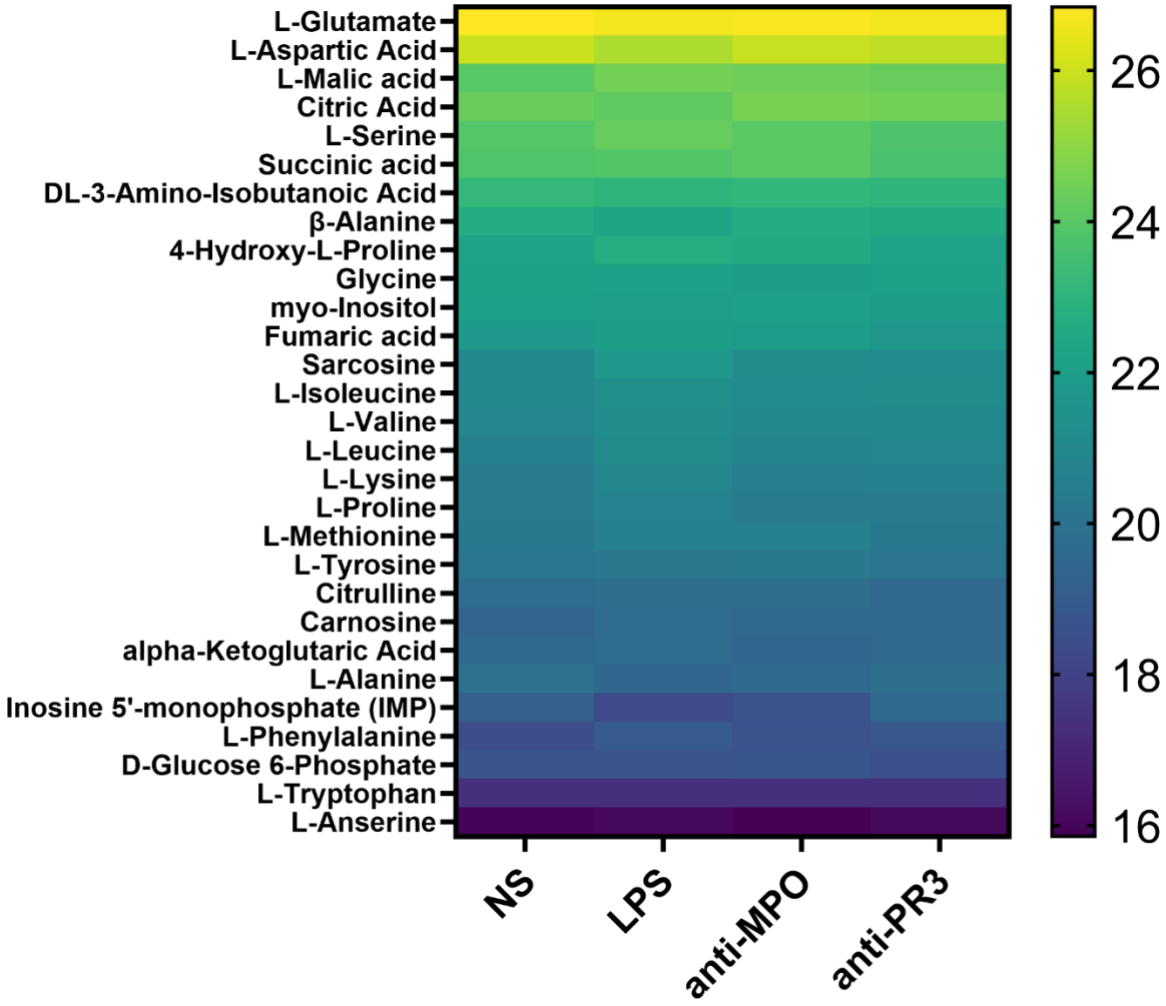


**Figure 5.3.13: Heatmap Analysis of Targeted Metabolites in ANCA- and LPS-Stimulated Monocytes in the Secondary Cohort.** CD14+ monocytes were isolated from PBMCs of healthy controls by MACS separation (n=24). Cells were plated and stimulated @37°C for 4 hours with 5µg/ml monoclonal antibody (mAb) directed against MPO, PR3, or 200ng/ml LPS. ANCA- and LPS-stimulated monocytes were analysed by LC-MS and targeted metabolomic analysis of 53 metabolites was completed. 29 of the 53 metabolites were detected in experiment samples. Intergroup values are reported as BCA and $Log_2$ normalised AUCs.

| Compound | ANOVA P Value | LPS | | | | anti-MPO | | | | anti-PR3 | | | |
|---|---|---|---|---|---|---|---|---|---|---|---|---|---|
| | | Mean Diff. | Fold Change | Q Value | P Value | Mean Diff. | Fold Change | Q Value | P Value | Mean Diff. | Fold Change | Q Value | P Value |
| 4-Hydroxy-L-Proline | 0.0014 | -0.5147 | 1.4287 | <0.0001 | <0.0001 | -0.2526 | 1.1913 | 0.0204 | 0.0136 | -0.0210 | 1.0147 | 0.8471 | 0.8471 |
| β-alanine | 0.0004 | 0.4022 | -1.3215 | <0.0001 | <0.0001 | 0.0884 | -1.0632 | 0.2633 | 0.2633 | 0.1508 | -1.1102 | 0.0555 | 0.0370 |
| Fumaric acid | 0.0059 | -0.1274 | 1.0923 | 0.0004 | 0.0002 | -0.1400 | 1.1019 | 0.0004 | 0.0003 | 0.0350 | -1.0246 | 0.5040 | 0.5040 |
| Aspartic Acid | 0.0001 | 0.4735 | -1.3885 | <0.0001 | <0.0001 | 0.0991 | -1.0711 | 0.2287 | 0.2287 | 0.1793 | -1.1323 | 0.0235 | 0.0157 |
| Isoleucine | 0.0014 | -0.5070 | 1.4211 | <0.0001 | <0.0001 | -0.2847 | 1.2182 | <0.0001 | <0.0001 | -0.2832 | 1.2169 | 0.0007 | 0.0007 |
| Leucine | 0.0008 | -0.5847 | 1.4997 | <0.0001 | <0.0001 | -0.2947 | 1.2266 | 0.0001 | <0.0001 | -0.3361 | 1.2623 | 0.0005 | 0.0005 |
| Lysine | 0.0012 | -0.3820 | 1.3031 | <0.0001 | <0.0001 | -0.1389 | 1.1011 | 0.0177 | 0.0118 | -0.1270 | 1.0920 | 0.0532 | 0.0532 |
| Phenylalanine | 0.0012 | -0.6178 | 1.5345 | 0.0002 | <0.0001 | -0.2372 | 1.1787 | 0.0283 | 0.0283 | -0.3993 | 1.3189 | 0.0118 | 0.0079 |
| Proline | 0.0178 | -0.3308 | 1.2577 | <0.0001 | <0.0001 | -0.0700 | 1.0497 | 0.3375 | 0.2250 | -0.0204 | 1.0142 | 0.7473 | 0.7473 |
| Serine | 0.0000 | -0.2873 | 1.2204 | 0.0011 | 0.0004 | -0.0883 | 1.0631 | 0.1796 | 0.1796 | 0.1216 | -1.0880 | 0.1796 | 0.1549 |
| Sarcosine | 0.0009 | -0.7809 | 1.7182 | 0.0007 | 0.0002 | -0.2557 | 1.1939 | 0.2054 | 0.2054 | -0.1619 | 1.1187 | 0.2054 | 0.1657 |

**Table 5.3.2: Statistical Results of Significantly Altered Metabolites in Targeted Analysis of Secondary Cohort.** Fold Change was calculated relative to unstimulated cells.

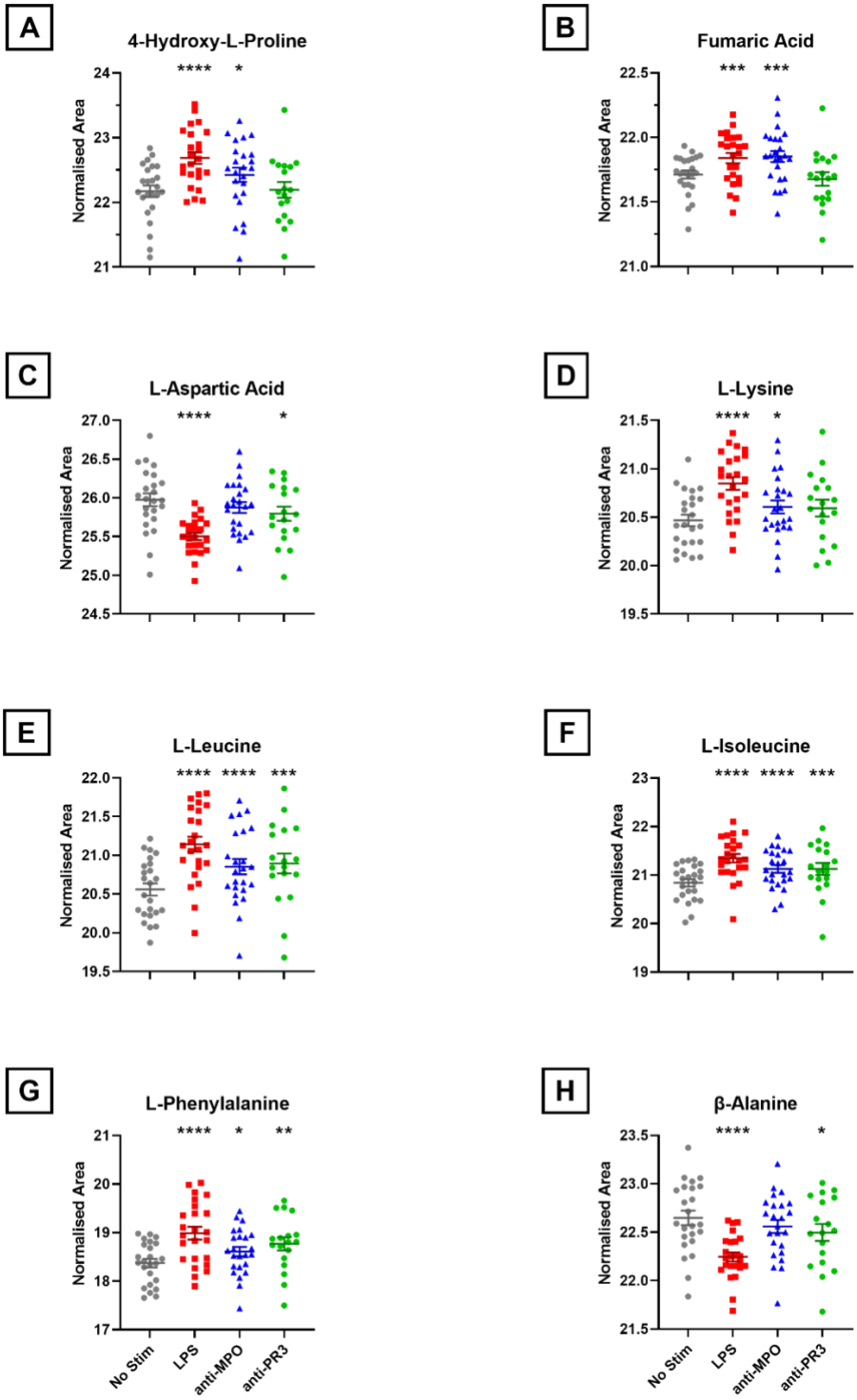


**Figure 5.3.14: Significantly Altered Metabolites in Targeted Analysis of ANCA- and LPS-Stimulated Monocytes in the Secondary Cohort.** CD14+ monocytes were isolated from PBMCs of healthy controls by MACS separation (n=24). Cells were plated and stimulated @37°C for 4 hours with 5µg/ml monoclonal antibody (mAb) directed against MPO, PR3, or 200ng/ml LPS. ANCA- and LPS-stimulated monocytes were analysed by LC-MS and targeted metabolomic analysis of 53 metabolites was completed. 29 of the 53 metabolites were detected in experiment samples. BCA and $Log_2$ normalised AUC values were analysed by 2-way ANOVA with a Benjamini-Hochberg FDR correction. Results for significantly altered metabolites in 2 or more treatment groups are displayed as individual dot plots (A-H).

### 5.3.10 Untargeted Analysis of the Larger Secondary Cohort Reveals Additional Metabolite Alterations in LPS- and ANCA-Stimulated Primary Monocytes.

Untargeted analysis of ANCA- and LPS-stimulated monocytes was carried out as described in Sections 2.9.7 and 2.9.8. A summary of the untargeted workflow for the Secondary cohort is shown in Figure 5.3.15A. A total of 1,804 features were detected using RFE wizard in ESI-. After manual chromatography review and removal of peaks present in extraction blank samples 1,380 features were imported into MPP in .CEF format. These were assigned tentative metabolite IDs in ID browser, where 457 entities were assigned metabolite IDs and a further 733 were assigned formulae. Of those assigned metabolite IDs 58.86% had an overall ID score ≥70. Significantly altered entities were identified by Mann-Whitney paired testing with a Benjamini-Hochberg FDR correction. Only metabolites with a fold change ≥1.5 and a p value <0.05 were considered significant. There were 146, 59, and 60 significantly altered metabolites in the LPS-, anti-MPO-, and anti-PR3-activated cells compared to unstimulated cells, respectively (Figure 5.3.15B). This amounted to 225 significantly altered entities in this Secondary cohort. Seven were common to all three groups, and two were shared between both ANCAs. 33 and 44 features were unique to anti-MPO and anti-PR3-stimulated cells respectively. Volcano plots comparing treatment groups to unstimulated cells are shown in Figure 5.3.16.

To better compare differences between all treatment groups we measured differences to unstimulated cells by ANOVA and Benjamini-Hochberg FDR correction. This highlighted 83 metabolites which were significantly different across LPS- and ANCA-stimulated monocytes. PCA plots for all untargeted peaks (n=1,380) and statistically significant features (n=225) are shown in Figure 5.3.17A & 5.3.17B, respectively. Considering just the significant peaks greatly improved separation of the LPS and unstimulated cells in particular, proving that ANCA-stimulated cells can be discriminated on the basis of specific metabolic pathways. Anti-PR3 treated cells continued to cluster with unstimulated cells, further demonstrating their meagre metabolic response. Anti-MPO stimulated cells sat between the unstimulated/anti-PR3 and LPS groups.

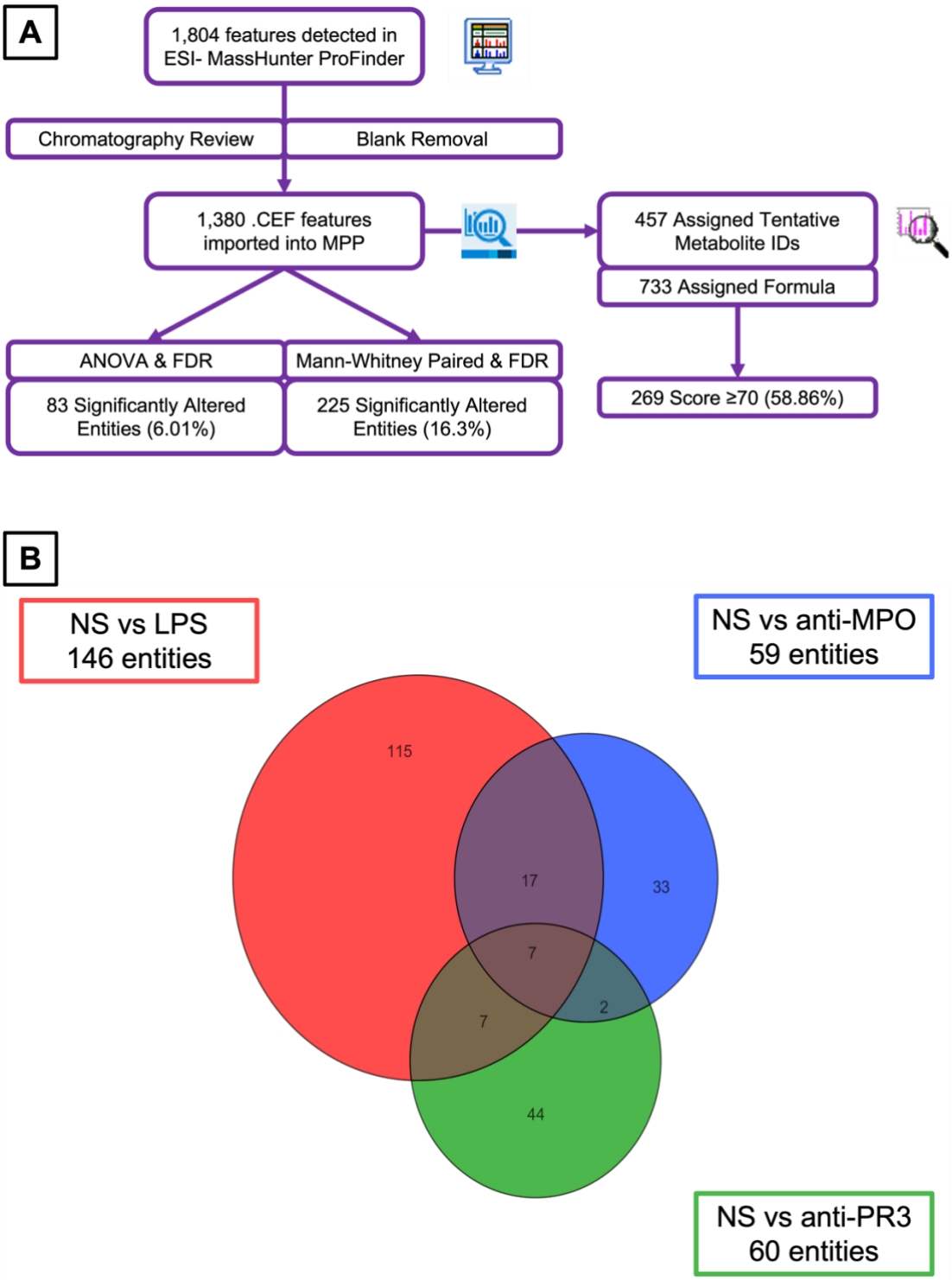


**Figure 5.3.15: Untargeted Analysis Workflow for Monocyte Metabolomic Secondary Cohort.** CD14+ monocytes were isolated from PBMCs of healthy controls by MACS separation (n=24). Cells were plated and stimulated @37°C for 4 hours with 5µg/ml monoclonal antibody (mAb) directed against MPO, PR3, or 200ng/ml LPS. ANCA- and LPS-stimulated monocytes were analysed by LC-MS and untargeted metabolomic analysis was completed. A summary workflow for the untargeted metabolomic analysis is shown here with the numbers of features/entities specified at each stage (A). A Venn diagram showing the shared and unique significantly altered entities by LPS (red), anti-MPO (blue), and anti-PR3 green) stimulation (B).

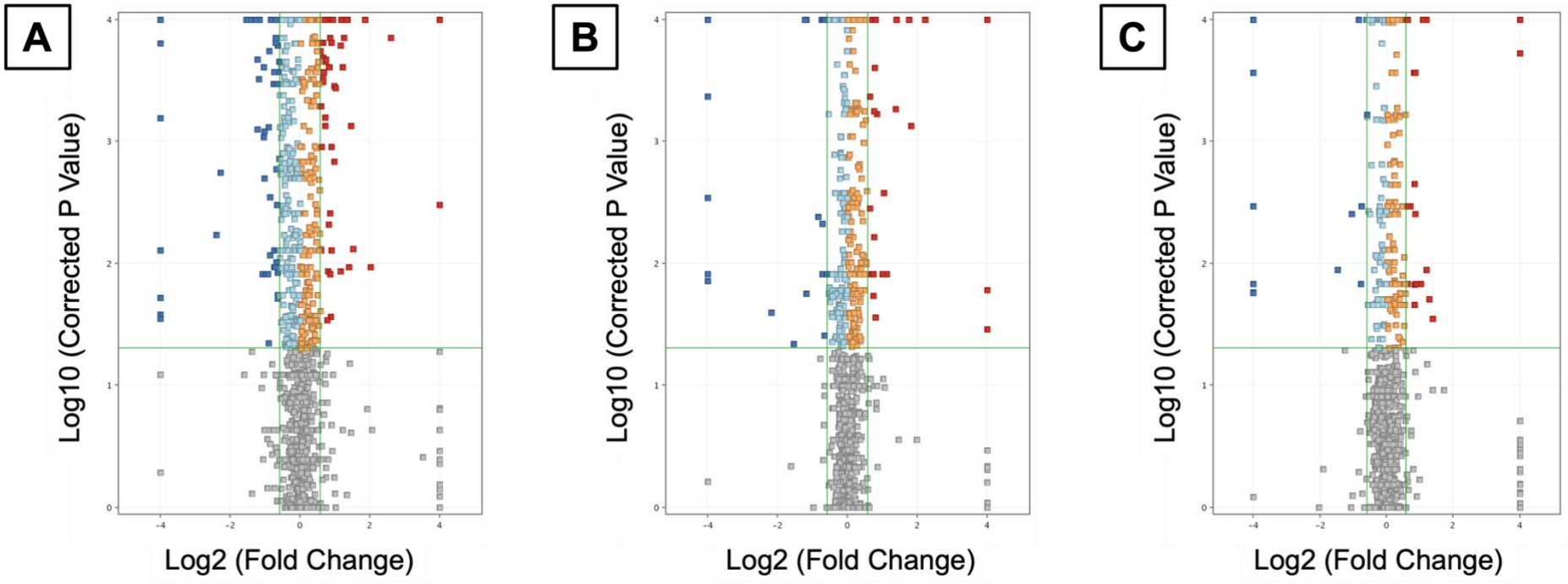


**Figure 5.3.16: Volcano Plot Analysis of Untargeted Metabolites in ANCA- and LPS-Stimulated Monocytes in the Secondary Cohort.** CD14+ monocytes were isolated from PBMCs of healthy controls by MACS separation (n=24). Cells were plated and stimulated @37°C for 4 hours with 5µg/ml monoclonal antibody (mAb) directed against MPO, PR3, or 200ng/ml LPS. Extracted metabolites were analysed by LC-MS and untargeted metabolomic analysis was completed. 1,804 features were initially detected and those present in extraction blanks were removed. Tentative metabolite ID were assigned in ID Browser. Features were analysed by Mann-Whitney paired test with a Benjamini-Hochberg FDR correction. Treatments were compared to unstimulated cells and features with fold change ≥1.5 and p value <0.05 were considered significant. In total 230 metabolites were significantly altered across treatment groups. Volcano plots for LPS- (A), MPO- (B), and PR3- (C) treated monocytes are shown and significantly upregulated features are highlighted in red and downregulated features in dark blue. Light blue and orange features did not meet the fold change threshold limits, and grey features were not significant. Fold change and p-value thresholds are shown in green lines on the X and Y axes respectively.

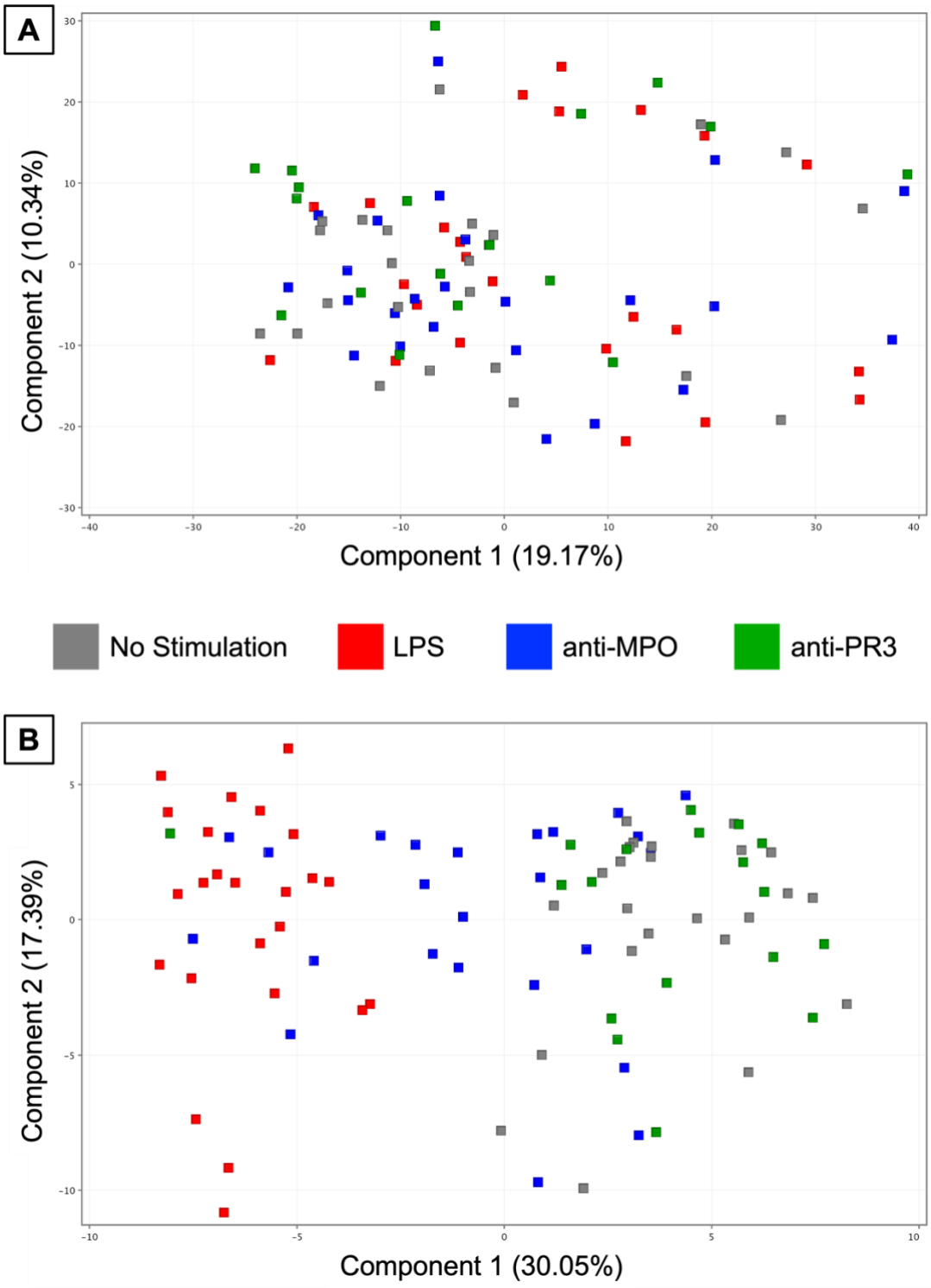


**Figure 5.3.17: Principal Component Analysis of Untargeted Metabolites in ANCA- and LPS-Stimulated Monocytes in the Secondary Cohort.** CD14+ monocytes were isolated from PBMCs of healthy controls by MACS separation. Cells were plated and stimulated @37°C for 4 hours with 5µg/ml monoclonal antibody (mAb) directed against MPO, PR3, or 200ng/ml LPS. ANCA- and LPS-stimulated monocytes were analysed by LC-MS and untargeted metabolomic analysis was completed on BCA-normalised AUC data. Principal Component Analysis (PCA) plots were generated for the four treatment groups (NS, LPS, MPO, and PR3) for all detectable entities (n=1,380, A) and entities that were significantly different compared to unstimulated cells as measured by ANOVA (n=83, B).

### 5.3.11 Class Predication Analysis Highlights Important Distinguishing Metabolites in Activated Monocytes

To better understand the specific influence and fundamental relations of these metabolites to the treatment matrices, class prediction analyses were carried out using partial least squares discriminant analysis (PLS-DA) and random forest (RF) analysis. Mean intragroup confidence measures were also higher in RF than PLS-DA. Variable importance in projection (VIP) scores and heatmaps for PLS-DA and RF are show in Figure 5.3.18A & 5.3.18B, respectively. VIP scores above 1 were considered significant. There were 29 and 17 metabolites above the VIP score threshold for the for PLS-DA and RF analyses, respectively, with eight metabolites common to both (see Table 5.3.3).

A heatmap for these metabolites is displayed in Figure 5.3.19. Where possible metabolites were annotated as proposed formulae, and where that was not attainable by their mass and RT values (e.g., 601.2048@4.95). As with the Primary cohort, we see an increase in a number of lipid-like molecules, particularly several glycerophosphoinositols (PI) and glycerophosphoserine (PS) species. Of note itaconic acid – an important modulator of inflammatory responses in macrophages – was found to be highly upregulated in LPS-activated cells at this early timepoint. *Myo*-inositol was previously reported as a urine biomarker of active AAV [261]. *Myo*-inositol mono- and diphosphate were increased in ANCA-stimulated cells, which may suggest increased activity through associated pathways. As MS/MS was not recorded in these metabolites we cannot be completely confident in these metabolite IDs. Additional validation experiments are required to confirm the influence of these metabolic pathways on monocyte function in AAV.

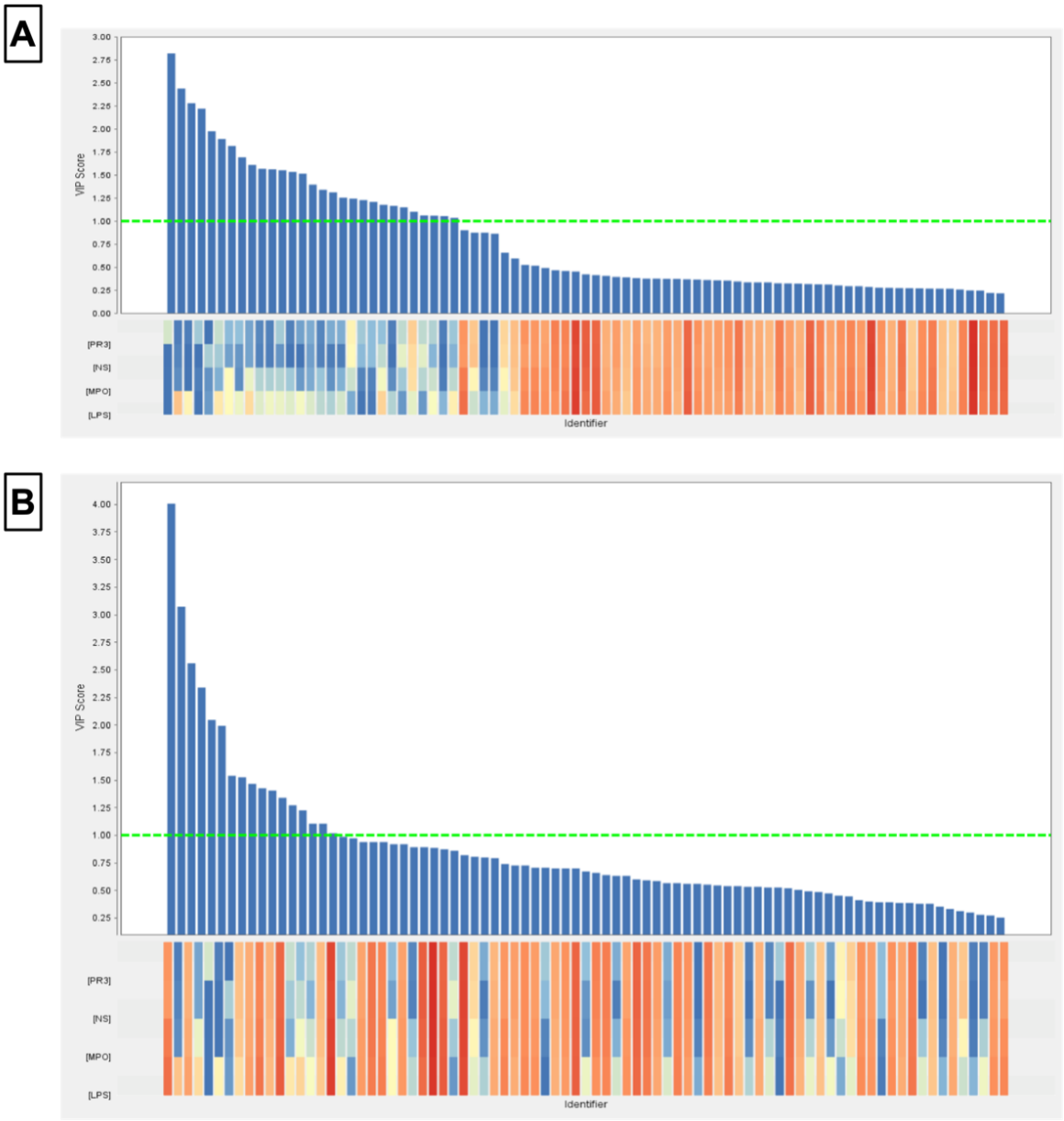


**Figure 5.3.18: Class Prediction Analyses of Significantly Altered Untargeted Metabolites in ANCA- and LPS-Stimulated Monocytes in the Secondary Cohort.** CD14+ monocytes were isolated from PBMCs of healthy controls by MACS separation (n=24). Cells were plated and stimulated @37°C for 4 hours with 5µg/ml monoclonal antibody (mAb) directed against MPO, PR3, or 200ng/ml LPS. ANCA- and LPS-stimulated monocytes were analysed by LC-MS and untargeted metabolomic analysis was completed. Features present in all four treatment groups (n=336) were compared to unstimulated cells using ANOVA with a Benjamini-Hochberg FDR correction. 83 significantly altered peaks were annotated using IDBrowser based on their accurate mass and isotopic distribution. Class prediction analysis was carried out by PLS-DA (A) and Random Forrest analysis (B), and VIP scores were plotted.

| | PLS-DA VIP Score | RF VIP Score |
|---|---|---|
| Hydroxytetradecanoyl-CoA | 1.0330 | |
| Glyerophosphoinositol | | 4.0067 |
| 419.1386@4.97 | | 2.5600 |
| 601.2048@4.95 | 1.3103 | |
| Aminomuconic acid | 2.2190 | |
| C14 H22 N4 O6 P3 | 1.5498 | |
| C24 H29 N22 O4 P2 | 1.3939 | |
| C32 H16 N7 O28 P3 S | 1.0602 | |
| C4 H9 N5 O S | 1.8895 | 1.2733 |
| C44 H83 N5 O10 P | | 1.4067 |
| C45 H90 O22 P2 | 1.2413 | |
| C5 H4 N2 | 1.2524 | |
| C6 H11 N O4 S | 1.5327 | |
| C7 H12 O3 P | 1.0529 | |
| C9 H21 N O5 | 1.6914 | |
| CL(1'-[18:2],3'-[18:2]) | 1.2270 | |
| Asparagine | | 1.3400 |
| *myo*-Inositol-1,3-diphosphate | 1.5128 | |
| *myo*-Inositol-3-phosphate | 1.8131 | |
| Erythronic acid | | 1.4267 |
| Glu Thr Met | 1.9722 | 1.5400 |
| Itaconic acid | 2.4361 | 3.0733 |
| Lactic acid | | 1.0200 |
| Ribulose 5-phosphate | 1.1641 | |
| PI(35:1) | 1.5658 | |
| PI(38:6) | 1.1757 | 1.2267 |
| PI(20:4) | 1.1478 | |
| PI(45:2) | 1.3391 | |
| PI(40:7) | 1.6075 | 2.3400 |
| PI(40:7) | | 1.5267 |
| PS(40:3) | 1.1001 | |
| PS(42:3) | | 1.1067 |
| PS(40:6) | 1.5597 | |
| PS(44:7) | 1.0578 | 1.1067 |
| Succinic aldehyde | 2.2783 | 1.9933 |
| Tos-Arg-CH2Cl | | 1.4667 |
| Tragopogonsaponin M | 1.2068 | |
| Tromethamine | 2.8172 | 2.0467 |

**Table 5.3.3: Class Prediction Variable Importance in Prediction (VIP) Scores for Secondary Metabolomic Profiling Cohort (n=24).** PLS-DA: Partial Least Squares Discriminant Analysis; RF: Random Forrest.

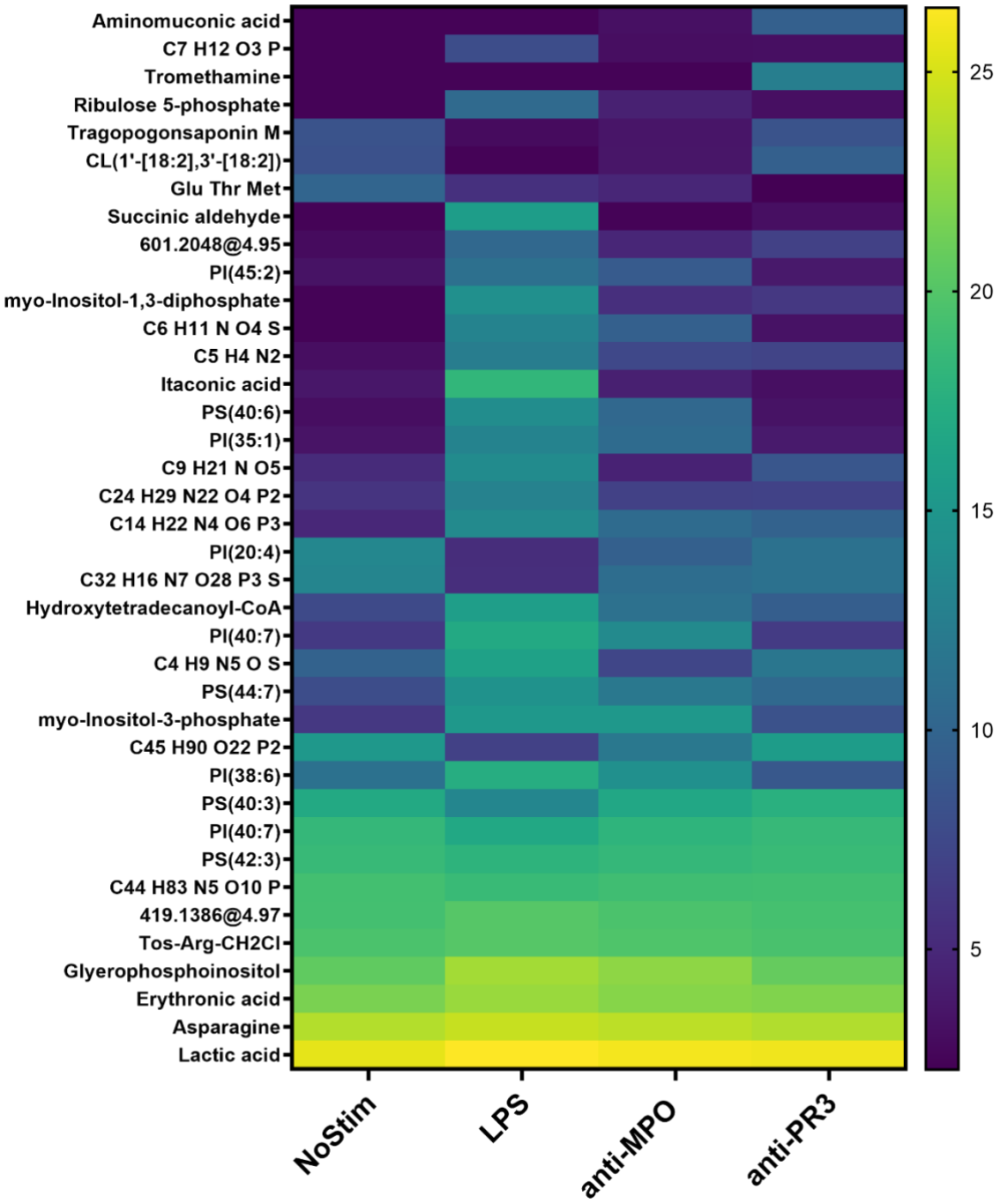


**Figure 5.3.19: Significantly Altered Metabolites in Untargeted Analysis of ANCA- and LPS-Stimulated Monocytes in the Secondary Cohort.** CD14+ monocytes were isolated from PBMCs of healthy controls by MACS separation (n=24). Cells were plated and stimulated @37°C for 4 hours with 5µg/ml monoclonal antibody (mAb) directed against MPO, PR3, or 200ng/ml LPS. ANCA- and LPS-stimulated monocytes were analysed by LC-MS and untargeted metabolomic analysis was completed. Features were compared to unstimulated cells using ANOVA with a Benjamini-Hochberg FDR correction. 83 significantly altered features were annotated by ID Browser based on their accurate mass and isotopic distribution. Class prediction analysis was carried out by PLS-DA and Random Forrest analysis and entities with a VIP score >1 are plotted on the heatmap.

### 5.3.12 Pathway Analysis of Untargeted Metabolomics Data

Pathway analysis for all 1,380 metabolites detected in the untargeted analysis was carried out using MetaboAnalyst (Version 5.0, https://www.metaboanalyst.ca/). Figure 5.3.20 shows annotated bubble plots for the most significantly altered metabolites in LPS- (A), MPO- (B), and PR3-stimulated monocytes (C). Inositol phosphate metabolism and phosphatidylinositol signalling were among the most significantly enriched pathways in LPS- and anti-MPO-treated cells. This effect was far more profound in the LPS-stimulated monocytes as indicated by the difference in scale of the X axis (Figure 5.3.20A). However, both of these pathways had a very low pathway coverage and thus a low pathway impact score. Glycolysis, gluconeogenesis, and the pentose phosphate pathway (PPP) were all significantly altered in anti-MPO group (Figure 5.3.20B). This indicates increased utilisation of glucose by early branches of the glycolysis pathway. There were no significantly altered pathways in the anti-PR3-treated cells (Figure 5.3.20C). Pathway analysis for the 83 significantly altered metabolites did not return any substantial results due to low pathway coverage and impact scores (data not shown). Here, implicated pathways included fatty acid elongation & degradation, valine, leucine and isoleucine degradation & biosynthesis, glycolysis/gluconeogenesis, and pyruvate metabolism. However, these are only tentative metabolite IDs [25], and we cannot be 100% certain that these annotations are correct. For instance, a number of di- and tri-peptides IDs were assigned but we cannot determine the exact configuration/order of these peptide bonds. It is however promising that 20 of the 29 metabolites in the synthetic standards mixture were identified in the untargeted analysis at the appropriate RTs. Additional analyses are needed to improve coverage of these metabolite pathways and confirm their important to ANCA- and LPS-activated inflammation.

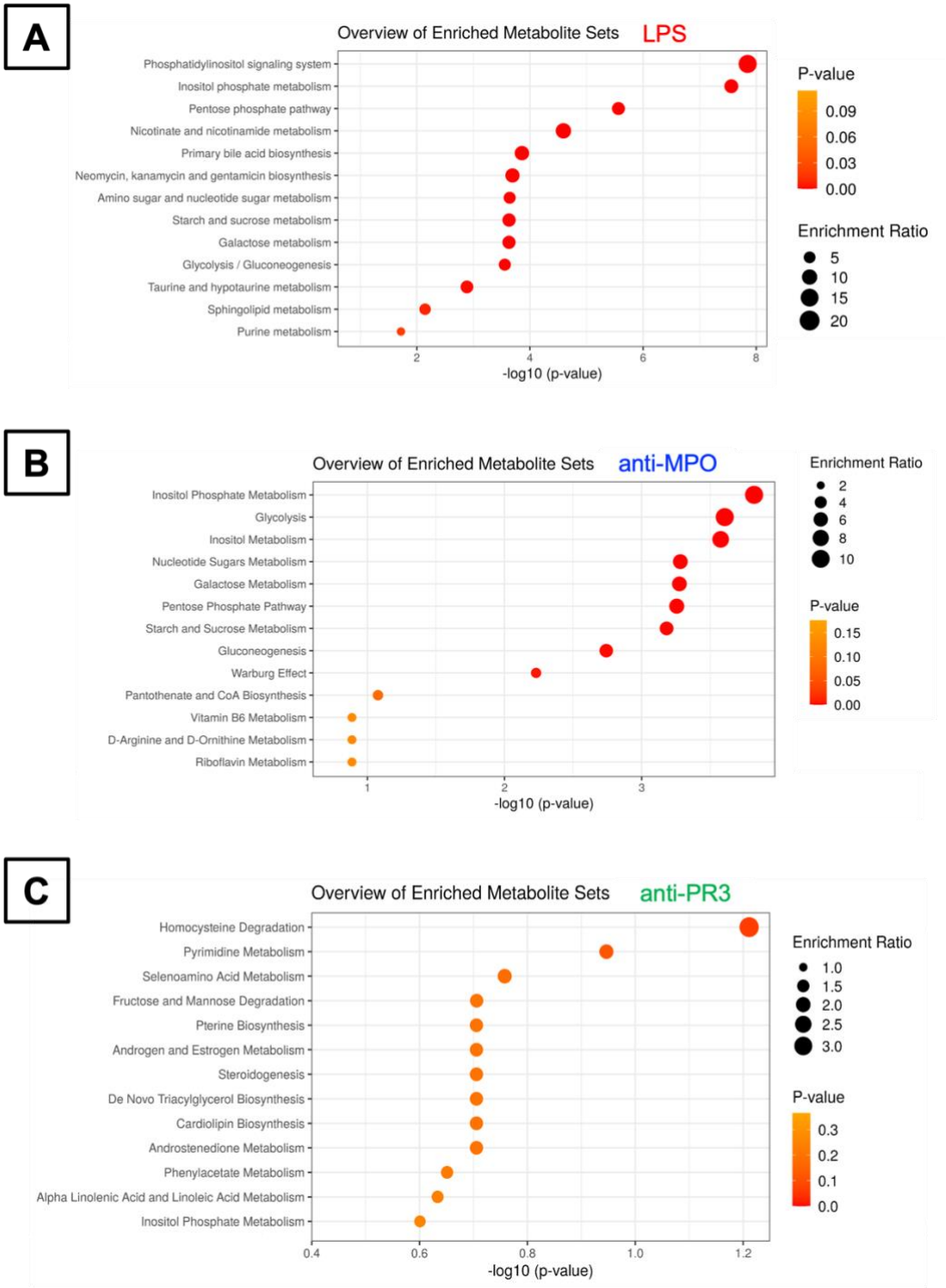


**Figure 5.3.20: Pathway Analysis of Significantly Altered Metabolites Identified in Untargeted Analysis.** CD14+ monocytes were isolated from PBMCs of healthy controls by MACS separation (n=24). Cells were plated and stimulated @37°C for 4 hours with 5µg/ml monoclonal antibody (mAb) directed against MPO, PR3, or 200ng/ml LPS. ANCA- and LPS-stimulated monocytes were analysed by LC-MS and untargeted metabolomic analysis was completed. Peaks (n=1,380) were annotated using IDBrowser based on their accurate mass and isotopic distribution. Pathway analysis was performed on the online MetaboAnalyst platform (Version 5.0, https://www.metaboanalyst.ca/) comparing unstimulated cells to LPS- (A), MPO- (B), and PR3-activated monocytes (C). **NB:** scales are not consistent between panels.

### 5.3.13 Cytokine Production and Protein Content Differ between Primary and Secondary Cohorts

One of the key functional readouts in ANCA- and LPS-stimulated monocytes was cytokine production (see Section 2.3), namely of IL-1β, IL-6, and TNF-α. All three cytokines were significantly increased in LPS-stimulated monocytes in both the Primary and Secondary cohorts (Figure 5.3.21). Anti-MPO stimulation also increased cytokine levels, though the effects were only significant in the Secondary cohort. Only TNF-α was significantly increased in anti-PR3 treated monocytes, and only in the Secondary cohort. CXCL10 was also measured but was not detectable in any of the treatment groups/cohorts (data not shown). Additionally, there were no differences in LDH release – a surrogate marker for cell death – from stimulated cells compared to unstimulated (data not shown). Considering both cohorts, we can conclude that LPS and anti-MPO increase cytokine production in primary monocytes, without affecting cell viability.

There was a notable difference in TNF-α levels detected between the Primary and Secondary cohorts (Figure 5.3.21C). The Primary cohort (open shapes) had substantially lower TNF-α production than the Secondary cohort (closed shaped). This phenomenon is particularly evident in LPS-stimulated cells. Furthermore, the Secondary cohort had significantly higher protein levels in the metabolite fraction than the Primary cohort (Figure 5.3.21D). There were no significant differences in protein levels between treatment groups in either cohort, but inter-batch differences in protein levels accounted for 88.16% of total variation. PooledQC values for the respective cohorts are highlighted in purple. These results confirm that metabolomic profiling data from two cohorts should be considered as separate experiments.

We examined the relationship of cytokine production and intracellular metabolite concentrations in the targeted analysis of the Secondary cohort. While a number of metabolites did appear to have a significant correlation with cytokine production, these associations were very minor. All Pearson $R^2$ values were below 0.2 (data not shown). Furthermore, the majority of these significant correlations were driven by high pro-inflammatory cytokine production in the LPS-activated cells. From these data we can conclude that these specific metabolites likely do not drive pro-inflammatory cytokine production in ANCA-stimulated cells.

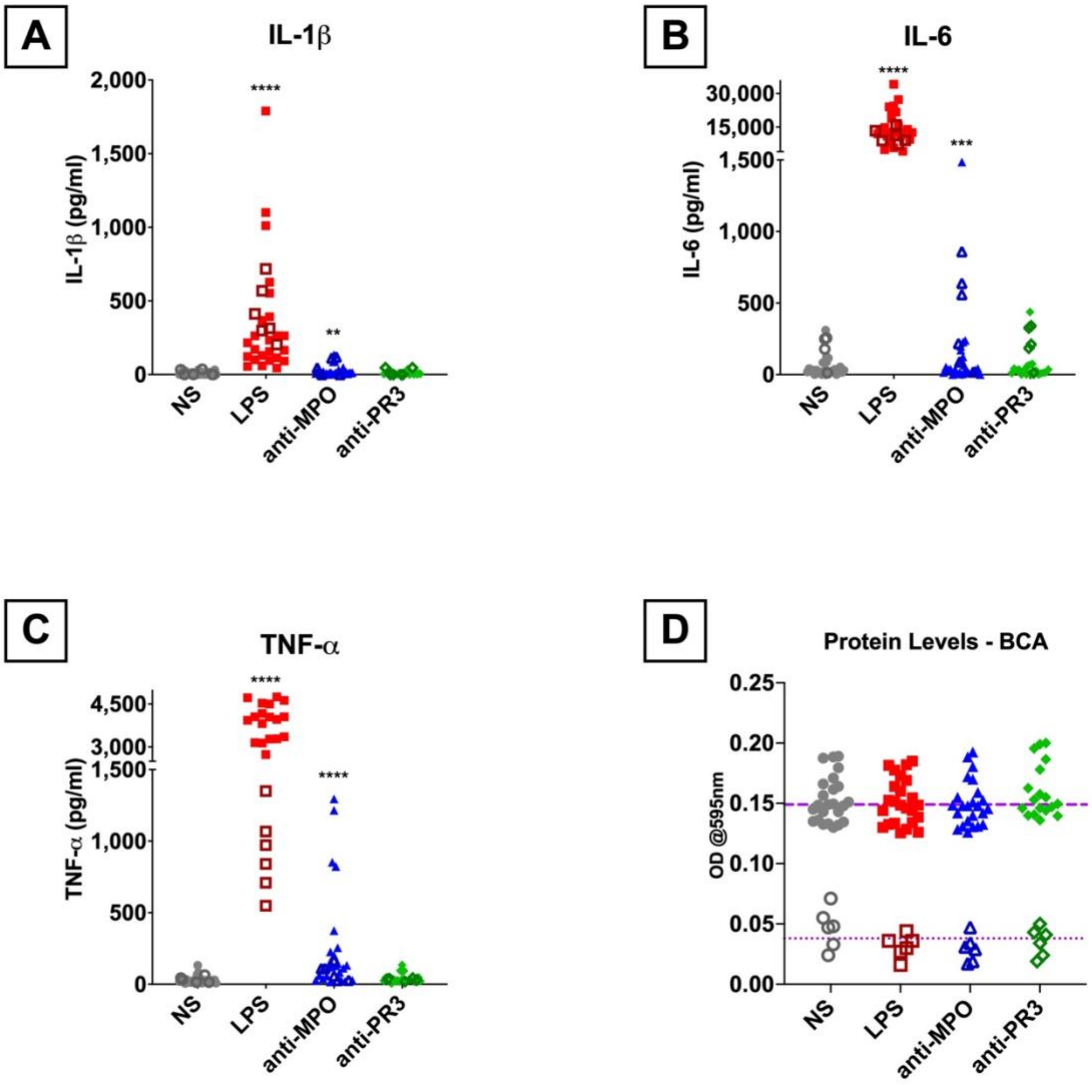


**Figure 5.3.21: Comparison of Cytokine Production and Protein Levels Across Metabolomic Profiling Experiments.** CD14+ monocytes were isolated from the PBMCs of healthy controls by MACS separation. Cells were plated and stimulated for 4 hours with 200ng/ml LPS, 5µg/ml monoclonal anti-MPO, or 5µg/ml monoclonal anti-PR3. Supernatants were removed and levels of IL-1β (A), IL-6 (B), and TNF-α (C) measured by ELISA. Results were analysed by Friedman's ANOVA and data are presented as the mean with standard error of the mean (SEM) (n=30). Primary profiling replicates (n=6) are open shapes and Secondary cohort samples (n=24) are filled. Following metabolite extraction residual protein levels in the metabolite fraction (MF) were measured by Pierce™ BCA Assay and reported as OD values at 595nm (D). PooledQC protein levels are marked with a dotted and dashed line for the primary and Secondary cohorts, respectively.

### 5.3.14 Monocyte MPO Surface Expression Reflects Intracellular Metabolite Concentrations.

Previously we have shown a relationship between the percentage of MPO+CD14+ monocytes and subsequent IL-1β production upon ANCA stimulation (Figure 3.3.14). In the Secondary metabolomic profiling cohort we revealed that there are three distinct groups of isolated monocytes which could be distinguished by the level of MPO expression (Figure 3.3.12B). We next determined if the degree of MPO expression was linked to intracellular metabolite concentration. Using the significantly altered metabolites identified in the targeted analysis of the Secondary cohort (see Figure 5.3.14), we found several significant relationships with MPO expression. These relationships were strongest for isoleucine (Figure 5.3.22D), leucine (Figure 5.3.22E), and phenylalanine (Figure 5.3.22G). This finding suggests that as well as being influenced the different treatments, some metabolite levels are also influenced by the degree of MPO surface expression. This finding should be further investigated and validated in AAV patients.

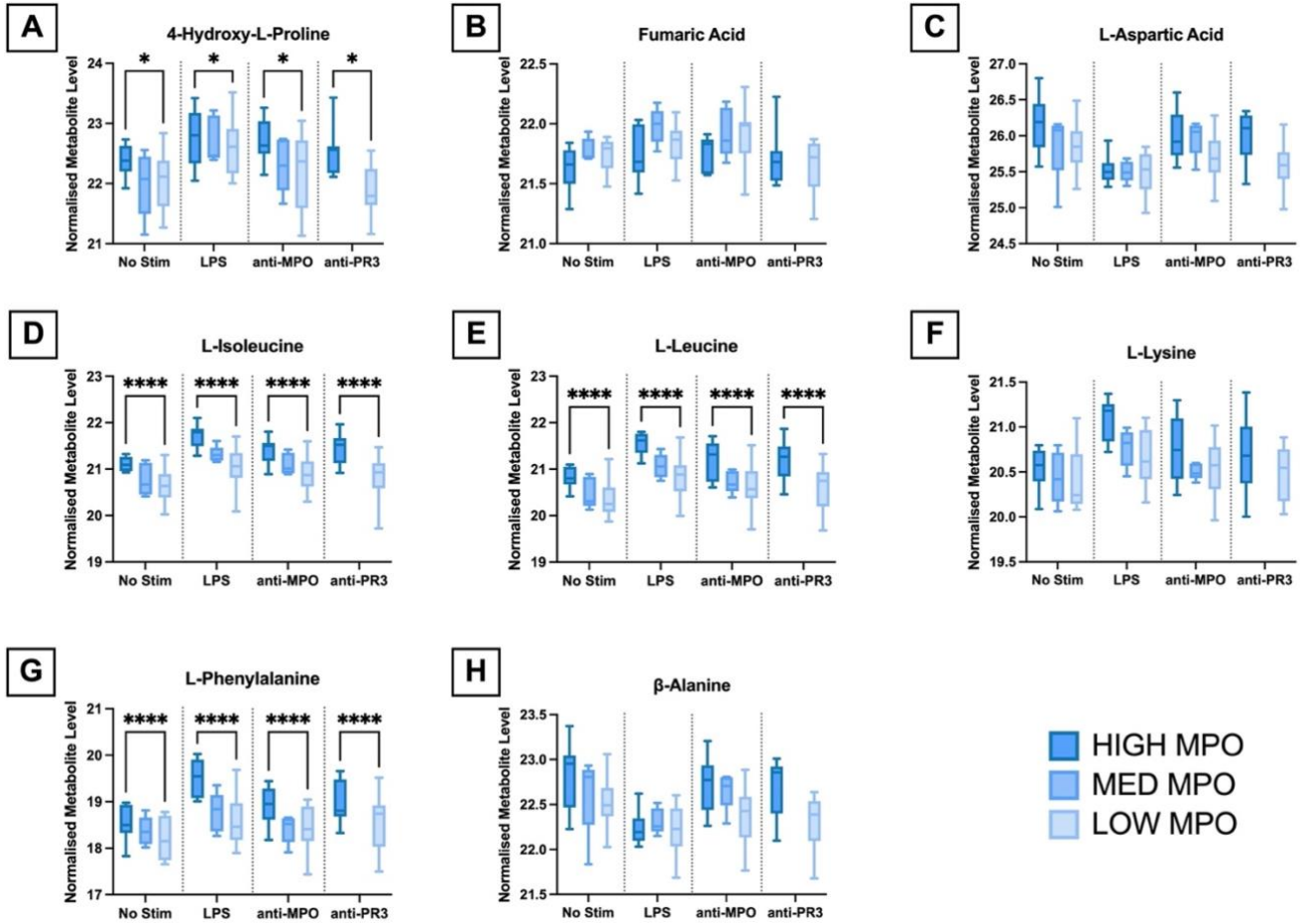


**Figure 5.3.22: Relationship of MPO Surface Expression and Intracellular Metabolite Levels in Stimulated Monocytes.** CD14+ monocytes were isolated from PBMCs of healthy controls by MACS separation (n=24). MPO expression was measured immediately after isolation by flow cytometry. Cells were plated and stimulated @37°C for 4 hours with 5µg/ml monoclonal antibody (mAb) directed against MPO, PR3, or 200ng/ml LPS. ANCA- and LPS-stimulated monocytes were analysed by LC-MS and targeted metabolomic analysis of 53 metabolites was completed. Monocytes were classified as “HIGH”, “MEDIUM”, or “LOW” based on their MPO surface expression and grouped accordingly separated further by treatment group. Intergroup comparisons were measured by2-way ANOVA with a Tukey adjustment for multiple comparisons.

## 5.4 Discussion

### 5.4.1 Combining Results from both Metabolomic Profiling Experiments

Here we have profiled the early metabolomic response of primary monocytes to LPS and ANCA stimulation using optimised LC-MS sample preparation protocols and analysis workflows (see Chapter 4). Metabolomic analyses were carried out in a Primary pilot cohort (n=6) and a larger Secondary cohort (n=24). Due to logistical issues, there were only 18 anti-PR3 replicates compared to 24 for other treatments. This may have impacted the statistical relevance of these cells as there were fewer degrees of freedom. As well as providing an initial insight into ANCA-induced changes in monocyte metabolism, the Primary analysis was used to conduct a power analysis to confirm required samples sizes (Figure 5.3.7). Studies carried out in mammalian cell lines typically use a very low number of replicates (n=3-15, [58]) as conditions can be tightly controlled throughout the experiment. The added complexity of primary human cells [47, 73-75] means a higher number of biological replicates are required to achieve consistent, reproducible results. Our power analyses determined this number was 24, and this was achieved in our subsequent validation experiment. This analysis also confirmed that measuring residual protein content in the metabolite fraction reduces the required number of biological replicates by controlling for technical and interpersonal variation.

Despite our best optimisation efforts LC–MS-based metabolomics assays will always be susceptible to signal and sensitivity variations [381]. There was a 12-month interval between LC-MS analysis of the Primary and Secondary cohorts. The use of a consistent synthetic standard mixture between both cohorts was intended to assess (and potentially correct for) inter-batch variance. The numbers of detectable metabolites in this synthetic standard mixture were consistent between both cohorts, with only minor differences in RTs and %CVs, and with the negative ionisation mode slightly outperforming the positive (Figure 5.3.8). The use of PooledQC samples is another effective strategy for monitoring and correcting within-batch effects. Both the Primary and Secondary cohorts contained all 4 treatment groups for all biological replicates (n=24 and n=90 samples, respectively). The metabolomic differences between these PooledQCs – though derived from identical experimental systems – were too great to disregard (Figure 5.3.9). Regrettably these inconsistencies could not be rectified by baselining, data

transformation or LOESS correction. Further issues with the ESI+ meant that these data were excluded from analysis in the Secondary cohort (Figure 5.3.10), adding to the discordance between these experimental groups. Advanced batch correction algorithms can be used in some instances to account for instrument variation [99-101, 106], however, further differences in cytokine production were evident between our cohorts (Figure 5.3.21). For these reasons the metabolomic profiling data from each cohort was analysed independently. Until appropriate validation experiments can be conceived and completed, we will consider the results from both cohorts as standalone works.

Results of metabolomic profiling of the Primary cohort are reported for metabolites detected in both positive and negative ionisation modes. However, all significantly altered metabolites detected in the untargeted analysis of this sample set were features detected in the negative ionisation mode (Figure 5.3.4). Additional technical variation in the Secondary cohorts ESI+ LC-MS run caused significant variation in the later PooledQC samples (Figure 5.3.10). More metabolites were detected by ESI- and with lower %CVs in PooledQC samples. Nicotinamide adenine dinucleotide (NAD) and trimethylamine n-oxide (TMAO) not detected in the negative ionisation mode but did not show any significant differences between treatment groups in ESI+ (Figure 5.3.11). The isomers 1- and 3-methyl-L-histidine were only effectively separated in positive mode, and significantly less 3-methyl-L-histidine was detected compared to 1-methyl-L-histidine. Only 3-methyl-L-histidine is formed endogenously in humans, and 1-methyl-L-histidine is often used as a marker of meat intake [382]. Given the consistency of the ESI- run, only metabolites and features detected by this method are considered in the analysis of the Secondary profiling cohort.

### 5.4.2 Results of Targeted Metabolomic Analyses

All LC-MS methods developed/referenced in this work are untargeted. This method is used for biomarker discovery and hypothesis generation and allows relative quantitation by comparing metabolite differences from one group to another. Previous investigations of AAV metabolism had identified potential metabolite biomarkers [238, 261]. These findings were used to develop a synthetic standard mixture of metabolites of interest we were hoping to reliably identify in our analysis (see Section 2.9.2.2). As such we have adopted a targeted approach to our data

analysis by prioritising the specific metabolites in this mixture. Because these metabolites are measured with known RTs derived from synthetic standards, the IDs are stronger than features annotated in the untargeted analysis, which can only be considered tentative IDs [25].

Targeted analysis of the Primary cohort identified α-ketoglutarate (aKG), ethanolamine, and histidine were all significantly increased in stimulated cells. However, none of these metabolites were found to be significantly altered in the Secondary cohort (Figure 5.3.14). Here a total of eleven metabolites were significantly altered (see Table 5.3.2), most of which were amino acids. Both fumarate and aKG are TCA cycle metabolites which were enriched by anti-MPO (and LPS) stimulation. These metabolites have been reported to play a role in innate immune training in monocyte-lineage cells [20]. Glutaminolysis – the breakdown of glutamine into TCA cycle intermediates – facilitates epigenetic changes in trained cells. This increased aKG and fumarate can enhance pro-inflammatory cytokine production in monocytes and macrophages [20, 299]. The aKG/succinate ratio is important for macrophage polarisation: a high ratio promotes M2 differentiation, and a low ratio strengthens the pro-inflammatory M1 phenotype [22]. This ratio can also control gene expression in murine embryonic stem cells [383]. Although we did not note any significant differences in the aKG/succinate ratio between treatment groups, the LPS-treated cells had a slightly higher ratio and the anti-MPO group were slightly lower than unstimulated cells (data not shown). These findings suggest a link between aKG levels and pro-inflammatory cytokine expression in ANCA-activated cells, one which demands further investigation.

Leucine and isoleucine levels were significantly increased in ACNA-activated cells in the Secondary cohort (Figure 5.3.14). These isomers (along with valine) are branched chained amino acids (BCAAs). BCAAs are used as fuel sources to support the rapid proliferation and activation of immune cells [384]. In particular, leucine has been reported to regulate innate and adaptive immune responses and drive inflammation via mTOR [384]. Levels of both isomers also appeared to be linked to surface MPO expression (Figure 5.3.22). In contrast, Zhang *et al.* found substantial decreases in leucine and isoleucine in THP-1 cells which persisted into the resolving stage of inflammation [96]. This has been attributed to a systemic immunoparalysis

affecting cellular metabolism in acute sepsis [385]. Whether these metabolites have specific role in ANCA-induce inflammation or are fuelling standard cellular functions remains to be determined.

The ANCA-induced alterations in 4-hydroxy-L-proline and serine found at 24h (Figure 3.3.7) were also seen at 4h in the Secondary cohort. Serine and phenylalanine were also tightly correlated with increases in ECAR (Figure 3.3.8), suggesting that glycolysis fuels the accumulation in these amino acids. Increased amino acid metabolism is essential for protein synthesis following immune cell activation. Amino acids have more recently been recognised for their roles in supporting cellular and organismal function via ATP generation, nucleotide synthesis, maintenance of redox balance and cellular communication [386, 387]. Metabolic requirements for immune cell subtypes vary based on their functions. To support metabolic reprogramming, immune cells utilise a range of amino acid receptors to selectively meet their energy demands [388]. In particular, SLC7A5 (the light chain of CD98) is particularly relevant in primary monocytes. Leucine influx via SLC7A5 contributes to metabolic reprogramming and IL-1β production [389]. This marker is also upregulated on monocytes of RA patients where it correlated with disease severity markers. The increase in amino acid anabolism seen in ANCA-stimulated monocytes may also be mediated via SLC7A5. Targeting amino acid transport has been suggested as a novel therapy for autoimmune diseases [390]. Future studies should investigate metabolic markers on immune cell subtypes in AAV patients to confirm if it is a viable treatment target.

### 5.4.3 Results of Untargeted Metabolomic Analyses

In the untargeted analysis similar feature numbers were detected in the Primary (n=1,515 ESI- only after blank removal) and Secondary cohorts (n=1,380). These features were assigned tentative IDs by matching parent ion exact mass and isotopic patterns with the Agilent METLIN Metabolomics Database and Library [25, 68]. Of the significantly altered metabolites that were assigned metabolite IDs, many of these were lipids and lipid-like molecules (Figures 5.3.5 & 5.3.19). This was without optimising the LC-MS method or sample preparation procedure for detecting lipid species and speaks to the strength of HILIC chromatography. Many of these compounds eluted in the void volume, and the mean/median RT of the compounds displayed in Figure 5.3.5 was 1.63/0.99mins. However, without further

fragmentation of these lipid entities they cannot be fully annotated. Developing targeted assays for these purposes – while feasible – is currently beyond the scope of this work. More polar lipids such as phospholipids (PE, PG, PC), lyso-PC and DG can be detected by HILIC chromatography [345]. Indeed, the synthetic standard ethanolamine was detected in ESI+ at 3.12 and 3.21 mins in the primary and secondary PooledQC samples, and was significantly upregulated by MPO-stimulation in the former (Figure 5.3.11). Our optimised methanol extraction protocol would also be suitable for analysis using a C18 column and the appropriate mobile phases, which may allow detection of additional lipid species. In subsequent experiments we will seek to verify the contributions of these metabolites to ANCA-induced inflammation.

Despite these uncertainties, lipid metabolism has been established as an immunomodulatory process in monocytes. The most significantly altered metabolite in the untargeted analysis of the Primary cohort was annotated as palmitic (hexadecenoic) acid and was increased in both anti-MPO- and anti-PR3-stimulated cells (Figure 5.3.6). Palmitic acid is the most common saturated fatty acid in the human body, accounting for 20–30% of total fatty acids in membrane phospholipids and adipose triacylglycerols [391]. Palmitate is a 16-carbon saturated fatty acid produced via the fatty acid synthesis pathway and is the precursor to many other longer fatty acids [391, 392]. Increased synthesis by ANCA activation (Figure 5.3.6) at this early timepoint may precede production of additional fatty acids species with greater functional relevance. Indeed, additional fatty acid metabolites were implicated in the untargeted analysis of the Primary cohort, including 10-methyl-hexadecanoic acid and (+)-isostearic acid (Figure 5.3.6). These metabolites (and others from closely related pathways [393]) have direct functional relevance to monocytes. Palmitate can promote atherogenesis, increase pro-inflammatory cytokine production, and enhance monocyte migration and endothelial binding [394-396]. It can modulate innate immunity via regulation of PRR activation to coordinate activity of infiltrating cells at sites of inflammation [397]. Metabolic memory by palmitate overload can induce insulin sensitivity, inducing further metabolic (and inflammatory) dysfunction [398]. In a similar vein, cholesterol synthesis – in particular mevalonate production – is also essential for innate immune memory in monocytes [20, 21].

Time (and dose) dependent effects of LPS stimulation on cytokine production, OCR, glycolysis, and fatty acid metabolism have been reported [97]. Enrichment of a similar variety of lipid species seen in our metabolomic profiling cohorts has been reported in LPS-activated primary monocytes [97, 302]. Lipid droplets also accumulate over time in LPS-activated cells and are used as a measure of (phospho-) lipid synthesis [85]. Macrophages enhance fatty acid uptake into lipid droplets after LPS stimulation, while simultaneously decreasing lipolysis and fatty acid oxidation [399], however these lipid droplets were primarily triacylglycerols (TAG), a lipid species much better detected by ESI+ [400]. α-linoleic acid was another lipid annotation identified in the Primary untargeted analysis. This is an essential omega-3 polyunsaturated fatty acid (PUFA) and was significantly upregulated in anti-MPO activated cells ($p=0.0110$) with a trend toward increase ($p=0.0663$) with anti-PR3 stimulation. PUFAs were also increased after LPS stimulation of THP-1 monocytes [96]. PUFAs can feed into any number of diverse metabolic pathways, and further work is needed to correctly classify them and determine their role in AAV.

Lipid metabolism has been implicated in monocyte dysfunction in other conditions as well. Fatty acid oxidation was essential for CCL20 production in RA monocytes [86], and dysregulation of monocyte subsets in human obesity has been correlated with lipid metabolism [401]. Most recently SARS-CoV-2 exposure promoted lipid droplet accumulation and upregulation of lipid metabolism targets in monocytes, which promoted production of pro-inflammatory cytokines, viral replication, and cell death [402]. Immune dysregulation in aging is characterized by persistent inflammatory responses; termed inflammaging. Aged monocytes have dysfunctional TLR signalling, cytokine production, and surface receptor expression [403-405]. Lipid metabolism has been suggested as a pathogenic contributor to inflammaging in monocytes. Plasma fatty acid levels increase with age and correlate with blood cytokine levels [394]. Saturated fatty acids primed monocytes to induce higher cytokine response to LPS stimulation, and controlled macrophage polarization. These effects were mediated in part by peroxisome proliferator-activated receptor γ (PPAR-γ) [394]. PPAR-γ activation reduced cytokine production in monocytes [406] and expression was decreased by LPS stimulation [97]. The

effect of this transcription factor in ANCA-induced inflammation should be a focus of future work.

Previous work from our group validated urinary *myo*-inositol as a urinary biomarker of AAV relapse [261]. This metabolite was included in the synthetic standard mix for this reason but was also picked up in the untargeted analysis with several metabolic precursors. Lower levels of bi- and mono-phospho-*myo*-inositol were detected than *myo*-inositol, indicating an accumulation of *myo*-inositol upon ANCA-stimulation. While *myo*-inositol levels were not significantly different between treatment groups, inositol phosphate metabolism and phosphatidylinositol signalling among the most significantly enriched pathways in the pathway analysis (Figure 5.3.20), and bi- and mono-phospho-*myo*-inositol had high-ranking VIP scores in the PLS-DA class prediction analysis (Figure 5.3.18). This was particularly relevant for anti-MPO activated cells. Indeed, when the anti-MPO and anti-PR3 treatment groups were compared by volcano plot analysis, D-*myo*-Inositol 1,3-diphosphate and 1-(sn-Glycero-3-phospho)-1D-*myo*-inositol were among the 79 differentiating metabolites IDs with scores of 80.15 and 96.58, respectively (data not shown). On a cellular level, phosphatidylinositol species acutely generated by activated macrophages regulate innate immune responses [407]. ANCA treatment reduced inositol signalling in neutrophils but increased it in endothelial cells [408, 409]. There are a number of different metabolic pathways that can drive *myo*-inositol accumulation (Figure 5.4.1). *Myo*-inositol can also be obtained from dietary sources, where it can affect monocyte differentiation in the gut [202]. The various mechanisms of *myo*-inositol production should be targeted to assess the effects of their metabolic manipulation on cytokine production.

Class prediction analyses were also carried out in the Secondary cohort to determine the optimal metabolic discriminators of cellular activation (Table 5.3.3). Among the top ranked metabolites were succinic aldehyde, itaconic acid, glyerophosphoinositol, PI(40:7), and tromethamine. The precise identities of the latter three could be disputed, however the relationship of succinate and itaconate in LPS-mediated macrophage immunometabolism has been well established. Succinic (semi-)aldhehyde is a precursor of succinate, and itaconate is formed from aconitate in the TCA cycle. Secondary to their roles in energy generation these

metabolites are important for pro- and anti-inflammatory responses in macrophages [321]. Itaconate was first recognised as an anti-microbial metabolite, but has recently been shown to decrease production of proinflammatory mediators in LPS-treated macrophages via Nrf2 [365, 410, 411]. Itaconate was highly increased in LPS-treated cells after 4h stimulation, consistent with other published data at 24h (Figure 5.3.19)[97, 302]. No differences were noted in either MPO- or PR3-ANCA-activated monocytes. Succinate alone does not appear to be important for inflammatory or metabolic response in ANCA-activated monocytes, but its relationship to other metabolites is intriguing, and deserves further study.

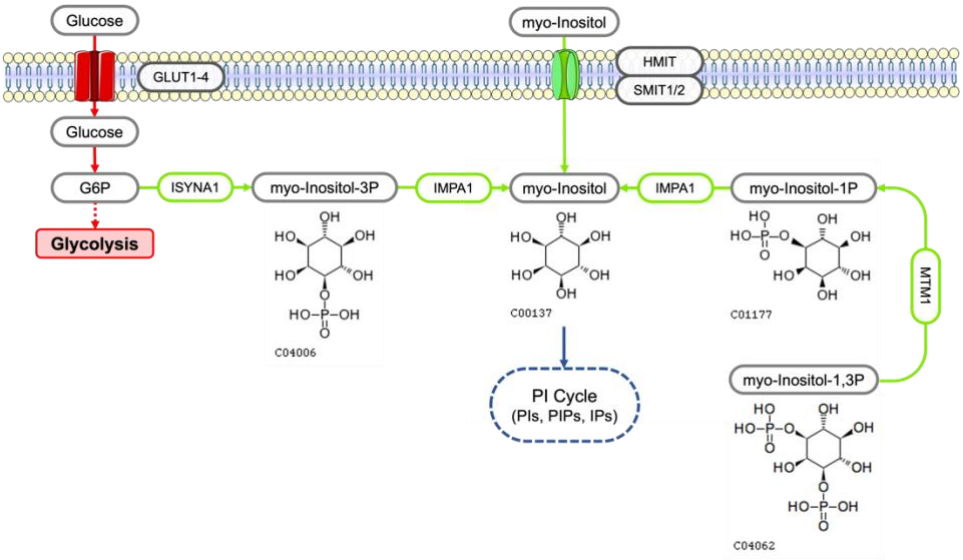


**Figure 5.4.1: Different Routes of *myo*-Inositol Production and Import in Human Cells.** *Myo*-inositol can be produced directly from glycolysis, by dephosphorylation reactions, or imported directly into the cell. G6P: Glucose 6-Phosphate; ISYNA1: *myo*-inositol 1-phosphate synthase; IMPA1: myo-inositol 1(or 3)-monophosphatase; MTM1: myotubularin; PI Cycle: Phosphoinositol Cycle

### 5.4.4 Functional Readouts – Cytokines & MPO Expression

Despite differences between metabolomic profiling cohorts, we confirm that anti-MPO stimulation increases pro-inflammatory cytokine production in primary monocytes. The intermediate monocyte subset are the primary producers of pro-inflammatory cytokines in response to anti-MPO, but do not react to anti-PR3 [203]. Our analysis did not find any significant correlation with intracellular metabolite levels and cytokine production. Where links between metabolic activity and cytokine production have been reported these studies have used specific metabolic inhibitors to uncover these relationships [97, 124, 302]. Future validation experiments should measure cytokine production as a primary functional readout for ANCA-activated

cells. Additional flow cytometry experiments were carried out in the Secondary profiling cohort to assess surface MPO expression (see Figure 5.2.1 and 3.3.12B). We have reported that intracellular levels of certain metabolites are linked to MPO surface expression (Figure 5.3.22). This novel finding is the first functional link between metabolite levels and AAV physiology reported in primary monocytes. Our experiments were carried out in monocytes isolated by CD14+ isolation. This would predominantly preserve the classical monocyte subset above all others. Given the differing functions of the monocyte subsets, differences in energy utilisation are to be expected. Indeed, metabolic distinctions between monocyte subsets have been reported, with classical monocytes favouring glycolysis and intermediate/non-classical opting for oxidative mitochondrial energy production [412]. The intermediate subset also expresses more surface MPO than classical and non-classical monocytes [203]. Further validation experiments should attempt to tease out the role of these specific cells in ANCA-induced inflammation.

The monocyte response to LPS stimulation is well established, albeit at the later timepoint of 24h. Similar to their macrophage counterparts, monocytes activated by LPS adopt Warburg metabolism and favour glycolysis for their energy production [97]. ANCA-activated monocytes (particularly anti-MPO) increase both glycolysis (ECAR) and OXPHOS (OCR), a phenomenon usually reserved for stimulation with complex whole micro-organisms [97, 124, 302]. At earlier timepoints broad decreases in metabolite levels after LPS-stimulation have been reported [85, 96]. Here we have identified novel early metabolic changes in LPS-activated cells, with a more profound (and expected) inflammatory response to LPS stimulation in our Secondary profiling cohort (Figure 5.3.21). This was accompanied by decreases in metabolites such as aspartic acid (confirmed by Raulien *et al.* [85]) and β-alanine (Figure 5.3.14). As with the alanine/sarcosine isomers, leucine and isoleucine were previously distinguished by running separate, individual synthetic standards for both isomers using the optimised LC-MS method, confirming that leucine eluted at the earlier timepoint. These early changes in the monocyte metabolome that precede inflammatory reactions highlight the metabolic flexibility of these cells. Additional metabolomic investigations at this early timepoint will be necessary to confirm these findings.

# Chapter 6: Discussion

## 6.1 Optimised LC-MS Methods for Metabolomic Analysis of Primary Immune Cells

In this work we have described an optimised LC-MS workflow for analysis of primary immune cells using healthy monocytes. Standardized protocols for primary cell metabolite and lipid extraction for LC-MS analysis do not currently exist in the literature [59]. There have been limited reports of cellular metabolomic investigations in primary cells, and even fewer in monocytes. Those who have explored the monocyte metabolome have not sufficiently detailed their sample preparation and LC-MS analysis methods. In some cases these investigations have been outsourced to collaborators or commercial entities (see Section 1.2) who may not necessarily optimise for the sample material or application at hand. This presented an opportunity for us to define optimum LC-MS conditions for metabolomic profiling of primary monocytes. Many cellular metabolomics optimisations have been carried out in mammalian cell lines [58, 59, 61, 62], which are metabolically distinct from primary human cells [413]. Furthermore, many of these cell lines are cancer-derived and have distinct metabolic requirements from healthy cells. Our methods were optimised in non-adherent primary immune cells, and with minor modifications can be valid and adaptable to other cell types. This LC-MS method used here has been applied to other primary cells and cell lines [364, 414].

Neutrophils have an established role in AAV pathogenesis, but immunometabolic investigations in these cells to date have been limited. Metabolic reprograming in these cells is only beginning to be recognised to impact their function [415-417]. Similarly, B cells are the source of ANCA and their unique metabolism links closely to their diverse functions. Like neutrophils they contain very few mitochondria, and activated B cells have increased glucose uptake and glycolysis [315, 418] which feed into the ribonucleotide biosynthesis pathway to support sustained production of antibodies [419]. Autoreactive B cells have prolonged and sustained energy demands which can deplete ATP and cause cell stress, worsening autoimmune diseases [418, 420]. T cells on the other hand have long been recognised as metabolically distinct subtypes [421-423], and are attractive targets for metabolic therapies in autoimmune disease [424, 425]. Disruption of T cell subsets and their respective cytokine profiles have been reported in AAV [185], with persistent Th cell activation (particularly Th17) and impaired suppressive functioning of regulatory T

cells (Tregs). The metabolism of these (and other) immune cells and how it relates to their function in AAV pathogenesis should be a focus of future investigations, and should incorporate the optimised protocols described in this work. Further, how they link to systemic metabolic changes and clinical characteristics should be explored [260]. We would encourage collaborators and research groups to employ the optimised sample preparation protocols developed here to other cell (and sample) types in AAV.

Given that our sample preparation methods have been optimised for polar metabolite detection, it is intriguing that several of the significantly altered metabolites in ANCA-stimulated monocytes were lipid species (Figures 5.3.6 & 5.3.19). The benefit of this optimisation protocol is that the non-polar, lipid fraction is preserved and can be extracted from the lysate for further analysis [426, 427]. This will improve metabolome coverage allow further characterisation of additional lipid species too hydrophobic to be detected by HILIC. DNA, RNA, and certain proteins may also be maintained for further analyses [295, 296]. These materials can be analysed to validate the findings of this work and potentially uncover new biomarkers for further investigation.

## 6.2 Attempting to Combine Metabolomic and Functional Readouts

Advancements in LC-MS technologies have expanded its capabilities beyond traditional untargeted metabolomic profiling [428]. MS imaging and single cell metabolomics have further advanced the capabilities of LC-MS for metabolomic profiling [429-432]. However, these methods require their own protocol optimisation. LC-MS metabolomics measures the direct output of metabolism – i.e. metabolites – but the strength of this method increases exponentially when combined with additional functional readouts [26]. The utility of these advanced MS methods as a compliment to the metabolomic profiling described here could be explored in future investigations.

Some researchers suggest using whole blood exclusively to prevent sample preparation- related variation in immunologic investigations [339]. A newly developed flow cytometry assay monitors rapid changes in protein translation upon using various inhibitors to allow complex metabolic profiling even with low cell

numbers [433]. This can be useful for revealing metabolic capacities and dependencies in diverse populations but cannot give more detailed info about specific metabolites that LC-MS provides. Methods have advanced to be able to profile the metabolome in low cell numbers [352], but isolation is still required to measure the specific metabolic phenotype of the cells of interest. We have seen in our work that the process of cell isolation appears to affect cell surface markers on monocytes (see Section 3.4.2). Cytokine production is also sensitive to the effects of monocytes isolation [434]. Here we have prioritised cytokine production as the key functional readout in parallel experiments using IL-1β as our key measure of monocyte activation. It is possible that the process of monocyte isolation primes the cells to respond to anti-MPO alone. However, monocytes are unique in that they can produce IL-1β without a priming stimulus in response to LPS [121, 435]. The phenotypic modification of cells during isolation seems to be unavoidable. Even sorting cells by flow cytometry can alter their metabolome [293]. These concerns cannot be addressed in the current work, but should be taken into consideration when planning future experiments.

Many researchers' first foray into immunometabolism involves extracellular flux analysis using the Seahorse [300]. Indeed our preliminary work found both glycolysis and OXPHOS to be increased by ANCA stimulation, particularly anti-MPO [238]. This is an excellent litmus test for investigating the baseline metabolic wiring of cellular metabolism, but cannot give more detailed info about the metabolic pathways being fed from the major nodes of glycolysis and OXPHOS [26]. Our attempts to utilise cells stimulated in a Seahorse analyser for subsequent metabolomic profiling were unsuccessful (see Section 3.3.10). However, parallel analysis of Seahorse results with LC-MS profiling did yield some interesting findings. A number of amino acids correlated with increased rates of glycolysis (Figure 3.3.8), suggesting their anabolism is fuelled by the breakdown of glucose. Seahorse analysis has been used to confirm the shift to Warburg metabolism in LPS-activated primary monocytes. These studies have also investigated phagocytosis, transcriptomics/qPCR, cell migration, ROS production, and surface marker expression [85, 86, 97, 124, 302] in parallel experiments distinct from the primary metabolomic profiling.

Contrary to Warburg metabolism, primary monocytes increase rates of both OXPHOS and glycolysis upon ANCA stimulation [238]. As such the metabolic changes in these cells may not be entirely applicable to their macrophage counterparts. Indeed, the activation of both glycolysis in OXPHOS seen with LPS and anti-MPO stimulation is more similar to activated T cells than either M1 or M2 macrophages [14, 436]. Future works should further investigate the monocyte-T cell crosstalk in the circulation and at disease sites. T cells have established and diverse metabolic requirements, which have not been elucidated in AAV. Inhibition of CD28 suppressed murine large-vessel vasculitis by disrupting T-cell metabolic fitness [246], and expansion of CD4+CD28- cells was recently reported in AAV patients [**Error! Hyperlink reference not valid.**]. Dekkema *et al.* [438] recently identified a range of differentially expressed miRNAs in Tregs of GPA patients, several of which have been shown to play a role in metabolism of these cells [439].

AAV monocytes increase T cell activation and proliferation [230]. These cells (and neutrophils) form the core of granulomas where they can orchestrate systemic T cell responses [187]. Activated monocytes preferentially induce infiltrating CD4+ T cells to produce IL-17 and promote Th17 differentiation [440]. These cells are subsequently rereleased into the circulation and are among the main pathogenic drivers in AAV [187, 441]. Within AAV granulomas T cells and monocytes/macrophages drive repeated destructive cycles of cell recruitment and activation [441]. Given their overlapping metabolic demands this creates a unique immune and metabolic microenvironment. The monocyte-T cell interaction in AAV should be a focus of future research, particularly the metabolic crosstalk and nutrient competition between these populations.

## 6.3 Cell Priming

A number of compounds are used in the ANCA literature to “prime” immune cells prior to stimulation. In neutrophils, pre-activation/priming activates the p38 and ERK Mitogen Activated Protein (MAP) kinase pathways, triggering MPO/PR3 translocation to the plasma membrane [212-217]. This allows external ANCA binding and subsequent cellular activation [173]. Given that ANCA titres do not necessarily correlate with disease severity [209], priming events which facilitate ANCA binding and cellular activation may be crucial for disease development.

Despite its routine use in neutrophils, TNF-α does not appear to be an appropriate priming factor for primary monocytes (Figures 3.3.4 & 3.3.5). IL-1β production was lower in monocytes primed with TNF-α even after subsequent ANCA stimulation. LPS was much more effective in inducing pro-inflammatory responses in these cells. Use of LPS as an ANCA-primer for monocytes has not been widely reported. Hattar *et al*. found co-stimulation of monocytes with ANCA and LPS increased IL-6, IL-8, and TNF-α production [226]. In cases of bacterial infection or disease [210, 211], systemic LPS could potentially trigger priming *in vivo* directly by PAMP stimulation, or via the resulting production of pro-inflammatory cytokines [173, 182, 184]. Animal models have used it at the time of ANCA-transfer to induce a more severe disease phenotype [442]. AAV patient monocytes also express more CD14, making them more susceptible to activation from bacterial antigens such as LPS [223] and potentially exacerbating ANCA flares. LPS also has established effects on monocyte metabolism, which may facilitate enhances pro-inflammatory activity by subsequent ANCA stimulation. Despite the synergistic effects of LPS and ANCA on monocytes activation, we opted not to use it as a priming agent in these works as the metabolic changes induced by LPS could mask/overtake and ANCA-specific effects.

We have previously proposed a role for priming in the metabolic activation of cells [186]. Both TNF-α and LPS can alter metabolic phenotypes of immune cells. Hypoxia-inducible factor (HIF)-1α is induced by TNF-α to promote expression of lactate dehydrogenase (LDH) and pyruvate dehydrogenase kinase (PDK) [315], supporting increased glycolysis in activated immune cells [316, 317]. TNF-α stimulation can alter glucose, lipid, and adipocytokine levels in arthritic murine joints [318], and is also crucial for insulin resistance development in obese mice [319]. Clinically relevant endotoxaemia triggers insulin resistance and cytokine release [443-445]. *In vitro* concentrations of LPS have differing effects on IL-1β production and cellular metabolism in monocytes [97]. It's unlikely that a single priming factor is responsible for cellular activation in ANCA, and a milieu of inflammatory and metabolic compounds are bound to contribute. The relationship between ANCA and priming agents does warrant further study though, and LPS priming alone should be incorporated as a control in future works.

### 6.3.1 Fatty Acids as Primers

Monocyte-lineage cells in RA and other autoimmune conditions adopt a "hypermetabolic" phenotype which drives inflammation [86, 147, 151, 422]. Specific lipid molecules may promote this primed phenotype at a cellular level. Oxidized phospholipids reprogrammed macrophages away from Warburg metabolism to simultaneously engage glycolysis and OXPHOS to enhance IL-1β production [446]. These molecules can function as TLR4 antagonists and are increased in the presence of MPO-ANCA [197]. The NLRP3 inflammasome can sense metabolites such as palmitate and cholesterol to drive IL-1β by macrophages [397]. A recent investigation of community-acquired pneumonia found that a majority of the immune tolerance phenotype in monocytes can be accounted for by coordinated shifts in cholesterol biosynthesis gene expression and its relationship to DNA methylation levels and cytokine production [447]. This suggests that dysfunctional lipid metabolism could create a pro-inflammatory environment for pre-clinical AAV.

Activated monocytes use the lipid chemoattractant sphingosine 1-phosphate (S1P) to coordinate T cell migration from lymph nodes [448]. S1P can promote disruption of endothelial barrier integrity in the presence of MPO-ANCA [449, 450], and systemic levels increase during active disease where they correlate with disease activity [451]. However, S1P was not identified in the untargeted analyses of our sample cohorts. Not all lipid species are pro-inflammatory, however. Some lipid mediators can suppress cytokine production in TNF-α primed macrophages [314]. As we cannot 100% confirm the identity of the lipid compounds identified in the untargeted analyses, we cannot validate their influence on ANCA-induced inflammation. It is possible however that a lipid-rich microenvironment primes monocytes to respond to ANCA.

## 6.4 Metabolomic Profiling

There were disparities in metabolites implicated in the Primary and Secondary cohorts. The primary cohort experiment is too underpowered to draw meaningful conclusions alone. Use of batch correction techniques may allow us to combine the results of these two cohorts in future analyses [99-101, 106]. Below we have discussed some of the metabolic alterations we have discovered in ANCA-activated monocytes, many of which have been shown to induce epigenetic changes in monocyte-derived cells.

### 6.4.1 Serine

Serine has been implicated multiple times in various analyses within this work. In two pilot experiments we found intracellular serine to be enriched by ANCA stimulation after 24 hours (Figure 3.3.7), and also to correlate with increased glycolysis measured by Seahorse at 4 hours (Figure 3.3.8). We hypothesised that the increased glycolysis was feeding serine synthesis via the *de novo* serine synthesis pathway (Figure 6.4.1). Serine can be produced by directly from glycolysis by converting 3-phosphoglycerate (3PG) to 3-phosphohydroxypyruvate (3PHP) via 3-phosphoglycerate dehydrogenase (PHGDH). Inhibiting this process temporarily limited IL-1β production in activated monocytes (Figure 3.3.9). Serine synthesis is essential for IL-1β (and TNF-α) production in murine macrophages [335], and this appears to be the case in human monocytes too. In cancer cells serine synthesis is essential to support proliferation via nucleotide synthesis and replenishment of the one-carbon pool [331-333]. Investigating the subsequent breakdown and utilisation of serine (perhaps by fluxomics) may be useful for determining its role in ANCA-induced inflammation. In macrophages the one-carbon pool facilitates epigenetic changes during M1 differentiation, fed in part by serine synthesis [387, 452]. Further confirming the compensatory mechanisms used by monocytes to overcome PHGDH inhibition – by increased serine import or synthesis via alternative pathways – may aid in this.

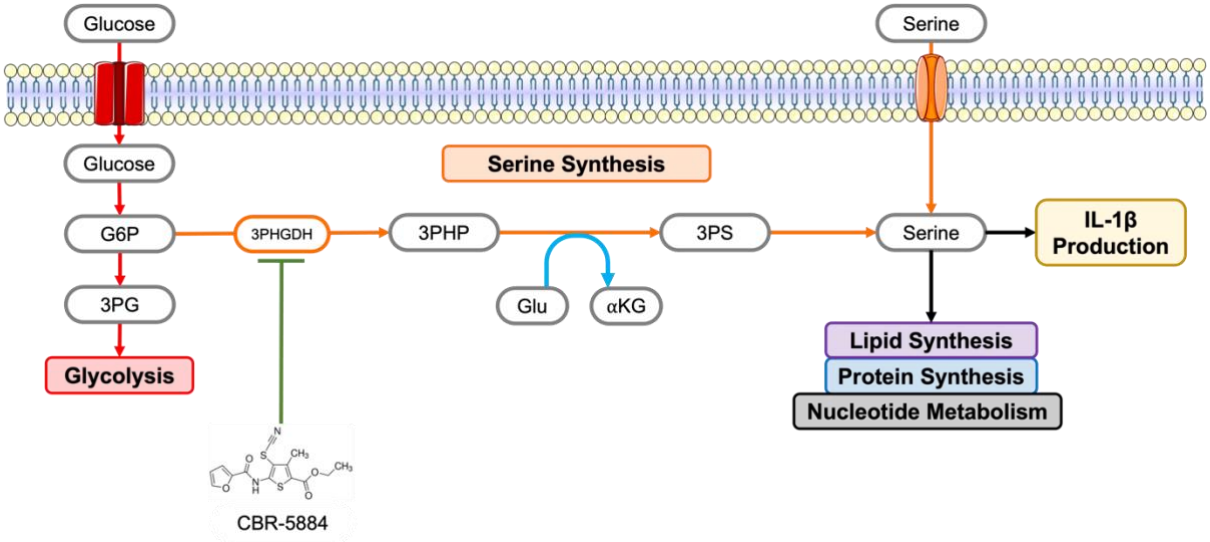


**Figure 6.4.1: Serine Synthesis via the *de novo* Synthesis Pathway.** Inhibition of 3-phosphoglycerate dehydrogenase (PHGDH) by CBR-5884 can limit short-term IL-1β production in activated monocytes.

### 6.4.2 *Myo*-inositol

*Myo*-inositol was previously identified as a urinary biomarker of AAV relapse [261]. Specifically, the *myo*-inositol:citrate ratio differentiated AAV from other kidney conditions and returned to normal levels following successful treatment. Monocyte-lineage cells are the most abundant infiltrates in early glomerular lesions [193], and this increase in *myo*-inositol metabolism in ANCA-activated monocytes may explain the increase urine levels in renal-disease. *Myo*-inositol can be synthesised *de novo* from glucose or directly imported into cells by a variety of transporters (HMIT [SLC2A13], SMIT1 [SLC5A3], or SMIT2 [SLC5A11])[453]. While not significantly altered in between treatment groups in the targeted analysis, precursor metabolites of *myo*-inositol (and other inositols) were identified in the untargeted analysis and were implicated in the pathway (Figure 5.3.20) and class prediction analyses (Figure 5.3.18). *Myo*-inositol metabolism appears to be involved in monocyte activation by anti-MPO.

### 6.4.3 Lipid Metabolism

The hypermetabolic phenotype described in RA [86, 147, 151, 422] can be influenced at the systemic level by nutrient exposure and availability. Cholesterol and other fatty acids are known to create a pro-inflammatory environment in atherosclerosis [454, 455], in part by increased FA uptake [155] promoting a pro-inflammatory phenotype. The systemic changes in fatty acid profile that accompany healthy ageing [394] may be driving systemic inflammation to prime circulating monocytes to react to ANCA. Increased PUFA and other lipid metabolites have been reported in AAV patients [258, 456], however one study found that serum lipid levels actually only increase during AAV remission [457]. This study also found this effect to be more pronounced in PR3+ AAV. Lipid lowering medications such as statins may provide anti-inflammatory effects and could be an easily integrated into AAV treatment protocols. Indeed statin use is associated with reduced relapse risk [273] and can inhibit respiratory burst in ANCA-stimulated neutrophils *in vitro* [216]. Further to its cholesterol-lowering effects, statin use can inhibit TLR4 signalling in LPS-activated monocytes to limit inflammation [156, 158], meaning its protective effects may be specifically relevant to monocytes. We did observe increases in several lipid species in ANCA stimulated cells (Figures 5.3.5, 5.3.6, & 5.3.19). The use of statins as part of the AAV treatment protocol has not been thoroughly

investigated but may improve patient outcomes by inhibiting pathogenic metabolism in inflammatory cells.

## 6.5 Future Work

This untargeted metabolomic profiling has been hypothesis-generating, and the metabolites implicated here must be further examined to confirm their roles in ANCA-induced inflammation. There are a number of ways to achieve this [19, 26] but given the availability of linked material we will first examine changes in gene expression by qPCR before examining the effects of various metabolic inhibitors on the ANCA response. We will specifically target metabolites significantly altered in the metabolomic profiling experiments (see Sections 5.4.2 & 5.4.3) and implicated in the pathway analysis (Figure 5.3.20). We will also complete more comprehensive inhibition experiments of using a broad spectrum of lipid metabolism inhibitors á la Chen *et al*. [458]. The optimised sample preparation protocol also preserves cell lysates for protein analysis by Western blot. Here we would target the master metabolic regulators – mTOR, AMPK, PPARγs, and sirtuins – to see how ANCA stimulation effects their activation at this early timepoint. Additional validation experiments using confocal microscopy to stain monocyte lipid droplets [402, 459, 460] would also aid in validating the role of lipid metabolism in these cells. Many of the implicated metabolites have established effects on epigenetic regulation. We would like to collaborate with other expert research groups to confirm these findings and would seek expert opinions on how to go about this.

An early LC-MS profiling experiment on monocyte supernatants extracted with 1:1 80% MeOH did not detect any changes in the exometabolome (data not shown). Despite not optimising our extraction protocols for spent media, these changes may have also been too subtle to detect at this early timepoint. Changes in nutrient transport may have begun to enrich intracellular concentrations of required metabolites. We have reported alterations in lipid, amino acid, and glucose metabolism in this work and will examine changes in corresponding nutrient transporters such as SLC7A5 (amino acid transport), ABCA1, CD36, GPR120 (lipid transport) SLC2A13, SLC5A3, and SLC5A11 (*myo*-inositol transport). We will first examine potential changes in expression patterns of these receptors, before validating our findings in a suitable patient cohort.

The effects of trained immunity by BCG include an increase in both glycolysis and OXPHOS – similar to that of ANCA. Innate immune training protocols occur over several days and track the monocyte lifecycle from circulation to macrophage differentiation. These experiments have similarities to our monocyte priming work (see Figure 3.3.5), albeit more long-term. Metabolic stimuli can strongly influence macrophage polarisation [14, 461-463]. Whether ANCA can further manipulate this polarisation and differentiation has not been fully investigated. Initial findings suggest MPO-ANCA increase monocyte survival and differentiation and have an altered inflammatory phenotype [197]. We would like to adopt innate immune training protocols to further investigate this phenomenon. The use of LPS as a priming agent should also be investigated in this context to confirm the metabolic effects involved in enhancing ANCA responses in these cells. The goal here is to determine if the hypermetabolic phenotype seen in other autoimmune conditions drives inflammation in AAV monocytes.

Another piece of this work which could not be expanded upon appropriately was the effect of MPO inhibition (see Figure 3.3.11). This approach has been validated as a potential therapy in a rodent AAV model [304]. MPO binds more rapidly to pathogenic MPO antibodies in the presence of hypochlorite acid, the main product of its catalytic reaction [337]. The MPO-catalyzing reaction also increases the antigenicity of MPO, indicating that the activity of MPO itself may drive inflammation in MPO-AAV. Additional metabolic effects of MPO enzyme activity may drive inflammation in AAV. The non-glycolytic acidification seen in ANCA-stimulated monocytes [238] may be driven by increased HOCl production by MPO. Macrophage exposure to MPO-derived HOSCN alters mitochondrial metabolism and increases cytokine production [464, 465]. The effects of MPO activity/inhibition on real time cellular metabolism can be easily measured by Seahorse. This would confirm if the non-glycolytic acidification observed is a result of increased MPO activity, or another compound as lactate [466] [467]. Further elucidating the role of MPO in inflammasome activation (see Figure 3.3.5) should also feature in these investigations.

The Rare Kidney Disease (RKD) biobank contains longitudinal biospecimens for over 800 Irish AAV patients. The availability of linked clinical data would allow us to

monitor patient relapse and further investigate the influence of statin on relapse seen in the Japanese cohort [273]. Serum samples are also obtained during routine clinic visits, and could be profiled to confirm the metabolic changes observed in active disease by Geetha *et al*. [260]. Given that monocytes are circulating cells their relationship with the systemic blood macroenvironment is an important source of nutrients which can change rapidly during disease/infection. Recent work combining cellular and serum metabolomics identified systemic amino acid deprivation as a mechanism of monocyte hypoactivation in a variant of psoriasis [468]. Improvements in sample workflows have allowed the routine collection of PBMCs by the RKD Biobank. This would facilitate the nutrient transporter study described above. This invaluable resource should be better utilised to profile the metabolic phenotype of systemic and cellular AAV.

The metabolic alterations in ANCA-stimulated monocytes are summarised in Figure 6.5.1. This untargeted metabolomic profiling has been hypothesis-generating. We hope that the data presented here will inspire other research groups to pursue these links of investigation through their own lens to confirm how metabolism affects ANCA-induced inflammation and disease pathogenesis.

## 6.6 Final Remarks

1. **Metabolomic analysis of immune cells requires careful consideration.** Sample preparation protocols, analysis pipelines, and parallel experimental readouts should all be optimised to appropriately address the experimental question. The methods described in this work are broadly applicable to other primary, non-adherent immune cells and should be used to profile cellular metabolism in AVV. We have also validated metabolite fraction BCA as a suitable and effective normalisation strategy for cellular metabolomics.
2. **Lipid metabolism links priming and ANCA responses in primary monocytes.** A lipid-rich environment creates a pro-inflammatory environment which acts as a primer for ANCA-induced metabolism. Limiting cholesterol metabolism with statins may mitigate monocyte activation and the subsequent inflammatory milieu.
3. **The inchoate metabolic response to ANCA in primary monocytes drives epigenetic modification.** Metabolites increased by ANCA stimulation such as fumarate, aKG, itaconate, serine and cholesterol, have been shown to influence innate immune cell activation and phenotype via chromatin modifications. The early increases in these metabolites are likely contributing to the inflammatory response by altering gene expression.

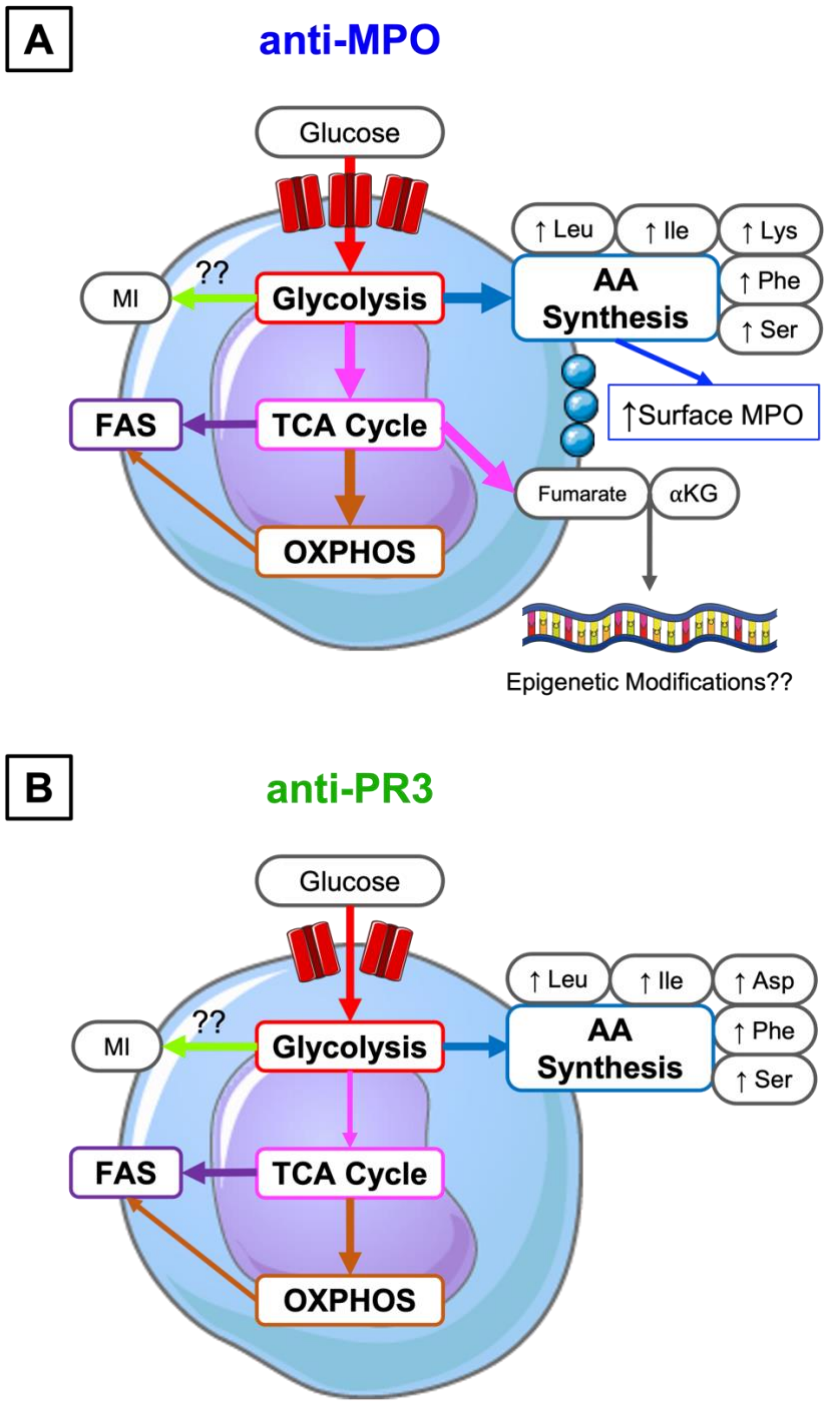


**Figure 6.5.1 Summary of Metabolomic Alterations in Primary Monocytes by anti-MPO (A) and anti-PR3 (B) Stimulation.** Monocyte activation with MPO-ANCA induces more profound metabolic changes than PR3-ANCA. Anti-MPO treated cells have higher glucose uptake than anti-PR3 and greater rates of glycolysis. This increased glycolysis feeds into the TCA cycle to drive FAS and fumarate/α-KG. These metabolites are known to induce epigenetic changes in monocytes and may control pro-inflammatory gene expression in AAV. AA synthesis is increased for both ANCAs, and intracellular Ile, Leu and Phe levels correlate with surface MPO expression. α-KG: alpha-Ketoglutarate; AA: Amino Acid; Asp: Aspartic Acid; FAS: Fatty Acid Synthesis; Ile: Isoleucine; Leu: Leucine; MI: *myo*-Inositol; OXPHOS: Oxidative Phosphorylation; Phe: Phenylalanine; Ser: Serine.

# References


1. Vegting, Y., et al., *Monocytes and macrophages in ANCA-associated vasculitis.* Autoimmunity Reviews, 2021: p. 102911.
2. Orwell, G., *Nineteen Eighty-Four*. Penguin books ; 972. 1954, Harmondsworth, Eng: Penguin in association with Secker & Warburg.
3. Hames, D. and N. Hooper, *Biochemistry*. 3rd ed. BIOS Instant Notes, ed. B.D. Hames. 2005: Taylor & Francis. 438.
4. Warburg, O., *On the Origin of Cancer Cells.* Science, 1956.
5. Pfeiffer, T., S. Schuster, and S. Bonhoeffer, *Cooperation and competition in the evolution of ATP-producing pathways.* Science, 2001. **292**(5516): p. 504-7.
6. Cheng, S.C., et al., *mTOR- and HIF-1alpha-mediated aerobic glycolysis as metabolic basis for trained immunity.* Science, 2014. **345**(6204): p. 1250684.
7. Ryan, D.G. and L.A.J. O'Neill, *Krebs Cycle Reborn in Macrophage Immunometabolism.* Annu Rev Immunol, 2020.
8. Tannahill, G.M., et al., *Succinate is an inflammatory signal that induces IL-1beta through HIF-1alpha.* Nature, 2013. **496**(7444): p. 238-42.
9. Italiani, P. and D. Boraschi, *From Monocytes to M1/M2 Macrophages: Phenotypical vs. Functional Differentiation.* Front Immunol, 2014. **5**: p. 514.
10. Viola, A., et al., *The Metabolic Signature of Macrophage Responses.* Frontiers in Immunology, 2019. **10**.
11. O'Neill, L.A., R.J. Kishton, and J. Rathmell, *A guide to immunometabolism for immunologists.* Nat Rev Immunol, 2016. **16**(9): p. 553-65.
12. Liu, Y., et al., *Metabolic reprogramming in macrophage responses.* Biomark Res, 2021. **9**(1): p. 1.
13. Jha, A.K., et al., *Network integration of parallel metabolic and transcriptional data reveals metabolic modules that regulate macrophage polarization.* Immunity, 2015. **42**(3): p. 419-30.
14. Abuawad, A., et al., *Metabolic characterisation of THP-1 macrophage polarisation using LC-MS-based metabolite profiling.* Metabolomics, 2020. **16**(3): p. 33.
15. Suzuki, H., et al., *Glycolytic pathway affects differentiation of human monocytes to regulatory macrophages.* Immunol Lett, 2016. **176**: p. 18-27.
16. Ismail, I.T., M.R. Showalter, and O. Fiehn, *Inborn Errors of Metabolism in the Era of Untargeted Metabolomics and Lipidomics.* Metabolites, 2019. **9**(10).
17. Mussap, M., M. Zaffanello, and V. Fanos, *Metabolomics: a challenge for detecting and monitoring inborn errors of metabolism.* Ann Transl Med, 2018. **6**(17): p. 338.
18. Causon, T.J. and S. Hann, *Review of sample preparation strategies for MS-based metabolomic studies in industrial biotechnology.* Anal Chim Acta, 2016. **938**: p. 18-32.
19. Guijas, C., et al., *Metabolomics activity screening for identifying metabolites that modulate phenotype.* Nat Biotechnol, 2018. **36**(4): p. 316-320.
20. Arts, R.J., et al., *Glutaminolysis and Fumarate Accumulation Integrate Immunometabolic and Epigenetic Programs in Trained Immunity.* Cell Metab, 2016. **24**(6): p. 807-819.
21. Bekkering, S., et al., *Metabolic Induction of Trained Immunity through the Mevalonate Pathway.* Cell, 2018. **172**(1-2): p. 135-146 e9.
22. Liu, P.S., et al., *alpha-ketoglutarate orchestrates macrophage activation through metabolic and epigenetic reprogramming.* Nat Immunol, 2017. **18**(9): p. 985-994.
23. Wishart, D.S., et al., *HMDB 4.0: the human metabolome database for 2018.* Nucleic Acids Res, 2018. **46**(D1): p. D608-D617.
24. Dettmer, K., P.A. Aronov, and B.D. Hammock, *Mass spectrometry-based metabolomics.* Mass Spectrom Rev, 2007. **26**(1): p. 51-78.
25. Schrimpe-Rutledge, A.C., et al., *Untargeted Metabolomics Strategies-Challenges and Emerging Directions.* J Am Soc Mass Spectrom, 2016. **27**(12): p. 1897-1905.
26. Voss, K., et al., *A guide to interrogating immunometabolism.* Nature Reviews Immunology, 2021.
27. Lu, W., et al., *Metabolite Measurement: Pitfalls to Avoid and Practices to Follow.* Annu Rev Biochem, 2017. **86**: p. 277-304.
28. Rhee, E.P., et al., *Variability of Two Metabolomic Platforms in CKD.* Clin J Am Soc Nephrol, 2019. **14**(1): p. 40-48.
29. Griffin, J.L., et al., *Standard reporting requirements for biological samples in metabolomics experiments: mammalian/in vivo experiments.* Metabolomics, 2007. **3**(3): p. 179-188.
30. Leuthold, P., et al., *Comprehensive Metabolomic and Lipidomic Profiling of Human Kidney Tissue: A Platform Comparison.* J Proteome Res, 2017. **16**(2): p. 933-944.
31. Onorato, J.M., et al., *Applications of HILIC for targeted and non-targeted LC/MS analyses in drug discovery.* J Sep Sci, 2010. **33**(6-7): p. 923-9.
32. Tang, D.Q., et al., *HILIC-MS for metabolomics: An attractive and complementary approach to RPLC-MS.* Mass Spectrom Rev, 2016. **35**(5): p. 574-600.
33. Akiyama, M., et al., *Neutrophil Extracellular Traps Induce Tissue-Invasive Monocytes in Granulomatosis With Polyangiitis.* Front Immunol, 2019. **10**: p. 2617.
34. Le, A., J. Mak, and T.M. Cowan, *Metabolic profiling by reversed-phase/ion-exchange mass spectrometry.* J Chromatogr B Analyt Technol Biomed Life Sci, 2020. **1143**: p. 122072.
35. Schwaiger, M., et al., *Merging metabolomics and lipidomics into one analytical run.* Analyst, 2018. **144**(1): p. 220-229.
36. Greco, G. and T. Letzel, *Main interactions and influences of the chromatographic parameters in HILIC separations.* J Chromatogr Sci, 2013. **51**(7): p. 684-93.
37. Mallet, C.R., Z. Lu, and J.R. Mazzeo, *A study of ion suppression effects in electrospray ionization from mobile phase additives and solid-phase extracts.* Rapid Commun Mass Spectrom, 2004. **18**(1): p. 49-58.
38. Fountain, K.J., et al., *Influence of stationary phase chemistry and mobile-phase composition on retention, selectivity, and MS response in hydrophilic interaction chromatography.* J Sep Sci, 2010. **33**(6-7): p. 740-51.
39. Tan, A. and J.C. Fanaras, *Use of high-pH (basic/alkaline) mobile phases for LC-MS or LC-MS/MS bioanalysis.* Biomed Chromatogr, 2019. **33**(1): p. e4409.
40. Kiefer, P., N. Delmotte, and J.A. Vorholt, *Nanoscale ion-pair reversed-phase HPLC-MS for sensitive metabolome analysis.* Anal Chem, 2011. **83**(3): p. 850-5.
41. Gika, H., et al., *Untargeted LC/MS-based metabolic phenotyping (metabonomics/metabolomics): The state of the art.* J Chromatogr B Analyt Technol Biomed Life Sci, 2019. **1117**: p. 136-147.

42. Hsiao, J.J., et al., *Improved LC/MS Methods for the Analysis of Metal-Sensitive Analytes Using Medronic Acid as a Mobile Phase Additive.* Anal Chem, 2018. **90**(15): p. 9457-9464.
43. Ren, D.-B., et al., *Effects of injection volume on chromatographic features and resolution in the process of counter-current chromatography.* Journal of Chromatography A, 2013. **1277**: p. 7-14.
44. Wu, Z.E., et al., *Tissue-Specific Sample Dilution: An Important Parameter to Optimise Prior to Untargeted LC-MS Metabolomics.* Metabolites, 2019. **9**(7).
45. Chernushevich, I.V., A.V. Loboda, and B.A. Thomson, *An introduction to quadrupole-time-of-flight mass spectrometry.* J Mass Spectrom, 2001. **36**(8): p. 849-65.
46. Zhou, J. and Y. Yin, *Strategies for large-scale targeted metabolomics quantification by liquid chromatography-mass spectrometry.* Analyst, 2016. **141**(23): p. 6362-6373.
47. Gonzalez-Riano, C., et al., *Recent Developments along the Analytical Process for Metabolomics Workflows.* Anal Chem, 2020. **92**(1): p. 203-226.
48. Annesley, T.M., *Ion Suppression in Mass Spectromtery.* Clinical Chemistry, 2003: p. 1041-1044.
49. Zhou, B., et al., *LC-MS-based metabolomics.* Mol Biosyst, 2012. **8**(2): p. 470-81.
50. Leon, Z., et al., *Mammalian cell metabolomics: experimental design and sample preparation.* Electrophoresis, 2013. **34**(19): p. 2762-75.
51. Assmann, N., et al., *Srebp-controlled glucose metabolism is essential for NK cell functional responses.* Nat Immunol, 2017. **18**(11): p. 1197-1206.
52. Luo, X., X. Gu, and L. Li, *Development of a simple and efficient method of harvesting and lysing adherent mammalian cells for chemical isotope labeling LC-MS-based cellular metabolomics.* Anal Chim Acta, 2018. **1037**: p. 97-106.
53. Bordag, N., et al., *Fast Filtration of Bacterial or Mammalian Suspension Cell Cultures for Optimal Metabolomics Results.* PLoS One, 2016. **11**(7): p. e0159389.
54. Bi, H., et al., *Optimization of harvesting, extraction, and analytical protocols for UPLC-ESI-MS-based metabolomic analysis of adherent mammalian cancer cells.* Anal Bioanal Chem, 2013. **405**(15): p. 5279-89.
55. Coman, C., et al., *Simultaneous Metabolite, Protein, Lipid Extraction (SIMPLEX): A Combinatorial Multimolecular Omics Approach for Systems Biology.* Mol Cell Proteomics, 2016. **15**(4): p. 1453-66.
56. Leuthold, P., et al., *Simultaneous Extraction of RNA and Metabolites from Single Kidney Tissue Specimens for Combined Transcriptomic and Metabolomic Profiling.* J Proteome Res, 2018. **17**(9): p. 3039-3049.
57. Sapcariu, S.C., et al., *Simultaneous extraction of proteins and metabolites from cells in culture.* MethodsX, 2014. **1**: p. 74-80.
58. Hayton, S., et al., *Experimental design and reporting standards for metabolomics studies of mammalian cell lines.* Cell Mol Life Sci, 2017. **74**(24): p. 4421-4441.
59. Ulmer, C.Z., et al., *Liquid Chromatography-Mass Spectrometry Metabolic and Lipidomic Sample Preparation Workflow for Suspension-Cultured Mammalian Cells using Jurkat T lymphocyte Cells.* J Proteomics Bioinform, 2015. **8**(6): p. 126-132.
60. Birsoy, K., et al., *Metabolic determinants of cancer cell sensitivity to glucose limitation and biguanides.* Nature, 2014. **508**(7494): p. 108-112.
61. Luo, Y., et al., *Effects of harvesting and extraction methods on metabolite recovery from adherently growing mammalian cells.* Anal Methods, 2020. **12**(19): p. 2491-2498.
62. Dietmair, S., et al., *A Multi-Omics Analysis of Recombinant Protein Production in Hek293 Cells.* PLOS ONE, 2012. **7**(8): p. e43394.
63. Broadhurst, D., et al., *Guidelines and considerations for the use of system suitability and quality control samples in mass spectrometry assays applied in untargeted clinical metabolomic studies.* Metabolomics, 2018. **14**(6): p. 72.
64. Dunn, W.B., et al., *Procedures for large-scale metabolic profiling of serum and plasma using gas chromatography and liquid chromatography coupled to mass spectrometry.* Nat Protoc, 2011. **6**(7): p. 1060-83.
65. Schiffman, C., et al., *Filtering procedures for untargeted LC-MS metabolomics data.* BMC Bioinformatics, 2019. **20**(1): p. 334.
66. Wei, R., et al., *Missing Value Imputation Approach for Mass Spectrometry-based Metabolomics Data.* Sci Rep, 2018. **8**(1): p. 663.
67. Guijas, C., et al., *METLIN: A Technology Platform for Identifying Knowns and Unknowns.* Anal Chem, 2018. **90**(5): p. 3156-3164.
68. Smith, C.A., et al., *METLIN: A Metabolite Mass Spectral Database.* Therapeutic Drug Monitoring, 2005. **27**(6): p. 747-751.
69. Horai, H., et al., *MassBank: a public repository for sharing mass spectral data for life sciences.* Journal of Mass Spectrometry, 2010. **45**(7): p. 703-714.
70. Sud, M., et al., *LMSD: LIPID MAPS structure database.* Nucleic Acids Research, 2007. **35**(suppl_1): p. D527-D532.
71. Muschet, C., et al., *Removing the bottlenecks of cell culture metabolomics: fast normalization procedure, correlation of metabolites to cell number, and impact of the cell harvesting method.* Metabolomics, 2016. **12**(10): p. 151.
72. Ejigu, B.A., et al., *Evaluation of normalization methods to pave the way towards large-scale LC-MS-based metabolomics profiling experiments.* OMICS, 2013. **17**(9): p. 473-85.
73. Robinson, J.L., et al., *An atlas of human metabolism.* Science Signaling, 2020. **13**(624).
74. Misra, B.B., *Data normalization strategies in metabolomics: Current challenges, approaches, and tools.* Eur J Mass Spectrom (Chichester), 2020. **26**(3): p. 165-174.
75. Wu, Y. and L. Li, *Sample normalization methods in quantitative metabolomics.* J Chromatogr A, 2016. **1430**: p. 80-95.
76. Warrack, B.M., et al., *Normalization strategies for metabonomic analysis of urine samples.* J Chromatogr B Analyt Technol Biomed Life Sci, 2009. **877**(5-6): p. 547-52.
77. Kohl, S.M., et al., *State-of-the art data normalization methods improve NMR-based metabolomic analysis.* Metabolomics, 2012. **8**(Suppl 1): p. 146-160.
78. Gagnebin, Y., et al., *Metabolomic analysis of urine samples by UHPLC-QTOF-MS: Impact of normalization strategies.* Anal Chim Acta, 2017. **955**: p. 27-35.
79. Eisenberg, E. and E.Y. Levanon, *Human housekeeping genes, revisited.* Trends in Genetics, 2013. **29**(10): p. 569-574.
80. Cook, T., Y. Ma, and S. Gamagedara, *Evaluation of statistical techniques to normalize mass spectrometry-based urinary metabolomics data.* J Pharm Biomed Anal, 2020. **177**: p. 112854.

81. Vogl, F.C., et al., *Evaluation of dilution and normalization strategies to correct for urinary output in HPLC-HRTOFMS metabolomics.* Anal Bioanal Chem, 2016. **408**(29): p. 8483-8493.
82. Ruiz-Aracama, A., et al., *An untargeted multi-technique metabolomics approach to studying intracellular metabolites of HepG2 cells exposed to 2,3,7,8-tetrachlorodibenzo-p-dioxin.* BMC Genomics, 2011. **12**: p. 251.
83. Cao, B., et al., *GC-TOFMS analysis of metabolites in adherent MDCK cells and a novel strategy for identifying intracellular metabolic markers for use as cell amount indicators in data normalization.* Anal Bioanal Chem, 2011. **400**(9): p. 2983-93.
84. Tanner, L.B., et al., *Four Key Steps Control Glycolytic Flux in Mammalian Cells.* Cell Syst, 2018. **7**(1): p. 49-62 e8.
85. Raulien, N., et al., *Fatty Acid Oxidation Compensates for Lipopolysaccharide-Induced Warburg Effect in Glucose-Deprived Monocytes.* Front Immunol, 2017. **8**: p. 609.
86. Rodgers, L.C., et al., *The rheumatoid synovial environment alters fatty acid metabolism in human monocytes and enhances CCL20 secretion.* Rheumatology (Oxford), 2020. **59**(4): p. 869-878.
87. Wulff, J.E. and M.W. Mitchell, *A Comparison of Various Normalization Methods for LC/MS Metabolomics Data.* Advances in Bioscience and Biotechnology, 2018. **09**(08): p. 339-351.
88. Silva, L.P., et al., *Measurement of DNA concentration as a normalization strategy for metabolomic data from adherent cell lines.* Anal Chem, 2013. **85**(20): p. 9536-42.
89. Zhao, C., et al., *Metabolomic analysis revealed glycylglycine accumulation in astrocytes after methionine enkephalin administration exhibiting neuron protective effects.* Journal of Pharmaceutical and Biomedical Analysis, 2015. **115**: p. 48-54.
90. Huang, S.-M., et al., *Metabolomics Studies Show Dose-Dependent Toxicity Induced by SiO2 Nanoparticles in MRC-5 Human Fetal Lung Fibroblasts.* Advanced Healthcare Materials, 2012. **1**(6): p. 779-784.
91. Purwaha, P., et al., *Targeted metabolomic analysis of amino acid response to L-asparaginase in adherent cells.* Metabolomics : Official journal of the Metabolomic Society, 2014. **10**(5): p. 909-919.
92. Shimada, H., et al., *Normalization using ploidy and genomic DNA copy number allows absolute quantification of transcripts, proteins and metabolites in cells.* Plant Methods, 2010. **6**(1): p. 29.
93. Modrzejewska, M., M. Gawronski, and D. Gackowski, *Normalization of metabolic data to total thymine content and its application to determination of 2-hydroxyglutarate.* Anal Biochem, 2021. **618**: p. 114129.
94. Abdel Rahman, A.M., et al., *Targeted metabolomics in cultured cells and tissues by mass spectrometry: Method development and validation.* Analytica Chimica Acta, 2014. **845**: p. 53-61.
95. Wallace, M., H. Whelan, and L. Brennan, *Metabolomic analysis of pancreatic beta cells following exposure to high glucose.* Biochimica et Biophysica Acta (BBA) - General Subjects, 2013. **1830**(3): p. 2583-2590.
96. Zhu, X., et al., *Frontline Science: Monocytes sequentially rewire metabolism and bioenergetics during an acute inflammatory response.* J Leukoc Biol, 2019.
97. Lachmandas, E., et al., *Microbial stimulation of different Toll-like receptor signalling pathways induces diverse metabolic programmes in human monocytes.* Nat Microbiol, 2016. **2**: p. 16246.
98. Lin, J., X. Yi, and Y. Zhuang, *Medium optimization based on comparative metabolomic analysis of chicken embryo fibroblast DF-1 cells.* RSC Advances, 2019. **9**(47): p. 27369-27377.
99. Bararpour, N., et al., *DBnorm as an R package for the comparison and selection of appropriate statistical methods for batch effect correction in metabolomic studies.* Sci Rep, 2021. **11**(1): p. 5657.
100. Sanchez-Illana, A., et al., *Model selection for within-batch effect correction in UPLC-MS metabolomics using quality control - Support vector regression.* Anal Chim Acta, 2018. **1026**: p. 62-68.
101. Luan, H., et al., *statTarget: A streamlined tool for signal drift correction and interpretations of quantitative mass spectrometry-based omics data.* Anal Chim Acta, 2018. **1036**: p. 66-72.
102. Li, B., et al., *NOREVA: normalization and evaluation of MS-based metabolomics data.* Nucleic Acids Res, 2017. **45**(W1): p. W162-W170.
103. De Livera, A.M., et al., *NormalizeMets: assessing, selecting and implementing statistical methods for normalizing metabolomics data.* Metabolomics, 2018. **14**(5): p. 54.
104. Wang, S. and H. Yang, *pseudoQC: A Regression-Based Simulation Software for Correction and Normalization of Complex Metabolomics and Proteomics Datasets.* Proteomics, 2019. **19**(19): p. e1900264.
105. Ernest, B., et al., *MetabR: an R script for linear model analysis of quantitative metabolomic data.* BMC Research Notes, 2012. **5**(1): p. 596.
106. Thonusin, C., et al., *Evaluation of intensity drift correction strategies using MetaboDrift, a normalization tool for multi-batch metabolomics data.* Journal of chromatography. A, 2017. **1523**: p. 265-274.
107. Willforss, J., A. Chawade, and F. Levander, *NormalyzerDE: Online Tool for Improved Normalization of Omics Expression Data and High-Sensitivity Differential Expression Analysis.* Journal of Proteome Research, 2019. **18**(2): p. 732-740.
108. Wang, S., et al., *MetaboGroupS: A Group Entropy-Based Web Platform for Evaluating Normalization Methods in Blood Metabolomics Data from Maintenance Hemodialysis Patients.* Analytical Chemistry, 2018. **90**(18): p. 11124-11130.
109. Fan, S., et al., *Systematic Error Removal Using Random Forest for Normalizing Large-Scale Untargeted Lipidomics Data.* Anal Chem, 2019. **91**(5): p. 3590-3596.
110. Yang, Q., et al., *NOREVA: enhanced normalization and evaluation of time-course and multi-class metabolomic data.* Nucleic Acids Res, 2020. **48**(W1): p. W436-W448.
111. Ziegler-Heitbrock, L., *Monocyte subsets in man and other species.* Cell Immunol, 2014. **289**(1-2): p. 135-9.
112. Boyette, L.B., et al., *Phenotype, function, and differentiation potential of human monocyte subsets.* PLoS One, 2017. **12**(4): p. e0176460.
113. Martinez, F.O., *The transcriptome of human monocyte subsets begins to emerge.* J Biol, 2009. **8**(11): p. 99.
114. Wong, K.L., et al., *Gene expression profiling reveals the defining features of the classical, intermediate, and nonclassical human monocyte subsets.* Blood, 2011. **118**(5): p. e16-31.
115. Segura, V., et al., *In-Depth Proteomic Characterization of Classical and Non-Classical Monocyte Subsets.* Proteomes, 2018. **6**(1).
116. Ong, S.M., et al., *The pro-inflammatory phenotype of the human non-classical monocyte subset is attributed to senescence.* Cell Death Dis, 2018. **9**(3): p. 266.
117. Guilliams, M., A. Mildner, and S. Yona, *Developmental and Functional Heterogeneity of Monocytes.* Immunity, 2018. **49**(4): p. 595-613.
118. Serbina, N.V., et al., *Monocyte-mediated defense against microbial pathogens.* Annu Rev Immunol, 2008. **26**: p. 421-52.

119. Awad, F., et al., *Impact of human monocyte and macrophage polarization on NLR expression and NLRP3 inflammasome activation.* PLoS One, 2017. **12**(4): p. e0175336.
120. Gov, L., et al., *NLRP3 and Potassium Efflux Drive Rapid IL-1beta Release from Primary Human Monocytes during Toxoplasma gondii Infection.* J Immunol, 2017. **199**(8): p. 2855-2864.
121. Gaidt, M.M., et al., *Human Monocytes Engage an Alternative Inflammasome Pathway.* Immunity, 2016. **44**(4): p. 833-46.
122. Deshmane, S.L., et al., *Monocyte chemoattractant protein-1 (MCP-1): an overview.* J Interferon Cytokine Res, 2009. **29**(6): p. 313-26.
123. Jakubzick, C.V., G.J. Randolph, and P.M. Henson, *Monocyte differentiation and antigen-presenting functions.* Nat Rev Immunol, 2017. **17**(6): p. 349-362.
124. Dominguez-Andres, J., et al., *Rewiring monocyte glucose metabolism via C-type lectin signaling protects against disseminated candidiasis.* PLoS Pathog, 2017. **13**(9): p. e1006632.
125. Takeuchi, O., et al., *Differential roles of TLR2 and TLR4 in recognition of gram-negative and gram-positive bacterial cell wall components.* Immunity, 1999. **11**(4): p. 443-51.
126. Hornung, V., et al., *Quantitative expression of toll-like receptor 1-10 mRNA in cellular subsets of human peripheral blood mononuclear cells and sensitivity to CpG oligodeoxynucleotides.* J Immunol, 2002. **168**(9): p. 4531-7.
127. Dorrington, M.G. and I.D.C. Fraser, *NF-kappaB Signaling in Macrophages: Dynamics, Crosstalk, and Signal Integration.* Front Immunol, 2019. **10**: p. 705.
128. McGettrick, A.F. and L.A. O'Neill, *How metabolism generates signals during innate immunity and inflammation.* J Biol Chem, 2013. **288**(32): p. 22893-8.
129. Yang, K., et al., *Low Cellular NAD(+) Compromises Lipopolysaccharide-Induced Inflammatory Responses via Inhibiting TLR4 Signal Transduction in Human Monocytes.* J Immunol, 2019.
130. Duroux-Richard, I., et al., *miR-125b controls monocyte adaptation to inflammation through mitochondrial metabolism and dynamics.* Blood, 2016. **128**(26): p. 3125-3136.
131. Billingham, L.K. and N.S. Chandel, *NAD-biosynthetic pathways regulate innate immunity.* Nat Immunol, 2019.
132. Nikiforov, A., V. Kulikova, and M. Ziegler, *The human NAD metabolome: Functions, metabolism and compartmentalization.* Crit Rev Biochem Mol Biol, 2015. **50**(4): p. 284-97.
133. Jones, N., et al., *Fructose reprogrammes glutamine-dependent oxidative metabolism to support LPS-induced inflammation.* Nature Communications, 2021. **12**(1).
134. Ratter, J.M., et al., *In vitro and in vivo Effects of Lactate on Metabolism and Cytokine Production of Human Primary PBMCs and Monocytes.* Front Immunol, 2018. **9**: p. 2564.
135. Palmer, C.S., et al., *Glucose transporter 1-expressing proinflammatory monocytes are elevated in combination antiretroviral therapy-treated and untreated HIV+ subjects.* J Immunol, 2014. **193**(11): p. 5595-603.
136. Lee, M.K.S., et al., *Glycolysis Is Required for LPS-Induced Activation and Adhesion of Human CD14+CD16− Monocytes.* Frontiers in Immunology, 2019. **10**.
137. Palmer, C.S., et al., *Glucose Metabolism in T Cells and Monocytes: New Perspectives in HIV Pathogenesis.* EBioMedicine, 2016. **6**: p. 31-41.
138. Pence, B.D., *Atypical monocytes in COVID-19: Lighting the fire of cytokine storm?* J Leukoc Biol, 2020.
139. Merad, M. and J.C. Martin, *Pathological inflammation in patients with COVID-19: a key role for monocytes and macrophages.* Nat Rev Immunol, 2020. **20**(6): p. 355-362.
140. Schulte-Schrepping, J., et al., *Severe COVID-19 Is Marked by a Dysregulated Myeloid Cell Compartment.* Cell, 2020.
141. Chevrier, S., et al., *A distinct innate immune signature marks progression from mild to severe COVID-19.* Cell Rep Med, 2021. **2**(1): p. 100166.
142. Carmona, L., et al., *Rheumatoid arthritis.* Best Practice & Research Clinical Rheumatology, 2010. **24**(6): p. 733-745.
143. Rantapaa-Dahlqvist, S., et al., *Up regulation of monocyte chemoattractant protein-1 expression in anti-citrulline antibody and immunoglobulin M rheumatoid factor positive subjects precedes onset of inflammatory response and development of overt rheumatoid arthritis.* Ann Rheum Dis, 2007. **66**(1): p. 121-3.
144. Tsukamoto, M., et al., *CD14(bright)CD16+ intermediate monocytes are induced by interleukin-10 and positively correlate with disease activity in rheumatoid arthritis.* Arthritis Res Ther, 2017. **19**(1): p. 28.
145. Rossol, M., et al., *The CD14(bright) CD16+ monocyte subset is expanded in rheumatoid arthritis and promotes expansion of the Th17 cell population.* Arthritis Rheum, 2012. **64**(3): p. 671-7.
146. Chara, L., et al., *The number of circulating monocytes as biomarkers of the clinical response to methotrexate in untreated patients with rheumatoid arthritis.* Journal of Translational Medicine, 2015. **13**(1): p. 2.
147. Zeisbrich, M., et al., *Hypermetabolic macrophages in rheumatoid arthritis and coronary artery disease due to glycogen synthase kinase 3b inactivation.* Ann Rheum Dis, 2018. **77**(7): p. 1053-1062.
148. Weyand, C.M., M. Zeisbrich, and J.J. Goronzy, *Metabolic signatures of T-cells and macrophages in rheumatoid arthritis.* Curr Opin Immunol, 2017. **46**: p. 112-120.
149. Fearon, U., et al., *Altered metabolic pathways regulate synovial inflammation in rheumatoid arthritis.* Clin Exp Immunol, 2018.
150. Littlewood-Evans, A., et al., *GPR91 senses extracellular succinate released from inflammatory macrophages and exacerbates rheumatoid arthritis.* J Exp Med, 2016. **213**(9): p. 1655-62.
151. McGarry, T., et al., *Rheumatoid arthritis CD14+ monocytes display metabolic and inflammatory dysfunction, a phenotype that precedes clinical manifestation of disease.* Clinical & Translational Immunology, 2021. **10**(1).
152. Bae, S., et al., *alpha-Enolase expressed on the surfaces of monocytes and macrophages induces robust synovial inflammation in rheumatoid arthritis.* J Immunol, 2012. **189**(1): p. 365-72.
153. Pamukcu, B., et al., *The role of monocytes in atherosclerotic coronary artery disease.* Ann Med, 2010. **42**(6): p. 394-403.
154. Groh, L., et al., *Monocyte and macrophage immunometabolism in atherosclerosis.* Semin Immunopathol, 2018. **40**(2): p. 203-214.
155. Fernandez-Ruiz, I., et al., *Differential lipid metabolism in monocytes and macrophages: influence of cholesterol loading.* J Lipid Res, 2016. **57**(4): p. 574-86.
156. Methe, H., et al., *Statins decrease Toll-like receptor 4 expression and downstream signaling in human CD14+ monocytes.* Arterioscler Thromb Vasc Biol, 2005. **25**(7): p. 1439-45.
157. Nakagomi, A., et al., *Effects of statin therapy on the production of monocyte pro-inflammatory cytokines, cardiac function, and long-term prognosis in chronic heart failure patients with dyslipidemia.* Circ J, 2012. **76**(9): p. 2130-8.

158. Hodgkinson, C.P. and S. Ye, *Statins inhibit toll-like receptor 4-mediated lipopolysaccharide signaling and cytokine expression.* Pharmacogenet Genomics, 2008. **18**(9): p. 803-13.
159. Zhu, J., et al., *NLRP3 inflammasome expression in peripheral blood monocytes of coronary heart disease patients and its modulation by rosuvastatin.* Mol Med Rep, 2019. **20**(2): p. 1826-1836.
160. Kedzierska, K. and S.M. Crowe, *The role of monocytes and macrophages in the pathogenesis of HIV-1 infection.* Curr Med Chem, 2002. **9**(21): p. 1893-903.
161. Campbell, J.H., et al., *The importance of monocytes and macrophages in HIV pathogenesis, treatment, and cure.* AIDS, 2014. **28**(15): p. 2175-87.
162. Prabhu, V.M., et al., *Monocyte Based Correlates of Immune Activation and Viremia in HIV-Infected Long-Term Non-Progressors.* Front Immunol, 2019. **10**: p. 2849.
163. Kalra, S., et al., *Understanding diabetes in patients with HIV/AIDS.* Diabetology & Metabolic Syndrome, 2011. **3**(1): p. 2.
164. Sitole, L.J., A.A. Williams, and D. Meyer, *Metabonomic analysis of HIV-infected biofluids.* Mol Biosyst, 2013. **9**(1): p. 18-28.
165. Sitole, L.J., F. Tugizimana, and D. Meyer, *Multi-platform metabonomics unravel amino acids as markers of HIV/combination antiretroviral therapy-induced oxidative stress.* J Pharm Biomed Anal, 2019. **176**: p. 112796.
166. Babu, H., et al., *Plasma Metabolic Signature and Abnormalities in HIV-Infected Individuals on Long-Term Successful Antiretroviral Therapy.* Metabolites, 2019. **9**(10).
167. Scarpellini, B., et al., *Plasma Metabolomics Biosignature According to HIV Stage of Infection, Pace of Disease Progression, Viremia Level and Immunological Response to Treatment.* PLoS One, 2016. **11**(12): p. e0161920.
168. Bowman, E.R., et al., *Altered Lipidome Composition Is Related to Markers of Monocyte and Immune Activation in Antiretroviral Therapy Treated Human Immunodeficiency Virus (HIV) Infection and in Uninfected Persons.* Front Immunol, 2019. **10**: p. 785.
169. Yeoh, H.L., et al., *Immunometabolic and Lipidomic Markers Associated With the Frailty Index and Quality of Life in Aging HIV+ Men on Antiretroviral Therapy.* EBioMedicine, 2017. **22**: p. 112-121.
170. Peltenburg, N.C., et al., *Persistent metabolic changes in HIV-infected patients during the first year of combination antiretroviral therapy.* Sci Rep, 2018. **8**(1): p. 16947.
171. Watad, A., et al., *Autoimmunity in the Elderly: Insights from Basic Science and Clinics - A Mini-Review.* Gerontology, 2017. **63**(6): p. 515-523.
172. Cooper, G.S. and B.C. Stroehla, *The epidemiology of autoimmune diseases.* Autoimmunity Reviews, 2003. **2**(3): p. 119-125.
173. Kettritz, R., *How anti-neutrophil cytoplasmic autoantibodies activate neutrophils.* Clin Exp Immunol, 2012. **169**(3): p. 220-8.
174. Kitching, A.R., et al., *ANCA-associated vasculitis.* Nat Rev Dis Primers, 2020. **6**(1): p. 71.
175. Hilhorst, M., et al., *Proteinase 3-ANCA Vasculitis versus Myeloperoxidase-ANCA Vasculitis.* J Am Soc Nephrol, 2015. **26**(10): p. 2314-27.
176. Berti, A., et al., *The Epidemiology of Antineutrophil Cytoplasmic Autoantibody-Associated Vasculitis in Olmsted County, Minnesota: A Twenty-Year US Population-Based Study.* Arthritis Rheumatol, 2017. **69**(12): p. 2338-2350.
177. Pearce, F.A., et al., *Incidence of ANCA-associated vasculitis in a UK mixed ethnicity population.* Rheumatology (Oxford), 2016. **55**(9): p. 1656-63.
178. Tan, J.A., et al., *Mortality in ANCA-associated vasculitis: ameta-analysis of observational studies.* Annals of the Rheumatic Diseases, 2017. **76**(9): p. 1566.
179. Nakazawa, D., et al., *Pathogenesis and therapeutic interventions for ANCA-associated vasculitis.* Nat Rev Rheumatol, 2019. **15**(2): p. 91-101.
180. Davies, D.J., et al., *Segmental necrotising glomerulonephritis with antineutrophil antibody: possible arbovirus aetiology?* Br Med J (Clin Res Ed), 1982. **285**(6342): p. 606.
181. Jennette, J.C., R.J. Falk, and A.H. Gasim, *Pathogenesis of antineutrophil cytoplasmic autoantibody vasculitis.* Curr Opin Nephrol Hypertens, 2011. **20**(3): p. 263-70.
182. Xiao, H., et al., *Overview of the Pathogenesis of ANCA-Associated Vasculitis.* Kidney diseases (Basel, Switzerland), 2016. **1**(4): p. 205-215.
183. Berti, A., et al., *Brief Report: Circulating Cytokine Profiles and Antineutrophil Cytoplasmic Antibody Specificity in Patients With Antineutrophil Cytoplasmic Antibody-Associated Vasculitis.* Arthritis Rheumatol, 2018. **70**(7): p. 1114-1121.
184. Jarrot, P.A. and G. Kaplanski, *Pathogenesis of ANCA-associated vasculitis: An update.* Autoimmun Rev, 2016. **15**(7): p. 704-13.
185. von Borstel, A., et al., *Cellular immune regulation in the pathogenesis of ANCA-associated vasculitides.* Autoimmun Rev, 2018. **17**(4): p. 413-421.
186. Leacy, E., G. Brady, and M.A. Little, *Pathogenesis of ANCA-associated vasculitis: an emerging role for immunometabolism.* Rheumatology (Oxford), 2020. **59**(Supplement_3): p. iii33-iii41.
187. Brunini, F., et al., *The role of monocytes in ANCA-associated vasculitides.* Autoimmun Rev, 2016. **15**(11): p. 1046-1053.
188. Ingersoll, M.A., et al., *Monocyte trafficking in acute and chronic inflammation.* Trends Immunol, 2011. **32**(10): p. 470-7.
189. Jonsson, N., et al., *Monocyte Chemoattractant Protein-1 in Antineutrophil Cytoplasmic Autoantibody-Associated Vasculitis: Biomarker Potential and Association with Polymorphisms in the MCP-1 and the CC Chemokine Receptor-2 Gene.* Mediators Inflamm, 2018. **2018**: p. 6861257.
190. Tam, F.W., et al., *Urinary monocyte chemoattractant protein-1 (MCP-1) is a marker of active renal vasculitis.* Nephrol Dial Transplant, 2004. **19**(11): p. 2761-8.
191. Ramirez, G.A., et al., *Plasma levels of M-CSF are increased in ANCA-associated vasculitides with active nephritis.* Results Immunol, 2015. **5**: p. 33-6.
192. Weidner, S., et al., *Antineutrophil cytoplasmic antibodies induce human monocytes to produce oxygen radicals in vitro.* Arthritis Rheum, 2001. **44**(7): p. 1698-706.
193. Zhao, L., et al., *M2 macrophage infiltrates in the early stages of ANCA-associated pauci-immune necrotizing GN.* Clin J Am Soc Nephrol, 2015. **10**(1): p. 54-62.
194. O'Reilly, V.P., et al., *Urinary Soluble CD163 in Active Renal Vasculitis.* J Am Soc Nephrol, 2016. **27**(9): p. 2906-16.

195. Dekkema, G.J., et al., *Urinary and serum soluble CD25 complements urinary soluble CD163 to detect active renal anti-neutrophil cytoplasmic autoantibody-associated vasculitis: a cohort study.* Nephrol Dial Transplant, 2019. **34**(2): p. 234-242.
196. Rousselle, A., R. Kettritz, and A. Schreiber, *Monocytes Promote Crescent Formation in Anti-Myeloperoxidase Antibody-Induced Glomerulonephritis.* Am J Pathol, 2017. **187**(9): p. 1908-1915.
197. Popat, R.J., et al., *Anti-myeloperoxidase antibodies attenuate the monocyte response to LPS and shape macrophage development.* JCI Insight, 2017. **2**(2): p. e87379.
198. Tan, D.S.Y., et al., *Thymic Deletion and Regulatory T Cells Prevent Antimyeloperoxidase GN.* Journal of the American Society of Nephrology, 2013. **24**(4): p. 573.
199. Ooi, J.D., et al., *The immunodominant myeloperoxidase T-cell epitope induces local cell-mediated injury in antimyeloperoxidase glomerulonephritis.* Proceedings of the National Academy of Sciences, 2012. **109**(39): p. E2615.
200. Ruth, A.J., et al., *Anti-neutrophil cytoplasmic antibodies and effector CD4+ cells play nonredundant roles in anti-myeloperoxidase crescentic glomerulonephritis.* J Am Soc Nephrol, 2006. **17**(7): p. 1940-9.
201. Roberts, C.A., A.K. Dickinson, and L.S. Taams, *The Interplay Between Monocytes/Macrophages and CD4(+) T Cell Subsets in Rheumatoid Arthritis.* Front Immunol, 2015. **6**: p. 571.
202. Kapellos, T.S., et al., *Human Monocyte Subsets and Phenotypes in Major Chronic Inflammatory Diseases.* Frontiers in Immunology, 2019. **10**.
203. O'Brien, E.C., et al., *Intermediate monocytes in ANCA vasculitis: increased surface expression of ANCA autoantigens and IL-1beta secretion in response to anti-MPO antibodies.* Sci Rep, 2015. **5**: p. 11888.
204. Matsumoto, K., et al., *Significant association between clinical characteristics and immuno-phenotypes in patients with ANCA-associated vasculitis.* Rheumatology (Oxford), 2020. **59**(3): p. 545-553.
205. Matsumoto, K., et al., *Longitudinal immune cell monitoring identified CD14(++) CD16(+) intermediate monocyte as a marker of relapse in patients with ANCA-associated vasculitis.* Arthritis Res Ther, 2020. **22**(1): p. 145.
206. Connaughton, E.P., et al., *Phenotypic and functional heterogeneity of human intermediate monocytes based on HLA-DR expression.* Immunol Cell Biol, 2018.
207. Dolff, S., O. Witzke, and B. Wilde, *Th17 cells in renal inflammation and autoimmunity.* Autoimmun Rev, 2019. **18**(2): p. 129-136.
208. van Sleen, Y., et al., *Involvement of Monocyte Subsets in the Immunopathology of Giant Cell Arteritis.* Sci Rep, 2017. **7**(1): p. 6553.
209. Csernok, E., *ANCA testing: the current stage and perspectives.* Clinical and Experimental Nephrology, 2013. **17**(5): p. 615-618.
210. Tidman, et al., *Patients hospitalized because of small vessel vasculitides with renal involvement in the period 1975–95: organ involvement, anti-neutrophil cytoplasmic antibodies patterns, seasonal attack rates and fluctuation of annual frequencies.* Journal of Internal Medicine, 1998. **244**(2): p. 133-141.
211. Weiner, M. and M. Segelmark, *The clinical presentation and therapy of diseases related to anti-neutrophil cytoplasmic antibodies (ANCA).* Autoimmun Rev, 2016. **15**(10): p. 978-82.
212. Harper, L., et al., *Neutrophil priming and apoptosis in anti-neutrophil cytoplasmic autoantibody-associated vasculitis.* Kidney Int, 2001. **59**(5): p. 1729-38.
213. Choi, M., et al., *Endothelial NF-kappaB Blockade Abrogates ANCA-Induced GN.* J Am Soc Nephrol, 2017. **28**(11): p. 3191-3204.
214. Ben-Smith, A., et al., *Antineutrophil cytoplasm autoantibodies from patients with systemic vasculitis activate neutrophils through distinct signaling cascades: comparison with conventional Fc gamma receptor ligation.* Blood, 2001. **98**(5): p. 1448-1455.
215. Radford, D.J., J.M. Lord, and C.O. Savage, *The activation of the neutrophil respiratory burst by anti-neutrophil cytoplasm autoantibody (ANCA) from patients with systemic vasculitis requires tyrosine kinases and protein kinase C activation.* Clin Exp Immunol, 1999. **118**(1): p. 171-9.
216. Choi, M., et al., *Extracellular signal-regulated kinase inhibition by statins inhibits neutrophil activation by ANCA.* Kidney Int, 2003. **63**(1): p. 96-106.
217. Kettritz, R., et al., *Role of mitogen-activated protein kinases in activation of human neutrophils by antineutrophil cytoplasmic antibodies.* J Am Soc Nephrol, 2001. **12**(1): p. 37-46.
218. Schreiber, A., et al., *Neutrophil serine proteases promote IL-1beta generation and injury in necrotizing crescentic glomerulonephritis.* J Am Soc Nephrol, 2012. **23**(3): p. 470-82.
219. Volk, A.P., et al., *Priming of neutrophils and differentiated PLB-985 cells by pathophysiological concentrations of TNF-alpha is partially oxygen dependent.* J Innate Immun, 2011. **3**(3): p. 298-314.
220. Pfister, H., et al., *Antineutrophil cytoplasmic autoantibodies against the murine homolog of proteinase 3 (Wegener autoantigen) are pathogenic in vivo.* Blood, 2004. **104**(5): p. 1411-8.
221. Noronha, I.L., et al., *In situ production of TNF-α, IL-1β and IL-2R in ANCA-positive glomerulonephritis.* Kidney International, 1993. **43**(3): p. 682-692.
222. Zamani, F., et al., *Induction of CD14 Expression and Differentiation to Monocytes or Mature Macrophages in Promyelocytic Cell Lines: New Approach.* Advanced pharmaceutical bulletin, 2013. **3**(2): p. 329-332.
223. Tarzi, R.M., et al., *CD14 expression is increased on monocytes in patients with anti-neutrophil cytoplasm antibody (ANCA)-associated vasculitis and correlates with the expression of ANCA autoantigens.* Clin Exp Immunol, 2015. **181**(1): p. 65-75.
224. Tadema, H., et al., *Increased expression of Toll-like receptors by monocytes and natural killer cells in ANCA-associated vasculitis.* PLoS One, 2011. **6**(9): p. e24315.
225. Nowack, R., et al., *Upregulation of CD14 and CD18 on monocytes In vitro by antineutrophil cytoplasmic autoantibodies.* J Am Soc Nephrol, 2000. **11**(9): p. 1639-46.
226. Hattar, K., et al., *Anti-proteinase 3 antibodies (c-ANCA) prime CD14-dependent leukocyte activation.* J Leukoc Biol, 2005. **78**(4): p. 992-1000.
227. Falk, R.J., et al., *Anti-neutrophil cytoplasmic autoantibodies induce neutrophils to degranulate and produce oxygen radicals in vitro.* Proc Natl Acad Sci U S A, 1990. **87**(11): p. 4115-9.
228. Yang, J.J., et al., *Circumvention of normal constraints on granule protein gene expression in peripheral blood neutrophils and monocytes of patients with antineutrophil cytoplasmic autoantibody-associated glomerulonephritis.* J Am Soc Nephrol, 2004. **15**(8): p. 2103-14.
229. Yang, J., et al., *Histone modification signature at myeloperoxidase and proteinase 3 in patients with anti-neutrophil cytoplasmic autoantibody-associated vasculitis.* Clin Epigenetics, 2016. **8**: p. 85.

230. Zeisbrich, M., et al., *CMTM6-Deficient Monocytes in ANCA-Associated Vasculitis Fail to Present the Immune Checkpoint PD-L1.* Frontiers in Immunology, 2021. **12**.
231. Wikman, A., et al., *Antineutrophil Cytoplasmic Antibodies Induce Decreased CD62L Expression and Enhanced Metabolic Activity in Monocytes.* Scandinavian Journal of Immunology, 2003. **57**(2): p. 179-184.
232. Wikman, A., J. Lundahl, and S.H. Jacobson, *Sustained monocyte activation in clinical remission of systemic vasculitis.* Inflammation, 2008. **31**(6): p. 384-90.
233. Bjerkeli, V., et al., *Increased expression of fractalkine (CX3CL1) and its receptor, CX3CR1, in Wegener's granulomatosis--possible role in vascular inflammation.* Rheumatology (Oxford), 2007. **46**(9): p. 1422-7.
234. Haller, H., et al., *Circulating leukocyte integrin expression in Wegener's granulomatosis.* J Am Soc Nephrol, 1996. **7**(1): p. 40-8.
235. Muller Kobold, A.C., C.G. Kallenberg, and J.W. Tervaert, *Monocyte activation in patients with Wegener's granulomatosis.* Ann Rheum Dis, 1999. **58**(4): p. 237-45.
236. Johansson, A.C., et al., *Impaired phagocytosis and reactive oxygen species production in phagocytes is associated with systemic vasculitis.* Arthritis Res Ther, 2016. **18**: p. 92.
237. Wikman, A., et al., *Monocyte activation and relationship to anti-proteinase 3 in acute vasculitis.* Nephrol Dial Transplant, 2003. **18**(9): p. 1792-9.
238. O'Brien, E.C., et al., *Pro-inflammatory Stimulation of Monocytes by ANCA Is Linked to Changes in Cellular Metabolism.* Frontiers in Medicine, 2020. **7**.
239. Hoffmann, J.C., et al., *Cytokine profiling in anti neutrophil cytoplasmic antibody-associated vasculitis: a cross-sectional cohort study.* Rheumatol Int, 2019.
240. Hattar, K., et al., *Wegener's granulomatosis: antiproteinase 3 antibodies induce monocyte cytokine and prostanoid release-role of autocrine cell activation.* J Leukoc Biol, 2002. **71**(6): p. 996-1004.
241. Irmscher, S., et al., *Serum FHR1 binding to necrotic-type cells activates monocytic inflammasome and marks necrotic sites in vasculopathies.* Nat Commun, 2019. **10**(1): p. 2961.
242. Casselman, B.L., et al., *Antibodies to neutrophil cytoplasmic antigens induce monocyte chemoattractant protein-1 secretion from human monocytes.* Journal of Laboratory and Clinical Medicine, 1995. **126**(5): p. 495-502.
243. Moran, S.M., et al., *Urinary soluble CD163 and monocyte chemoattractant protein-1 in the identification of subtle renal flare in anti-neutrophil cytoplasmic antibody-associated vasculitis.* Nephrol Dial Transplant, 2020. **35**(2): p. 283-291.
244. O'Brien, E.C., *The role of monocytes in ANCA associated vasculitis*, in *School of Medicine*. 2017, Trinity College Dublin. p. 193.
245. Batten, I., et al., *Investigation of type I interferon responses in ANCA-associated vasculitis.* Scientific Reports, 2021. **11**(1).
246. Zhang, H., et al., *CD28 Signaling Controls Metabolic Fitness of Pathogenic T Cells in Medium and Large Vessel Vasculitis.* J Am Coll Cardiol, 2019. **73**(14): p. 1811-1823.
247. Ohashi, R., et al., *M1 macrophage is the predominant phenotype in coronary artery lesions following Kawasaki disease.* Vasc Med, 2019. **24**(6): p. 484-492.
248. Arts, R.J.W., et al., *Immunometabolic Pathways in BCG-Induced Trained Immunity.* Cell Rep, 2016. **17**(10): p. 2562-2571.
249. Lyons, P.A., et al., *Genetically distinct subsets within ANCA-associated vasculitis.* N Engl J Med, 2012. **367**(3): p. 214-23.
250. Lyons, P.A., et al., *Genome-wide association study of eosinophilic granulomatosis with polyangiitis reveals genomic loci stratified by ANCA status.* Nat Commun, 2019. **10**(1): p. 5120.
251. de Souza, A.W.S., et al., *M2 macrophage is the predominant phenotype in airways inflammatory lesions in patients with granulomatosis with polyangiitis.* Arthritis Res Ther, 2017. **19**(1): p. 100.
252. Clarke, B.E., et al., *Macrophages and Glomerular Crescent Formation. Studies with Rat Nephrotoxic Nephritis.* Pathology, 1983. **15**(1): p. 75-81.
253. Soussan, M., et al., *FDG-PET/CT in patients with ANCA-associated vasculitis: case-series and literature review.* Autoimmun Rev, 2014. **13**(2): p. 125-31.
254. Grayson, P.C., et al., *Metabolic pathways and immunometabolism in rare kidney diseases.* Annals of the Rheumatic Diseases, 2018. **77**(8): p. 1226.
255. Zheng, W., et al., *Metabolomic alterations associated with Behcet's disease.* Arthritis Res Ther, 2018. **20**(1): p. 214.
256. Ahn, J.K., et al., *Potential metabolomic biomarkers for reliable diagnosis of Behcet's disease using gas chromatography/ time-of-flight-mass spectrometry.* Joint Bone Spine, 2018. **85**(3): p. 337-343.
257. Guleria, A., et al., *NMR-Based Serum Metabolomics Discriminates Takayasu Arteritis from Healthy Individuals: A Proof-of-Principle Study.* Journal of Proteome Research, 2015. **14**(8): p. 3372-3381.
258. Misra, R., et al., *3-141 NMR based serum metabolomics revealed distinctive metabolic Patterns of ANCA-associated vasculitis*, in *21st Asia Pacific League of Associations for Rheumatology Congress*. 2019, International Journal of Rheumatic Diseases: Brisbane, QLD, Australia. p. 40-226.
259. Najem, C.E., et al., *Characterizing the Gut and Plasma Metabolomes in Patients with ANCA-Associated Vasculitis*, in *Arthritis & Rheumatology*. 2018.
260. Geetha, D., et al., *Serum and urinary metabolites discriminate disease activity in ANCA associated glomerulonephritis in a pilot study.* J Nephrol, 2021.
261. Al-Ani, B., et al., *Changes in urinary metabolomic profile during relapsing renal vasculitis.* Sci Rep, 2016. **6**: p. 38074.
262. Huang, N. and A. Perl, *Metabolism as a Target for Modulation in Autoimmune Diseases.* Trends Immunol, 2018. **39**(7): p. 562-576.
263. Bettencourt, I.A. and J.D. Powell, *Targeting Metabolism as a Novel Therapeutic Approach to Autoimmunity, Inflammation, and Transplantation.* J Immunol, 2017. **198**(3): p. 999-1005.
264. Sanchez-Lopez, E., A. Cheng, and M. Guma, *Can Metabolic Pathways Be Therapeutic Targets in Rheumatoid Arthritis?* J Clin Med, 2019. **8**(5).
265. Caputa, G., A. Castoldi, and E.J. Pearce, *Metabolic adaptations of tissue-resident immune cells.* Nat Immunol, 2019. **20**(7): p. 793-801.
266. Ursini, F., et al., *Metformin and Autoimmunity: A "New Deal" of an Old Drug.* Front Immunol, 2018. **9**: p. 1236.
267. Hou, H.W., et al., *Rapid and label-free microfluidic neutrophil purification and phenotyping in diabetes mellitus.* Sci Rep, 2016. **6**: p. 29410.

268. Vaez, H., et al., *Metformin Alleviates Lipopolysaccharide-induced Acute Lung Injury through Suppressing Toll-like Receptor 4 Signaling.* Iranian Journal of Allergy Asthma and Immunology, 2016. **15**(6): p. 498-507.
269. Zhang, X., et al., *The alleviative effects of metformin for lipopolysaccharide-induced acute lung injury rat model and its underlying mechanism.* Saudi Pharm J, 2017. **25**(4): p. 666-670.
270. Feng, X., et al., *Metformin, Macrophage Dysfunction and Atherosclerosis.* Frontiers in Immunology, 2021. **12**.
271. Constantinescu, A.R., M. Liang, and D.A. Laskow, *Sirolimus lowers myeloperoxidase and p-ANCA titers in a pediatric patient before kidney transplantation.* Am J Kidney Dis, 2002. **40**(2): p. 407-10.
272. Sha, L.L., et al., *Autophagy is induced by anti-neutrophil cytoplasmic Abs and promotes neutrophil extracellular traps formation.* Innate Immun, 2016. **22**(8): p. 658-665.
273. Yamaguchi, M., et al., *Association between statin use and incidence of relapse in anti-neutrophil cytoplasmic antibody-associated vasculitis: a single-center retrospective cohort study.* Rheumatol Int, 2020.
274. Sen, D., E.D. Rosenstein, and N. Kramer, *ANCA-positive vasculitis associated with simvastatin/ezetimibe: expanding the spectrum of statin-induced autoimmunity?* International Journal of Rheumatic Diseases, 2010. **13**(3): p. e29-e31.
275. Weyand, C.M. and J.J. Goronzy, *Medium- and Large-Vessel Vasculitis.* New England Journal of Medicine, 2003. **349**(2): p. 160-169.
276. Tremoulet, A.H., et al., *Phase I/IIa Trial of Atorvastatin in Patients with Acute Kawasaki Disease with Coronary Artery Aneurysm.* J Pediatr, 2019. **215**: p. 107-117 e12.
277. Cuadrado, A., et al., *Therapeutic targeting of the NRF2 and KEAP1 partnership in chronic diseases.* Nat Rev Drug Discov, 2019. **18**(4): p. 295-317.
278. Tsai, H.C. and M.H. Han, *Sphingosine-1-Phosphate (S1P) and S1P Signaling Pathway: Therapeutic Targets in Autoimmunity and Inflammation.* Drugs, 2016. **76**(11): p. 1067-79.
279. Hao, J.A., et al., *The interaction between C5a and sphingosine-1-phosphate in neutrophils for antineutrophil cytoplasmic antibody mediated activation.* Arthritis Research & Therapy, 2014. **16**(4).
280. Fox, R.I., et al., *Mechanism of action for leflunomide in rheumatoid arthritis.* Clinical Immunology, 1999. **93**(3): p. 198-208.
281. Mustapha, N., et al., *Efficacy of leflunomide in the treatment of vasculitis.* Clin Exp Rheumatol, 2021. **39 Suppl 129**(2): p. 114-118.
282. Chiaravalli, M., et al., *2-Deoxy-d-Glucose Ameliorates PKD Progression.* J Am Soc Nephrol, 2016. **27**(7): p. 1958-69.
283. Pelicano, H., et al., *Glycolysis inhibition for anticancer treatment.* Oncogene, 2006. **25**(34): p. 4633-46.
284. Raez, L.E., et al., *A phase I dose-escalation trial of 2-deoxy-D-glucose alone or combined with docetaxel in patients with advanced solid tumors.* Cancer Chemother Pharmacol, 2013. **71**(2): p. 523-30.
285. Ulmer, A.J., et al., *Isolation and Subfractionation of Human Peripheral Blood Mononuclear Cells (PBMC) by Density Gradient Centrifugation on Percoll.* Immunobiology, 1984. **166**(3): p. 238-250.
286. Miltenyi, S., et al., *High gradient magnetic cell separation with MACS.* Cytometry, 1990. **11**(2): p. 231-8.
287. Brown, G.R., et al., *Gene: a gene-centered information resource at NCBI.* Nucleic Acids Research, 2014. **43**(D1): p. D36-D42.
288. Thornton, B. and C. Basu, *Real-time PCR (qPCR) primer design using free online software.* Biochem Mol Biol Educ, 2011. **39**(2): p. 145-54.
289. Livak, K.J. and T.D. Schmittgen, *Analysis of Relative Gene Expression Data Using Real-Time Quantitative PCR and the 2−ΔΔCT Method.* Methods, 2001. **25**(4): p. 402-408.
290. Pitt, J.J., *Principles and Applications of Liquid Chromatography- Mass Spectrometry in Clinical Biochemistry.* 2009.
291. Zhou, L., et al., *Impact of human granulocyte and monocyte isolation procedures on functional studies.* Clin Vaccine Immunol, 2012. **19**(7): p. 1065-74.
292. Nielsen, M.C., M.N. Andersen, and H.J. Moller, *Monocyte isolation techniques significantly impact the phenotype of both isolated monocytes and derived macrophages in vitro.* Immunology, 2020. **159**(1): p. 63-74.
293. Llufrio, E.M., et al., *Sorting cells alters their redox state and cellular metabolome.* Redox Biol, 2018. **16**: p. 381-387.
294. Tedesco, S., et al., *Convenience versus Biological Significance: Are PMA-Differentiated THP-1 Cells a Reliable Substitute for Blood-Derived Macrophages When Studying in Vitro Polarization?* Front Pharmacol, 2018. **9**: p. 71.
295. Muller, E., et al., *The sequential isolation of metabolites, RNA, DNA, and proteins from a single, undivided mixed microbial community sample.* Protocol Exchange, 2014.
296. Roume, H., et al., *Sequential isolation of metabolites, RNA, DNA, and proteins from the same unique sample.* Methods Enzymol, 2013. **531**: p. 219-36.
297. Dinarello, C.A., *Immunological and inflammatory functions of the interleukin-1 family.* Annu Rev Immunol, 2009. **27**: p. 519-50.
298. Netea, M.G., et al., *Differential requirement for the activation of the inflammasome for processing and release of IL-1beta in monocytes and macrophages.* Blood, 2009. **113**(10): p. 2324-35.
299. Mills, E.L., et al., *Succinate Dehydrogenase Supports Metabolic Repurposing of Mitochondria to Drive Inflammatory Macrophages.* Cell, 2016. **167**(2): p. 457-470 e13.
300. Dranka, B.P., et al., *Assessing bioenergetic function in response to oxidative stress by metabolic profiling.* Free Radic Biol Med, 2011. **51**(9): p. 1621-35.
301. Daskalaki, E., et al., *The influence of culture media upon observed cell secretome metabolite profiles: The balance between cell viability and data interpretability.* Anal Chim Acta, 2018. **1037**: p. 338-350.
302. Kerstholt, M., et al., *Role of glutathione metabolism in host defense against Borrelia burgdorferi infection.* Proceedings of the National Academy of Sciences, 2018. **115**(10): p. E2320.
303. Mullarky, E., et al., *Identification of a small molecule inhibitor of 3-phosphoglycerate dehydrogenase to target serine biosynthesis in cancers.* Proceedings of the National Academy of Sciences, 2016. **113**(7): p. 1778.
304. Antonelou, M., et al., *Therapeutic Myeloperoxidase Inhibition Attenuates Neutrophil Activation, ANCA-Mediated Endothelial Damage, and Crescentic GN.* J Am Soc Nephrol, 2020. **31**(2): p. 350-364.
305. Kettle, A.J., et al., *Inhibition of myeloperoxidase by benzoic acid hydrazides.* Biochem J, 1995. **308 ( Pt 2)**: p. 559-63.
306. Kipkeu, B.J., et al., *Evaluation of the functional properties of cryopreserved buffy coat-derived monocytes for monocyte monolayer assay.* Transfusion, 2018. **58**(8): p. 2027-2035.
307. Grievink, H.W. and M. Moerland, *Sample Aging Profoundly Reduces Monocyte Responses in Human Whole Blood Cultures.* J Immunol Res, 2018. **2018**: p. 8901485.

308. Patel, A.A., F. Ginhoux, and S. Yona, *Monocytes, macrophages, dendritic cells and neutrophils: an update on lifespan kinetics in health and disease.* Immunology, 2021. **163**(3): p. 250-261.
309. Patel, A.A., et al., *The fate and lifespan of human monocyte subsets in steady state and systemic inflammation.* J Exp Med, 2017. **214**(7): p. 1913-1923.
310. Winters, A.C., et al., *Reassessing the safety concerns of utilizing blood donations from patients with hemochromatosis.* Hepatology, 2018. **67**(3): p. 1150-1157.
311. Stechemesser, L., et al., *Metabolomic profiling identifies potential pathways involved in the interaction of iron homeostasis with glucose metabolism.* Mol Metab, 2017. **6**(1): p. 38-47.
312. Cronin, S.J.F., et al., *The Role of Iron Regulation in Immunometabolism and Immune-Related Disease.* Front Mol Biosci, 2019. **6**: p. 116.
313. Richer, B.C., et al., *Changes in Neutrophil Metabolism upon Activation and Aging.* Inflammation, 2018. **41**(2): p. 710-721.
314. Tam, V.C., *Lipidomic profiling of bioactive lipids by mass spectrometry during microbial infections.* Semin Immunol, 2013. **25**(3): p. 240-8.
315. Pearce, E.L. and E.J. Pearce, *Metabolic pathways in immune cell activation and quiescence.* Immunity, 2013. **38**(4): p. 633-43.
316. Wang, T., et al., *HIF1alpha-Induced Glycolysis Metabolism Is Essential to the Activation of Inflammatory Macrophages.* Mediators Inflamm, 2017. **2017**: p. 9029327.
317. Cramer, T., et al., *HIF-1a Is Essential for Myeloid Cell-Mediated Inflammation.* Cell, 2003. **112**: p. 645–657.
318. Oliveira, M.C., et al., *Tumor Necrosis Factor, but Not Neutrophils, Alters the Metabolic Profile in Acute Experimental Arthritis.* PLoS One, 2016. **11**(1): p. e0146403.
319. Alwarawrah, Y., K. Kiernan, and N.J. MacIver, *Changes in Nutritional Status Impact Immune Cell Metabolism and Function.* Front Immunol, 2018. **9**: p. 1055.
320. Munoz-Grajales, C. and J.C. Pineda, *Pathophysiological Relationship between Infections and Systemic Vasculitis.* Autoimmune Dis, 2015. **2015**: p. 286783.
321. Murphy, M.P. and L.A.J. O'Neill, *Krebs Cycle Reimagined: The Emerging Roles of Succinate and Itaconate as Signal Transducers.* Cell, 2018. **174**(4): p. 780-784.
322. Fei, F., et al., *Age-associated metabolic dysregulation in bone marrow-derived macrophages stimulated with lipopolysaccharide.* Sci Rep, 2016. **6**: p. 22637.
323. Guthrie, L.A., et al., *Priming of neutrophils for enhanced release of oxygen metabolites by bacterial lipopolysaccharide. Evidence for increased activity of the superoxide-producing enzyme.* The Journal of Experimental Medicine, 1984. **160**(6): p. 1656.
324. Zuo, Y., et al., *Sodium azide induces mitochondria-mediated apoptosis in PC12 cells through Pgc-1α-associated signaling pathway.* Mol Med Rep, 2019. **19**(3): p. 2211-2219.
325. Park, C.Y., et al., *Sodium azide suppresses LPS-induced expression MCP-1 through regulating IkappaBzeta and STAT1 activities in macrophages.* Cell Immunol, 2017. **315**: p. 64-70.
326. Simms, H.H., et al., *Studies on phagocytosis in patients with acute bacterial infections.* J Clin Invest, 1989. **83**(1): p. 252-60.
327. Cianciolo, G.J. and R. Snyderman, *Monocyte responsiveness to chemotactic stimuli is a property of a subpopulation of cells that can respond to multiple chemoattractants.* J Clin Invest, 1981. **67**(1): p. 60-8.
328. Ishikawa, T., B.L. Zhu, and H. Maeda, *Effect of sodium azide on the metabolic activity of cultured fetal cells.* Toxicol Ind Health, 2006. **22**(8): p. 337-41.
329. Netea, M.G., et al., *Trained immunity: A program of innate immune memory in health and disease.* Science, 2016. **352**(6284): p. aaf1098.
330. van Splunter, M., et al., *Induction of Trained Innate Immunity in Human Monocytes by Bovine Milk and Milk-Derived Immunoglobulin G.* Nutrients, 2018. **10**(10).
331. Newman, A.C. and O.D.K. Maddocks, *Serine and Functional Metabolites in Cancer.* Trends Cell Biol, 2017. **27**(9): p. 645-657.
332. Labuschagne, C.F., et al., *Serine, but not glycine, supports one-carbon metabolism and proliferation of cancer cells.* Cell Rep, 2014. **7**(4): p. 1248-58.
333. Mattaini, K.R., M.R. Sullivan, and M.G. Vander Heiden, *The importance of serine metabolism in cancer.* J Cell Biol, 2016. **214**(3): p. 249-57.
334. McNamee, M.J., D. Michod, and M.V. Niklison-Chirou, *Can small molecular inhibitors that stop de novo serine synthesis be used in cancer treatment?* Cell Death Discov, 2021. **7**(1): p. 87.
335. Rodriguez, A.E., et al., *Serine Metabolism Supports Macrophage IL-1beta Production.* Cell Metab, 2019.
336. Xu, P.C., et al., *Influence of myeloperoxidase by anti-myeloperoxidase antibodies and its association with the disease activity in microscopic polyangiitis.* Rheumatology (Oxford), 2010. **49**(11): p. 2068-75.
337. Xu, P.C., et al., *Influence of myeloperoxidase-catalyzing reaction on the binding between myeloperoxidase and anti-myeloperoxidase antibodies.* Hum Immunol, 2012. **73**(4): p. 364-9.
338. STENT, G. and S.M. CROWE, *Effects of monocvte purification and culture on integrin expression.* APMIS, 1997. **105**: p. 663-670.
339. Brodin, P., D. Duffy, and L. Quintana-Murci, *A Call for Blood—In Human Immunology.* Immunity, 2019. **50**(6): p. 1335-1336.
340. Liu, Y., et al., *IL-17A and TNF-alpha exert synergistic effects on expression of CXCL5 by alveolar type II cells in vivo and in vitro.* J Immunol, 2011. **186**(5): p. 3197-205.
341. Disteldorf, E.M., et al., *CXCL5 drives neutrophil recruitment in TH17-mediated GN.* J Am Soc Nephrol, 2015. **26**(1): p. 55-66.
342. Antonelli, A., et al., *Chemokine (C-X-C motif) ligand (CXCL)10 in autoimmune diseases.* Autoimmun Rev, 2014. **13**(3): p. 272-80.
343. Corbera-Bellalta, M., et al., *Blocking interferon gamma reduces expression of chemokines CXCL9, CXCL10 and CXCL11 and decreases macrophage infiltration in ex vivo cultured arteries from patients with giant cell arteritis.* Ann Rheum Dis, 2016. **75**(6): p. 1177-86.
344. Vorreiter, F., et al., *Comparison and optimization of methods for the simultaneous extraction of DNA, RNA, proteins, and metabolites.* Anal Biochem, 2016. **508**: p. 25-33.
345. Fei, F., D.M. Bowdish, and B.E. McCarry, *Comprehensive and simultaneous coverage of lipid and polar metabolites for endogenous cellular metabolomics using HILIC-TOF-MS.* Anal Bioanal Chem, 2014. **406**(15): p. 3723-33.
346. Lagziel, S., E. Gottlieb, and T. Shlomi, *Mind your media.* Nat Metab, 2020.

347. Sima, M., et al., *Cell-Tak coating may cause misnormalization of Seahorse metabolic flux data.* 2021.
348. Gonzalez-Dominguez, R., et al., *Recommendations and Best Practices for Standardizing the Pre-Analytical Processing of Blood and Urine Samples in Metabolomics.* Metabolites, 2020. **10**(6).
349. Fernández-Peralbo, M.A. and M.D. Luque de Castro, *Preparation of urine samples prior to targeted or untargeted metabolomics mass-spectrometry analysis.* TrAC Trends in Analytical Chemistry, 2012. **41**: p. 75-85.
350. Emwas, A.H., et al., *Standardizing the experimental conditions for using urine in NMR-based metabolomic studies with a particular focus on diagnostic studies: a review.* Metabolomics, 2015. **11**(4): p. 872-894.
351. Haid, M., et al., *Long-Term Stability of Human Plasma Metabolites during Storage at -80 degrees C.* J Proteome Res, 2018. **17**(1): p. 203-211.
352. Luo, X. and L. Li, *Metabolomics of Small Numbers of Cells: Metabolomic Profiling of 100, 1000, and 10000 Human Breast Cancer Cells.* Anal Chem, 2017. **89**(21): p. 11664-11671.
353. Gunda, V., F. Yu, and P.K. Singh, *Validation of Metabolic Alterations in Microscale Cell Culture Lysates Using Hydrophilic Interaction Liquid Chromatography (HILIC)-Tandem Mass Spectrometry-Based Metabolomics.* PLoS One, 2016. **11**(4): p. e0154416.
354. Shurubor, Y.I., et al., *Biological variability dominates and influences analytical variance in HPLC-ECD studies of the human plasma metabolome.* BMC Clin Pathol, 2007. **7**: p. 9.
355. Sampson, J.N., et al., *Metabolomics in epidemiology: sources of variability in metabolite measurements and implications.* Cancer Epidemiol Biomarkers Prev, 2013. **22**(4): p. 631-40.
356. Liigand, J., et al., *Quantification for non-targeted LC/MS screening without standard substances.* Scientific Reports, 2020. **10**(1): p. 5808.
357. Meissen, J.K., et al., *Phenotyping hepatocellular metabolism using uniformly labeled carbon-13 molecular probes and LC-HRMS stable isotope tracing.* Anal Biochem, 2016. **508**: p. 129-37.
358. Lindahl, A., et al., *Tuning Metabolome Coverage in Reversed Phase LC-MS Metabolomics of MeOH Extracted Samples Using the Reconstitution Solvent Composition.* Anal Chem, 2017. **89**(14): p. 7356-7364.
359. Eriksson, L., et al., *Using chemometrics for navigating in the large data sets of genomics, proteomics, and metabonomics (gpm).* Analytical and Bioanalytical Chemistry, 2004. **380**(3): p. 419-429.
360. Dieterle, F., et al., *Probabilistic quotient normalization as robust method to account for dilution of complex biological mixtures. Application in H-1 NMR metabonomics.* Analytical Chemistry, 2006. **78**(13): p. 4281-4290.
361. Bolstad, B.M., et al., *A comparison of normalization methods for high density oligonucleotide array data based on variance and bias.* Bioinformatics, 2003. **19**(2): p. 185-193.
362. Dettmer, K., et al., *Metabolite extraction from adherently growing mammalian cells for metabolomics studies: optimization of harvesting and extraction protocols.* Anal Bioanal Chem, 2011. **399**(3): p. 1127-39.
363. Dietmair, S., et al., *Towards quantitative metabolomics of mammalian cells: development of a metabolite extraction protocol.* Anal Biochem, 2010. **404**(2): p. 155-64.
364. Nastasi, C., et al., *Inhibition of succinate dehydrogenase activity impairs human T cell activation and function.* Sci Rep, 2021. **11**(1): p. 1458.
365. O'Neill, L.A.J. and M.N. Artyomov, *Itaconate: the poster child of metabolic reprogramming in macrophage function.* Nat Rev Immunol, 2019. **19**(5): p. 273-281.
366. Krawczyk, C.M., et al., *Toll-like receptor-induced changes in glycolytic metabolism regulate dendritic cell activation.* Blood, 2010. **115**(23): p. 4742-9.
367. Kelly, B., et al., *Metformin Inhibits the Production of Reactive Oxygen Species from NADH:Ubiquinone Oxidoreductase to Limit Induction of Interleukin-1beta (IL-1beta) and Boosts Interleukin-10 (IL-10) in Lipopolysaccharide (LPS)-activated Macrophages.* J Biol Chem, 2015. **290**(33): p. 20348-59.
368. Borst, K., M. Schwabenland, and M. Prinz, *Microglia metabolism in health and disease.* Neurochem Int, 2019. **130**: p. 104331.
369. Ohlsson, S.M., et al., *Phagocytosis of apoptotic cells by macrophages in anti-neutrophil cytoplasmic antibody-associated systemic vasculitis.* Clin Exp Immunol, 2012. **170**(1): p. 47-56.
370. Schreiber, A., F.C. Luft, and R. Kettritz, *Phagocyte NADPH oxidase restrains the inflammasome in ANCA-induced GN.* J Am Soc Nephrol, 2015. **26**(2): p. 411-24.
371. O'Neill, L.A., *A broken krebs cycle in macrophages.* Immunity, 2015. **42**(3): p. 393-4.
372. O'Neill, L.A. and E.J. Pearce, *Immunometabolism governs dendritic cell and macrophage function.* J Exp Med, 2016. **213**(1): p. 15-23.
373. Ryan, D.G., et al., *Coupling Krebs cycle metabolites to signalling in immunity and cancer.* Nature Metabolism, 2018. **1**(1): p. 16-33.
374. Martinez-Reyes, I. and N.S. Chandel, *Mitochondrial TCA cycle metabolites control physiology and disease.* Nat Commun, 2020. **11**(1): p. 102.
375. Blacher, E., et al., *Microbiome-Modulated Metabolites at the Interface of Host Immunity.* J Immunol, 2017. **198**(2): p. 572-580.
376. Levy, M., E. Blacher, and E. Elinav, *Microbiome, metabolites and host immunity.* Curr Opin Microbiol, 2017. **35**: p. 8-15.
377. Shibata, N., J. Kunisawa, and H. Kiyono, *Dietary and Microbial Metabolites in the Regulation of Host Immunity.* Front Microbiol, 2017. **8**: p. 2171.
378. Faul, F., et al., *G*Power 3: a flexible statistical power analysis program for the social, behavioral, and biomedical sciences.* Behav Res Methods, 2007. **39**(2): p. 175-91.
379. Nyamundanda, G., et al., *MetSizeR: selecting the optimal sample size for metabolomic studies using an analysis based approach.* Bmc Bioinformatics, 2013. **14**.
380. Oliveros, J.C. *Venny. An interactive tool for comparing lists with Venn's diagrams.* 2007-2015 [cited 2021 21/01]; Available from: https://bioinfogp.cnb.csic.es/tools/venny/index.html.
381. Fuhrer, T. and N. Zamboni, *High-throughput discovery metabolomics.* Curr Opin Biotechnol, 2015. **31**: p. 73-8.
382. Holecek, M., *Histidine in Health and Disease: Metabolism, Physiological Importance, and Use as a Supplement.* Nutrients, 2020. **12**(3).
383. Carey, B.W., et al., *Intracellular alpha-ketoglutarate maintains the pluripotency of embryonic stem cells.* Nature, 2015. **518**(7539): p. 413-6.
384. Zhang, S., et al., *Novel metabolic and physiological functions of branched chain amino acids: a review.* J Anim Sci Biotechnol, 2017. **8**: p. 10.
385. Cheng, S.C., et al., *Broad defects in the energy metabolism of leukocytes underlie immunoparalysis in sepsis.* Nat Immunol, 2016. **17**(4): p. 406-13.

386. Kelly, B. and E.L. Pearce, *Amino Assets: How Amino Acids Support Immunity.* Cell Metab, 2020. **32**(2): p. 154-175.
387. Miyajima, M., *Amino acids: key sources for immunometabolites and immunotransmitters.* Int Immunol, 2020. **32**(7): p. 435-446.
388. Halaby, M.J. and T.L. McGaha, *Amino Acid Transport and Metabolism in Myeloid Function.* Frontiers in Immunology, 2021. **12**.
389. Yoon, B.R., et al., *Role of SLC7A5 in Metabolic Reprogramming of Human Monocyte/Macrophage Immune Responses.* Front Immunol, 2018. **9**: p. 53.
390. Mondanelli, G., et al., *Amino acid metabolism as drug target in autoimmune diseases.* Autoimmun Rev, 2019. **18**(4): p. 334-348.
391. Carta, G., et al., *Palmitic Acid: Physiological Role, Metabolism and Nutritional Implications.* Frontiers in Physiology, 2017. **8**(902).
392. Wong, E., *Cells: Molecules and Mechanisms*. 2009: Axolotl Academic Publishing Company.
393. Snodgrass, R.G., et al., *Docosahexaenoic acid and palmitic acid reciprocally modulate monocyte activation in part through endoplasmic reticulum stress.* J Nutr Biochem, 2016. **32**: p. 39-45.
394. Pararasa, C., et al., *Age-associated changes in long-chain fatty acid profile during healthy aging promote pro-inflammatory monocyte polarization via PPARγ.* Aging Cell, 2016. **15**(1): p. 128-139.
395. Gao, D., et al., *Palmitate promotes monocyte atherogenicity via de novo ceramide synthesis.* Free Radic Biol Med, 2012. **53**(4): p. 796-806.
396. Gao, W., et al., *Monocyte-derived extracellular vesicles upon treated by palmitate promote endothelial migration and monocytes attachment to endothelial cells.* Biochem Biophys Res Commun, 2020.
397. Tzeng, H.T., I.T. Chyuan, and W.Y. Chen, *Shaping of Innate Immune Response by Fatty Acid Metabolite Palmitate.* Cells, 2019. **8**(12).
398. Gao, D., C.J. Bailey, and H.R. Griffiths, *Metabolic memory effect of the saturated fatty acid, palmitate, in monocytes.* Biochem Biophys Res Commun, 2009. **388**(2): p. 278-82.
399. Huang, Y.L., et al., *Toll-like receptor agonists promote prolonged triglyceride storage in macrophages.* J Biol Chem, 2014. **289**(5): p. 3001-12.
400. Sokol, E., et al., *Profiling of lipid species by normal-phase liquid chromatography, nanoelectrospray ionization, and ion trap-orbitrap mass spectrometry.* Anal Biochem, 2013. **443**(1): p. 88-96.
401. Friedrich, K., et al., *Perturbation of the Monocyte Compartment in Human Obesity.* Front Immunol, 2019. **10**: p. 1874.
402. Dias, S.S.G., et al., *Lipid droplets fuel SARS-CoV-2 replication and production of inflammatory mediators.* PLoS Pathog, 2020. **16**(12): p. e1009127.
403. Hearps, A.C., et al., *Aging is associated with chronic innate immune activation and dysregulation of monocyte phenotype and function.* Aging Cell, 2012. **11**(5): p. 867-75.
404. Metcalf, T.U., et al., *Human Monocyte Subsets Are Transcriptionally and Functionally Altered in Aging in Response to Pattern Recognition Receptor Agonists.* J Immunol, 2017. **199**(4): p. 1405-1417.
405. Shaw, A.C., D.R. Goldstein, and R.R. Montgomery, *Age-dependent dysregulation of innate immunity.* Nat Rev Immunol, 2013. **13**(12): p. 875-87.
406. Jiang, C., A.T. Ting, and B. Seed, *PPAR-gamma agonists inhibit production of monocyte inflammatory cytokines.* Nature, 1998. **391**(6662): p. 82-6.
407. Gil-de-Gomez, L., et al., *A phosphatidylinositol species acutely generated by activated macrophages regulates innate immune responses.* J Immunol, 2013. **190**(10): p. 5169-77.
408. Lai, K.N. and C.M. Lockwood, *The effect of anti-neutrophil cytoplasm autoantibodies on the signal transduction in human neutrophils.* Clin Exp Immunol, 1991. **85**(3): p. 396-401.
409. Sibelius, U., et al., *Wegener's granulomatosis: anti-proteinase 3 antibodies are potent inductors of human endothelial cell signaling and leakage response.* J Exp Med, 1998. **187**(4): p. 497-503.
410. Yu, X.H., et al., *Itaconate: an emerging determinant of inflammation in activated macrophages.* Immunol Cell Biol, 2018.
411. Mills, E.L., et al., *Itaconate is an anti-inflammatory metabolite that activates Nrf2 via alkylation of KEAP1.* Nature, 2018. **556**(7699): p. 113-117.
412. Schmidl, C., et al., *Transcription and enhancer profiling in human monocyte subsets.* Blood, 2014. **123**(17): p. e90-9.
413. Dettmer, K., et al., *Distinct metabolic differences between various human cancer and primary cells.* Electrophoresis, 2013. **34**(19): p. 2836-47.
414. Maruyama, A., et al., *De novo deoxyribonucleotide biosynthesis regulates cell growth and tumor progression in small-cell lung carcinoma.* Scientific Reports, 2021. **11**(1): p. 13474.
415. Sadiku, P., et al., *Neutrophils Fuel Effective Immune Responses through Gluconeogenesis and Glycogenesis.* Cell Metabolism, 2020.
416. Kumar, S. and M. Dikshit, *Metabolic Insight of Neutrophils in Health and Disease.* Front Immunol, 2019. **10**: p. 2099.
417. Rodriguez-Espinosa, O., et al., *Metabolic requirements for neutrophil extracellular traps formation.* Immunology, 2015. **145**(2): p. 213-24.
418. Caro-Maldonado, A., et al., *Metabolic reprogramming is required for antibody production that is suppressed in anergic but exaggerated in chronically BAFF-exposed B cells.* J Immunol, 2014. **192**(8): p. 3626-36.
419. Waters, L.R., et al., *Initial B Cell Activation Induces Metabolic Reprogramming and Mitochondrial Remodeling.* iScience, 2018. **5**: p. 99-109.
420. Muschen, M., *Metabolic gatekeepers to safeguard against autoimmunity and oncogenic B cell transformation.* Nat Rev Immunol, 2019. **19**(5): p. 337-348.
421. MacIver, N.J., R.D. Michalek, and J.C. Rathmell, *Metabolic regulation of T lymphocytes.* Annu Rev Immunol, 2013. **31**: p. 259-83.
422. Bantug, G.R., et al., *The spectrum of T cell metabolism in health and disease.* Nat Rev Immunol, 2018. **18**(1): p. 19-34.
423. Buck, M.D., D. O'Sullivan, and E.L. Pearce, *T cell metabolism drives immunity.* J Exp Med, 2015. **212**(9): p. 1345-60.
424. O'Sullivan, D. and E.L. Pearce, *Targeting T cell metabolism for therapy.* Trends Immunol, 2015. **36**(2): p. 71-80.
425. Li, W., et al., *Targeting T Cell Activation and Lupus Autoimmune Phenotypes by Inhibiting Glucose Transporters.* Front Immunol, 2019. **10**: p. 833.

426. Sitnikov, D.G., C.S. Monnin, and D. Vuckovic, *Systematic Assessment of Seven Solvent and Solid-Phase Extraction Methods for Metabolomics Analysis of Human Plasma by LC-MS.* Sci Rep, 2016. **6**: p. 38885.
427. Aldana, J., A. Romero-Otero, and M.P. Cala, *Exploring the Lipidome: Current Lipid Extraction Techniques for Mass Spectrometry Analysis.* Metabolites, 2020. **10**(6).
428. Fessenden, M., *Metabolomics: Small molecules, single cells.* Nature, 2016. **540**(7631): p. 153-155.
429. Duncan, K.D., J. Fyrestam, and I. Lanekoff, *Advances in mass spectrometry based single-cell metabolomics.* Analyst, 2019. **144**(3): p. 782-793.
430. Gilmore, I.S., S. Heiles, and C.L. Pieterse, *Metabolic Imaging at the Single-Cell Scale: Recent Advances in Mass Spectrometry Imaging.* Annu Rev Anal Chem (Palo Alto Calif), 2019. **12**(1): p. 201-224.
431. Artyomov, M.N. and J. Van den Bossche, *Immunometabolism in the Single-Cell Era.* Cell Metab, 2020. **32**(5): p. 710-725.
432. Ganesh, S., et al., *Spatially resolved 3D metabolomic profiling in tissues.* Sci Adv, 2021. **7**(5).
433. Arguello, R.J., et al., *SCENITH: A Flow Cytometry-Based Method to Functionally Profile Energy Metabolism with Single-Cell Resolution.* Cell Metab, 2020. **32**(6): p. 1063-1075 e7.
434. Tripodi, G.L., M.B. Prieto, and D.S.P. Abdalla, *Inflammasome Activation in Human Macrophages Induced by a LDL (-) Mimetic Peptide.* Inflammation, 2020. **43**(2): p. 722-730.
435. Gritsenko, A., et al., *Priming Is Dispensable for NLRP3 Inflammasome Activation in Human Monocytes In Vitro.* Front Immunol, 2020. **11**: p. 565924.
436. Menk, A.V., et al., *Early TCR Signaling Induces Rapid Aerobic Glycolysis Enabling Distinct Acute T Cell Effector Functions.* Cell Rep, 2018. **22**(6): p. 1509-1521.
437. Żabińska, M., et al., *Immune Cells Profiling in ANCA-Associated Vasculitis Patients—Relation to Disease Activity.* Cells, 2021. **10**(7).
438. Dekkema, G.J., et al., *Increased miR-142-3p Expression Might Explain Reduced Regulatory T Cell Function in Granulomatosis With Polyangiitis.* Frontiers in Immunology, 2019. **10**.
439. Colamatteo, A., et al., *Metabolism and Autoimmune Responses: The microRNA Connection.* Frontiers in Immunology, 2019. **10**.
440. Evans, H.G., et al., *In vivo activated monocytes from the site of inflammation in humans specifically promote Th17 responses.* Proc Natl Acad Sci U S A, 2009. **106**(15): p. 6232-7.
441. Hilhorst, M., et al., *T cell-macrophage interactions and granuloma formation in vasculitis.* Front Immunol, 2014. **5**: p. 432.
442. Shochet, L., S. Holdsworth, and A.R. Kitching, *Animal Models of ANCA Associated Vasculitis.* Front Immunol, 2020. **11**: p. 525.
443. Cani, P.D., et al., *Metabolic Endotoxemia Initiates Obesity and Insulin Resistance.* Diabetes, 2007. **56**(7): p. 1761.
444. Liang, H., et al., *Effect of Lipopolysaccharide on Inflammation and Insulin Action in Human Muscle.* PLOS ONE, 2013. **8**(5): p. e63983.
445. Ulich, T.R., et al., *The intratracheal administration of endotoxin and cytokines. I. Characterization of LPS-induced IL-1 and TNF mRNA expression and the LPS-, IL-1-, and TNF-induced inflammatory infiltrate.* The American journal of pathology, 1991. **138**(6): p. 1485-1496.
446. Di Gioia, M., et al., *Endogenous oxidized phospholipids reprogram cellular metabolism and boost hyperinflammation.* Nat Immunol, 2019.
447. Brands, X., et al., *An epigenetic and transcriptomic signature of immune tolerance in human monocytes through multi-omics integration.* Genome Med, 2021. **13**(1): p. 131.
448. Baeyens, A., et al., *Monocyte-derived S1P in the lymph node regulates immune responses.* Nature, 2021.
449. Sun, X.J., M. Chen, and M.H. Zhao, *Sphingosine-1-phosphate (S1P) enhances glomerular endothelial cells activation mediated by anti-myeloperoxidase antibody-positive IgG.* J Cell Mol Med, 2018. **22**(3): p. 1769-1777.
450. Sun, X.J., M. Chen, and M.H. Zhao, *Rho GTPases are involved in S1P-enhanced glomerular endothelial cells activation with anti-myeloperoxidase antibody positive IgG.* J Cell Mol Med, 2018. **22**(9): p. 4550-4554.
451. Sun, X.J., et al., *Sphingosine-1-phosphate and its receptors in anti-neutrophil cytoplasmic antibody-associated vasculitis.* Nephrol Dial Transplant, 2017. **32**(8): p. 1313-1322.
452. Yu, W., et al., *One-Carbon Metabolism Supports S-Adenosylmethionine and Histone Methylation to Drive Inflammatory Macrophages.* Mol Cell, 2019. **75**(6): p. 1147-1160 e5.
453. Croze, M.L. and C.O. Soulage, *Potential role and therapeutic interests of myo-inositol in metabolic diseases.* Biochimie, 2013. **95**(10): p. 1811-27.
454. Kraaijenhof, J.M., et al., *The iterative lipid impact on inflammation in atherosclerosis.* Curr Opin Lipidol, 2021.
455. Rahman, M.S., A.J. Murphy, and K.J. Woollard, *Effects of dyslipidaemia on monocyte production and function in cardiovascular disease.* Nat Rev Cardiol, 2017. **14**(7): p. 387-400.
456. Petermann Smits, D.R., et al., *Metabolic syndrome in ANCA-associated vasculitis.* Rheumatology (Oxford), 2013. **52**(1): p. 197-203.
457. Wallace, Z.S., et al., *Disease Activity, ANCA-Type, and Lipid Levels in ANCA-Associated Vasculitis.* Arthritis & Rheumatology, 2019. **0**(ja).
458. Chen, R.R., et al., *Targeting of lipid metabolism with a metabolic inhibitor cocktail eradicates peritoneal metastases in ovarian cancer cells.* Commun Biol, 2019. **2**: p. 281.
459. Monson, E.A., et al., *Lipid droplet density alters the early innate immune response to viral infection.* PLoS One, 2018. **13**(1): p. e0190597.
460. Marschallinger, J., et al., *Lipid-droplet-accumulating microglia represent a dysfunctional and proinflammatory state in the aging brain.* Nature Neuroscience, 2020.
461. Galvan-Pena, S. and L.A. O'Neill, *Metabolic reprograming in macrophage polarization.* Front Immunol, 2014. **5**: p. 420.
462. Thapa, B. and K. Lee, *Metabolic influence on macrophage polarization and pathogenesis.* BMB Reports, 2019. **52**(6): p. 360-372.
463. Zhu, L., et al., *Cellular metabolism and macrophage functional polarization.* Int Rev Immunol, 2015. **34**(1): p. 82-100.
464. Love, D.T., et al., *The role of the myeloperoxidase-derived oxidant hypothiocyanous acid (HOSCN) in the induction of mitochondrial dysfunction in macrophages.* Redox Biol, 2020. **36**: p. 101602.
465. Pan, G.J., et al., *A pivotal role for NF-kappaB in the macrophage inflammatory response to the myeloperoxidase oxidant hypothiocyanous acid.* Arch Biochem Biophys, 2018. **642**: p. 23-30.

466. Erra Diaz, F., E. Dantas, and J. Geffner, *Unravelling the Interplay between Extracellular Acidosis and Immune Cells.* Mediators of Inflammation, 2018. **2018**: p. 11.
467. Dietl, K., et al., *Lactic acid and acidification inhibit TNF secretion and glycolysis of human monocytes.* J Immunol, 2010. **184**(3): p. 1200-9.
468. Yu, N., et al., *Circulating Metabolomic Signature in Generalized Pustular Psoriasis Blunts Monocyte Hyperinflammation by Triggering Amino Acid Response.* Frontiers in Immunology, 2021. **12**.